MULTIDISCIPLINARY CENTER FOR EARTHQUAKE ENGINEERING RESEARCH
A National Center of Excellence in Advanced Technology Applications

ISSN 1520-295X

Effect of Spatial Variation of Ground Motion on Highway Structures

by

Masanobu Shinozuka, Vinita Saxena and George Deodatis
Princeton University
Department of Civil Engineering and Operations Research
Princeton, New Jersey 08544

Technical Report MCEER-00-0013

December 31, 2000

This research was conducted at Princeton University and was supported by the Federal Highway Administration under contract number DTFH61-92-C-00106.

NOTICE

This report was prepared by Princeton University as a result of research sponsored by the Multidisciplinary Center for Earthquake Engineering Research (MCEER) through a contract from the Federal Highway Administration. Neither MCEER, associates of MCEER, its sponsors, Princeton University, nor any person acting on their behalf:

a. makes any warranty, express or implied, with respect to the use of any information, apparatus, method, or process disclosed in this report or that such use may not infringe upon privately owned rights; or

b. assumes any liabilities of whatsoever kind with respect to the use of, or the damage resulting from the use of, any information, apparatus, method, or process disclosed in this report.

Any opinions, findings, and conclusions or recommendations expressed in this publication are those of the author(s) and do not necessarily reflect the views of MCEER or the Federal Highway Administration.

MULTIDISCIPLINARY CENTER FOR EARTHQUAKE ENGINEERING RESEARCH
A National Center of Excellence in Advanced Technology Applications

Effect of Spatial Variation of Ground Motion on Highway Structures

by

Masanobu Shinozuka[1], Vinita Saxena[2] and George Deodatis[3]

Publication Date: December 31, 2000
Submittal Date: May 20, 1999

Technical Report MCEER-00-0013

Task Numbers 106-E-2.2 and 106-E-2.5

FHWA Contract Number DTFH61-92-C-00106

1 Fred Champion Chair in Civil Engineering, Civil Engineering Department, University of Southern California
2 Graduate Research Assistant, Civil Engineering & Operations Research Department, Princeton University
3 Associate Professor, Civil Engineering & Operations Research Department, Princeton University

MULTIDISCIPLINARY CENTER FOR EARTHQUAKE ENGINEERING RESEARCH
University at Buffalo, State University of New York
Red Jacket Quadrangle, Buffalo, NY 14261

Preface

The Multidisciplinary Center for Earthquake Engineering Research (MCEER) is a national center of excellence in advanced technology applications that is dedicated to the reduction of earthquake losses nationwide. Headquartered at the University at Buffalo, State University of New York, the Center was originally established by the National Science Foundation in 1986, as the National Center for Earthquake Engineering Research (NCEER).

Comprising a consortium of researchers from numerous disciplines and institutions throughout the United States, the Center's mission is to reduce earthquake losses through research and the application of advanced technologies that improve engineering, pre-earthquake planning and post-earthquake recovery strategies. Toward this end, the Center coordinates a nationwide program of multidisciplinary team research, education and outreach activities.

MCEER's research is conducted under the sponsorship of two major federal agencies, the National Science Foundation (NSF) and the Federal Highway Administration (FHWA), and the State of New York. Significant support is also derived from the Federal Emergency Management Agency (FEMA), other state governments, academic institutions, foreign governments and private industry.

The Center's FHWA-sponsored Highway Project develops retrofit and evaluation methodologies for existing bridges and other highway structures (including tunnels, retaining structures, slopes, culverts, and pavements), and improved seismic design criteria and procedures for bridges and other highway structures. Specifically, tasks are being conducted to:

- assess the vulnerability of highway systems, structures and components;
- develop concepts for retrofitting vulnerable highway structures and components;
- develop improved design and analysis methodologies for bridges, tunnels, and retaining structures, which include consideration of soil-structure interaction mechanisms and their influence on structural response;
- review and recommend improved seismic design and performance criteria for new highway systems and structures.

Highway Project research focuses on two distinct areas: the development of improved design criteria and philosophies for new or future highway construction, and the development of improved analysis and retrofitting methodologies for existing highway systems and structures. The research discussed in this report is a result of work conducted under the existing highway structures project, and was performed within Tasks 106-E-2.2 through 106-E-2.5, "Spatial Variation of Ground Motion" of that project as shown in the flowchart on the following page.

The overall objectives of these tasks were to assess and, to the extent possible, quantify the effect of spatial variability of ground motion on the seismic response of highway bridges and to provide guidelines for the seismic analysis and design of highway bridges which account for this effect. To accomplish these objectives, a methodology was developed to generate spatially varying ground motion time histories along the length of a long, multi-span bridge at its supports. Spatial

variability of seismic ground motion can be mainly attributed to the following three mechanisms: difference in arrival times of seismic waves at different locations, which is commonly known as the wave passage effect; loss of coherence of seismic waves due to multiple reflections and refractions as they propagate through the highly inhomogeneous soil medium, referred to as the incoherence effect; and change in the amplitude and frequency content of seismic ground motion due to different local soil conditions, known as the local soil effect. The methodology developed in this study to generate spatially varying seismic ground motion time histories at different locations reflects all three of these effects.

Representative highway bridges were analyzed using two cases of input ground motions at the bridge supports. In the first case, the input motions were identical at all supports; in the second case, different input motions were applied at each pier along the length of the bridge reflecting the wave passage effect, the incoherence effect, and the local soils effect. This was done to assess the effect of spatial variability of ground motion when compared to the standard assumption currently used in practice of identical support ground motion. An extensive sensitivity analysis was carried out as a function of various parameters controlling the spatial variability of ground motions. Based on the results from these studies, two guidelines were proposed: one for the analysis and design of highway bridges that are less than approximately 1,000-to-1,500 feet long and have all supports on the same local soil conditions, and the second for bridges that are more than approximately 1,500 feet long or bridges of any length that have supports on different local soil conditions.

SEISMIC VULNERABILITY OF EXISTING HIGHWAY CONSTRUCTION
FHWA Contract DTFH61-92-C-00106

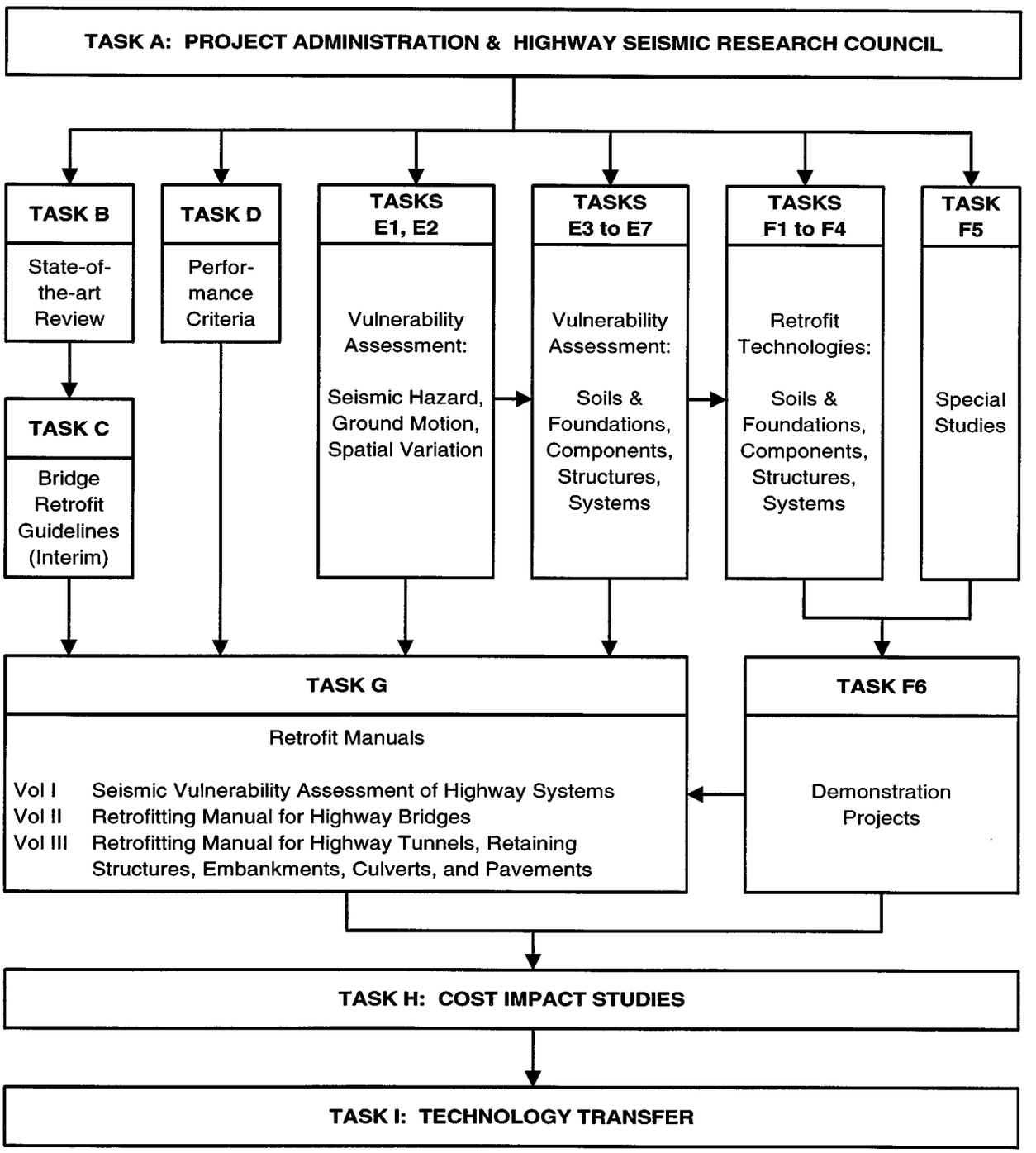

ABSTRACT

The two basic steps in the design of new bridge structures or the analysis of existing ones for strong earthquakes are the proper definition and representation of the seismic excitation and the subsequent computation of the structural response due to this input earthquake ground motion. It is very common in engineering practice today to determine the structural response by performing an equivalent linear static or a linear dynamic analysis of the bridge. For the case of a linear dynamic analysis, it is more common to perform a response spectrum analysis rather than performing a time history analysis. Furthermore, when deciding to perform a time history analysis, it is customary to assume that all of the bridge supports experience identical ground motion time histories, even for multi-span bridges of considerable overall length. It should be pointed out that the assumption of identical support ground motion is implicitly made also when performing an equivalent static or a response spectrum analysis.

Past research studies have demonstrated that seismic ground motion can vary significantly over distances comparable to the length of the majority of highway bridges on multiple supports. As a result, such bridges are subjected to ground motions at their supports that can differ considerably in amplitude, phase, as well as frequency content. These spatially varying seismic ground motions are referred to in the literature as differential or asynchronous support ground motions. In some cases, these differential motions can induce additional internal forces in the structure when compared to the case of identical support ground motion. This in turn might have a potentially detrimental effect on the safety of a bridge during a severe earthquake event. It is therefore of paramount importance to be able to account for the effect of spatial variability of earthquake ground motion on the response of highway bridges.

The objectives of this study are therefore to estimate the effect of spatial variability of ground motion on the seismic response of highway bridges and to provide guidelines for the seismic analysis and design of such structures to account for this effect. To accomplish the aforementioned objectives, a methodology is developed to generate spatially varying ground motion time histories at the different supports of a bridge. Spatial variability of seismic ground motion can be mainly attributed to the following three mechanisms: 1) difference in arrival times of seismic waves at different locations, commonly known as the "wave passage effect," 2) loss of coherence of seismic waves due to multiple reflections and refractions as they propagate through the highly inhomogeneous soil medium, referred to as the "incoherence effect," and 3) change in the amplitude and frequency content of seismic ground motion due to different local soil conditions, known as the "local soil effect". The "wave passage effect" is characterized by the apparent velocity of wave propagation, the "incoherence effect" is characterized by the so-called coherence function, while the "local soil effect" is characterized by defining different response (or power) spectra at different locations corresponding to their local soil conditions. The methodology that is developed in this study to generate spatially varying seismic ground motion time histories at different locations reflects all three of the aforementioned effects.

A set of representative highway bridges is then selected to be analyzed using identical support ground motions and differential (asynchronous) support ground motions, in order to estimate the effect of spatial variability of seismic ground motion. Extensive preliminary as well as rigorous sensitivity analyses are performed using a large variety of different spatially varying ground

motions. A Monte Carlo simulation approach is followed throughout. The following general conclusions are drawn.

1. The peak ductility demand at the columns can increase substantially when the bridge is analyzed using differential support ground motion and considering that different supports of the bridge are on different local soil conditions, compared to the case of identical support ground motion. Specifically, the ratio of the peak ductility demand at the columns using differential support ground motion and considering that different supports of the bridge are on different local soil conditions over the peak ductility demand using identical support ground motion is of the order of 2.0-2.5 for bridges of intermediate total length, and as high as 4.0 for longer bridges.

2. The peak ductility demand at the columns can increase by a smaller amount when the bridge is analyzed using differential support ground motion and considering that all supports of the bridge are on the same local soil conditions, compared to the case of identical support ground motion. Specifically, the ratio of the peak ductility demand at the columns using differential support ground motion and considering that all supports of the bridge are on the same local soil conditions over the peak ductility demand using identical support ground motion is of the order of 1.0-1.5 for bridges of intermediate total length, and as high as 4.0 for longer bridges.

3. Low apparent velocity of wave propagation might reduce in some cases the peak ductility demand of some of the columns, for the general case where both the wave propagation and loss of coherence effects are considered and all supports of the bridge are on the same type of local soil conditions. Further, a low value of the velocity might change the relative contribution of the wave passage and the incoherence effects in some of the columns.

4. The incoherence effect is in general more important than the wave passage effect. The wave passage effect becomes more important than the incoherence effect only for relatively longer bridges and for low velocities of wave propagation. But even in cases where the incoherence effect is more important, the wave passage effect is still substantial and its interaction with the incoherence effect cannot be predicted a priori. Therefore neglecting either one of these two effects might produce inaccurate results.

5. The relative contribution of the wave passage and incoherence effects to the peak ductility demand of the columns does not seem to be affected to any considerable degree by the assumption of different versus same local soil conditions at the supports of the bridge.

6. The identical support ground motion assumption seems to be generally unconservative, but much more so in the case of different local soil conditions. However, for relatively longer bridges, the identical support ground motion assumption severely underestimates the peak ductility demand at the columns by approximately the same amount for both same as well as different local soil conditions.

Based mainly on the general conclusions of the analyses performed in this study (presented above), and taking into account the observations and conclusions of other researchers' work, the

following guidelines are proposed for the analysis and design of highway bridges to account for the spatial variation of seismic ground motion.

I. For Bridges That Are Less Than Approximately 1,000 to 1,500 ft in Total Length, And Have All Their Supports on the Same Local Soil Conditions:

- For such bridges, we believe that the relatively small increases in the peak response values due to the spatial variability of seismic ground motion can be taken care of by the various safety margins built in current seismic codes.
- It is therefore recommended that such bridges be analyzed and designed using currently available seismic design practices that do not consider the spatial variability of seismic ground motion.

II. For Bridges That Are More Than Approximately 1,000 to 1,500 ft in Total Length, Or Bridges of Any Length That Have Supports on Different Local Soil Conditions:

- For such bridges, we believe that the significant increases in the peak response values due to the spatial variability of seismic ground motion can not be taken care of by the various safety margins built in current seismic codes without compromising the overall safety of the structure.
- It is therefore recommended to perform time history dynamic analyses for design purposes, involving response spectrum compatible asynchronous (differential) support ground motion time histories reflecting the (potentially) different local soil conditions, wave propagation and loss of coherence effects.
- The generation of such asynchronous support ground motion time histories can be performed using the methodology presented in this report or analogous methodologies suggested by other researchers.
- It is recommended to consider a minimum of twenty time history analyses of the bridge to get a reliable estimate of the peak response that will be used for design purposes.
- Dynamic analyses of a bridge using asynchronous support ground motion can be done without undue difficulty today using commercially available finite element codes.

ACKNOWLEDGEMENTS

The authors want to acknowledge the significant contributions of Professor J-M. Kim in the section: "Comparative Analysis of Eight Bridges," of Mr. Sanjay Arwade in the section dealing with the three-dimensional analysis of the SR14/I5 viaduct (based on his senior thesis at Princeton University), and of Ms. W-P. Kwan in the section dealing with the three-dimensional analysis of the typical three-span bridge (based on her senior thesis at Princeton University).

TABLE OF CONTENTS

TABLE OF CONTENTS (continued)

LIST OF ILLUSTRATIONS

LIST OF ILLUSTRATIONS (continued)

LIST OF ILLUSTRATIONS (continued)

LIST OF ILLUSTRATIONS (continued)

LIST OF ILLUSTRATIONS (continued)

LIST OF ILLUSTRATIONS (continued)

LIST OF ILLUSTRATIONS (continued)

LIST OF ILLUSTRATIONS (continued)

LIST OF ILLUSTRATIONS (continued)

LIST OF TABLES

SECTION1
INTRODUCTION

1.1 General Background

The two basic steps in the design of new bridge structures or the analysis of existing ones for strong earthquakes are the proper definition and representation of the seismic excitation and the subsequent computation of the structural response due to this input earthquake ground motion. It is very common in engineering practice today to determine the structural response by performing an equivalent linear static or a linear dynamic analysis of the bridge. For the case of a linear dynamic analysis, it is more common to perform a response spectrum analysis rather than performing a time history analysis. Furthermore, when deciding to perform a time history analysis, it is customary to assume that all of the bridge supports experience identical ground motion time histories, even for multi-span bridges of considerable overall length. It should be pointed out that the assumption of identical support ground motion is implicitly made also when performing an equivalent static or a response spectrum analysis.

Past research studies have demonstrated that seismic ground motion can vary significantly over distances comparable to the length of the majority of highway bridges on multiple supports. As a result, such bridges are subjected to ground motions at their supports that can differ considerably in amplitude, phase, as well as frequency content. These spatially varying seismic ground motions are referred to in the literature as differential or asynchronous support ground motions. In some cases, these differential motions can induce additional internal forces in the structure when compared to the case of identical support ground motion. This in turn might have a potentially detrimental effect on the safety of a bridge during a severe earthquake event. It is therefore of paramount importance to be able to account for the effect of spatial variability of earthquake ground motion on the response of highway bridges.

Spatial variability of seismic ground motion can be mainly attributed to the following three mechanisms: 1) difference in arrival times of seismic waves at different locations, commonly known as the "wave passage effect," 2) loss of coherence of seismic waves due to multiple reflections and refractions as they propagate through the highly inhomogeneous soil medium, referred to as the "incoherence effect," and 3) change in the amplitude and frequency content of seismic ground motion due to different local soil conditions, known as the "local soil effect". The "wave passage effect" is characterized by the apparent velocity of wave propagation, the "incoherence effect" is characterized by the so-called coherence function, while the "local soil effect" is characterized by defining different response (or power) spectra at different locations corresponding to their local soil conditions. The apparent velocity of wave propagation can be estimated from analysis of recorded data and can be considered to be constant or to vary with frequency (although in most cases it is assumed to be constant). The coherence function can be estimated from recorded data or from physical models. In either case it is a decaying function of frequency and separation between observation points.

Spatial variability of seismic ground motion can be treated deterministically or stochastically. In a deterministic approach, a recorded, simulated, or synthesized time history is applied at different structural supports by considering a simple delay in the arrival of the seismic waves according to the distance between supports and the apparent velocity of wave propagation. Such a deterministic approach obviously takes into account only the wave passage effect. In order to consider also the coherence and local soil effects, a stochastic approach has to be followed. In a stochastic approach, ground motion time histories at different locations on the ground surface are modeled as stochastic vector processes with prescribed spectral contents at every location. The spatial variability of ground motion is described by means of the coherence function and the apparent velocity of wave propagation that together define the cross-spectral density characteristics of the vector process.

It is generally acknowledged that it is most challenging to estimate the coherence function when studying the spatial variability of seismic ground motion. In 1978, the issue of estimating this spatial variability was addressed during an international workshop in Hawaii (Iwan 1979), where the deployment of strong ground motion arrays in seismically active regions such as California, Taiwan and Japan was suggested. Following this suggestion, the study of spatial variability of seismic ground motion acquired a new dimension when high-density arrays of accelerometers were installed at several locations all over the world. One of the most important and influential arrays was the SMART-1 array in Lotung, Taiwan, whose recorded data from numerous seismic events have been used to conduct significant research to develop various models to describe the spatial variability of seismic ground motion. Over the years, different analytical expressions have been suggested to model the coherence decay using recorded data from different arrays on different local soil conditions and numerous seismic events in each array. It has to be mentioned, however, that most of these expressions for the coherence function were based on recorded accelerograms at the SMART-1 array.

1.2 Models for the Spatial Variability of Seismic Ground Motion

In one of the early papers dealing with the issue of spatial variability of seismic ground motion, Bolt et al. (1982) studied seismic wave coherency, local magnitude variation across the array, and cross correlation of motions between stations. They found the acceleration waveforms to vary significantly across the array for each event they studied. Loh (1985) developed a mathematical model for the spatial variation of ground displacements using the wave number spectrum and the cross-spectral density function between two spatial locations of the array data. Such a model can be useful for the random vibration analysis of elongated structures subjected to multi-support excitation. Luco and Wong (1986) gave an analytical model for the coherence function developed from the analysis of wave propagation through random media. Harichandran and Vanmarcke (1986) and Harichandran (1991) did a comprehensive analysis of several earthquake events recorded at the SMART-1 array, and formulated a model for the coherence function whose parameters could be determined from the recorded data of specific events (e.g. they provided values for the model parameters based on events 20 and 24). Loh and Yeh (1988) developed a similar model with parameters being determined from events 39 and 40. Hao et al. (1989) suggested another model for the

coherence function with parameters established using recorded data from events 24 and 45. Abrahamson (1985) examined the coherence of specific events recorded at the SMART-1 array. Abrahamson et al. (1991) formulated a spatial coherency model using data from 15 earthquake events recorded at the SMART-1 array and established an expression for the coherence function from a non-linear regression analysis of the data. They found that the results were comparable with the coherencies computed at the EPRI Parkfield array, indicating that these coherence functions might be applicable to other regions. Abrahamson (1993) suggested a model for the coherence function based on recorded data from a number of different seismic arrays located in a variety of soil conditions.

Schneider et al. (1992) compared the coherencies from ten dense seismic arrays situated in different soil conditions and coherencies observed were different in different soil conditions. Essentially all models proposed for the spatial variability of ground motion included the wave passage and incoherence effects, but did not take into account the local soil effect (effect of different local soil conditions). Der Kiureghian (1996) proposed a model for the coherence function using a linear random vibration approach and included for the first time all three different effects of spatial variability: the wave passage effect, the incoherence effect, and the local soil effect.

1.3 Effect of Spatial Variability of Seismic Ground Motion on Structural Response

The study of the effect of spatial variability of seismic ground motion on the response of a structure can generally be performed with two different approaches: (1) using random vibration theory (frequency domain analysis), and (2) using a Monte Carlo simulation approach (time domain analysis). The random vibration approach is generally computationally more efficient but it assumes stationary input excitation and linear structural response. On the other hand, the Monte Carlo simulation approach though computationally less efficient, does not operate on the strict assumptions of stationarity and linearity.

Many researchers have investigated the response of long span structures to differential (asynchronous) support excitations. Most of them have used relatively simple models to describe the structure (e.g. simple or continuous beams). Most of the early studies were essentially deterministic and focussed only on the wave passage effect on the response of structures (e.g. Masri 1976, Scanlan 1976, Werner and Lee 1979, Werner et. al. 1979). In these papers comparisons were made with the case of identical support ground motions (a norm in engineering practice) in order to evaluate the significance of the wave passage effect on the structural response. Abdel-Ghaffar (1982) examined the earthquake induced vertical response of suspension bridges subjected to correlated or uncorrelated multi-support excitation. Existing ground displacements recorded at locations within distances similar to the span of the suspension bridge were used to establish the cross-spectral density function of the input ground motion. These bridges were analyzed in the frequency domain using a random vibration approach. It was shown that the earthquake response associated with correlated multiple support excitation was significantly different (the cable tension was lower in this case) from the uncorrelated case.

Zerva et al. (1986) provided an empirical expression for differential ground motions. This empirical expression was obtained through least-square error minimization of the results of an analytical stochastic model developed earlier by the authors. Differential ground motions obtained using this empirical expression, as well as the analytical model developed earlier, were used as input motions in the evaluation of the dynamic response of a two-degree-of-freedom model for a pipeline. The analysis indicated that the empirical expression described the effect of differential ground motion on the response of the pipeline with adequate accuracy. In this paper the authors have also introduced the concept of the differential response spectrum for design purposes. The results of the analysis performed demonstrated that the assumption of perfectly correlated motion at the supports is inadequate for the analysis and design of pipelines. Zerva (1988) used simply supported and continuous beams to model extended structures. It was concluded that the effect of differential support ground motion was not significant for single span simply supported bridges and that the identical support ground motion assumption was a valid approximation for such bridges. However, for continuous pipelines on multiple supports, partially correlated motions yielded higher stresses than perfectly correlated motions.

Harichandran et al. (1988) considered both the effects of wave passage and incoherence in their model to estimate the response of a single span beam using a random vibration approach. They concluded that by considering only the wave passage effect, the beam response is underestimated, and that the assumption of identical support ground motion was overly conservative for the case of a single span beam. In a later paper, Harichandran and Wang (1990) analyzed a two-span continuous beam modeled using finite elements. The response was again computed using a linear random vibration approach, and the relative significance of the incoherence and wave propagation effects was examined for various span lengths. The results were compared to the case with identical support ground motion and to the case where only the wave passage effect was considered. It was found that when these effects were considered, the estimate of the structural response could become overly conservative for some beam configurations and unconservative for others. They concluded that it is very important to consider both the wave passage and incoherence effects, when estimating the response of multiple supported structures. Another observation was that for cases where the apparent velocity of wave propagation is large, the incoherence effect becomes more important than the wave passage effect. Finally, they concluded that the identical support ground motion assumption yields inaccurate results for such structures. Harichandran and Wang (1990) investigated also multiple-span continuous beams and observed a similar behavior.

Abdel-Ghaffar (1991) studied the effect of spatial variation of ground motion on cable stayed bridges. A non-linear time history analysis using a three-dimensional model of the bridge was performed. Existing strong motion records were used as representative input ground motions. The nonlinearity was due to changes in the geometry of the bridge due to large deformations including changes in the geometry of the cables. A tangent stiffness iterative procedure was used to capture the non-linear response. The results indicated that differential support ground motion tends to considerably alter the

structural response when compared to the case of identical support ground motion. In some cases, it increased the response while in other cases it decreased the response. Lower values for the apparent velocity of wave propagation generally tend to produce higher values for the response quantities, and a non-linear analysis seems to be inevitable for such long span structures with complex geometry. In a later paper, Abdel-Ghaffar (1992) examined the response of several existing cable-stayed bridges. It was found that the structural response increased substantially when using differential support ground motion, especially for more rigid bridges and bridges with supports on different local soil conditions. The increase of the structural response was found to be dependent on the specific bridge configuration (e.g. span length rigidity, structural redundancy etc.)

Zerva (1991) examined the relative effects of wave passage and incoherence for lifelines modeled as two and three-span continuous beams. The author concluded that the loss of coherence effect overshadows the wave passage effect (for realistic values of the apparent velocity of wave propagation), and in fact the wave propagation effect may be neglected at sites where ground motion is expected to be incoherent. But as seismic ground motion becomes more coherent, the wave passage effect may produce higher or lower response than the one induced by identical support ground motions. For low values of the apparent velocity of wave propagation, the contribution to the overall response from the quasi-static term is higher than that of the dynamic term. As the velocity of wave propagation increases, the contribution of the quasi-static term drops and that of the dynamic term increases. However, if the frequency of the first mode of the structure is much higher than the dominant frequencies of the input motion, then the total response may not increase that much when compared to the case of identical support ground motion. Zerva (1992) did a study to analyze the relative contribution of the incoherence and wave passage effects to seismic strains in near source regions. The ground motions were generated using the spectral representation method and considering different models for the coherence function available in the literature. It was shown that the wave propagation assumption for analysis and design of buried pipelines underestimates their response in near source regions, and there exists a critical apparent velocity of wave propagation for the seismic ground motions. For apparent velocities of wave propagation higher than the critical value, seismic strains (response) are essentially constant and controlled by the incoherence of ground motions. For apparent velocities of wave propagation lower than the critical value, the strains gradually increase and eventually become inversely proportional to the propagation velocity.

Harichandran et. al. (1996) studied the effect of spatial variability of ground motion on existing long span suspension and arch bridges. They studied stationary and transient linear stochastic response with ground motions generated using the Harichandran and Vanmarcke model for the coherence function (1986). These bridges were analyzed using two-dimensional finite element models. They concluded that the assumption of identical support ground motion is unacceptable as it underestimates the response in some cases and it overestimates it in others. The consideration of only the wave passage effect can significantly underestimate the response when analyzing bridges with long center spans, and therefore the incoherence effect should always be included.

Zerva (1994) analyzed the effect of spatial variability of seismic ground motion on the response of lifelines. Two commonly utilized models for the coherence function (Harichandran and Vanmarcke, and Luco and Wang) were compared to determine their relative effects on the structural response. The structural response was estimated using the concept of the differential response spectrum (Zerva 1992). The results suggest that models for the coherence function with partial correlation at low frequencies and with slow exponential decay as frequency and separation distance increase will produce significantly high response in lifelines. It was shown that considering the wave passage effect alone will underestimate the response, and that at high values of the apparent velocity of wave propagation the incoherence effect overshadows the wave passage effect. One of the most important effects of spatial incoherence on the response is the introduction of high quasi-static internal forces in the structure with the simultaneous reduction in the dynamic forces. The highest dynamic response is induced by identical support ground motion.

Der Kiureghian et al. (1997) used the multi support response spectrum (MSRS) method to analyze bridge response under spatially varying ground motion. They used the coherency model that Der Kiureghian (1996) has developed that includes the incoherence, wave passage and local soil effects. Using the MSRS method, the expected maximum of a generic response quantity is calculated with input support ground motions specified through a set of displacement response spectra for each of the support degrees of freedom, and a set of coherence functions for every pair of support degrees of freedom. The authors concluded that depending on local soil conditions, span lengths of more than 50 ft. may require differential support ground motion analysis. Such analysis may be required for even shorter spans if their supports are located on sites with significantly different local soil conditions. Extensive parametric studies were performed on two example bridge structures. The results of the analyses of these two bridges indicated that:

1. The spatial variability of seismic ground motion can amplify or de-amplify the bridge response by as much as a factor of two or possibly more.
2. For a multi-span bridge with 240-ft. spans, the wave passage effect has the dominant influence with the local soil effect a close second, while for a multi-span bridge with 120-ft. spans, the local soil effect has the dominant influence.
3. The currently practiced method of using the envelope response spectra uniformly at all supports of a multi-span bridge is inaccurate and potentially unconservative.

In order to check the accuracy of the MSRS method, the results were compared by performing Monte Carlo simulations. However the MSRS method is based on the fundamentals of stationary random vibration theory while actual ground motions are non stationary in nature. It is further limited to linear structures whereas the bridge response under peak ground acceleration that can cause damage to the structure is nonlinear.

Monti et al. (1996) examined the inelastic response of multi-span bridges using a Monte Carlo simulation approach and the spectral representation method (Shinozuka and

Deodatis 1991) to generate the spatially varying ground motion time histories. They did a parametric analysis of three bridge models with varying stiffnesses using both differential and identical support ground motion excitations for comparison purposes. The Luco and Wang model (1986) for the coherence function was selected. The authors have considered the incoherence and wave passage effects, but did not include the local soil effect (different soil conditions at different supports). The ground motion time histories were generated according to Kanai-Tajimi power spectral density functions for accelerations. The nonlinear model of the bridge consisted of a Takeda-type plastic zone at the base of the piers. All structural supports were assumed to be on the same type of local soil conditions, and the wave passage and incoherence effects were made to vary between their respective extremes. Three bridge models were selected and the relative importance of the two spatial variability effects was evaluated by considering a variety of cases. In almost all cases, a certain amount of incoherence acts toward reducing the ductility demand for the central piers and increasing it for the piers close to the two ends of the bridge, compared to the case of identical support ground motion. Another observation was that the structural response to differential support ground motion is not significantly influenced by the wave passage effect when high levels of incoherence are present.

1.4 Some Observations from Past Research Work

Studying the results from past work of other researchers (presented briefly in section 1.3), it becomes very difficult to draw general conclusions concerning the effect of spatial variability of seismic ground motion on the response of elongated structures on multiple supports. First, it is quite difficult to make comparisons among the results of the different studies presented in section 1.3, as different researchers use different structures, different ways to model their structures, different models for the spatial variability of seismic ground motion, different approaches to analyze the structures and different quantities to measure the response of a structure. Therefore some of the conclusions reached by different researchers might seem contradictory because of differences in the case studies that they have considered. There isn't even agreement about whether the assumption of spatial variability of seismic ground motion is beneficial or detrimental to the structural response (compared to the case of identical support ground motion). The only common conclusion that can be deduced is that the effect of spatial variability of ground motion on the response of the structure is very complex and depends on various parameters describing the structure and the characteristics of earthquake ground motion.

SECTION 2
GENERATION OF SPATIALLY VARYING SEISMIC GROUND MOTION TIME HISTORIES

In this chapter, a methodology is proposed to generate earthquake ground motion time histories at several specified locations on the ground surface, according to user-supplied response (or power) spectra. It should be mentioned that different locations can correspond to different local soil conditions, and consequently different response (or power) spectra can be assigned to each location. This makes possible the analysis of bridges with supports on different local soil conditions. In addition, a duration of strong ground motion can be specified through a modulating (envelope) function, and the generated time histories will reflect a prescribed apparent velocity of wave propagation and a specified loss of coherence law through a complex coherence function.

At this point, the following important note has to be made concerning the case of differential (asynchronous) support ground motion when the bridge supports are on different local soil conditions. As mentioned earlier, the way to approach such a case is by assigning different response (or power) spectra to the various bridge supports according to the corresponding local soil conditions. Such an approach makes necessary the use of a coherence function between bridge supports on different local soil conditions that would account for this change in local soil conditions. Unfortunately, such a coherence function is not currently available, as every model for the coherence in the literature has been established for uniform (homogeneous) soil conditions. Consequently, throughout this report, coherence functions for uniform (homogeneous) soil conditions are used for the cases involving different local soil conditions. Although this is definitely an approximation, it has been determined to be a reasonable one, as in such cases the effect from the difference in amplitude and frequency content is the dominant one (compared to loss of coherence and wave passage). A similar argument can be made for the apparent velocity of wave propagation (although in this case it is possible to assign equivalent "average" velocities between points).

The methodology is now described by considering that the acceleration time histories at a specified number of locations on the ground surface constitute a multi-variate, non-stationary, stochastic process (non-stationary stochastic vector process). The remaining part of this chapter is reprinted from *Probabilistic Engineering Mechanics*, Vol. 11, No. 3, Deodatis, G., "Non-Stationary Stochastic Vector Processes: Seismic Ground Motion Applications," pp. 149-167, Copyright (1996), with permission from Elsevier Science Ltd.

2.1 Introduction

One of the most important parts of the Monte Carlo simulation methodology is the generation of sample functions of the stochastic processes, fields or waves involved in the problem. The generated sample functions must accurately describe the probabilistic characteristics of the corresponding stochastic processes, fields or waves that may be either stationary or non-stationary, homogeneous or non-homogeneous, one-dimensional or multi-dimensional, uni-variate or multi-variate, Gaussian or non-Gaussian. Among the various methods that

have been developed to generate such sample functions (for a review of these methods, the reader is referred to Elishakoff 1983, Kozin 1988, Soong and Grigoriu 1993, Grigoriu 1995, and Deodatis 1996a), the spectral representation method is one of the most widely used today. Although the concept of the method existed for some time (Rice 1954), it was Shinozuka (Shinozuka and Jan 1972, Shinozuka 1972) who first applied it for simulation purposes including multi-dimensional, multi-variate and non-stationary cases. Yang (1972, 1973) showed that the Fast Fourier Transform (FFT) technique can be used to dramatically improve the computational efficiency of the spectral representation algorithm, and proposed a formula to simulate random envelope processes. Shinozuka (1974) extended the application of the FFT technique to multi-dimensional cases. Recently, Deodatis and Shinozuka (1989) further extended the spectral representation method to simulate stochastic waves, Yamazaki and Shinozuka (1988) developed an iterative procedure to simulate non-Gaussian stochastic fields, and Grigoriu (1993) compared two different spectral representation models. Four recent review papers on the subject of simulation using the spectral representation method were written by Shinozuka (1987) and Shinozuka and Deodatis (1988, 1991, 1996).

A spectral-representation-based algorithm (Shinozuka and Jan 1972, Shinozuka 1987, Shinozuka and Deodatis 1988, Li and Kareem 1991) is used in this chapter to simulate non-stationary stochastic vector processes with evolutionary power. If the components of the vector process correspond to different locations in space (as in the seismic ground motion examples provided later in this chapter), then the process can also be non-homogeneous in space (in addition to being non-stationary in time). The simulation algorithm is simple and straightforward and generates sample functions of the vector process according to a prescribed non-stationary cross-spectral density matrix.

For the important application of earthquake ground motion simulation which is the main objective of this report, acceleration, velocity, or displacement time histories can be generated at several locations on the ground surface according to a target cross-spectral density matrix. The only drawback in this approach is that it is often preferable to work with time histories that are compatible with prescribed response spectra, rather than with prescribed power spectral density functions (cross-spectral density matrix). In order to address this issue, an iterative scheme is proposed in this chapter, based on the suggested simulation algorithm, to generate seismic ground motion time histories at several points on the ground surface that are compatible with prescribed response spectra, are correlated according to a given coherence function, include the wave propagation effect, and have a specified duration of strong ground motion.

Finally, from the rich bibliography related to the various methods currently available to generate sample functions of stochastic processes, fields and waves, the following representative publications dealing with simulation of multi-variate stochastic processes are mentioned here: Shinozuka and Jan 1972 (simulation of multi-variate processes by spectral representation), Gersch and Yonemoto 1977 (multi-variate ARMA model), Mignolet and Spanos 1987a, 1987b (stability and invertibility aspects of AR to ARMA procedures for multi-variate random processes), Li and Kareem 1991 (simulation of non-stationary vector processes using an FFT-based approach), Li and Kareem 1993 (simulation of multi-

variate processes using a hybrid discrete Fourier transform and digital filtering approach), Ramadan and Novak 1993 (asymptotic and approximate spectral techniques to simulate multi-dimensional and multi-variate processes and fields), and Deodatis 1996b (simulation of ergodic multi-variate stochastic processes). From this list, the Li and Kareem 1991 and Ramadan and Novak 1993 papers considered non-stationary vector processes. At this juncture it should be mentioned that a very promising development with potential applications to simulation of non-stationary multi-variate stochastic processes is the use of wavelets (e.g. Gurley and Kareem 1995, and Spanos and Zeldin 1995).

In the following, the theory, the simulation algorithm, and the iterative scheme are presented for tri-variate non-stationary stochastic vector processes (dimension of vector process is three). This is done for the sake of simplicity in the notation. The simulation algorithm and the iterative scheme can be extended in a straightforward fashion to any other dimension of the vector process.

2.2 Tri-Variate Non-Stationary Stochastic Processes

Consider a 1D-3V (one-dimensional, tri-variate) non-stationary stochastic vector process with components $f_1^0(t)$, $f_2^0(t)$ and $f_3^0(t)$, having mean value equal to zero:

$$\mathcal{E}[f_j^0(t)] = 0 \quad ; \quad j = 1,2,3 \tag{2-1}$$

cross-correlation matrix given by:

$$\mathbf{R}^0(t,t+\tau) = \begin{bmatrix} R_{11}^0(t,t+\tau) & R_{12}^0(t,t+\tau) & R_{13}^0(t,t+\tau) \\ R_{21}^0(t,t+\tau) & R_{22}^0(t,t+\tau) & R_{23}^0(t,t+\tau) \\ R_{31}^0(t,t+\tau) & R_{32}^0(t,t+\tau) & R_{33}^0(t,t+\tau) \end{bmatrix} \tag{2-2}$$

and cross-spectral density matrix given by:

$$\mathbf{S}^0(\omega,t) = \begin{bmatrix} S_{11}^0(\omega,t) & S_{12}^0(\omega,t) & S_{13}^0(\omega,t) \\ S_{21}^0(\omega,t) & S_{22}^0(\omega,t) & S_{23}^0(\omega,t) \\ S_{31}^0(\omega,t) & S_{32}^0(\omega,t) & S_{33}^0(\omega,t) \end{bmatrix} \tag{2-3}$$

Note that because of the non-stationarity of the vector process, the cross-correlation matrix is a function of two time instants: t and $t+\tau$ (t = time and τ = time lag), while the cross-spectral density matrix is a function of both frequency ω and time t.

Adopting the theory of evolutionary power spectra for non-stationary stochastic processes (Priestley 1965 and 1988), the elements of the cross-spectral density matrix are defined as:

$$S_{jj}^0(\omega,t) = |A_j(\omega,t)|^2 \; S_j(\omega) \quad ; \quad j = 1,2,3 \tag{2-4}$$

$$S_{jk}^0(\omega,t) = A_j(\omega,t)A_k(\omega,t) \; \sqrt{S_j(\omega)S_k(\omega)} \; \Gamma_{jk}(\omega) \quad ; \quad j,k = 1,2,3 \; ; \; j \neq k \tag{2-5}$$

where $A_j(\omega,t)$; $j=1,2,3$ are the modulating functions of $f_1^0(t)$, $f_2^0(t)$ and $f_3^0(t)$, respectively, $S_j(\omega)$; $j=1,2,3$ are the (stationary) power spectral density functions of $f_1^0(t)$, $f_2^0(t)$ and $f_3^0(t)$, respectively, and $\Gamma_{jk}(\omega)$; $j,k=1,2,3$; $j\neq k$ are the complex coherence functions between $f_j^0(t)$ and $f_k^0(t)$.

It should be pointed out that Eqs. (2-4) and (2-5) imply that the modulating function $A_j(\omega,t)$ represents the change in the evolutionary power spectrum, relative to the (stationary) power spectral density function $S_j(\omega)$.

Consequently, for any time instant t, the diagonal elements of the cross-spectral density matrix are real and non-negative functions of ω satisfying:

$$S_{jj}^0(\omega,t)=S_{jj}^0(-\omega,t) \quad ; \quad j=1,2,3 \quad \text{and for every } t \tag{2-6}$$

while the off-diagonal elements are generally complex functions of ω satisfying:

$$S_{jk}^0(\omega,t)=S_{jk}^{0*}(-\omega,t) \quad ; \quad j,k=1,2,3\ ;\ j\neq k \quad \text{and for every } t \tag{2-7}$$

$$S_{jk}^0(\omega,t)=S_{kj}^{0*}(\omega,t) \quad ; \quad j,k=1,2,3\ ;\ j\neq k \quad \text{and for every } t \tag{2-8}$$

where the asterisk denotes the complex conjugate. Equation (2-8) indicates that the cross-spectral density matrix $\mathbf{S}^0(\omega,t)$ is Hermitian for any value of t.

The elements of the cross-correlation matrix are related to the corresponding elements of the cross-spectral density matrix through
the following transformations:

$$R_{jj}^0(t,t+\tau)=\int_{-\infty}^{\infty} A_j(\omega,t)A_j(\omega,t+\tau)\ e^{i\omega\tau}\ S_j(\omega)\ d\omega \quad ; \quad j=1,2,3 \tag{2-9}$$

$$R_{jk}^0(t,t+\tau)=\int_{-\infty}^{\infty} A_j(\omega,t)A_k(\omega,t+\tau)\ e^{i\omega\tau}\ \sqrt{S_j(\omega)S_k(\omega)}\ \Gamma_{jk}(\omega)\ d\omega \quad ; \quad j,k=1,2,3\ ;\ j\neq k \tag{2-10}$$

2.2.1 Special Case: Uniformly Modulated Non-Stationary Stochastic Vector Process

For the special case of a uniformly modulated non-stationary stochastic vector process, the modulating functions $A_j(\omega,t)$; $j=1,2,3$ are independent of the frequency ω:

$$A_j(\omega,t)=A_j(t) \quad ; \quad j=1,2,3 \tag{2-11}$$

and Eqs. (2-9) and (2-10) reduce to:

$$R_{jj}^0(t,t+\tau)=A_j(t)A_j(t+\tau)\int_{-\infty}^{\infty} S_j(\omega)\ e^{i\omega\tau}\ d\omega \quad ; \quad j=1,2,3 \tag{2-12}$$

$$R^0_{jk}(t,t+\tau) = A_j(t)A_k(t+\tau)\int_{-\infty}^{\infty}\sqrt{S_j(\omega)S_k(\omega)}\;\Gamma_{jk}(\omega)\;\mathrm{e}^{i\omega\tau}\;d\omega \quad ; \quad j,k=1,2,3\;;\; j\neq k \qquad (2-13)$$

In such a case, the three components of the non-stationary stochastic vector process are expressed as:

$$f^0_j(t) = A_j(t)\;g^0_j(t) \quad ; \quad j=1,2,3 \qquad (2-14)$$

where $g^0_j(t);\ j=1,2,3$ are the three components of a stationary stochastic vector process, having mean value equal to zero:

$$\mathcal{E}[g^0_j(t)] = 0 \quad ; \quad j=1,2,3 \qquad (2-15)$$

and cross-spectral density matrix given by:

$$\mathbf{S}^0(\omega) = \begin{bmatrix} S_1(\omega) & \sqrt{S_1(\omega)S_2(\omega)}\Gamma_{12}(\omega) & \sqrt{S_1(\omega)S_3(\omega)}\Gamma_{13}(\omega) \\ \sqrt{S_2(\omega)S_1(\omega)}\Gamma_{21}(\omega) & S_2(\omega) & \sqrt{S_2(\omega)S_3(\omega)}\Gamma_{23}(\omega) \\ \sqrt{S_3(\omega)S_1(\omega)}\Gamma_{31}(\omega) & \sqrt{S_3(\omega)S_2(\omega)}\Gamma_{32}(\omega) & S_3(\omega) \end{bmatrix} \qquad (2-16)$$

Note that the elements of matrix $\mathbf{S}^0(\omega)$ shown in Eq. (2-16) consist of terms that have been defined in Eqs. (2-4) and (2-5).

2.3 Simulation Formula

In the following, distinction will be made between the non-stationary stochastic vector process $f^0_j(t);\ j=1,2,3$ and its simulation $f_j(t);\ j=1,2,3$.

In order to simulate the 1D-3V non-stationary stochastic process $f^0_j(t);\ j=1,2,3$, its cross-spectral density matrix $\mathbf{S}^0(\omega,t)$ must be decomposed at every time instant t under consideration, into the following product:

$$\mathbf{S}^0(\omega,t) = \mathbf{H}(\omega,t)\;\mathbf{H}^{T*}(\omega,t) \qquad \text{for every } t \text{ under consideration} \qquad (2-17)$$

where superscript ^{T} denotes the transpose of a matrix. This decomposition can be performed using Cholesky's method, in which case $\mathbf{H}(\omega,t)$ is a lower triangular matrix:

$$\mathbf{H}(\omega,t) = \begin{bmatrix} H_{11}(\omega,t) & 0 & 0 \\ H_{21}(\omega,t) & H_{22}(\omega,t) & 0 \\ H_{31}(\omega,t) & H_{32}(\omega,t) & H_{33}(\omega,t) \end{bmatrix} \qquad (2-18)$$

whose diagonal elements are real and non-negative functions of ω and whose off-diagonal elements are generally complex functions of ω.

The following relation is satisfied by the diagonal elements of $\mathbf{H}(\omega,t)$:

$$H_{jj}(\omega,t) = H_{jj}(-\omega,t) \quad ; \quad j=1,2,3 \quad \text{and for every } t \qquad (2-19)$$

If the off-diagonal elements $H_{jk}(\omega,t)$ are written in polar form as:

$$H_{jk}(\omega,t) = |H_{jk}(\omega,t)|\, e^{i\theta_{jk}(\omega,t)} \quad ; \quad j=2,3;\ k=1,2;\ j>k \qquad (2-20)$$

where:

$$\theta_{jk}(\omega,t) = \tan^{-1}\left(\frac{\mathrm{Im}[H_{jk}(\omega,t)]}{\mathrm{Re}[H_{jk}(\omega,t)]}\right) \qquad (2-21)$$

with Im and Re denoting the imaginary and the real part of a complex number, respectively, then the following relations are satisfied:

$$|H_{jk}(\omega,t)| = |H_{jk}(-\omega,t)| \quad ; \quad j=2,3;\ k=1,2;\ j>k \quad \text{and for every } t \qquad (2-22)$$

$$\theta_{jk}(\omega,t) = -\theta_{jk}(-\omega,t) \quad ; \quad j=2,3;\ k=1,2;\ j>k \quad \text{and for every } t \qquad (2-23)$$

Once matrix $\mathbf{S}^0(\omega,t)$ is decomposed according to Eqs. (2-17)-(2-18), the non-stationary stochastic vector process $f_j^0(t)$; $j=1,2,3$ can be simulated by the following series as $N\to\infty$

$$f_j(t) = 2\sum_{m=1}^{3}\sum_{l=1}^{N} |H_{jm}(\omega_l,t)|\sqrt{\Delta\omega}\,\cos[\omega_l\, t - \theta_{jm}(\omega_l,t) + \Phi_{ml}] \quad ; \quad j=1,2,3 \qquad (2-24)$$

or explicitly

$$f_1(t) = 2\sum_{l=1}^{N} |H_{11}(\omega_l,t)|\sqrt{\Delta\omega}\,\cos[\omega_l\, t - \theta_{11}(\omega_l,t) + \Phi_{1l}] \qquad (2-25a)$$

$$\begin{aligned} f_2(t) =& 2\sum_{l=1}^{N} |H_{21}(\omega_l,t)|\sqrt{\Delta\omega}\,\cos[\omega_l\, t - \theta_{21}(\omega_l,t) + \Phi_{1l}] + \\ &+2\sum_{l=1}^{N} |H_{22}(\omega_l,t)|\sqrt{\Delta\omega}\,\cos[\omega_l\, t - \theta_{22}(\omega_l,t) + \Phi_{2l}] \end{aligned} \qquad (2-25b)$$

$$\begin{aligned} f_3(t) =& 2\sum_{l=1}^{N} |H_{31}(\omega_l,t)|\sqrt{\Delta\omega}\,\cos[\omega_l\, t - \theta_{31}(\omega_l,t) + \Phi_{1l}] + \\ &+2\sum_{l=1}^{N} |H_{32}(\omega_l,t)|\sqrt{\Delta\omega}\,\cos[\omega_l\, t - \theta_{32}(\omega_l,t) + \Phi_{2l}] + \\ &+2\sum_{l=1}^{N} |H_{33}(\omega_l,t)|\sqrt{\Delta\omega}\,\cos[\omega_l\, t - \theta_{33}(\omega_l,t) + \Phi_{3l}] \end{aligned} \qquad (2-25c)$$

where:

$$\omega_l = l\Delta\omega \quad ; \quad l = 1, 2, \ldots, N \tag{2-26}$$

$$\Delta\omega = \frac{\omega_u}{N} \tag{2-27}$$

$$\theta_{jm}(\omega_l, t) = \tan^{-1}\left(\frac{\mathrm{Im}[H_{jm}(\omega_l, t)]}{\mathrm{Re}[H_{jm}(\omega_l, t)]}\right) \tag{2-28}$$

In Eq. (2-27), ω_u represents an upper cut-off frequency beyond which the elements of the cross-spectral density matrix [Eq. (2-3)] may be assumed to be zero for any time instant t. As such, ω_u is a fixed value and hence $\Delta\omega \to 0$ as $N \to \infty$ so that $N\Delta\omega = \omega_u$. A criterion to estimate the value of ω_u can be found in Shinozuka and Deodatis (1991).

The Φ_{1l}, Φ_{2l}, Φ_{3l}; $l = 1, 2, \ldots, N$ appearing in Eqs. (2-24)-(2-25) are three sequences of independent random phase angles distributed uniformly over the interval $[0, 2\pi]$.

It should be noted that the simulated non-stationary stochastic vector process $f_j(t)$; $j = 1, 2, 3$ is asymptotically Gaussian as $N \to \infty$ because of the central limit theorem (Shinozuka and Deodatis 1991).

A sample function $f_j^{(i)}(t)$; $j = 1, 2, 3$ of the simulated non-stationary stochastic vector process $f_j(t)$; $j = 1, 2, 3$ can be obtained by replacing the three sequences of random phase angles Φ_{1l}, Φ_{2l}, Φ_{3l}; $l = 1, 2, \ldots, N$ with their respective i-th realizations $\phi_{1l}^{(i)}$, $\phi_{2l}^{(i)}$, $\phi_{3l}^{(i)}$; $l = 1, 2, \ldots, N$:

$$f_j^{(i)}(t) = 2\sum_{m=1}^{3}\sum_{l=1}^{N} |H_{jm}(\omega_l, t)|\sqrt{\Delta\omega}\,\cos[\omega_l\, t - \theta_{jm}(\omega_l, t) + \phi_{ml}^{(i)}] \quad ; \quad j = 1, 2, 3 \tag{2-29}$$

The generated values of $f_j^{(i)}(t)$ according to Eq. (2-29) are bounded as follows:

$$f_j^{(i)}(t) \leq 2\sum_{m=1}^{3}\sum_{l=1}^{N} |H_{jm}(\omega_l, t)|\sqrt{\Delta\omega} \quad ; \quad j = 1, 2, 3 \tag{2-30}$$

For a given form of the cross-spectral density matrix, the above bound is large enough for all practical applications, even for relatively small values of N (Deodatis 1996b). It is obvious that this bound can be easily calculated for any form of the cross-spectral density matrix to be used.

It will be shown now that the ensemble expected value $\mathcal{E}[f_j(t)]$; $j = 1, 2, 3$ and the ensemble auto-/cross-correlation function $R_{jk}(t, t+\tau)$; $j, k = 1, 2, 3$ of the simulated non-stationary stochastic vector process $f_j(t)$ are identical to the corresponding targets, $\mathcal{E}[f_j^0(t)] = 0$; $j = 1, 2, 3$ and $R_{jk}^0(t, t+\tau)$; $j, k = 1, 2, 3$, respectively.

(1) Show that: $\mathcal{E}[f_j(t)] = \mathcal{E}[f_j^0(t)] = 0$; $j = 1, 2, 3$

Proof:

This proof is trivial and similar to the corresponding one for 1D-1V processes (Shinozuka and Deodatis 1991).

(2) Show that: $R_{jk}(t,t+\tau) = R^0_{jk}(t,t+\tau);\ j,k = 1,2,3$

Proof:

Utilizing the property that the operations of mathematical expectation and summation are commutative, the ensemble auto-/cross-correlation function of the simulated non-stationary stochastic vector process $f_j(t);\ j = 1,2,3$ can be written as:

$$
\begin{aligned}
&R_{jk}(t,t+\tau) = \mathcal{E}[f_j(t) f_k(t+\tau)] = \\
&= 4 \sum_{m_1=1}^{3} \sum_{m_2=1}^{3} \sum_{l_1=1}^{N} \sum_{l_2=1}^{N} |H_{jm_1}(\omega_{l_1},t)|\ |H_{km_2}(\omega_{l_2},t+\tau)|\ \Delta\omega \\
&\quad \cdot \mathcal{E}\Big\{ \cos\left[\omega_{l_1}\ t - \theta_{jm_1}(\omega_{l_1},t) + \Phi_{m_1 l_1}\right] \cos\left[\omega_{l_2}(t+\tau) - \theta_{km_2}(\omega_{l_2},t+\tau) + \Phi_{m_2 l_2}\right] \Big\} = \\
&= 2 \sum_{m_1=1}^{3} \sum_{m_2=1}^{3} \sum_{l_1=1}^{N} \sum_{l_2=1}^{N} |H_{jm_1}(\omega_{l_1},t)|\ |H_{km_2}(\omega_{l_2},t+\tau)|\ \Delta\omega \\
&\quad \cdot \mathcal{E}\Big\{ \cos\left[(\omega_{l_1}+\omega_{l_2})t + \omega_{l_2}\ \tau - \theta_{jm_1}(\omega_{l_1},t) - \theta_{km_2}(\omega_{l_2},t+\tau) + \Phi_{m_1 l_1} + \Phi_{m_2 l_2}\right] + \\
&\quad + \cos\left[(\omega_{l_2}-\omega_{l_1})t + \omega_{l_2}\ \tau + \theta_{jm_1}(\omega_{l_1},t) - \theta_{km_2}(\omega_{l_2},t+\tau) - \Phi_{m_1 l_1} + \Phi_{m_2 l_2}\right] \Big\}
\end{aligned}
\qquad (2-31)
$$

Since the Φ's are independent random variables distributed uniformly over the interval $[0, 2\pi]$, the expected value appearing in Eq. (2-31) is different from zero only when:

$$
m_1 = m_2 = m \qquad \text{and} \qquad l_1 = l_2 = l \qquad (2-32)
$$

Under the conditions of Eq. (2-32), Eq. (2-31) can be written as:

$$
\begin{aligned}
R_{jk}(t,t+\tau) = 2 \sum_{m=1}^{3} \sum_{l=1}^{N} &|H_{jm}(\omega_l,t)|\ |H_{km}(\omega_l,t+\tau)|\ \Delta\omega \\
&\cdot \cos\left[\omega_l\ \tau + \theta_{jm}(\omega_l,t) - \theta_{km}(\omega_l,t+\tau)\right]
\end{aligned}
\qquad (2-33)
$$

Taking into account Eqs. (2-19), (2-22) and (2-23), the expression for $R_{jk}(t,t+\tau)$ in Eq. (2-33) can be written in the limit as $\Delta\omega \to 0$ and $N \to \infty$ (while keeping in mind that $\omega_u = N\Delta\omega$ is constant and that the elements of the cross-spectral density matrix $\mathbf{S}^0(\omega,t)$ are zero for $|\omega| \geq \omega_u$ at any time instant t) in the following way:

$$
R_{jk}(t,t+\tau) = \int_{-\infty}^{\infty} \sum_{m=1}^{3} |H_{jm}(\omega,t)|\ |H_{km}(\omega,t+\tau)|\ \mathrm{e}^{i[\omega\tau + \theta_{jm}(\omega,t) - \theta_{km}(\omega,t+\tau)]}\ d\omega \qquad (2-34)
$$

Using now the polar form representation of the elements of the $\mathbf{H}(\omega, t)$ matrix [Eq. (2-20)], Eq. (2-34) is written as:

$$R_{jk}(t, t+\tau) = \int_{-\infty}^{\infty} \sum_{m=1}^{3} H_{jm}(\omega, t)\, H_{km}^{*}(\omega, t+\tau)\, \mathrm{e}^{i\omega\tau}\, d\omega \qquad (2-35)$$

Then, using the decomposition shown in Eq. (2-17) in conjunction with Eqs. (2-4) and (2-5), it is straightforward to show that:

$$R_{jj}(t, t+\tau) = \int_{-\infty}^{\infty} A_j(\omega, t) A_j(\omega, t+\tau)\, S_j(\omega)\, \mathrm{e}^{i\omega\tau}\, d\omega \quad ; \quad j = 1, 2, 3 \qquad (2-36)$$

$$R_{jk}(t, t+\tau) = \int_{-\infty}^{\infty} A_j(\omega, t) A_k(\omega, t+\tau)\, \sqrt{S_j(\omega) S_k(\omega)}\, \Gamma_{jk}(\omega)\, \mathrm{e}^{i\omega\tau}\, d\omega \quad ; \quad j, k = 1, 2, 3 \; ; \; j \neq k \qquad (2-37)$$

Comparing finally Eqs. (2-9) and (2-10) to Eqs. (2-36) and (2-37), it is evident that:

$$R_{jk}(t, t+\tau) = R_{jk}^{0}(t, t+\tau) \quad ; \quad j, k = 1, 2, 3 \qquad (2-38)$$

2.3.1 Special Case: Uniformly Modulated Non-Stationary Stochastic Vector Process

For the special case of a uniformly modulated non-stationary stochastic vector process, simulation can be performed on the basis of Eq. (2-14), instead of using Eq. (2-24). The simulation formula corresponding to Eq. (2-14) is:

$$f_j(t) = A_j(t)\, g_j(t) \quad ; \quad j = 1, 2, 3 \qquad (2-39)$$

where $g_j(t)$ is the simulation of the stationary stochastic vector process $g_j^0(t)$ having mean value equal to zero and cross-spectral density matrix shown in Eq. (2-16). It should be mentioned that the simulation of stationary and ergodic stochastic vector processes can be performed with great computational efficiency using the Fast Fourier Transform (FFT) technique, as described by Deodatis (1996b).

2.3.2 Comments on Computational Efficiency

At this juncture, it should be pointed out that it is not possible to take advantage of the FFT technique when using the (non-stationary) simulation formula shown in Eq. (2-24), in contrast to the corresponding formula for simulation of stationary stochastic vector processes (Deodatis 1996b). This is due to the fact that the coefficients $|H_{jm}(\omega_l, t)|\sqrt{\Delta\omega}$ in the double summation of Eq. (2-24) are now functions of both frequency and time. However, this shouldn't be of any great concern computationally, since in most cases of practical interest the non-stationary stochastic vector process $f_j^0(t)$; $j = 1, 2, 3$ is limited to relatively short durations by the modulating functions $A_j(\omega, t)$; $j = 1, 2, 3$ (e.g. ground

motion acceleration time histories). A case of non-stationary stochastic vector processes where the FFT technique can be used in the simulation formula is that of uniformly modulated processes [Eq. (2-39)]. At this juncture, it should be noted that Li and Kareem (1991) have proposed a methodology to simulate non-stationary vector processes taking advantage of FFT.

2.4 Simulation of Seismic Ground Motion Compatible With Prescribed Response Spectra

The simulation algorithm presented earlier in this chapter can generate sample functions of a general non-stationary stochastic vector process with evolutionary power, according to a prescribed non-stationary cross-spectral density matrix. A very important application is simulation of earthquake ground motion time histories. In such a case, acceleration, velocity, or displacement time histories can be generated at several locations on the ground surface according to a target cross-spectral density matrix. This will be demonstrated in the first two numerical examples presented later in this chapter. The only drawback in this approach is that it is often preferable to work with time histories that are compatible with prescribed response spectra, rather than with prescribed power spectral density functions (cross-spectral density matrix). An obvious reason for this preference is that it is much easier and more reliable to find a response spectrum specified for a given location, rather than a power spectral density function. For example, design codes usually provide response spectra as a function of local site conditions.

In order to address this issue, a methodology is proposed now to simulate seismic ground motion compatible with the following three prescribed quantities: (1) response spectra, (2) complex coherence functions, and (3) modulating functions. Although the methodology is presented in the following for accelerations, it is straightforward to modify it to accommodate velocities or displacements. The choice of accelerations is done solely for demonstration purposes.

According to the proposed methodology, the acceleration time histories at three points on the ground surface are considered to be a uniformly modulated, tri-variate, non-stationary stochastic vector process. In general, the three points correspond to different local soil conditions. Consequently, a different target acceleration response spectrum $RSA_j(\omega)$; $j = 1, 2, 3$ is assigned to each one of the three points. In addition, complex coherence functions $\Gamma_{jk}(\omega)$; $j, k = 1, 2, 3$; $j \neq k$ are prescribed between pairs of points, and modulating functions $A_j(t)$; $j = 1, 2, 3$ are assigned at each point. The simulation of the acceleration time histories is then performed according to the iterative scheme shown in Table 2-1. This scheme is not expected to perfectly converge at all frequencies as the number of iterations increases (perfect convergence at frequency $\omega = \omega^*$ is expressed as: $\frac{RSA_j(\omega^*)}{RSA^{(f_j)}(\omega^*)} = 1$; $j = 1, 2, 3$, where $RSA^{(f_j)}(\omega)$ is defined in Table 2-1). This is why no convergence criterion is included in the flowchart of Table 2-1. As will be shown in the third numerical example that is presented later in this chapter, only a small number of iterations is usually needed (in most cases less than ten) for a sufficiently accurate convergence at every frequency.

At this point it should be mentioned that the idea for upgrading the individual power

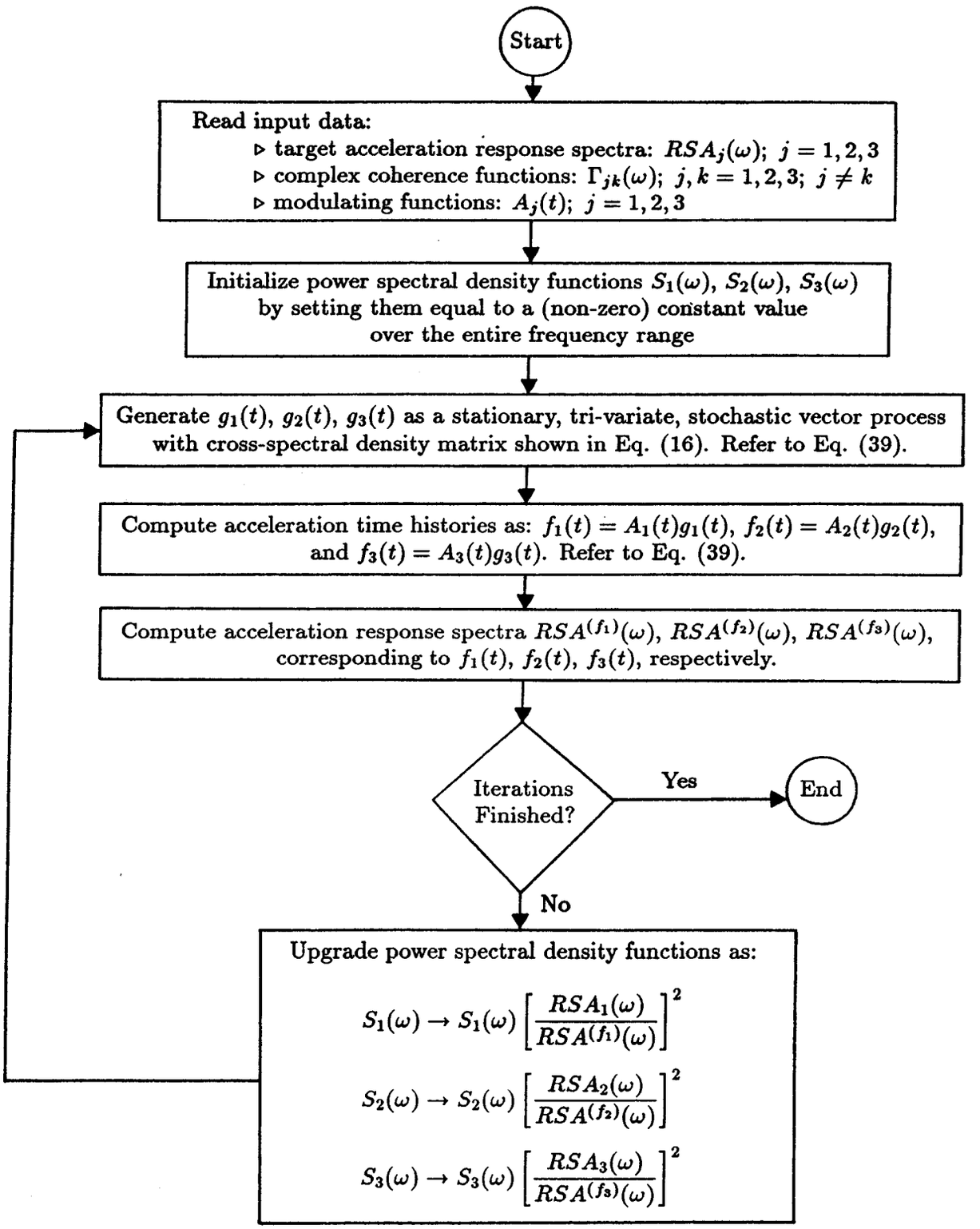

TABLE 2-1 Iterative Scheme to Simulate Response Spectrum Compatible Acceleration Time Histories at Three Points On the Ground Surface.

spectral density functions depicted in Table 2-1 has been suggested by Gasparini and Vanmarcke (1976) for one-dimensional and uni-variate stochastic processes.

Two alternative methodologies to generate ground motion time histories compatible with prescribed response spectra, coherence function, velocity of wave propagation, and duration of strong ground motion, have been suggested by Hao et al. (1989) and by Abrahamson (1993). The Hao et al. methodology and the methodology proposed in this report in Table 2-1 are conceptually similar, while the Abrahamson (1993) approach is a conceptually different time-domain-based methodology.

According to Hao et al. (1989), a spectral-representation-based simulation algorithm (Shinozuka and Jan 1972) is first used to generate stationary time histories that are compatible with a coherence function and a velocity of wave propagation, but not with the prescribed response spectrum. After multiplying these stationary time histories by an appropriate envelope function to introduce non-stationarity, Hao et al. are then adjusting each non-stationary time history independently to make it compatible with the prescribed response spectrum. This adjustment is performed by Fourier transforming each non-stationary time history to the frequency domain, multiplying its frequency domain Fourier transform by the ratio of the prescribed response spectrum over the computed response spectrum of the non-stationary time history, and then inverse transforming the product back to the time domain. This adjustment procedure is usually repeated a few times.

On the other hand, the methodology proposed in this report in Table 2-1 is starting by using a different spectral-representation-based simulation algorithm (Deodatis 1996b) to generate ergodic, stationary time histories (the Shinozuka and Jan 1972 algorithm is generating time histories that are not ergodic) that are again compatible with a coherence function and a velocity of wave propagation, but not with the prescribed response spectrum. After multiplying these stationary time histories by an appropriate envelope function to introduce non-stationarity, the methodology proposed in this report is upgrading the power spectral density functions of the components of the vector process as indicated in Table 2-1, generates new stationary time histories according to the upgraded cross-spectral density matrix, and multiplies them again by the envelope function to introduce non-stationarity. This upgrading procedure is repeated a few times to make the time histories response spectrum compatible to the desired degree.

2.5 Numerical Examples

In order to demonstrate the capabilities of the proposed algorithms to simulate non-stationary stochastic vector processes, three examples involving simulation of earthquake ground motion are selected. In the first example, ground motion time histories are modeled as a uniformly modulated non-stationary stochastic vector process, and sample functions are generated according to a target cross-spectral density matrix. In the second example, ground motion time histories are modeled as a non-stationary stochastic vector process with amplitude and frequency modulation, and sample functions are again generated according to a target cross-spectral density matrix. Finally, in the third example, ground motion time histories are modeled as a uniformly modulated non-stationary stochastic vector process, but unlike the first example, sample functions are generated to be compatible

with prescribed response spectra.

2.5.1 Example 1

In this numerical example, ground motion time histories are modeled as a uniformly modulated non-stationary stochastic vector process, and sample functions will be generated according to a target cross-spectral density matrix. Specifically, the acceleration time histories at three points on the ground surface along the line of main wave propagation are considered to be a tri-variate non-stationary stochastic vector process. The configuration of the three points is shown in Fig. 2-1 where the arrow indicates the direction of wave propagation. The simulated earthquake ground motion at points 1, 2 and 3 will have the following characteristics:

(1) Points 1, 2 and 3 correspond to different local soil conditions. Specifically, point 1 is characterized by stiff soil conditions, point 2 by intermediate soil conditions and point 3 by soft soil conditions. This is a very desirable capability of the method, being able to simulate ground motion at neighboring points on the ground surface with different local soil conditions and consequently different frequency contents. Such a case is encountered, for example, at the supports of intermediate to long-span bridges located in areas with abrupt changes in soil conditions along the axis of the bridge.

(2) In addition to different frequency contents at points 1, 2 and 3, the acceleration time histories at these three points will also be correlated according to a specified coherence function and they will reflect the wave propagation effect according to a specified velocity of wave propagation. The method is therefore capable to simulate ground motion time histories that, at the same time, are spatially correlated, include the wave propagation effect and correspond to different local soil conditions.

(3) Finally, the acceleration time histories at points 1, 2 and 3 will reflect the non-stationary characteristics of ground motion according to specified modulating functions $A_j(\omega, t)$; $j = 1, 2, 3$.

The three components of the tri-variate non-stationary stochastic vector process describing the acceleration time histories at points 1, 2 and 3 (see Fig. 2-1) are denoted by $f_1^0(t)$, $f_2^0(t)$ and $f_3^0(t)$, respectively. The mean value of the process is equal to zero [see Eq. (2-1)], while the elements of its cross-spectral density matrix [see Eq. (2-3)] are defined as follows:

$$S_{jj}^0(\omega, t) = |A_j(\omega, t)|^2 \; S_j(\omega) \quad ; \quad j = 1, 2, 3 \tag{2-40}$$

$$S_{jk}^0(\omega, t) = A_j(\omega, t) A_k(\omega, t) \; \sqrt{S_j(\omega) S_k(\omega)} \; \gamma_{jk}(\omega) \; \exp\left[-i \frac{\omega \; \xi_{jk}}{v}\right] \quad ; \quad j, k = 1, 2, 3 \; ; \; j \neq k \tag{2-41}$$

where $\gamma_{jk}(\omega)$ are the (stationary) coherence functions between $f_j^0(t)$ and $f_k^0(t)$, and $\exp\left[-i \frac{\omega \; \xi_{jk}}{v}\right]$ is the wave propagation term, with ξ_{jk} being the distance between points j and k and v being the velocity of wave propagation.

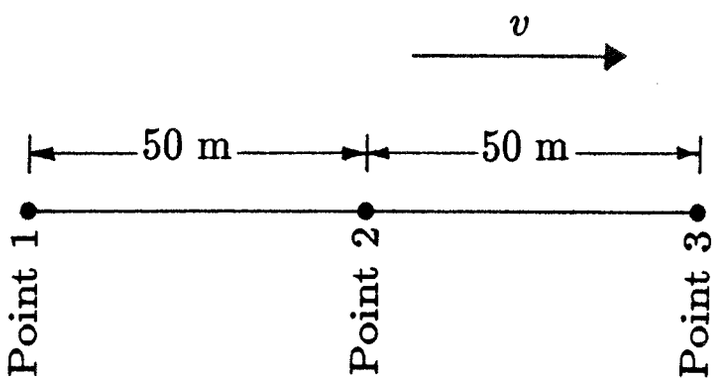

FIGURE 2-1 Configuration of points 1, 2 and 3 on the ground surface along the line of main wave propagation, for Example 1. Point 1 corresponds to rock or stiff soil conditions, point 2 corresponds to deep cohesionless soils and point 3 corresponds to soft to medium clays and sands.

At this juncture, it should be pointed out that the expressions shown in Eqs. (2-40) and (2-41) describe earthquake ground motion that is non-homogeneous in space (since $S_1(\omega) \neq S_2(\omega) \neq S_3(\omega)$) and non-stationary in time.

The Clough-Penzien acceleration spectrum (Clough and Penzien 1975) is selected to model the (stationary) power spectral density functions $S_j(\omega)$; $j = 1, 2, 3$ of the acceleration time histories $f_j^0(t)$; $j = 1, 2, 3$, respectively:

$$S_j(\omega) = S_{0j} \left[\frac{1 + 4\zeta_{gj}^2 \left[\frac{\omega}{\omega_{gj}}\right]^2}{\left\{1 - \left[\frac{\omega}{\omega_{gj}}\right]^2\right\}^2 + 4\zeta_{gj}^2 \left[\frac{\omega}{\omega_{gj}}\right]^2} \right] \cdot \left[\frac{\left[\frac{\omega}{\omega_{fj}}\right]^4}{\left\{1 - \left[\frac{\omega}{\omega_{fj}}\right]^2\right\}^2 + 4\zeta_{fj}^2 \left[\frac{\omega}{\omega_{fj}}\right]^2} \right] \quad ; \quad j = 1, 2, 3 \qquad (2-42)$$

where S_{0j} is a constant determining the intensity of acceleration at point j, ω_{gj} and ζ_{gj} can be thought of as some characteristic frequency and damping ratio of the ground at point j, and ω_{fj} and ζ_{fj} are filtering parameters for point j.

The Harichandran-Vanmarcke model (Harichandran and Vanmarcke 1986) is chosen to describe the (stationary) coherence functions $\gamma_{jk}(\omega)$; $j, k = 1, 2, 3$; $j \neq k$ between $f_j^0(t)$ and $f_k^0(t)$:

$$\gamma_{jk}(\omega) = A \exp\left[-\frac{2\xi_{jk}}{\alpha\, \theta(\omega)}(1 - A + \alpha A)\right] + (1 - A) \exp\left[-\frac{2\xi_{jk}}{\theta(\omega)}(1 - A + \alpha A)\right] \quad ; \quad j, k = 1, 2, 3 \; ; \; j \neq k \qquad (2-43)$$

where ξ_{jk} is the distance between points j and k, $\theta(\omega)$ is the frequency-dependent correlation distance:

$$\theta(\omega) = k \left[1 + \left(\frac{\omega}{\omega_0}\right)^b\right]^{-1/2} \qquad (2-44)$$

and A, α, k, ω_0 and b are model parameters.

Since the acceleration time histories $f_j^0(t)$; $j = 1, 2, 3$ are modeled as a uniformly modulated non-stationary stochastic vector process, the modulating functions $A_j(\omega, t)$; $j = 1, 2, 3$ will be functions of time only. The Bogdanoff-Goldberg-Bernard model (Bogdanoff, Goldberg and Bernard 1961) is used for this purpose:

$$A_1(\omega, t) = A_1(t) = a_1\, t \exp(-a_2\, t) \qquad \text{for } t > 0 \qquad (2-45a)$$

$$A_2(\omega, t) = A_2(t) = \begin{cases} a_1 \left(t - \frac{\xi_{21}}{v}\right) \exp\left[-a_2 \left(t - \frac{\xi_{21}}{v}\right)\right] & \text{for } t > \frac{\xi_{21}}{v} \\ 0 & \text{for } 0 < t < \frac{\xi_{21}}{v} \end{cases} \qquad (2-45b)$$

$$A_3(\omega, t) = A_3(t) = \begin{cases} a_1 \left(t - \frac{\xi_{31}}{v}\right) \exp\left[-a_2 \left(t - \frac{\xi_{31}}{v}\right)\right] & \text{for } t > \frac{\xi_{31}}{v} \\ 0 & \text{for } 0 < t < \frac{\xi_{31}}{v} \end{cases} \qquad (2-45c)$$

where a_1 and a_2 are model parameters depending on such factors as earthquake magnitude and epicentral distance. It should be noted that Eq. (2-45) includes the wave propagation effect.

At this juncture, it should be pointed out that the models used for $S_j(\omega)$, $\gamma_{jk}(\omega)$ and $A_j(\omega, t)$ in Eqs. (2-42), (2-43) and (2-45), respectively, were selected for demonstration purposes only. There are several other models in the literature that can be used for $S_j(\omega)$, $\gamma_{jk}(\omega)$ and $A_j(\omega, t)$. At this point, the reader is referred to an important note concerning the case of differential (asynchronous) support ground motion when the bridge supports are on different local soil conditions found in the second paragraph of Chapter 2 "Generation of Spatially Varying Seismic Ground Motion Time Histories" (this is before the "Introduction" section of Chapter 2).

The next step is to select numerical values for the parameters appearing in Eqs. (2-42)-(2-45). Starting from ω_{gj} and ζ_{gj}; $j = 1, 2, 3$ appearing in Eq. (2-42), the values suggested by Ellingwood and Batts (1982) for three different soil conditions are used in this study:

Point 1: Rock or stiff soil conditions: $\omega_{g1} = 8\pi$ rad/sec, $\zeta_{g1} = 0.60$ (2-46a)
Point 2: Deep cohesionless soils: $\omega_{g2} = 5\pi$ rad/sec, $\zeta_{g2} = 0.60$ (2-46b)
Point 3: Soft to medium clays and sands: $\omega_{g3} = 2.4\pi$ rad/sec, $\zeta_{g3} = 0.85$ (2-46c)

The filtering parameter ω_{fj} [Eq. (2-42)] is set equal to 0.10 of the corresponding ω_{gj} value, while the other filtering parameter ζ_{fj} [Eq. (2-42)] is set equal to the corresponding ζ_{gj} value, following the recommendation by Hindy and Novak (1980):

Point 1: Rock or stiff soil conditions: $\omega_{f1} = 0.8\pi$ rad/sec, $\zeta_{f1} = 0.60$ (2-47a)
Point 2: Deep cohesionless soils: $\omega_{f2} = 0.5\pi$ rad/sec, $\zeta_{f2} = 0.60$ (2-47b)
Point 3: Soft to medium clays and sands: $\omega_{f3} = 0.24\pi$ rad/sec, $\zeta_{f3} = 0.85$ (2-47c)

Finally, the last parameter appearing in Eq. (2-42), S_{0j}; $j = 1, 2, 3$, is computed so that the standard deviation of the Kanai-Tajimi part of the (stationary) power spectral density function is equal to 100 cm/sec^2 for all three points 1, 2 and 3:

$$S_{01} = 62.3 \text{ cm}^2/\text{sec}^3 \quad , \quad S_{02} = 99.7 \text{ cm}^2/\text{sec}^3 \quad , \quad S_{03} = 184.5 \text{ cm}^2/\text{sec}^3 \qquad (2-48)$$

For the various parameters appearing in Eqs. (2-43) and (2-44), the values estimated by Harichandran and Wang (1990) by analyzing data from the SMART-1 seismograph array will be used in this study for demonstration purposes:

$$A = 0.626, \quad \alpha = 0.022, \quad k = 19,700 \text{ m}, \quad \omega_0 = 12.692 \text{ rad/sec}, \quad b = 3.47 \qquad (2-49)$$

Parameters a_1 and a_2 appearing in the expressions for the modulating functions [Eq. (2-45)] are set equal to:

$$a_1 = 0.906 \qquad \text{and} \qquad a_2 = 1/3 \qquad (2-50)$$

so that the maximum value of $A_j(t)$; $j = 1, 2, 3$ occurs at time $t = \left(3 + \frac{\xi_{j1}}{v}\right)$ sec; $j = 1, 2, 3$ and is equal to unity (from Fig. 2-1 it is obvious that $\xi_{11} = 0$, $\xi_{21} = 50$ m, $\xi_{31} = 100$ m).

Finally, the velocity of wave propagation v is set equal to (Harichandran and Wang 1990):

$$v = 1,000 \text{ m/sec} \qquad (2-51)$$

Based on the numerical values given in Eqs. (2-46)-(2-51), the (stationary) power spectral density functions $S_j(\omega)$; $j = 1,2,3$ are plotted in Fig. 2-2, the (stationary) coherence functions $\gamma_{jk}(\omega)$; $j,k = 1,2,3$; $j \neq k$ are plotted in Fig. 2-3 and the modulating functions $A_j(t)$; $j = 1,2,3$ are plotted in Fig. 2-4.

Since the non-stationary stochastic vector process in this example is a uniformly modulated one, the generation of its sample functions will be performed using Eq. (2-39). It is reminded that the simulation of stationary stochastic vector processes involved in Eq. (2-39) is performed with great computational efficiency using the FFT technique, as described by Deodatis (1996b).

The upper cut-off frequency ω_u and the value of N [see Eq. (2-27)] are set equal to:

$$\omega_u = 126 \text{ rad/sec (20 Hz)} \qquad \text{and} \qquad N = 126 \qquad (2-52)$$

The simulation is performed at 3,072 time instants, with a time step $\Delta t = 6.14 \cdot 10^{-3}$ sec, over a length equal to $3,072 \cdot 6.14 \cdot 10^{-3} = 18.85$ sec. One generated sample function for the acceleration at points 1, 2 and 3 (see Fig. 2-1), denoted by $f_1(t)$, $f_2(t)$ and $f_3(t)$, respectively, is displayed in Fig. 2-5.

The most obvious characteristic of the acceleration time histories in Fig. 2-5 is their non-stationarity which is described by the modulating functions shown in Fig. 2-4. The different frequency contents of $f_1(t)$, $f_2(t)$ and $f_3(t)$ (making the acceleration non-homogeneous in space and described by the (stationary) power spectral density functions shown in Fig. 2-2) can also be detected in Fig. 2-5. Specifically, the characteristic frequency of the ground for $f_1(t)$ ($\omega_{g1} = 8\pi$ rad/sec) is higher than that for $f_2(t)$ ($\omega_{g2} = 5\pi$ rad/sec), which is then higher than that for $f_3(t)$ ($\omega_{g3} = 2.4\pi$ rad/sec). This characteristic is not as obvious as the non-stationarity one in Fig. 2-5, because of the relatively large bandwidths of $S_1(\omega)$, $S_2(\omega)$ and $S_3(\omega)$, which are controlled by ζ_{g1}, ζ_{g2} and ζ_{g3}, respectively.

The wave propagation effect and the correlation among $f_1(t)$, $f_2(t)$ and $f_3(t)$ cannot be observed in Fig. 2-5. For this reason, a segment of the acceleration time histories shown in Fig. 2-5 (specifically from time $t = 3.1$ sec up to time $t = 6.2$ sec) is magnified and displayed in Fig. 2-6. In this figure, the wave propagation effect is easily detected by following the movement of peak A in $f_1(t)$, $f_2(t)$ and $f_3(t)$, which reflects the $v = 1{,}000$ m/sec velocity of wave propagation. The correlation among $f_1(t)$, $f_2(t)$ and $f_3(t)$ is also easily detected in Fig. 2-6, as major peaks in the three time histories (like peak A) retain their general shape after some loss of coherence described by the (stationary) coherence functions shown in Fig. 2-3.

It is therefore obvious from Figs. 2-5 and 2-6 that the proposed algorithm is able to simulate non-stationary ground motion time histories that are spatially correlated according to a given coherence function, include the wave propagation effect and are non-homogeneous in space (or equivalently they correspond to different frequency contents). At this point,

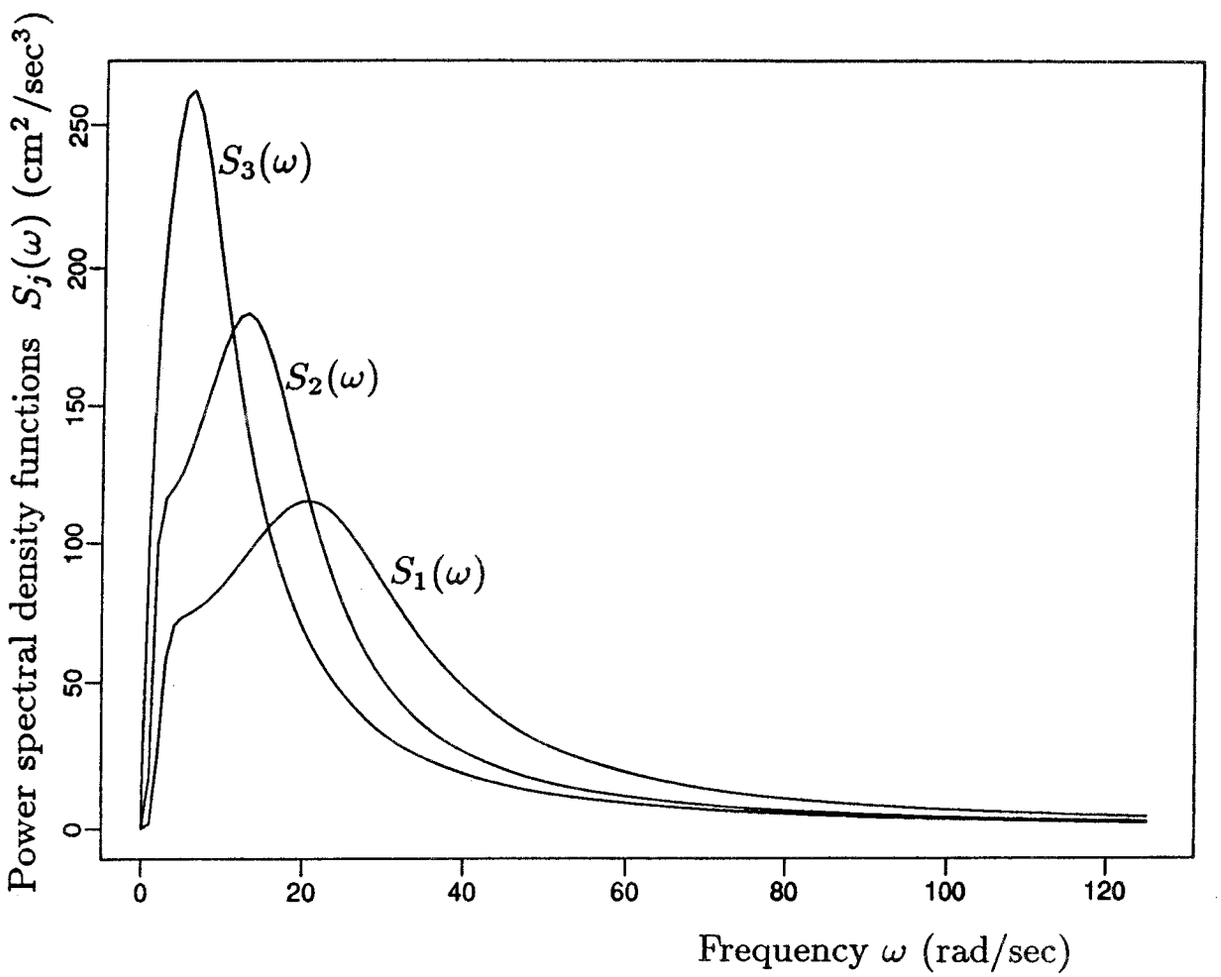

FIGURE 2-2 The power spectral density functions at points 1, 2 and 3, for Example 1: $S_1(\omega) \rightarrow$ rock or stiff soil conditions, $S_2(\omega) \rightarrow$ deep cohesionless soils and $S_3(\omega) \rightarrow$ soft to medium clays and sands.

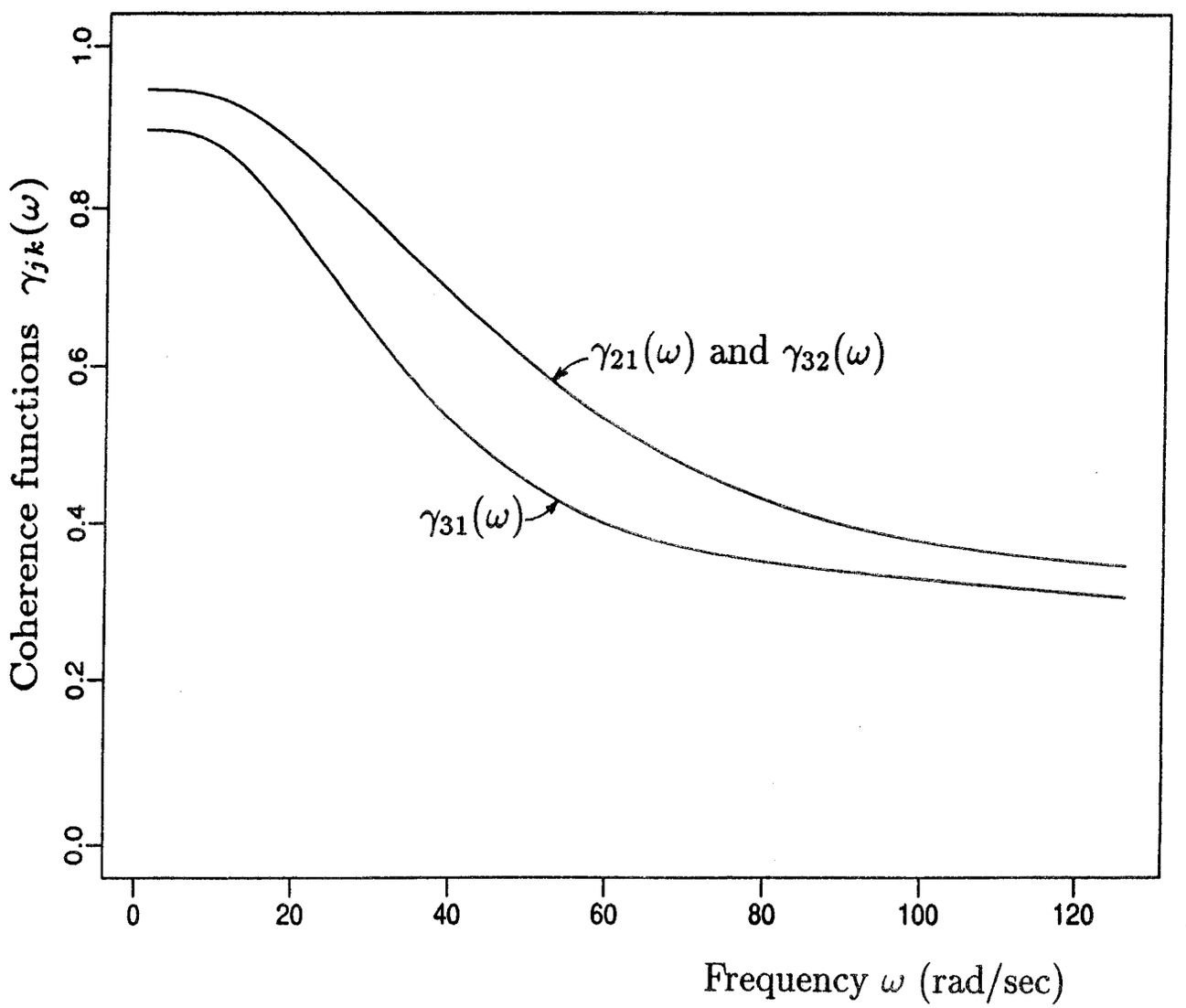

FIGURE 2-3 Coherence functions $\gamma_{21}(\omega)$, $\gamma_{31}(\omega)$ and $\gamma_{32}(\omega)$, for Example 1.

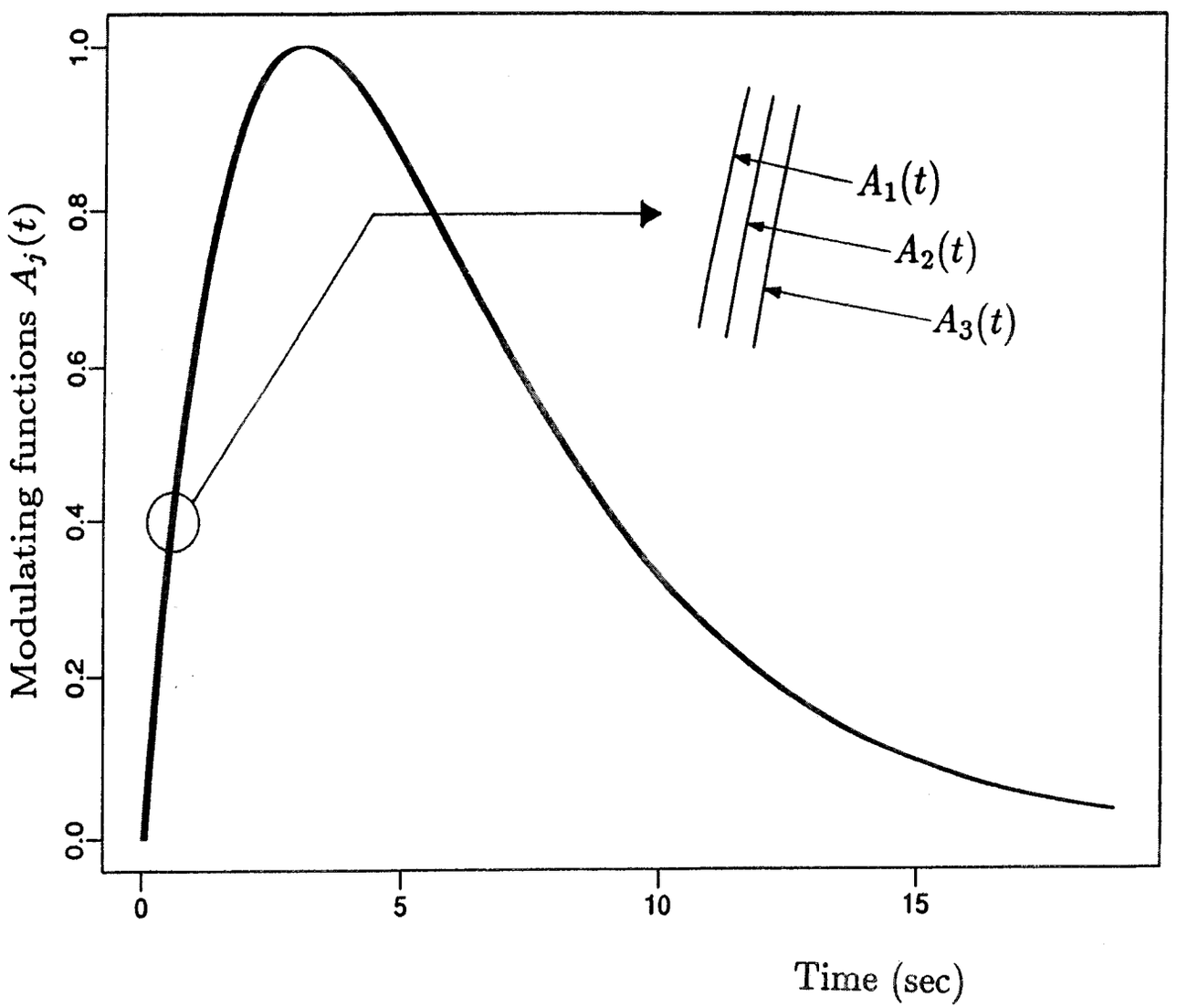

FIGURE 2-4 Modulating functions $A_1(t)$, $A_2(t)$ and $A_3(t)$, for Example 1.

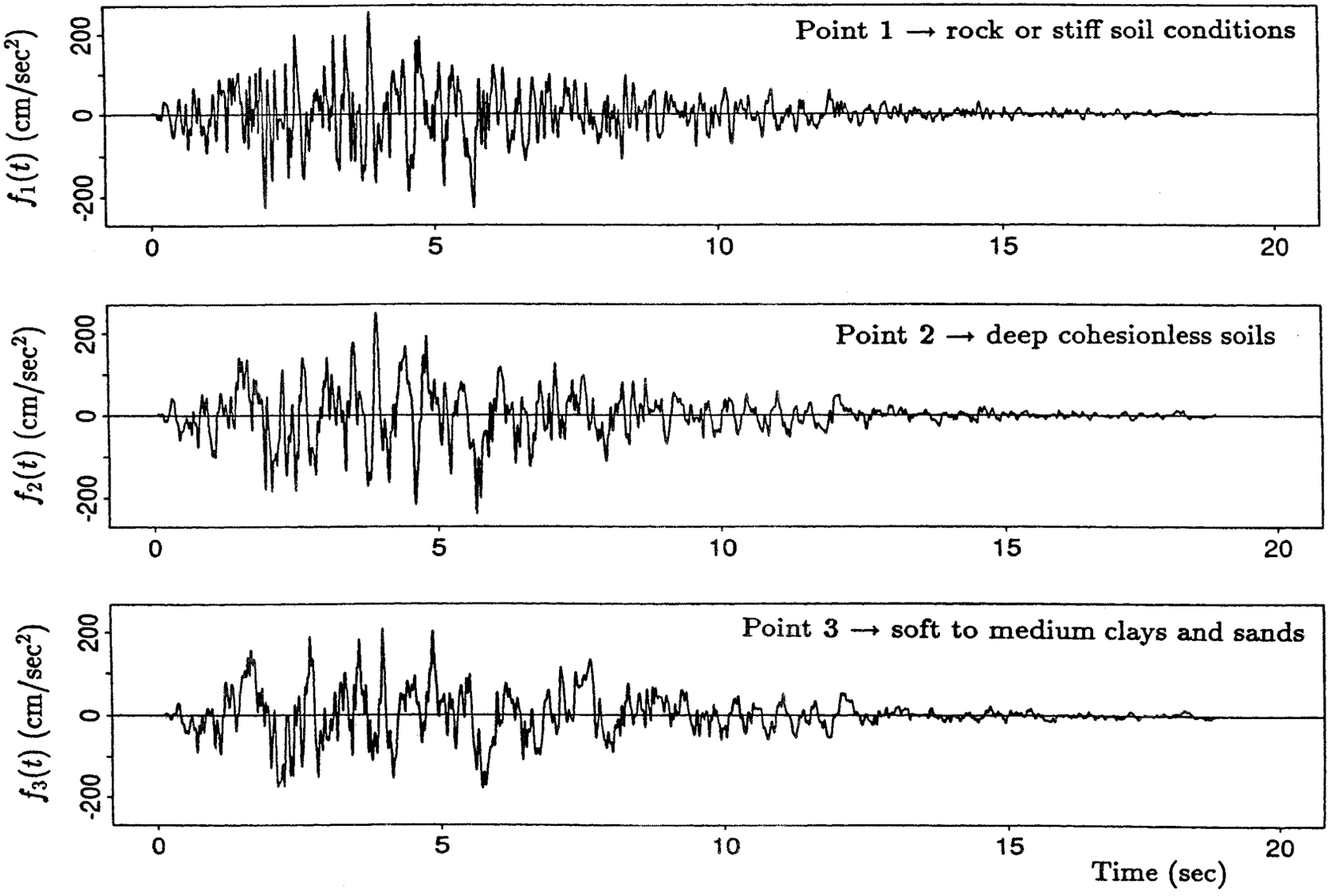

FIGURE 2-5 Generated sample function for the acceleration at points 1, 2 and 3, over a length equal to 18.85 sec (Example 1).

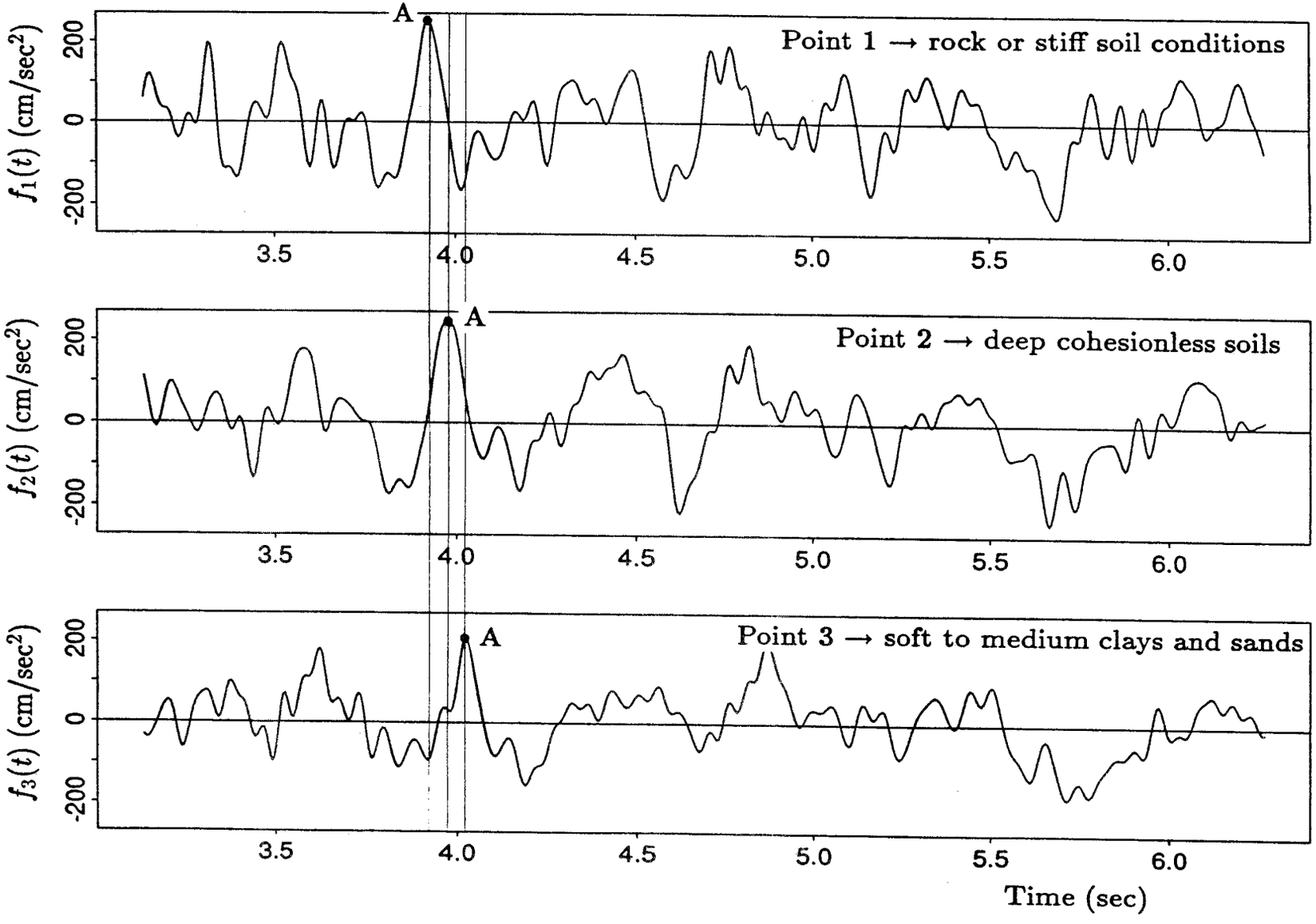

FIGURE 2-6 Generated sample function for the acceleration at points 1, 2 and 3 from $t = 3.1$ sec up to $t = 6.2$ sec (Example 1).

the reader is referred again to an important note concerning the case of differential (asynchronous) support ground motion when the bridge supports are on different local soil conditions found in the second paragraph of Chapter 2 "Generation of Spatially Varying Seismic Ground Motion Time Histories" (this is before the "Introduction" section of Chapter 2).

Finally, the ensemble auto-/cross-correlation function $R_{jk}(t, t+\tau)$ is computed from 1,000 sample functions at time instant $t = 3.14$ sec and plotted as a function of τ in Fig. 2-7 versus the target auto-/cross-correlation function $R^0_{jk}(t, t+\tau)$. As can be seen in Fig. 2-7, the agreement between $R^0_{jk}(t, t+\tau)$ and $R_{jk}(t, t+\tau)$ is very good, especially in the vicinity of the dominant peak of the auto-/cross-correlation functions. Some small differences can be observed away from this dominant peak in Fig. 2-7. However, these differences disappear when the ensemble auto-/cross-correlation function $R_{jk}(t, t+\tau)$ is computed from 100,000 sample functions, as can be seen in Fig. 2-8 where $R^0_{jk}(t, t+\tau)$ and $R_{jk}(t, t+\tau)$ practically coincide.

It should be noted that the agreement between $R^0_{jk}(t, t+\tau)$ and $R_{jk}(t, t+\tau)$ observed in Figs. 2-7 and 2-8 for time instant $t = 3.14$ sec is typical for any time instant from $t = 0$ up to $t = 18.85$ sec (the duration of the time histories shown in Fig. 2-5).

2.5.2 Example 2

Unlike the first example where ground motion time histories were modeled as a uniformly modulated non-stationary stochastic vector process, in this example they are modeled as a non-stationary stochastic vector process with amplitude and frequency modulation. This means that both the amplitude and the frequency content of ground motion change as a function of time (in the first example, it was only the amplitude of ground motion that was varying with time). As in the previous example, sample functions will be generated according to a target cross-spectral density matrix.

Figure 2-9 displays an acceleration record from the 1964 Niigata earthquake involving both amplitude and frequency content variation as a function of time. Specifically, this record shows an abrupt change of its frequency content between approximately 8 sec and 10 sec. During this 2 sec period, the frequency content is transformed from one containing a relatively broad band of frequencies to one containing essentially a single low frequency. It is believed that this phenomenon is due to soil liquefaction. The objective of this example will be to reproduce the general frequency and amplitude variation characteristics of the acceleration record shown in Fig. 2-9.

The acceleration time histories at three points on the ground surface are again considered to be a tri-variate non-stationary stochastic vector process. The configuration of the three points is shown in Fig. 2-10, indicating that it is not necessary for the points to be on a straight line, or to be equidistant (compare to previous example). For simplicity, no wave propagation will be considered in this example. The simulated earthquake ground motion at points 1, 2 and 3 will have the following characteristics:

(1) Points 1, 2 and 3 correspond to the same local soil conditions.

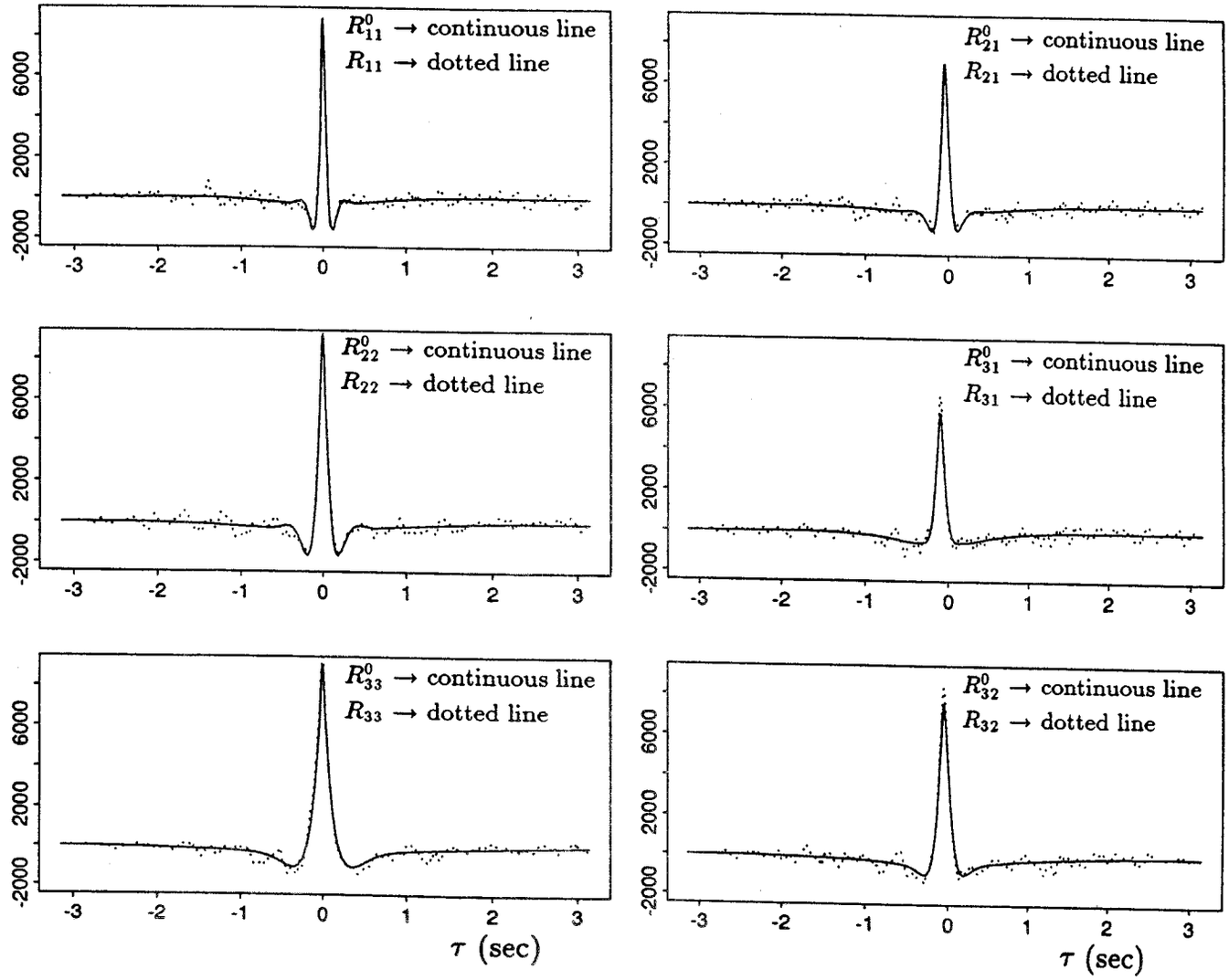

FIGURE 2-7 Ensemble auto-/cross-correlation functions $[R_{jk}(t, t+\tau)]$ computed from 1,000 sample functions versus the corresponding targets $[R^0_{jk}(t, t+\tau)]$. Both $R_{jk}(t, t+\tau)$ and $R^0_{jk}(t, t+\tau)$ are plotted at time instant $t = 3.14$ sec as a function of τ.

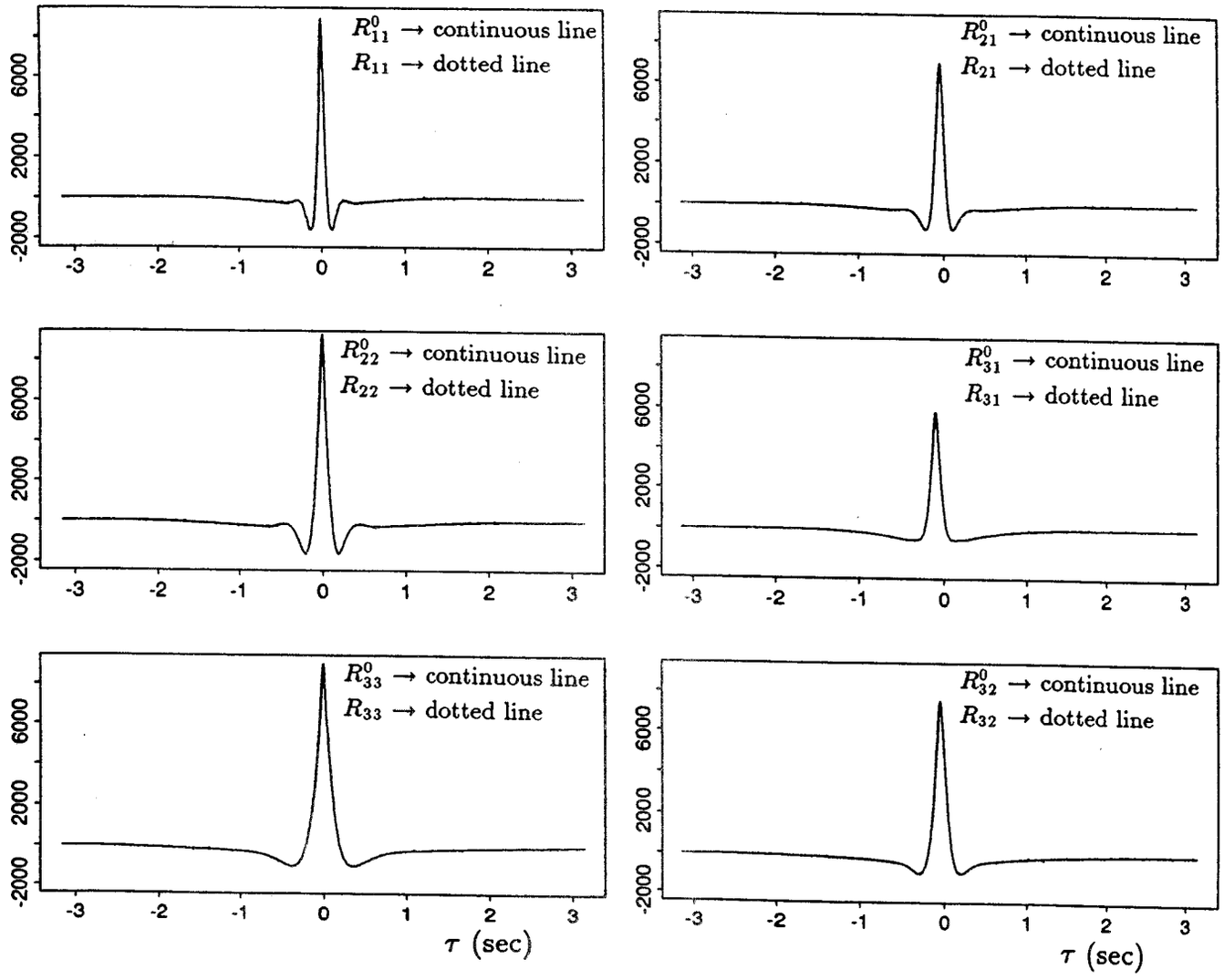

FIGURE 2-8 Ensemble auto-/cross-correlation functions $[R_{jk}(t, t+\tau)]$ computed from 100,000 sample functions versus the corresponding targets $[R^0_{jk}(t, t+\tau)]$. Both $R_{jk}(t, t+\tau)$ and $R^0_{jk}(t, t+\tau)$ are plotted at time instant $t = 3.14$ sec as a function of τ.

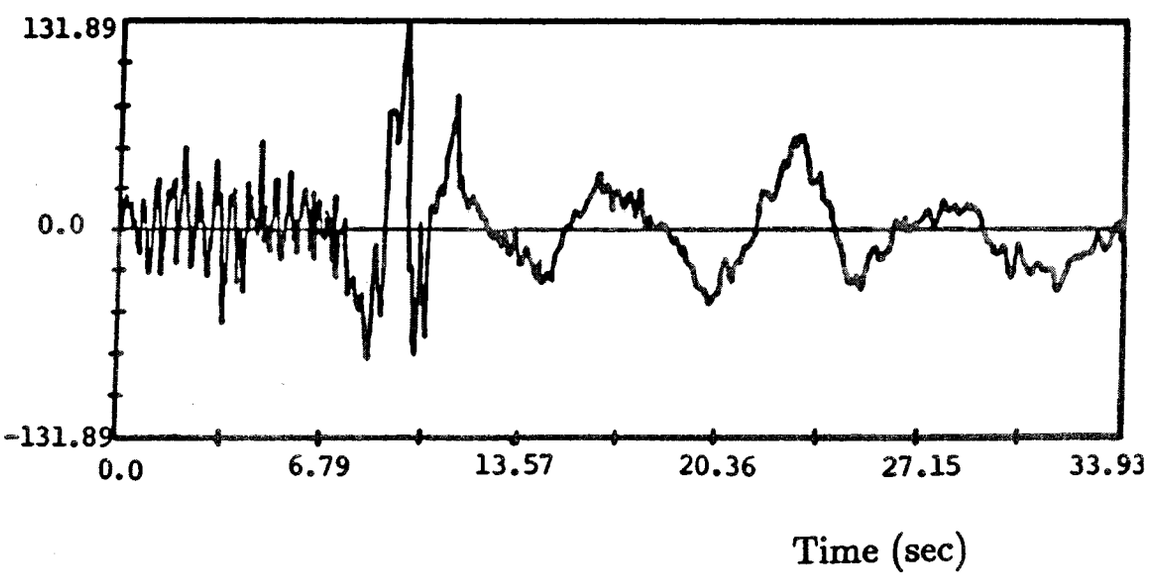

FIGURE 2-9 Acceleration record from the 1964 Niigata earthquake.

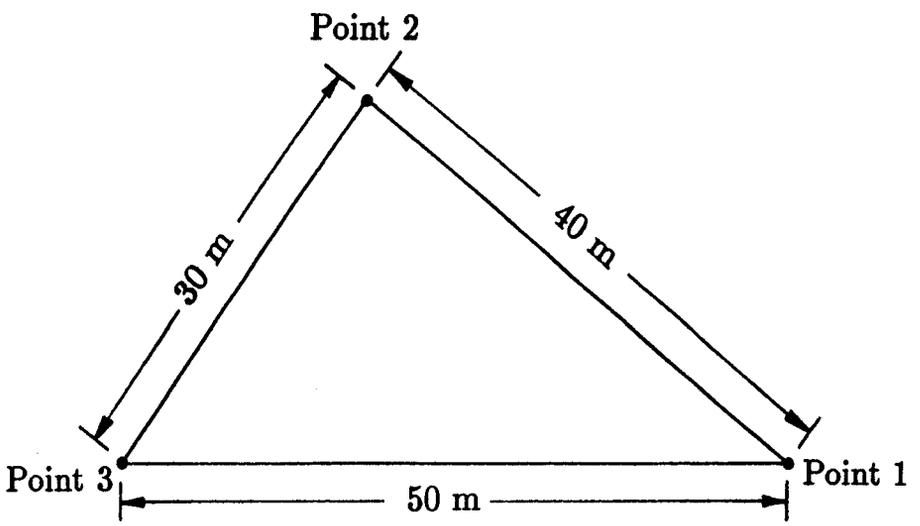

FIGURE 2-10 Configuration of points 1, 2 and 3 on the ground surface, for Example 2. Points 1, 2 and 3 correspond to the same local soil conditions.

(2) The frequency content of the acceleration time histories at these three points will change with time as will be described in the following, in order to capture the unique characteristics of the record shown in Fig. 2-9.

(3) The acceleration time histories at points 1, 2 and 3 will be correlated according to a specified coherence function.

(4) Finally, the amplitude variation as a function of time of the acceleration time histories at these three points will be described by prescribed modulating functions $A_j(\omega, t)$; $j = 1, 2, 3$.

The three components of the tri-variate non-stationary stochastic vector process describing the acceleration time histories at points 1, 2 and 3 (see Fig. 2-10) are denoted by $f_1^0(t)$, $f_2^0(t)$ and $f_3^0(t)$, respectively. The mean value of the process is equal to zero [see Eq. (2-1)], while the elements of its cross-spectral density matrix [see Eq. (2-3)] are given by the expressions shown in Eqs. (2-40) and (2-41). It should be pointed out, however, that since no wave propagation is considered in this example, the wave propagation term $\exp\left[-i\frac{\omega\ \xi_{jk}}{v}\right]$ in Eq. (2-41) should be set equal to unity ($v \to \infty$).

The Clough-Penzien acceleration spectrum shown in Eq. (2-42) is selected again to model the power spectral density functions $S_j(\omega)$; $j = 1, 2, 3$ of the acceleration time histories $f_j^0(t)$; $j = 1, 2, 3$, respectively. However, in order to account for the variation of the frequency content with time, the characteristic frequency and damping ratio of the ground are considered now to vary as a function of time as follows:

$$\omega_{gj}(t) = \begin{cases} 15.56 \text{ rad/sec} & \text{for } 0 \leq t \leq 4.5 \text{ sec} \\ 27.12t_p^3 - 40.68t_p^2 + 15.56 & \text{for } 4.5 \leq t \leq 5.5 \text{ sec} \\ 2.0 \text{ rad/sec} & \text{for } t \geq 5.5 \text{ sec} \end{cases} \quad ; \quad j = 1, 2, 3 \qquad (2-53)$$

$$\zeta_{gj}(t) = \begin{cases} 0.64 & \text{for } 0 \leq t \leq 4.5 \text{ sec} \\ 1.25t_p^3 - 1.875t_p^2 + 0.64 & \text{for } 4.5 \leq t \leq 5.5 \text{ sec} \\ 0.015 & \text{for } t \geq 5.5 \text{ sec} \end{cases} \quad ; \quad j = 1, 2, 3 \qquad (2-54)$$

where $t_p = t - 4.5$ sec and:

$$\omega_{fj}(t) = 0.1\omega_{gj}(t) \quad ; \quad \zeta_{fj}(t) = \zeta_{gj}(t) \quad ; \quad j = 1, 2, 3 \qquad (2-55)$$

The expressions for $\omega_{gj}(t)$ and $\zeta_{gj}(t)$ are taken from Deodatis and Shinozuka (1988) and describe a sudden drop in the values of the characteristic frequency and damping ratio during the one-second period from $t = 4.5$ sec to $t = 5.5$ sec. The constant determining the intensity of the acceleration is also going to be a function of time, so that the standard deviation of the Kanai-Tajimi part of the spectrum is equal to $\sigma = 100$ cm/sec^2 at every time instant:

$$S_{0j}(t) = \frac{\sigma^2}{\pi\omega_{gj}(t)\left[2\zeta_{gj}(t) + \frac{1}{2\zeta_{gj}(t)}\right]} \quad ; \quad j = 1, 2, 3 \qquad (2-56)$$

The Harichandran-Vanmarcke model shown in Eqs. (2-43) and (2-44) is chosen again to describe the coherence functions $\gamma_{jk}(\omega)$; $j, k = 1, 2, 3$; $j \neq k$ between $f_j^0(t)$ and $f_k^0(t)$. The

model parameters A, α, k, ω_0 and b are assigned the values from the previous example shown in Eq. (2-49).

The Bogdanoff-Goldberg-Bernard model is selected again for the modulating functions:

$$A_j(\omega, t) = A_j(t) = a_1 \; t \; \exp(-a_2 \; t) \quad ; \quad j = 1, 2, 3 \qquad (2-57)$$

with model parameters a_1 and a_2 set equal to:

$$a_1 = 0.680 \qquad \text{and} \qquad a_2 = 1/4 \qquad (2-58)$$

so that the maximum value of $A_j(t)$; $j = 1, 2, 3$ occurs at time $t = 4$ sec and is equal to unity.

At this juncture, it should be pointed out that the definitions for $S_j(\omega)$; $j = 1, 2, 3$ [see Eqs. (2-42), (2-53), (2-54), (2-55), (2-56)] and $A_j(\omega, t)$ [see Eq. (2-57)] do not imply anymore that the modulating function $A_j(\omega, t)$ represents the change in the evolutionary power spectrum, relative to the (stationary) power spectral density function $S_j(\omega)$ (note that $S_j(\omega)$ is now a function of both frequency and time since the characteristic frequency and damping ratio of the ground are functions of time, and $A_j(\omega, t)$ is a function of time only).

The evolutionary power spectra $S^0_{jj}(\omega, t)$; $j = 1, 2, 3$ [see Eq. (2-4)] are plotted in Fig. 2-11 at three time instants: $t = 1$ sec, $t = 4$ sec, and $t = 7$ sec. As seen in this figure, the sudden drop in the values of the characteristic frequency and damping ratio of the ground from 4.5 sec to 5.5 sec causes the formation of a very sharp peak in the evolutionary power spectra at frequency 2.0 rad/sec [refer to Eqs. (2-53) and (2-54)].

Since the non-stationary stochastic vector process in this example is not a uniformly modulated one, the generation of its sample functions can only be performed using Eq. (2-24). The upper cut-off frequency ω_u and the value of N [see Eq. (2-27)] are set equal to:

$$\omega_u = 128 \text{ rad/sec} \qquad \text{and} \qquad N = 1,024 \qquad (2-59)$$

The reason for using such a high value for N [compare to the corresponding value in Eq. (2-52)] is to describe accurately the very sharp peak in the evolutionary power spectra after time instant 5.5 sec (refer to Fig. 2-11).

The simulation is performed at 2,000 time instants, with a time step $\Delta t = 0.01$ sec, over a length equal to $2,000 \cdot 0.01 = 20$ sec. One generated sample function for the acceleration at points 1, 2 and 3 (see Fig. 2-10), denoted by $f_1(t)$, $f_2(t)$ and $f_3(t)$, respectively, is displayed in Fig. 2-12. It is obvious that the general frequency and amplitude variation characteristics of the acceleration record of the 1964 Niigata earthquake shown in Fig. 2-9 are reproduced very well in the sample function plotted in Fig. 2-12. This is accomplished by using the time-varying characteristic frequency and damping ratio of the ground shown in Eqs. (2-53) and (2-54), and the modulating function shown in Eq. (2-57). In addition, it is possible to detect the correlation among $f_1(t)$, $f_2(t)$ and $f_3(t)$ in Fig. 2-12, as major peaks in the three time histories retain their general shape after some loss of coherence

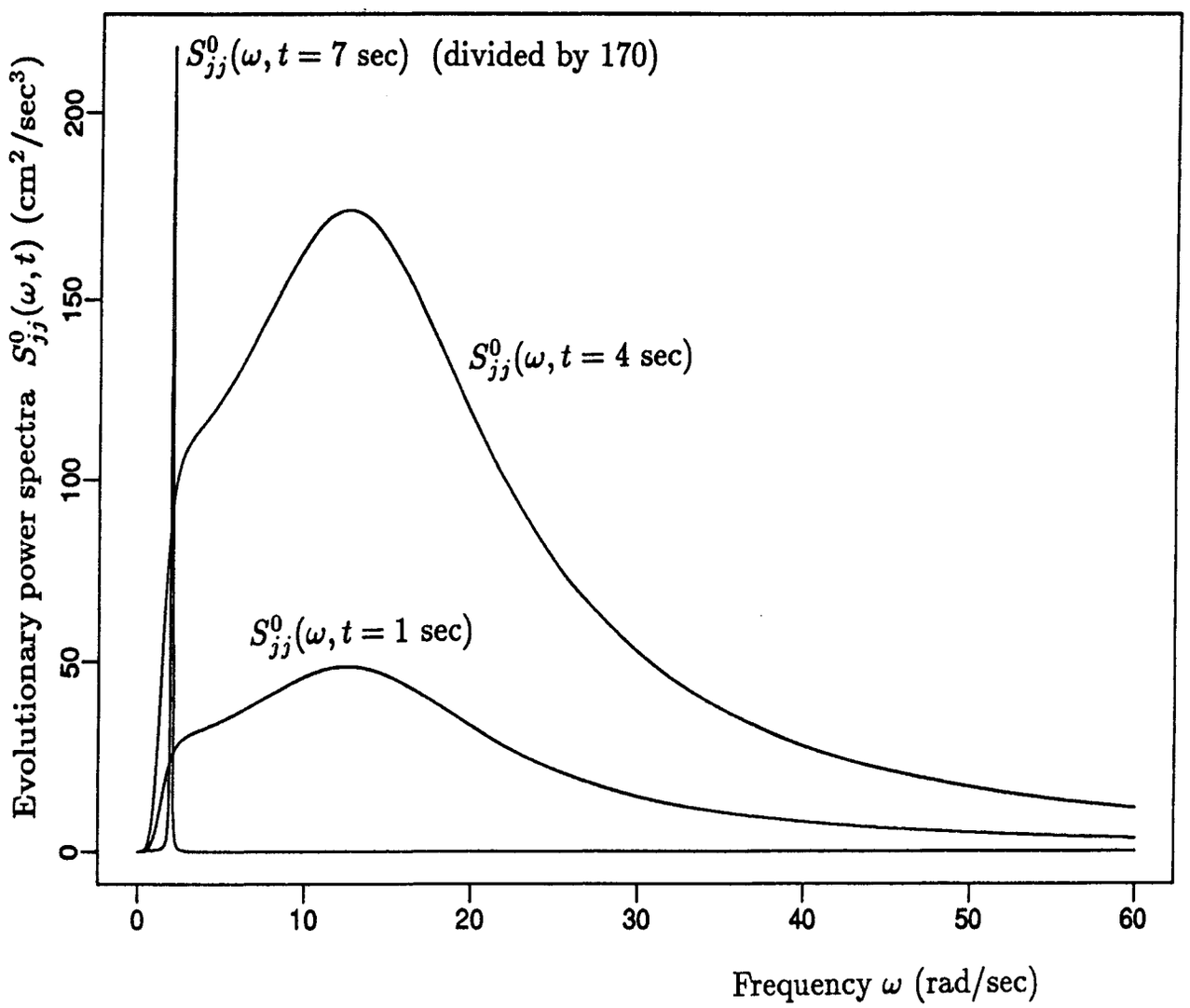

FIGURE 2-11 The evolutionary power spectra $S^0_{jj}(\omega, t)$; $j = 1, 2, 3$ at three time instants (Example 2).

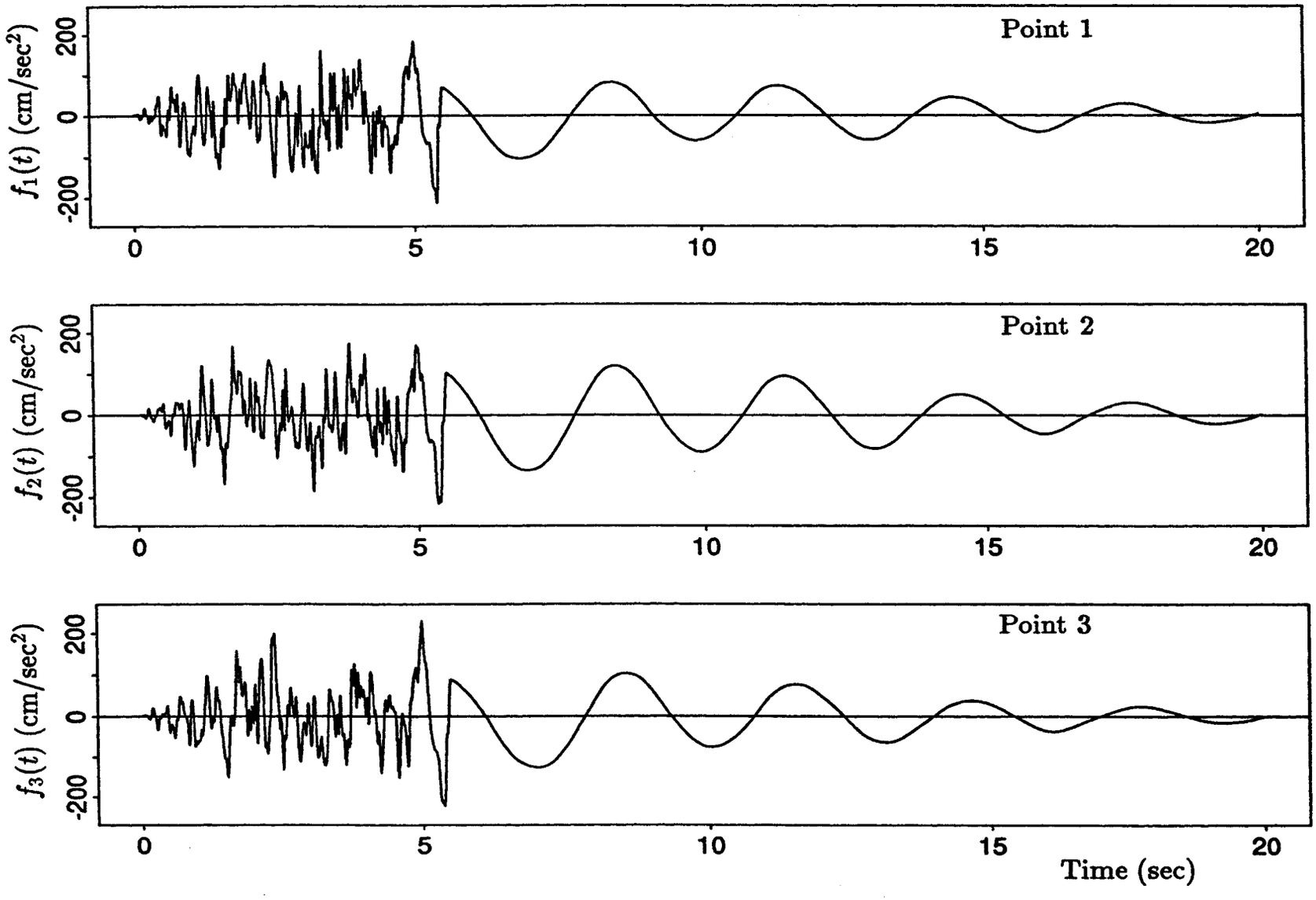

FIGURE 2-12 Generated sample function for the acceleration at points 1, 2 and 3, over a length equal to 20 sec (Example 2).

described by the coherence functions $\gamma_{jk}(\omega)$; $j,k = 1,2,3$; $j \neq k$ [refer to Eqs. (2-43), (2-44) and (2-49)]. Finally, it is possible to show that the ensemble auto-/cross-correlation function converges to the target auto-/cross-correlation function as the number of sample functions increases (refer to the first numerical example for a similar demonstration).

2.5.3 Example 3

In the first two numerical examples, sample functions of ground motion time histories were generated according to a target cross-spectral density matrix. The only drawback in this approach is that it is often preferable to work with time histories that are compatible with prescribed response spectra, rather than with prescribed power spectral density functions (cross-spectral density matrix), as indicated earlier in "Simulation of Seismic Ground Motion Compatible With Prescribed Response Spectra." In order to address this issue in this numerical example, ground motion time histories are modeled as a uniformly modulated non-stationary stochastic vector process, but unlike the first example, sample functions will be now generated to be compatible with prescribed response spectra.

The acceleration time histories at three points on the ground surface along the line of main wave propagation are considered one more time to be a tri-variate non-stationary stochastic vector process. The configuration of the three points is shown in Fig. 2-13 where the arrow indicates the direction of wave propagation. The simulated earthquake ground motion at points 1, 2 and 3 will have the following characteristics:

(1) Points 1, 2 and 3 correspond to different local soil conditions. Specifically, point 1 corresponds to the Uniform Building Code's Soil Type 1 (rock and stiff soils), point 2 to Soil Type 2 (deep cohesionless or stiff clay soils), and point 3 to Soil Type 3 (soft to medium clays and sands).

(2) The acceleration time histories at these three points will be correlated according to a prescribed coherence function and they will reflect the wave propagation effect according to a specified velocity of wave propagation.

(3) Finally, the amplitude variation as a function of time of the acceleration time histories at these three points will be described by prescribed modulating functions $A_j(\omega,t)$; $j = 1,2,3$.

The three components of the tri-variate non-stationary stochastic vector process describing the acceleration time histories at points 1, 2 and 3 (see Fig. 2-13) are denoted by $f_1^0(t)$, $f_2^0(t)$ and $f_3^0(t)$, respectively.

The acceleration response spectra specified by the Uniform Building Code (International Conference of Building Officials 1994) are selected for the three points in Fig. 2-13. For the purposes of this numerical example, the peak ground acceleration is set equal to 200 cm/sec^2 and the corresponding Uniform Building Code (UBC) acceleration response spectra $RSA_j(\omega)$; $j = 1,2,3$ are plotted in Fig. 2-14. It is reminded that sample functions of ground motion time histories will be generated to be compatible with these UBC response spectra.

The Abrahamson model (Abrahamson 1993) is chosen to describe the (stationary) coher-

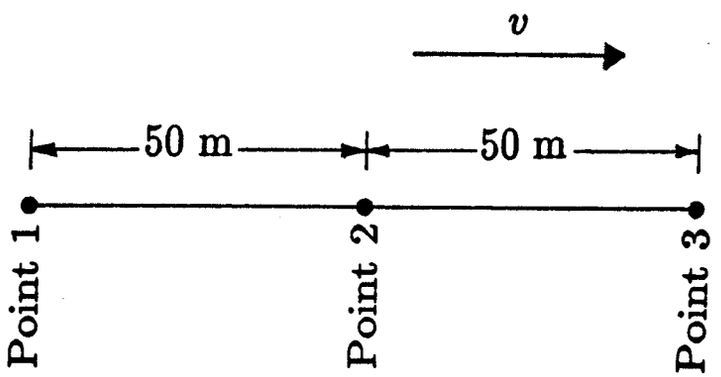

FIGURE 2-13 Configuration of points 1, 2 and 3 on the ground surface along the line of main wave propagation, for Example 3. Point 1 corresponds to rock and stiff soils (UBC Type 1), point 2 corresponds to deep cohesionless or stiff clay soils (UBC Type 2), and point 3 corresponds to soft to medium clays and sands (UBC Type 3).

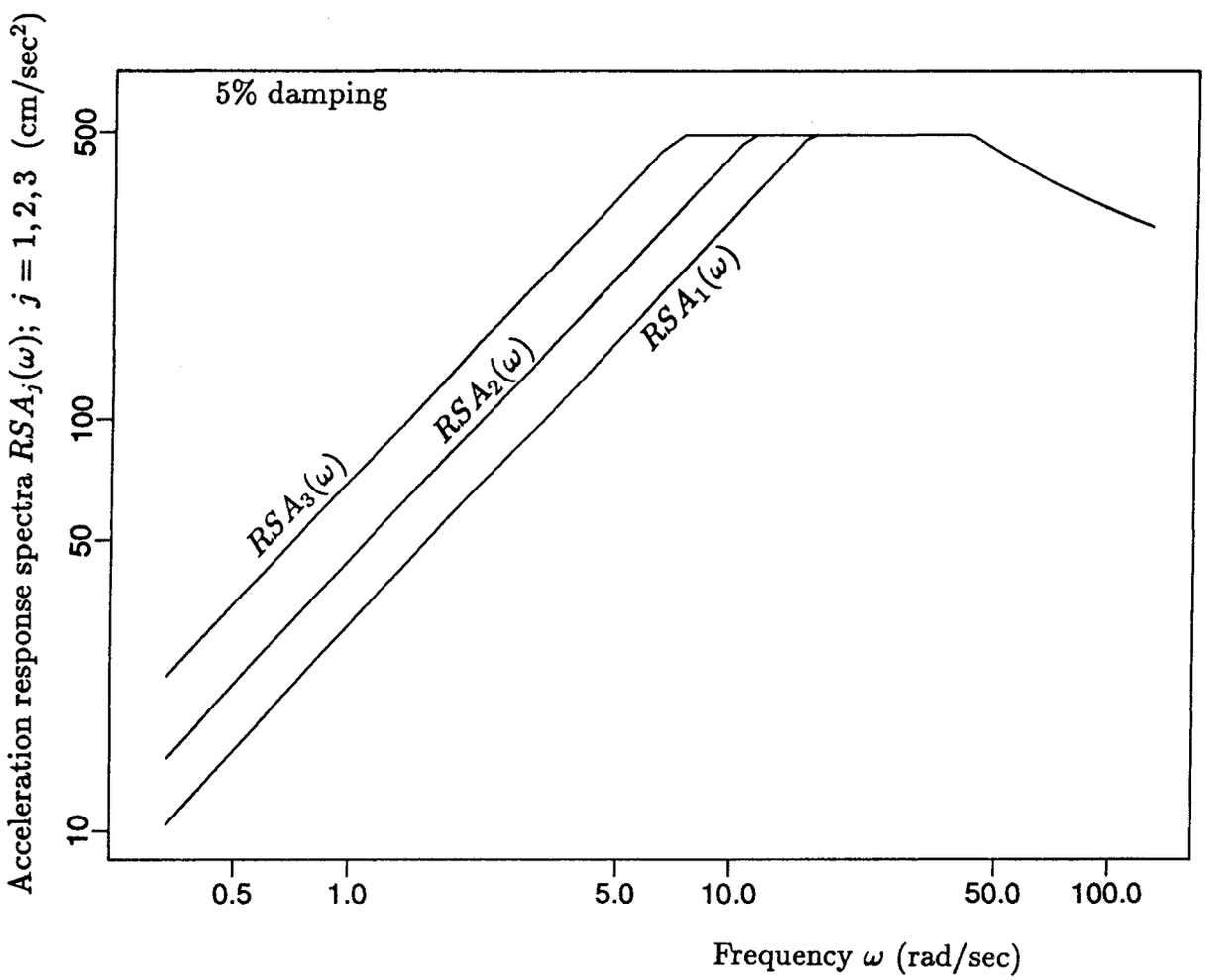

FIGURE 2-14 Uniform Building Code acceleration response spectra $RSA_j(\omega)$; $j = 1, 2, 3$, assigned to points 1, 2 and 3 (see Fig. 13), respectively. Point 1 corresponds to rock and stiff soils (UBC Type 1), point 2 corresponds to deep cohesionless or stiff clay soils (UBC Type 2), and point 3 corresponds to soft to medium clays and sands (UBC Type 3) (Example 3).

ence functions $\gamma_{jk}(\omega)$; $j,k=1,2,3$; $j \neq k$ between $f_j^0(t)$ and $f_k^0(t)$:

$$\gamma_{jk}(\omega) = \frac{1}{1+\left[\frac{\omega}{2\pi c_8(\xi_{jk})}\right]^6} \cdot \tanh\left\{ \frac{c_3(\xi_{jk})}{1+\frac{\omega}{2\pi}c_4(\xi_{jk})+\frac{\omega^2}{4\pi^2}c_7(\xi_{jk})} + [4.80 - c_3(\xi_{jk})] \cdot \right.$$
$$\left. \cdot \exp\left[c_6(\xi_{jk})\frac{\omega}{2\pi}\right] + 0.35 \right\} ; \quad j,k=1,2,3;\ j \neq k \quad (2-60)$$

where ξ_{jk} is the distance between points j and k, and:

$$c_3(\xi_{jk}) = \frac{3.95}{\left(1+0.0077\xi_{jk}+0.000023\xi_{jk}^2\right)} + 0.85\ \exp\{-0.00013\xi_{jk}\} \quad (2-61)$$

$$c_4(\xi_{jk}) = \frac{0.4\left[1-\frac{1}{1+\left(\frac{\xi_{jk}}{5}\right)^3}\right]}{\left[1+\left(\frac{\xi_{jk}}{190}\right)^8\right]\left[1+\left(\frac{\xi_{jk}}{180}\right)^3\right]} \quad (2-62)$$

$$c_6(\xi_{jk}) = 3\left(\exp\left\{-\frac{\xi_{jk}}{20}\right\}-1\right) - 0.0018\xi_{jk} \quad (2-63)$$

$$c_7(\xi_{jk}) = -0.598 + 0.106\ \ln(\xi_{jk}+325) - 0.0151\ \exp\{-0.6\xi_{jk}\} \quad (2-64)$$

$$c_8(\xi_{jk}) = \exp\{8.54 - 1.07\ \ln(\xi_{jk}+200)\} + 100\ \exp\{-\xi_{jk}\} \quad (2-65)$$

Abrahamson's model for the coherence function has the advantage that it can be used for a broad range of soil conditions (Abrahamson 1993). The $\gamma_{jk}(\omega)$; $j,k=1,2,3$; $j \neq k$ defined in Eqs. (2-60)-(2-65) are plotted in Fig. 2-15. The velocity of wave propagation v is set equal to:

$$v = 2{,}000 \text{ m/sec} \quad (2-66)$$

so that the complex coherence functions can be expressed as:

$$\Gamma_{jk}(\omega) = \gamma_{jk}(\omega) \cdot \exp\left[-i\ \frac{\omega\ \xi_{jk}}{v}\right] ; \quad j,k=1,2,3;\ j \neq k \quad (2-67)$$

At this point, the reader is referred to an important note concerning the case of differential (asynchronous) support ground motion when the bridge supports are on different local soil conditions found in the second paragraph of Chapter 2 "Generation of Spatially Varying Seismic Ground Motion Time Histories" (this is before the "Introduction" section of Chapter 2).

Since the acceleration time histories $f_j^0(t)$; $j=1,2,3$ are modeled as a uniformly modulated non-stationary stochastic vector process, the modulating functions $A_j(\omega,t)$; $j=1,2,3$ will be functions of time only. In order to control the duration of strong ground motion, the

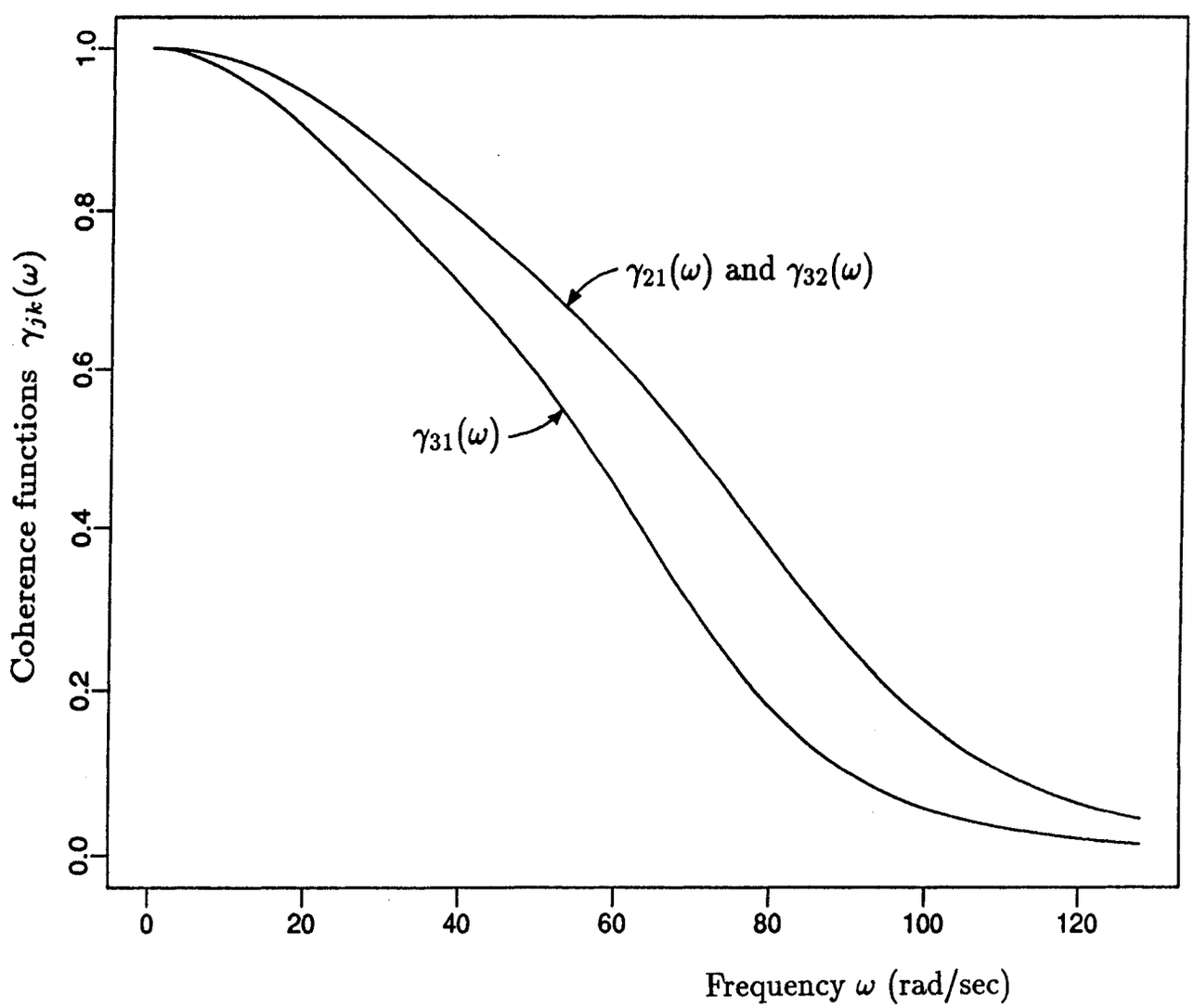

FIGURE 2-15 Coherence functions $\gamma_{21}(\omega)$, $\gamma_{31}(\omega)$ and $\gamma_{32}(\omega)$, for Example 3 (Abrahamson's model).

model suggested by Jennings, Housner and Tsai (1968) is selected for the modulating functions $A_j(t)$; $j = 1, 2, 3$. Figure 2-16 plots $A_1(t)$ and indicates the numerical values chosen for all the parameters [$A_2(t)$ and $A_3(t)$ have the same form as $A_1(t)$, but they are shifted by ξ_{21}/v and ξ_{31}/v, respectively, to include the wave propagation effect in the same way as in Eq. (2-45)].

The generation of sample functions of the acceleration time histories at the three points shown in Fig. 2-13 will be performed using the iterative scheme shown in Table 2-1 (refer to "Simulation of Seismic Ground Motion Compatible With Prescribed Response Spectra"). According to Table 2-1, the power spectral density functions $S_j(\omega)$; $j = 1, 2, 3$ must be initialized by setting them equal to a constant value over the entire frequency range. This value can be selected arbitrarily and in this example is set equal to:

$$S_j(\omega) = 100 \text{ cm}^2/\text{sec}^3 \; ; \quad j = 1, 2, 3 \qquad (2-68)$$

while the upper cut-off frequency ω_u and the value of N [see Eq. (2-27)] are set equal to:

$$\omega_u = 128 \text{ rad/sec} \qquad \text{and} \qquad N = 128 \qquad (2-69)$$

The simulation is performed at 6,144 time instants, with a time step $\Delta t = 3.07 \cdot 10^{-3}$ sec, over a length equal to $6,144 \cdot 3.07 \cdot 10^{-3} = 18.85$ sec. One sample function for the acceleration at points 1, 2 and 3 (see Fig. 2-13), denoted by $f_1(t)$, $f_2(t)$ and $f_3(t)$, respectively, is generated after 10 iterations and displayed in Fig. 2-17.

As in the previous two examples, it is possible to detect the following characteristics in the time histories shown in Fig. 2-17: (1) their mutual correlation according to the coherence functions defined in Eqs. (2-60)-(2-65), (2) the wave propagation effect according to a velocity of wave propagation $v = 2,000$ m/sec, (3) their amplitude variation as a function of time according to the modulating function plotted in Fig. 2-16. In this example, however, the main objective is to generate acceleration time histories that will be compatible with prescribed response spectra. For this purpose, the acceleration response spectra $RSA^{(f_j)}(\omega)$; $j = 1, 2, 3$ computed using the ground motion time histories shown in Fig. 2-17 should be compared with the target UBC response spectra $RSA_j(\omega)$; $j = 1, 2, 3$ plotted in Fig. 2-14. This comparison is carried out in Fig. 2-18, where it can be seen that the 10 iterations performed to obtain the sample function shown in Fig. 2-17 are enough for an excellent match at every frequency.

The iterative scheme shown in Table 2-1 is therefore capable to simulate seismic ground motion time histories that: (1) are compatible with prescribed response spectra (that can be different at different points on the ground surface), (2) are correlated according to a given coherence function, (3) include the wave propagation effect, and (4) have an amplitude variation as a function of time according to a prescribed modulating function. At this point, the reader is referred again to an important note concerning the case of differential (asynchronous) support ground motion when the bridge supports are on different local soil conditions found in the second paragraph of Chapter 2 "Generation of Spatially Varying Seismic Ground Motion Time Histories" (this is before the "Introduction" section of Chapter 2).

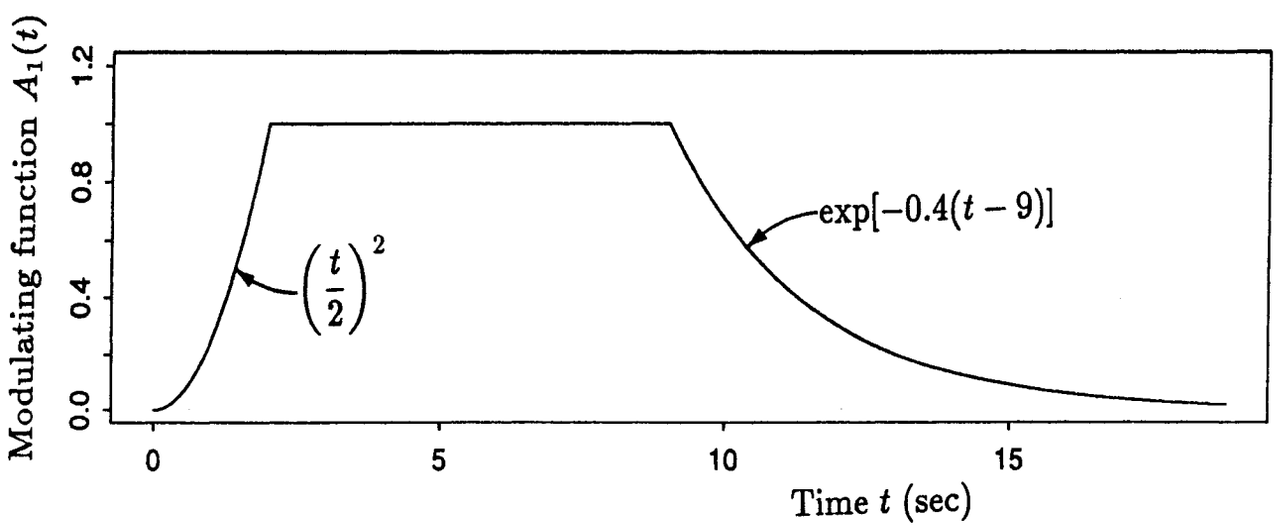

FIGURE 2-16 Modulating function $A_1(t)$, for Example 3 (Jennings, Housner, Tsai model).

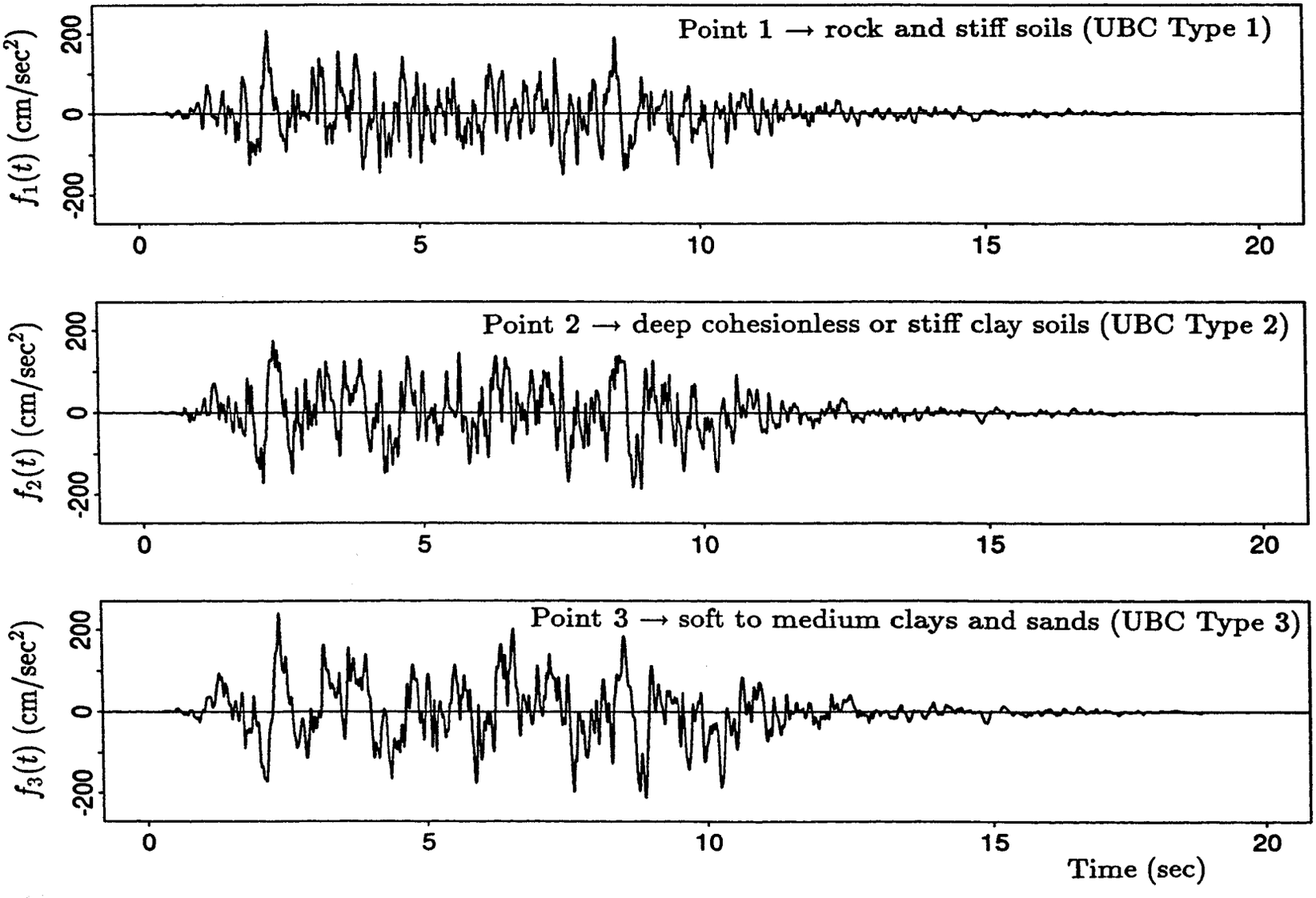

FIGURE 2-17 Generated sample function for the acceleration at points 1, 2 and 3, after 10 iterations, over a length equal to 18.85 sec (Example 3).

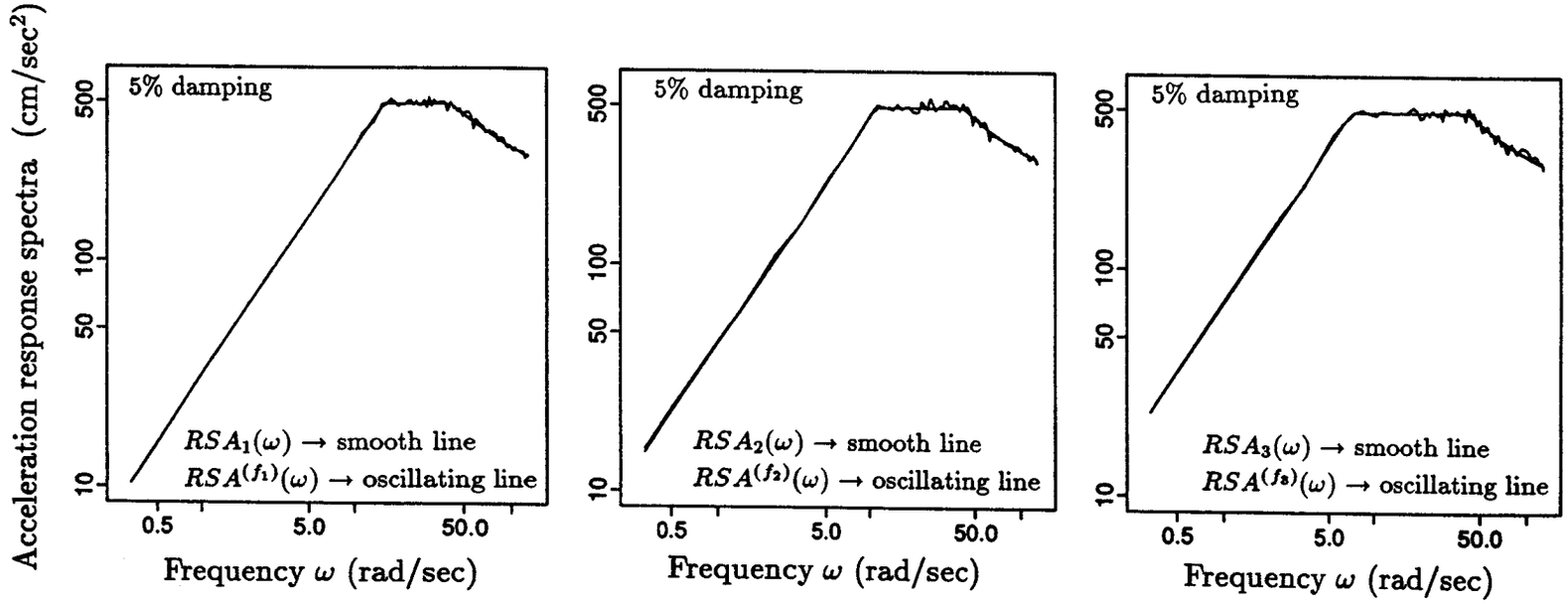

FIGURE 2-18 Acceleration response spectra $RSA^{(f_j)}(\omega)$; $j = 1, 2, 3$ computed using the generated acceleration time histories shown in Fig. 17 versus the UBC acceleration response spectra $RSA_j(\omega)$; $j = 1, 2, 3$.

2.6 Conclusions

A spectral-representation-based simulation algorithm was used to generate sample functions of a non-stationary, multi-variate stochastic process with evolutionary power, according to its prescribed non-stationary cross-spectral density matrix. If the components of the vector process correspond to different locations in space, then the process is also non-homogeneous in space (in addition to being non-stationary in time). The ensemble cross-correlation matrix of the generated sample functions is identical to the corresponding target and the generated sample functions are Gaussian in the limit as the number of terms in the frequency discretization of the cross-spectral density matrix approaches infinity.

For the important application of earthquake ground motion simulation which is the main objective of this report, an iterative scheme was introduced to generate seismic ground motion time histories at several locations on the ground surface that are compatible with prescribed response spectra, are correlated according to a given coherence function, include the wave propagation effect, and have a specified duration of strong ground motion.

Three examples involving simulation of earthquake ground motion were presented in order to demonstrate the capabilities of the proposed methodologies. In all three examples, the acceleration time histories at three points on the ground surface were considered to be a tri-variate, non-stationary stochastic vector process. In the first example, the time histories were modeled as a uniformly modulated non-stationary stochastic vector process, and sample functions were generated according to a target cross-spectral density matrix. In the second example, the time histories were modeled as a non-stationary stochastic vector process with amplitude and frequency modulation, and sample functions were again generated according to a target cross-spectral density matrix. Finally, in the third example, ground motion time histories were modeled as a uniformly modulated non-stationary stochastic vector process, but unlike the first example, sample functions were generated to be compatible with prescribed response spectra. The generated acceleration time histories at the three points were spatially correlated according to prescribed coherence functions (all three examples), included the wave propagation effect (examples one and three), and were non-homogeneous in space, or equivalently corresponded to different local soil conditions (examples one and three).

At this point, the reader is referred to an important note concerning the case of differential (asynchronous) support ground motion when the bridge supports are on different local soil conditions found in the second paragraph of Chapter 2 "Generation of Spatially Varying Seismic Ground Motion Time Histories" (this is before the "Introduction" section of Chapter 2).

The generated ground motion time histories can be directly used as input for the dynamic seismic analysis of elongated structures such as bridges, lifelines, retaining walls, etc., as will be demonstrated in Chapters 3 and 4.

SECTION 3
PRELIMINARY ANALYSIS OF A SET OF HIGHWAY BRIDGES TO ESTIMATE THE EFFECT OF SPATIAL VARIATION OF SEISMIC GROUND MOTION

3.1 Introduction - Objectives - Approach

The main objective of this chapter is to provide a first estimate of the effect of spatial variability of seismic ground motion on the response of a large range of different highway bridges subjected to a variety of input ground motions. Another important objective of this chapter is to determine which set of bridges and which cases of spatially varying seismic ground motion require a more detailed study, in order to eventually establish practical guidelines.

The methodology developed in Chapter 2 to generate spatially varying seismic ground motion time histories will be used in this chapter to provide the input for the dynamic time history analysis of a number of typical highway bridges. According to this methodology, seismic ground motion time histories are modeled as stochastic vector processes. Consequently, a Monte Carlo simulation approach will be followed to estimate the structural response by performing time history analyses. As the studies in this chapter were decided to be preliminary, it was attempted to examine a set of representative highway bridges under a very wide range of different cases of spatially varying seismic ground motion. For this reason, only a relatively small number of samples was considered along the lines of the Monte Carlo simulation approach. The objective, therefore, was not to estimate the statistics of the structural response with high accuracy, but to determine which bridges and which cases of ground motion necessitated further study.

In order to achieve the aforementioned objectives each one of the selected bridges is subjected to a number of scenario earthquakes. For each scenario earthquake, the bridge under consideration is analyzed (dynamically) using identical and differential support ground motion. The following ratio is then computed for each section of the bridge in order to quantify the effect of the spatial variation of ground motion on the response of the structure:

$$\rho = \frac{\text{max of response quantity computed using differential support ground motion}}{\text{max of same quantity computed using identical support ground motion}} \qquad (3-1)$$

The response quantity appearing in the above equation can be the moment at some critical point of the structure, the ductility demand at a certain location, the opening or closing of a hinge, etc.

It is obvious that the ratio ρ indicates the increase ($\rho > 1$) or decrease ($\rho < 1$) in the maximum value of the response quantity under consideration caused by differential support ground motion, compared to the corresponding case of identical support ground motion.

Eight bridges have been selected for a comparative study with total lengths ranging from 111 ft up to 1,584 ft, and with number of spans ranging from 3 up to 10. This selection was

done in an effort to relate the values of ρ in Eq. (3-1) to the length of the largest span or the total length of the bridge. Linear as well as nonlinear dynamic analyses of these eight bridges were performed using two-dimensional finite element models. All eight bridges in this group were subjected to the same ground motion cases for comparison purposes. It was also assumed that all the supports of these eight bridges are on the same local soil conditions.

In order to estimate the effect of different local soil conditions, one of the above eight bridges was then analyzed considering that some of its supports are on softer local soil conditions than the rest. Nonlinear dynamic analyses were performed using again a two-dimensional finite element model. This same bridge was also analyzed twenty times using twenty different sets of ground motion time histories reflecting the same scenario earthquake. This was done in order to examine the variation in the ρ values (Eq. (3-1)) resulting from the Monte Carlo simulation procedure that was followed (in most other cases there were only five different sets of ground motion time histories reflecting the same scenario earthquake).

Finally, two bridges were modeled linearly in three dimensions in order to study the effect of different angles of incidence of the seismic waves with respect to the axis of the bridge and to examine the effect of the vertical component of ground motion. It was assumed that all the supports of these two bridges were on the same local soil conditions. A detailed sensitivity analysis with respect to the value of the apparent velocity of wave propagation was carried out for one of these two bridges (in most other cases there were only three different apparent velocities of wave propagation that have been considered).

3.2 Comparative Analysis of Eight Bridges

3.2.1 Introduction

Eight bridges were selected for this comparative study representing a wide range of number of spans and total lengths. The reason for this selection is that an effort will be made to relate the values of ρ in Eq. (3-1) to the length of the largest span or the total length of a bridge. The total lengths of these eight bridges range from 111 ft to 1,584 ft. The number of spans range from 3 to 10. Linear and nonlinear dynamic analyses of these eight bridges are performed using two-dimensional finite element models. All eight bridges in this group are subjected to the same ground motion cases for comparison purposes. It is also assumed that all the supports of these eight bridges are on the same local soil conditions.

3.2.2 Description of the Eight Bridges

Table 3-1 provides information about the number of spans, largest span, total length, and number of expansion joints of the eight bridges considered.

The "Text Example Bridge" has three spans and a total length of 111 ft. The plan and the elevation of the bridge are displayed in Fig. 3-1. Table 3-2 provides information about the moment of inertia, cross sectional area, mass density, and elastic modulus of the girders and the columns of the bridge.

TABLE 3-1

Basic Characteristics of Eight Bridges
Considered in Comparative Study

Bridge Name	Number of Spans	Largest Span (ft)	Total Length (ft)	Number of Expansion Joints
Text Example Bridge	3	44	111	0
Aptos Creek Bridge	5	56	256	1
FHWA-No.2 Bridge	3	152	400	0
TY0H Example Bridge	5	175	795	0
TY1H Example Bridge	5	175	795	1
TY2H Example Bridge	5	175	795	2
Gavin Canyon Bridge	5	208	741	2
SR14/I5 Viaduct	10	206	1,584	4

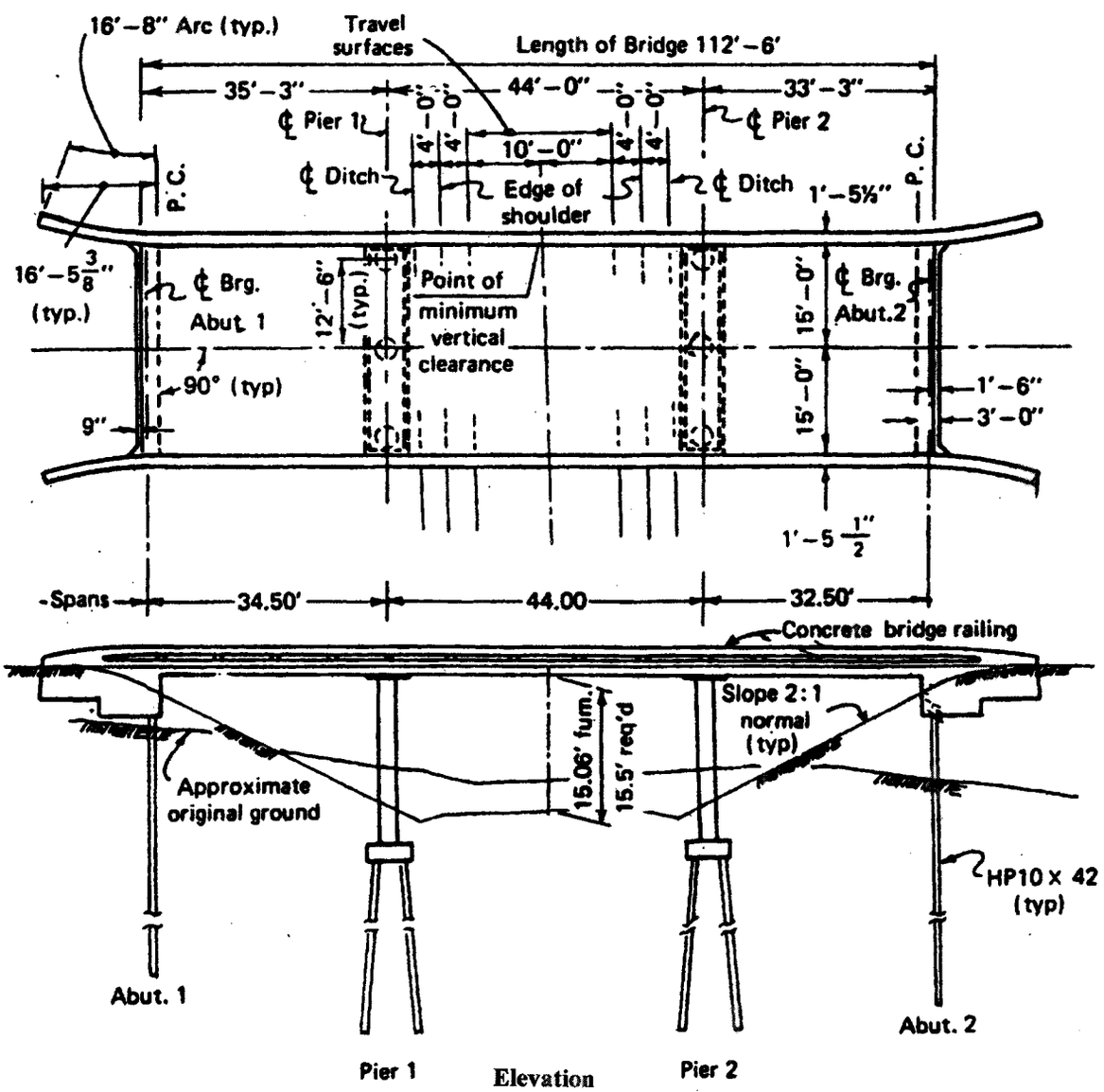

FIGURE 3-1 Plan and Elevation of Text Example Bridge (Heins and Lawrie (1984)).

TABLE 3-2 Material and Cross Sectional Properties of Analysis Model for TEXT Bridge Using SAP2000

Structural Component	Moment of Inertia (ft^4)	Cross Sectional Area (ft^2)	Mass Density (pcf)	Young's Modulus (Ksi)
Girders	10.89	62.09	150	3605
Piers	6.36	14.73	150	3605

The "Aptos Creek Bridge" has five spans and a total length of 256 ft. The elevation and section views of the bridge are displayed in Fig. 3-2. Table 3-3 provides information about the moment of inertia, cross sectional area, mass density, and elastic modulus of the deck and the columns of the bridge.

The "FHWA No. 2 Bridge" has three spans and a total length of 400 ft. The plan and elevation of the bridge are displayed in Fig. 3-3. Table 3-4 provides information about the moment of inertia, cross sectional area, mass density, and elastic modulus of the girders and the columns of the bridge.

The "TY0H Example Bridge" has five spans and a total length of 795 ft. The elevation and section views of the bridge are displayed in Fig. 3-4. Table 3-5 provides information about the moment of inertia, cross sectional area, mass density, and elastic modulus of the girders and the columns of the bridge.

The "TY1H Example Bridge" has five spans and a total length of 795 ft. The elevation and section views of the bridge are displayed in Fig. 3-5. Table 3-6 provides information about the moment of inertia, cross sectional area, mass density, and elastic modulus of the girders and the columns of the bridge.

The "TY2H Example Bridge" has five spans and a total length of 795 ft. The elevation and section views of the bridge are displayed in Fig. 3-6. Table 3-7 provides information about the moment of inertia, cross sectional area, mass density, and elastic modulus of the girders and the columns of the bridge.

The "Gavin Canyon Bridge" has five spans and a total length of 741 ft. The elevation and section views of the bridge are displayed in Fig. 3-7. Table 3-8 provides information about the moment of inertia, cross sectional area, mass density, and elastic modulus of the girders and the columns of the bridge.

The "SR14/I5 Viaduct" has ten spans and a total length of 1,584 ft. The elevation and section views of the bridge are displayed in Fig. 3-8. Table 3-9 provides information about the moment of inertia, cross sectional area, mass density, and elastic modulus of the girders and the columns of the bridge.

3.2.3 Finite Element Models of the Eight Bridges

The motion of interest in this comparative study is the motion of the center axis of each bridge. For this reason, each bridge is modeled in two dimensions using frame elements. The section properties of these elements are chosen to represent the actual cross-sections of the bridges. Information about the cross-sectional area and moment of inertia of the different sections of each bridge is provided in Tables 3-2 to 3-9.

The computer code SAP90 beta version is selected to perform the dynamic time history analyses. Both linear and nonlinear models are created for each bridge and corresponding analyses are carried out. A relatively simple model is used to perform the nonlinear dynamic analyses. This appears quite appropriate considering the various types of approximation in modeling the structures, and the uncertainty involved in specifying the input ground motion. The model used here for the piers of all eight bridges (the only

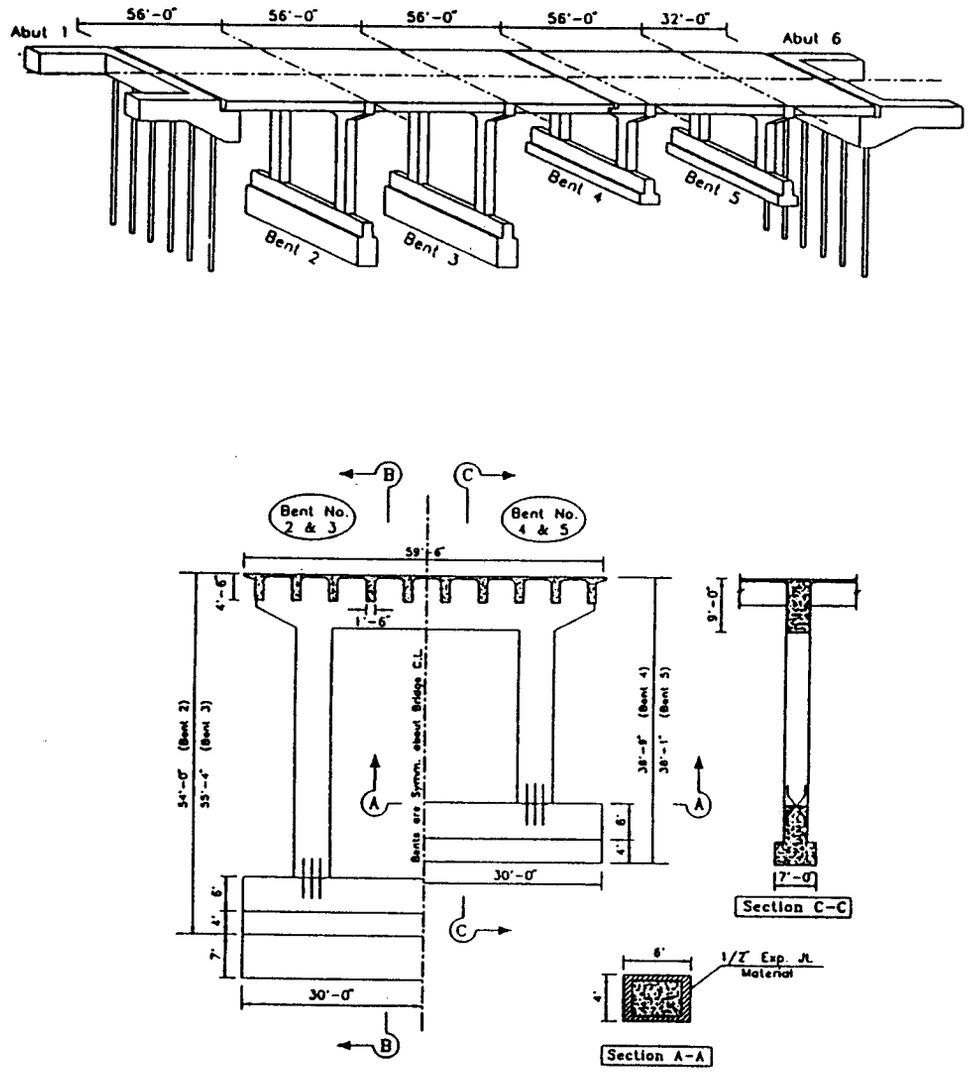

FIGURE 3-2 Schematic Drawing and Section Views of Aptos Creek Bridge (Abdel Ghaffar et al. (1997)).

TABLE 3-3 Material and Cross Sectional Properties of Analysis Model for Aptos Creek Bridge Using SAP2000

Structural Component	Moment of Inertia (ft^4)	Cross Sectional Area (ft^2)	Mass Density (pcf)	Young's Modulus (Ksi)
Deck	205.54	89.75	175	3122
Piers	64.00	48.00	150	3122

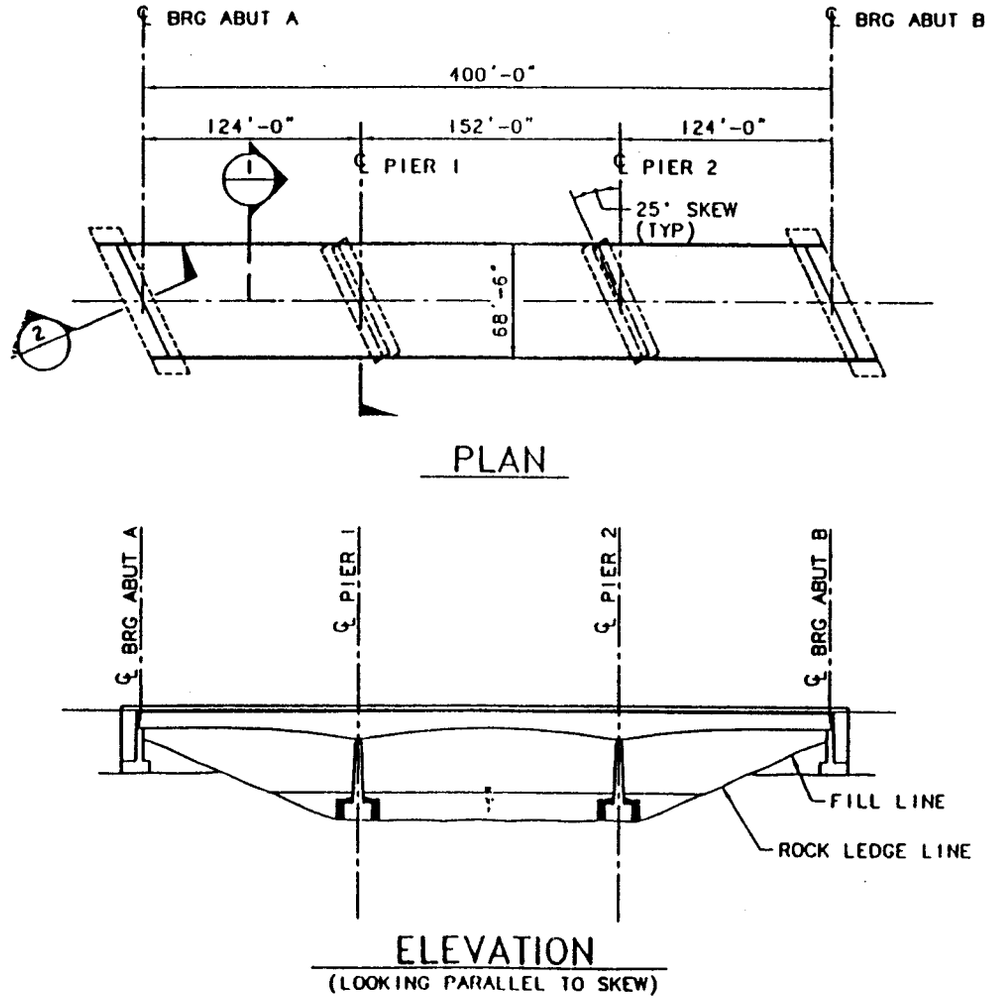

FIGURE 3-3 Plan and Elevation of FHWA-No.2 Example Bridge.

TABLE 3-4 Material and Cross Sectional Properties of Analysis Model for FHWA Bridge Using SAP2000

Structural Component	Moment of Inertia (ft^4)		Cross Sectional Area (ft^2)	Mass Density (pcf)	Young's Modulus (Ksi)
	About. Horizontal. Axis	About Vertical Axis			
Girder Section at A, F	296	36207	81.00	166	3605
Girder Section at B	311	36353	81.30	166	3605
Girder Section at C	473	37607	84.30	162	3605
Girder Section at D	996	45998	104.00	143	3605
Girder Section at E	417	37206	83.40	163	3605
Pier Section at G	12.56		12.56	150	3605
Pier Section at H	16.47		14.38	150	3605
Pier Section at I	21.22		16.33	150	3605
Pier Section at J	63.62		18.27	150	3605
Pier Section at K	3217.99		201.06	150	3605

TABLE 3-4 (cont'd) Material and Cross Sectional Properties of Analysis Model for FHWA Bridge Using SAP2000

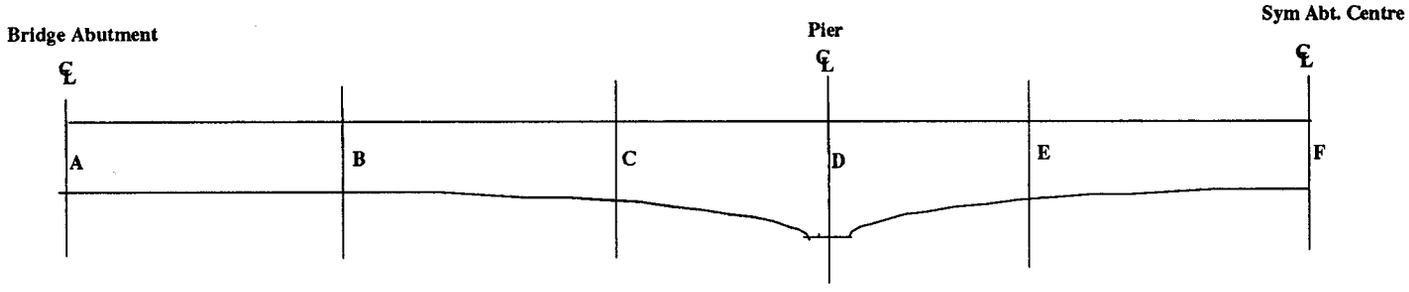

Girder Elevation

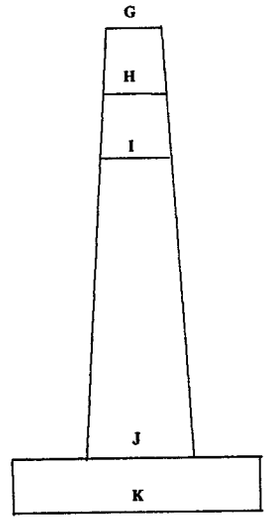

Typical Pier

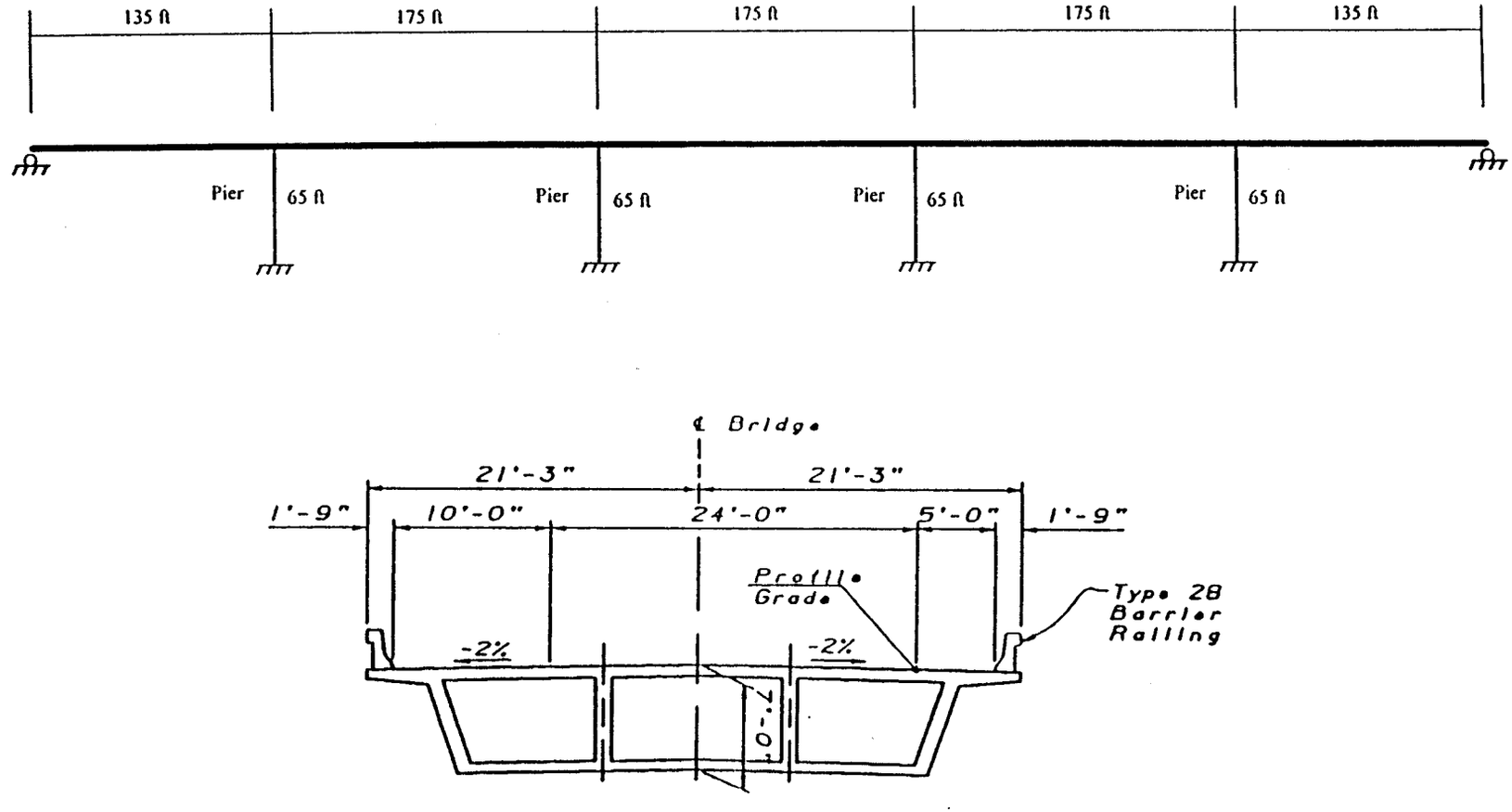

FIGURE 3-4 Elevation and Section Views of TY0H Example Bridge (Sultan).

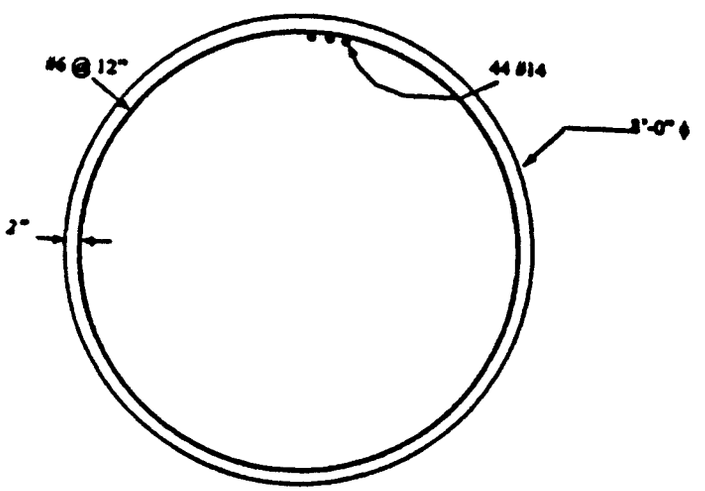

All reinforcement not shown.

FIGURE 3-4 (cont'd) Cross-Section of Piers of TY0H Example Bridge.

TABLE 3-5 Material and Cross Sectional Properties of Analysis Model for TYOH Bridge Using SAP2000

Structural Component	Moment of Inertia (ft^4)	Cross Sectional Area (ft^2)	Mass Density (pcf)	Young's Modulus (Ksi)
Girders	554.8	74.7	145	4031
Piers	201.1	50.3	145	4031

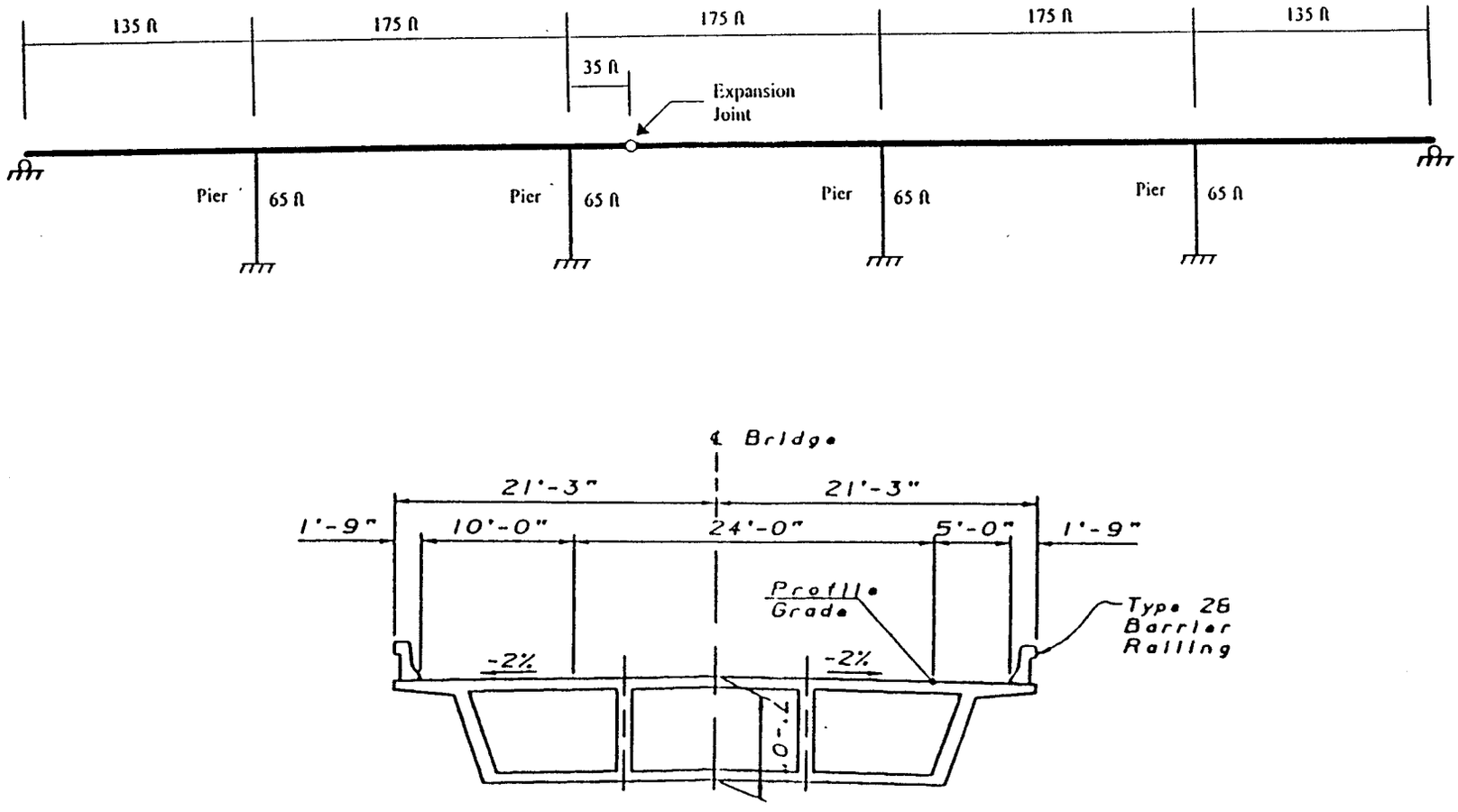

FIGURE 3-5 Elevation and Section Views of TY1H Example Bridge (Sultan).

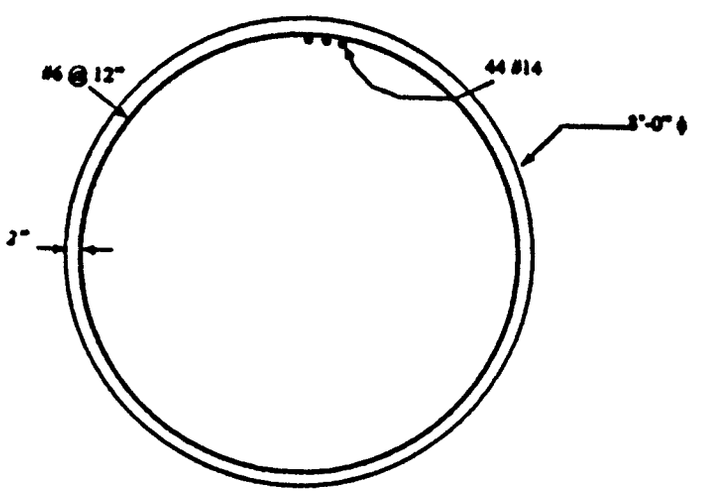

All reinforcement not shown.

FIGURE 3-5 (cont'd) Cross-Section of Piers of TY1H Example Bridge.

TABLE 3-6 Material and Cross Sectional Properties of Analysis Model for TY1H Bridge Using SAP2000

Structural Component	Moment of Inertia (ft^4)	Cross Sectional Area (ft^2)	Mass Density (pcf)	Young's Modulus (Ksi)
Girders	554.8	74.7	145	4031
Piers	201.1	50.3	145	4031

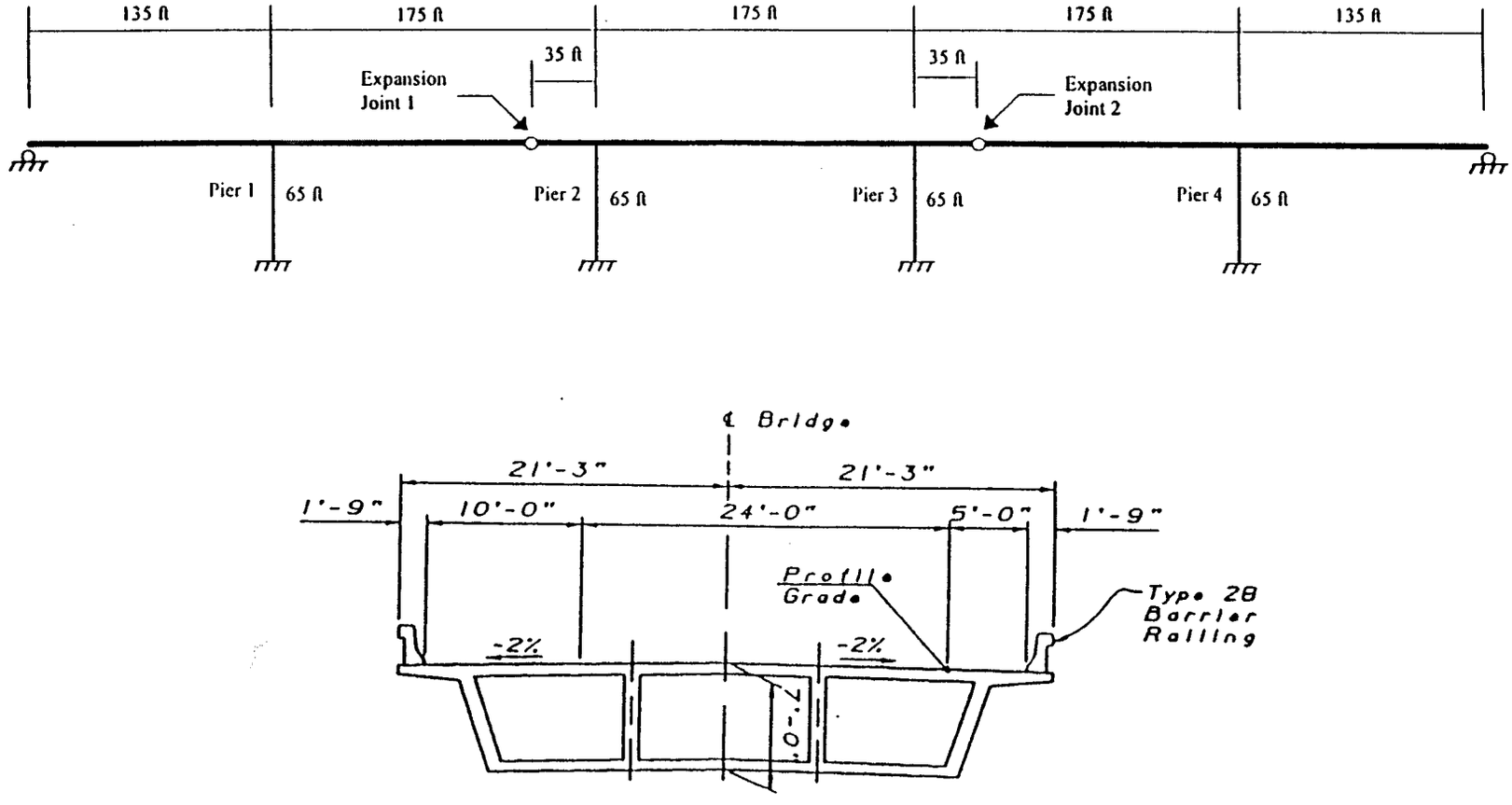

FIGURE 3-6 Elevation and Section Views of TY2H Example Bridge.

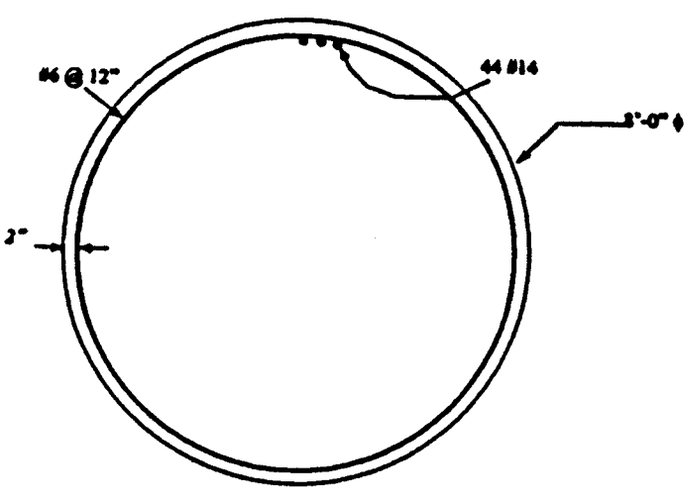

All reinforcement not shown.

FIGURE 3-6 (cont'd) Cross-Section of Piers of TY2H Example Bridge.

TABLE 3-7 Material and Cross Sectional Properties of Analysis Model for TY2H Bridge Using SAP2000

Structural Component	Moment of Inertia (ft^4)	Cross Sectional Area (ft^2)	Mass Density (pcf)	Young's Modulus (Ksi)
Girders	554.8	74.7	145	4031
Piers	201.1	50.3	145	4031

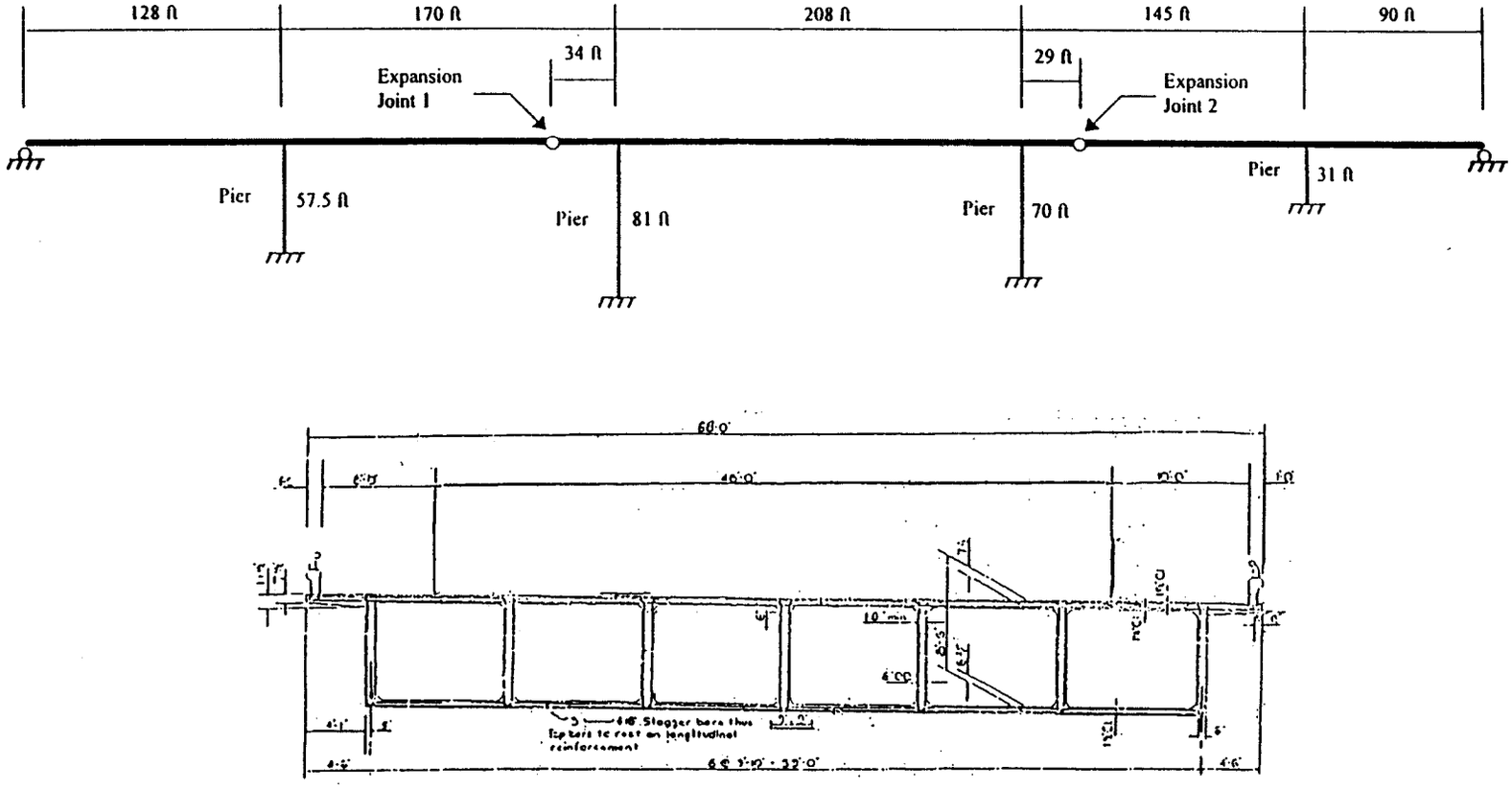

FIGURE 3-7 Elevation and Section Views of Gavin Canyon Bridge.

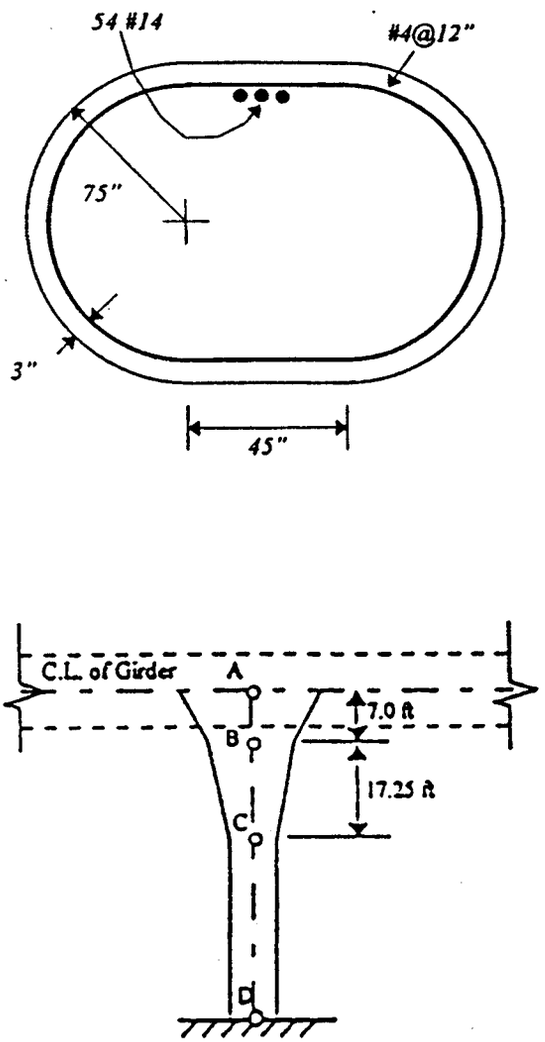

All reinforcement not shown. Weak axis ⟶ longitudinal direction.

FIGURE 3-7 (cont'd) Cross-Section and Elevation of Piers of Gavin Canyon Bridge.

TABLE 3-8 Material and Cross Sectional Properties of Analysis Model for Gavin Canyon Bridge Using SAP2000

Structural Component	Moment of Inertia (ft^4)	Cross Sectional Area (ft^2)	Mass Density (pcf)	Young's Modulus (Ksi)
RC Girders	1335.28	119.05	145	4031
PC Girders	1436.29	127.60	145	4415
Pier (AB*)	867.00	281.80	145	4031
Piers (BC*)	435.40	147.80	145	4031
Piers (CD*)	319.40	111.60	145	4031

Note = *

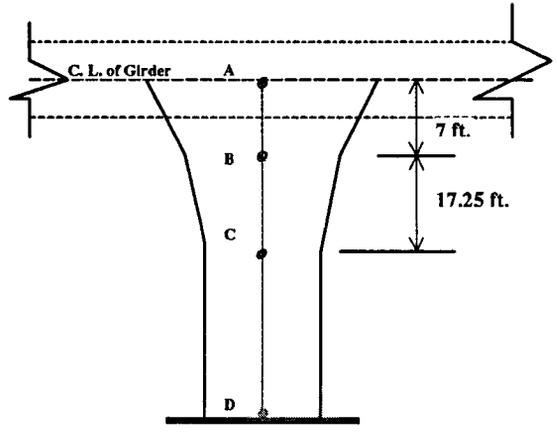

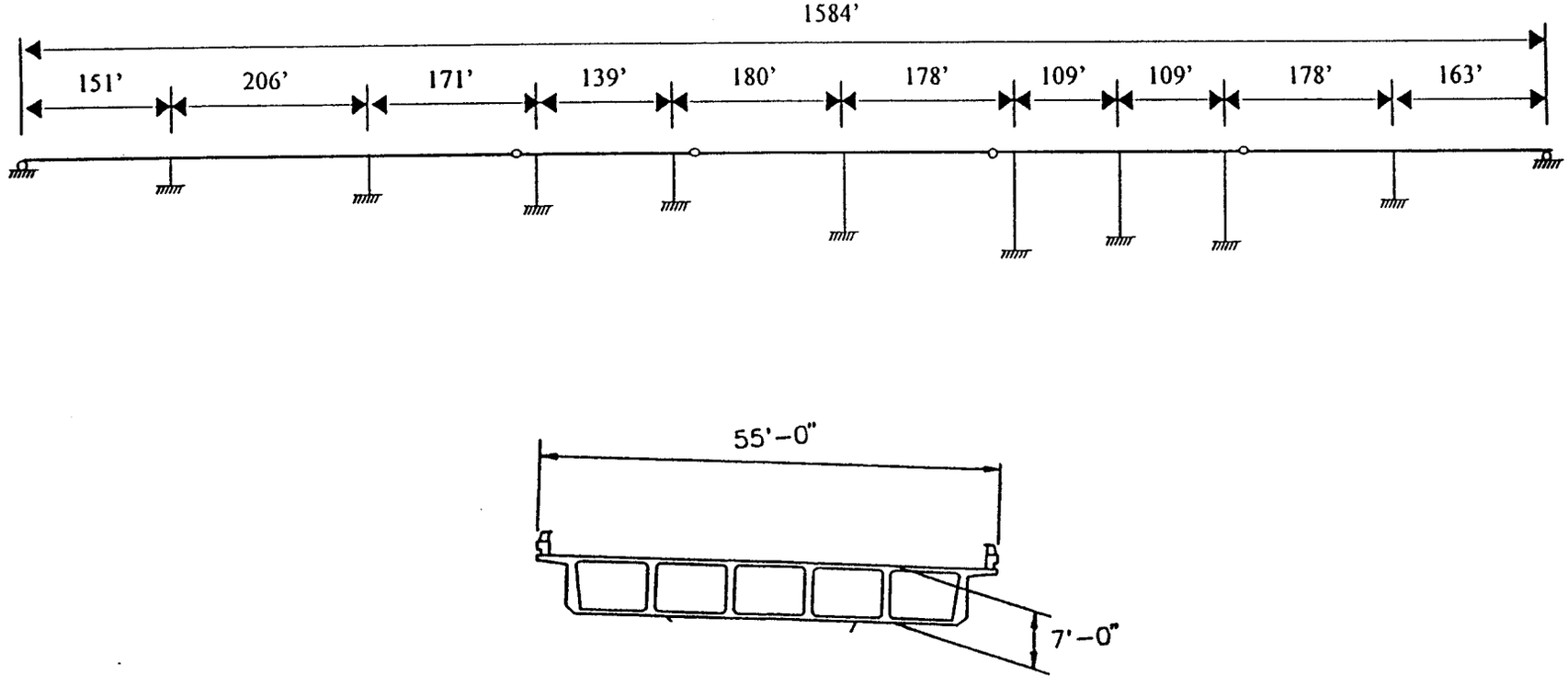

FIGURE 3-8 Elevation and Section Views of SR14/I5 Interchange.

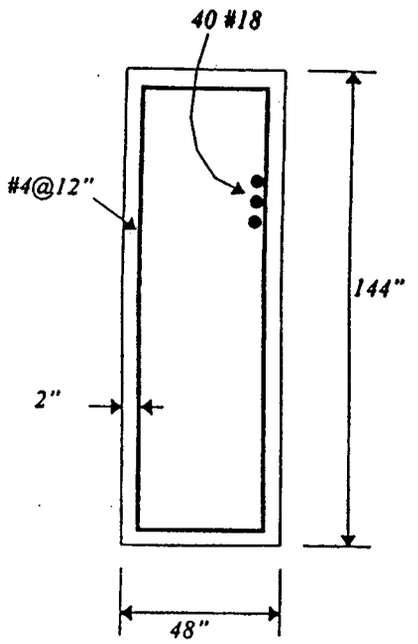

Piers 1&2

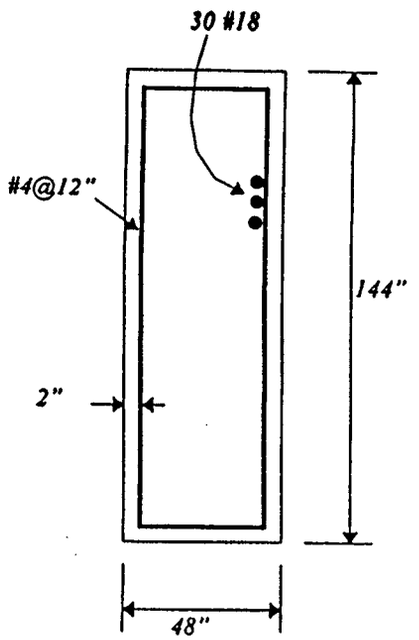

Piers 3,4 & 9

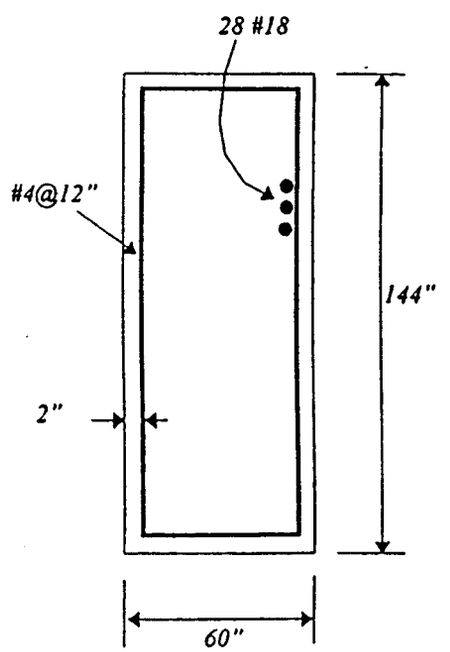

Pier 5

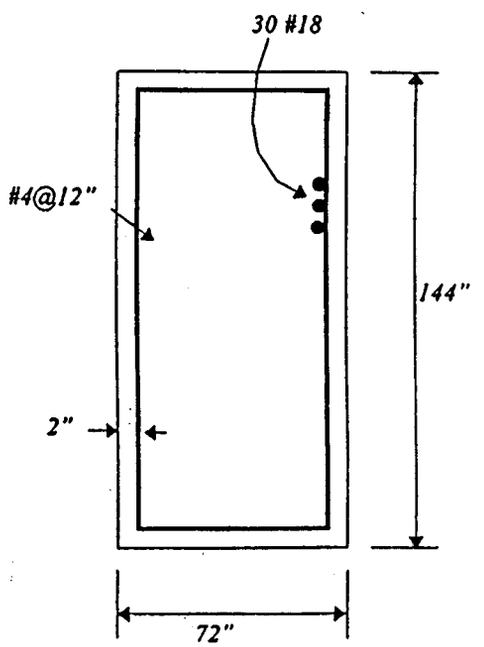

Piers 6,7 & 8

All reinforcement not shown.

Weak axis ⟶ longitudinal direction.

FIGURE 3-8 (cont'd) Cross-Section of Piers of SR14/I5 Interchange.

TABLE 3-9 Material and Cross Sectional Properties of Analysis Model for SR14/15 Bridge Using SAP2000

Structural Component	Moment of Inertia (ft^4)			Cross Sectional Area (ft^2)			Mass Density (pcf)	Young's Modulus (Ksi)
RC Girders	392.87			74.72			150	4031
Pier Type 1	AB*	BC*	CD*	AB*	BC*	CD*	150	4031
	131.17	94.03	56.90	101.27	73.27	45.27		
Pier Type 2	244.50	171.68	98.86	109.5	74.5	39.5	150	4031
Pier Type 3	407.98	281.63	155.76	127.25	85.125	43.125	150	4031

Note = *

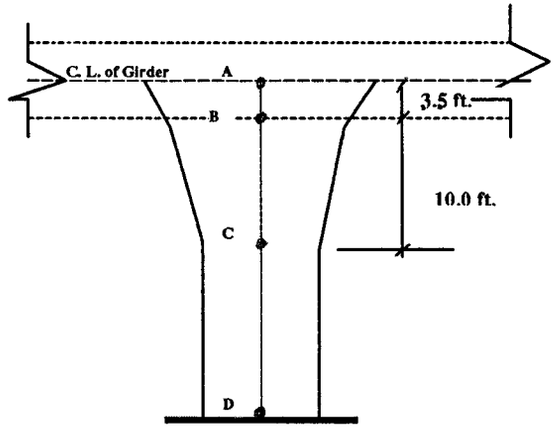

members considered to exhibit nonlinear behavior in this study) is depicted in Fig. 3-9a. According to this model, a pier is modeled as an elastic column of length $2H_e$, with a pair of plastic zones of length L_p at each end of the column, as shown in Fig. 3-9a. The total length H of the pier from the ground to the soffit of the girder is therefore equal to $2(H_e + L_p)$. The plastic zone is then modeled to consist of a nonlinear rotational spring and a rigid element of length L_p as shown in Fig. 3-9b. The typical moment-rotation relationship used in this study for the nonlinear springs is shown in Fig. 3-9c. Its parameters are established using the *Column Ductility Program* COLx (Caltrans 1993). The specific moment-curvature relationships resulting from the COLx program are displayed in Figs. 3-10 to 3-14 (it should be mentioned that the Aptos Creek bridge is analyzed only linearly). For those bridges with expansion joints (the Aptos Creek, TY1H, TY2H, Gavin Canyon, and SR14/I5 bridges), the joints are modeled by allowing the two sections of the bridge converging to the joint to move independently in the horizontal direction and to rotate independently, and by constraining them to move by the same amount in the vertical direction.

3.2.4 Ground Motion

All eight bridges were subjected to response spectrum compatible, spatially varying ground motions to examine whether differential support ground motion can lead to increased bridge response, when compared to the case of identical support ground motion. The methodology described in Chapter 2 of this report is used to generate the ground motion time histories.

A total of 15 scenario earthquakes were examined for each one of the eight bridges by considering three different apparent velocities of seismic wave propagation v (1,000, 1,500, and 2,000 m/sec), and five different scenario earthquakes for each value of v by varying the seed for the random number generator. These 15 cases are described in Table 3-10.

The Uniform Building Code (International Conference of Building Officials 1994) acceleration response spectrum for Type I soil, 5% damping, and 0.5g peak ground acceleration was selected for all supports of each one of the eight bridges (with the exception of the FHWA/ABAM-No.2 bridge for which the UBC response spectrum for Type II soil was used for 5% damping and 0.3g peak ground acceleration). These two response spectra are shown in Fig. 3-15.

Abrahamson's coherence law (Abrahamson 1993) was chosen to describe the coherence loss between pairs of supports. The functional form of this law is provided in Eqs. (2-60)-(2-65) and is plotted in Fig. 3-16. Abrahamson's model for the coherence function has the advantage that it can be used for a broad range of soil conditions.

Finally, the Jennings et al. envelope (Jennings et al. 1968) was used to define the duration of strong ground motion with parameters shown in Fig. 2-4. It should be pointed out that as two-dimensional models of the eight bridges were considered, only the horizontal component of ground motion parallel to the axis of the bridge has been generated.

For each set of differential (asynchronous) support ground motion time histories, the corresponding set of identical support ground motion time histories is obtained by considering that the acceleration time history at the first support of the bridge is applied at all the

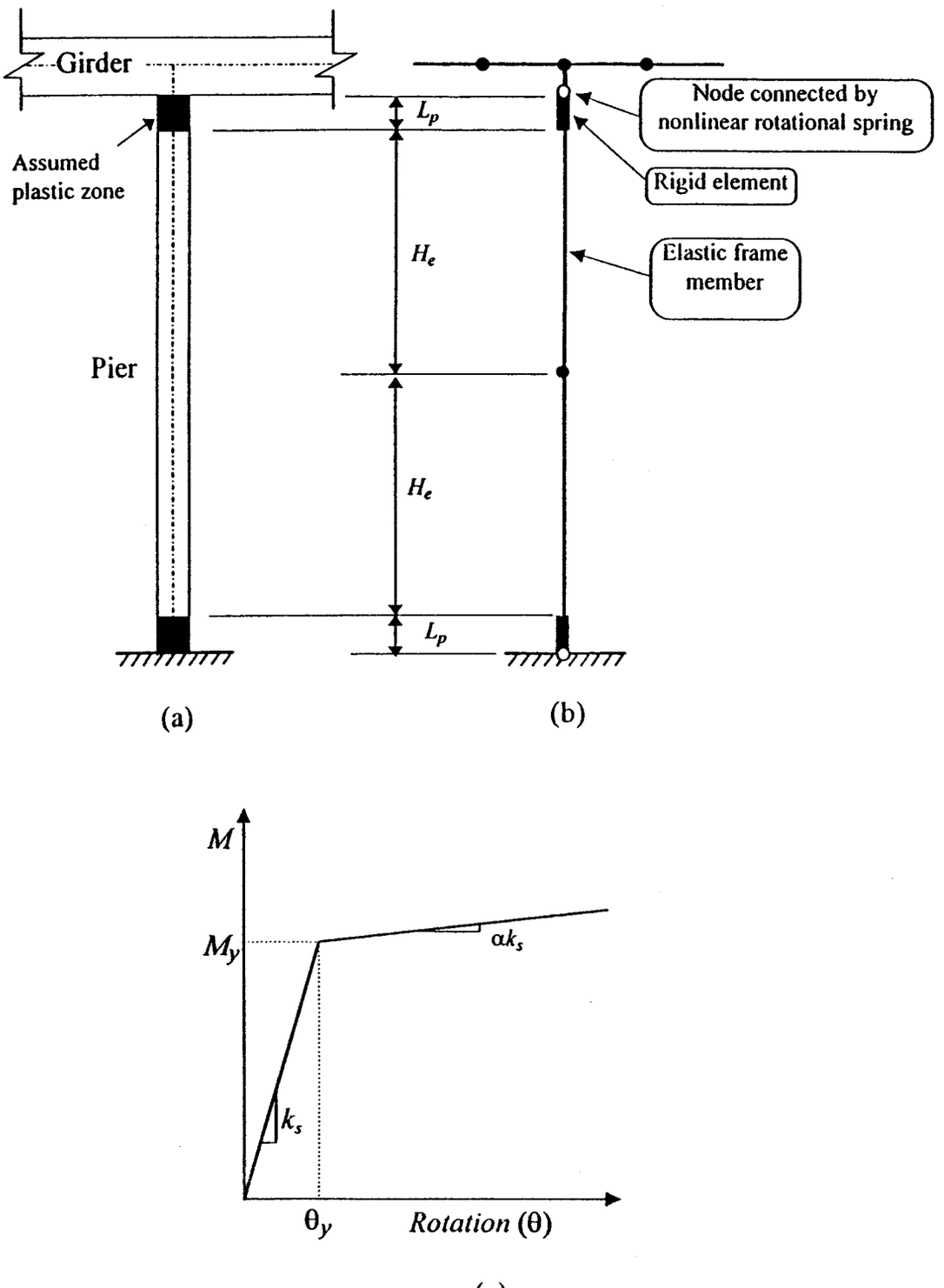

FIGURE 3-9 Nonlinear Model for the Bridge Piers: (a) Model of Pier, (b) Finite Element Model of Pier, (c) Moment-Curvature Relationship of Nonlinear Rotational Spring.

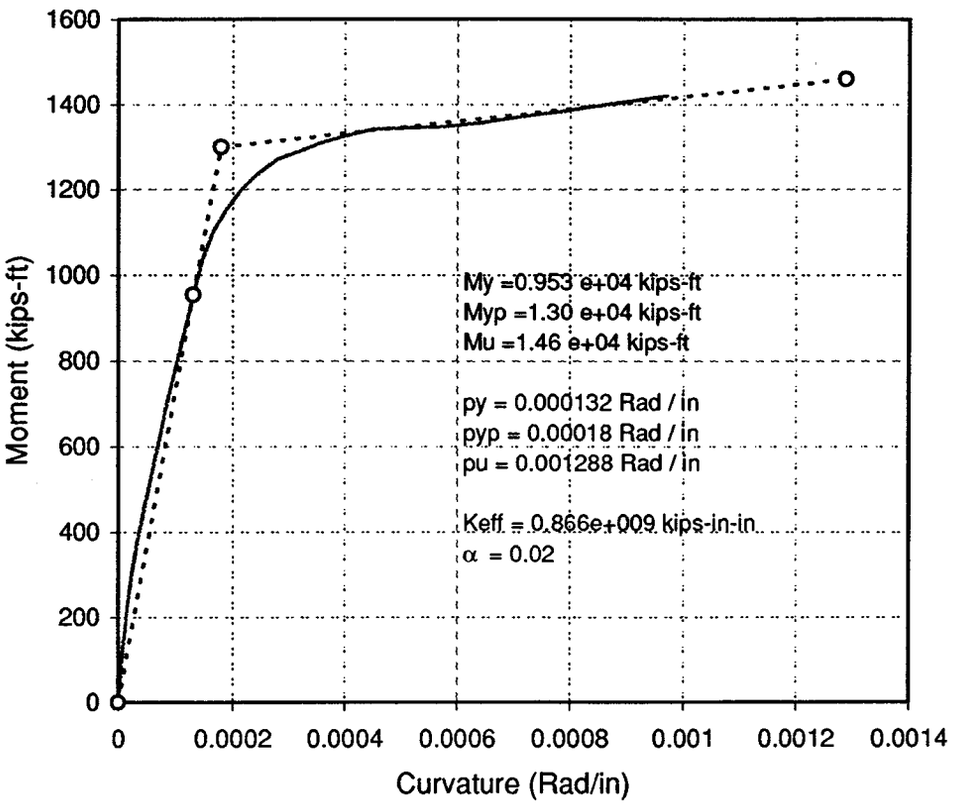

FIGURE 3-10 Moment - Curvature Relationships for the Piers of TEXT bridge resullting from the COLx Column Ductility Program (Caltrans 1993)

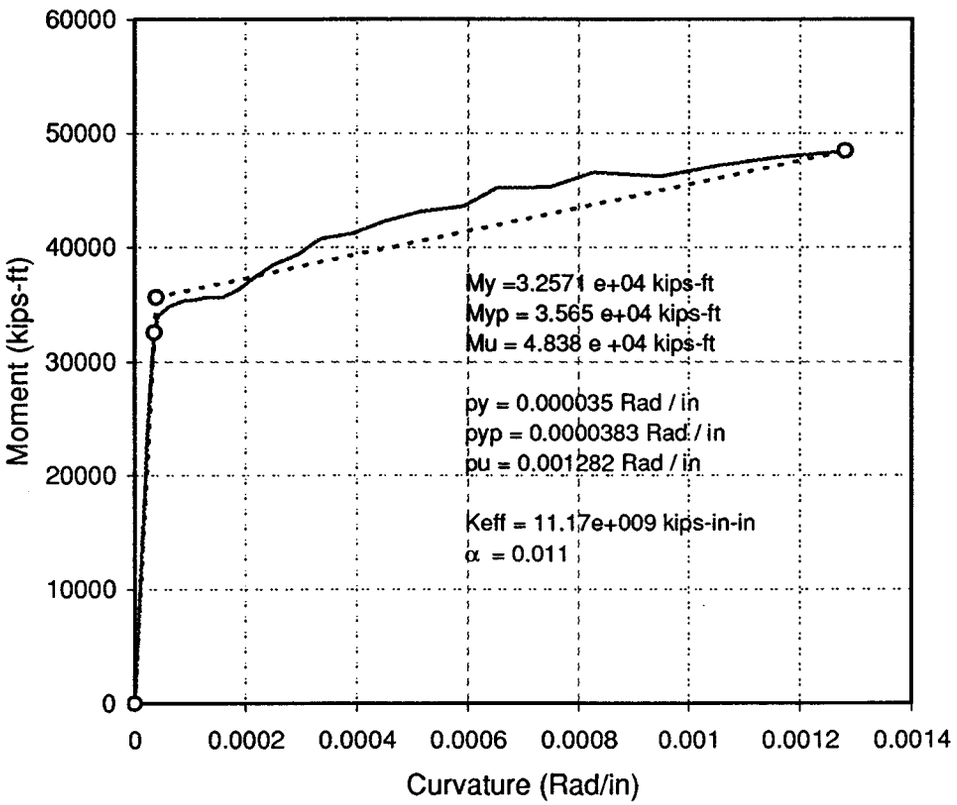

FIGURE 3-11 Moment - Curvature Relationships for the Piers of FHWA bridge resullting from the COLx Column Ductility Program (Caltrans 1993)

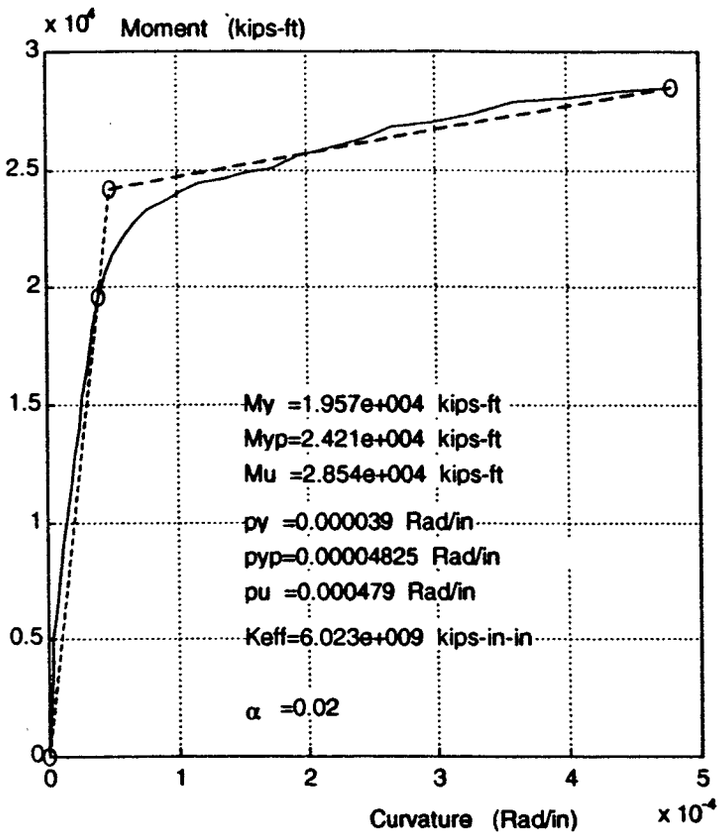

FIGURE 3-12 Moment-Curvature Relationship for the Piers of the TY0H, TY1H, and TY2H Example Bridges, Resulting from the COLx Column Ductility Program (Caltrans 1993).

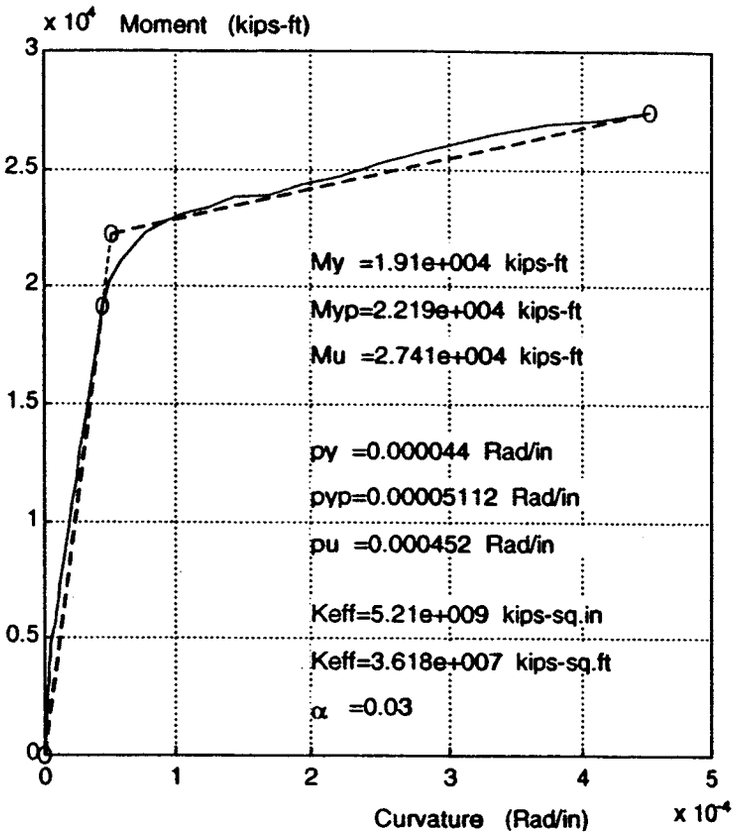

FIGURE 3-13 Moment-Curvature Relationship for the Piers of the Gavin Canyon Bridge, Resulting from the COLx Column Ductility Program (Caltrans 1993).

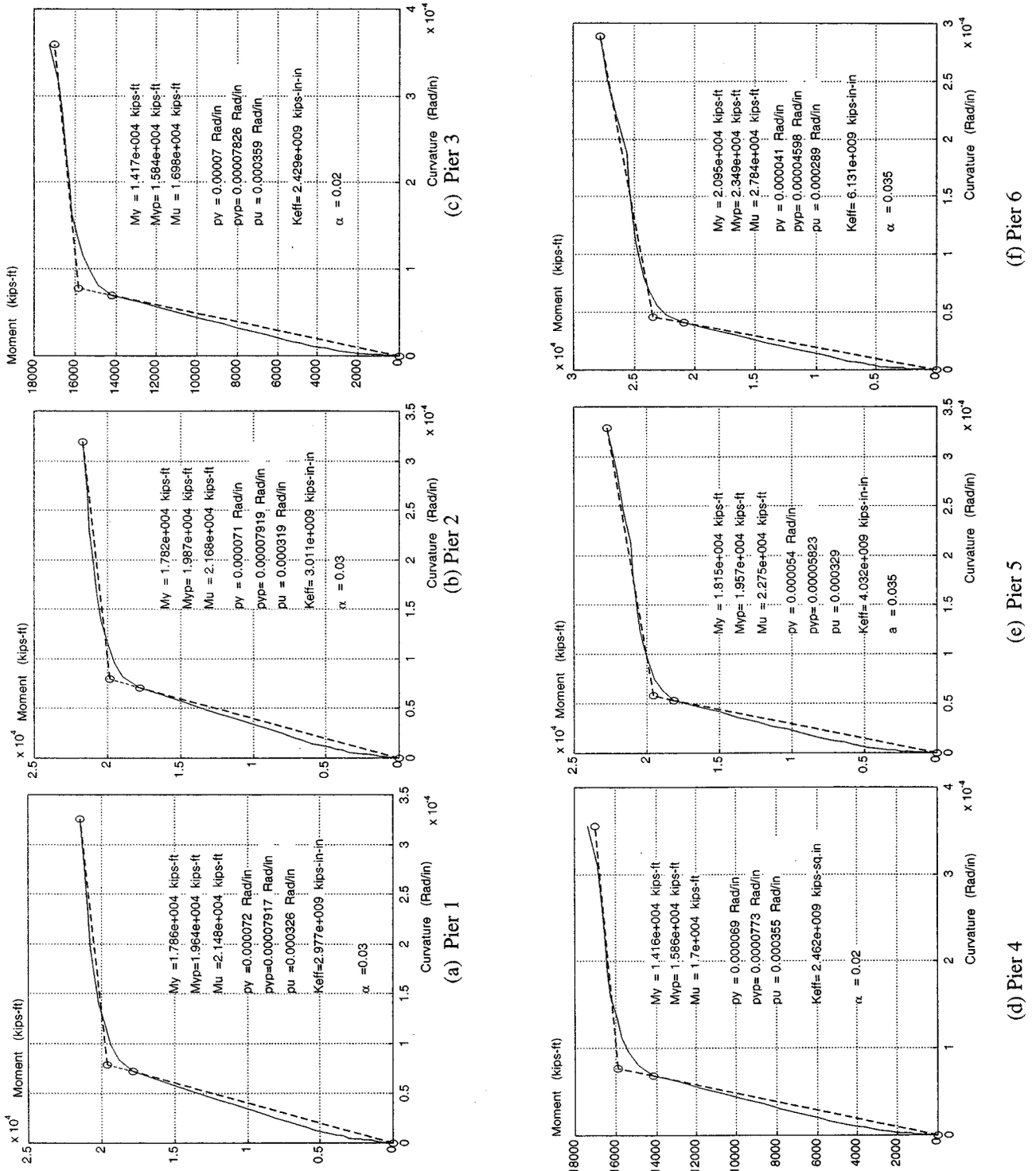

FIGURE 3-14 Moment-Curvature Relationships for the Piers of the SR14/I5 Viaduct, Resulting from the COLx Column Ductility Program (Caltrans 1993).

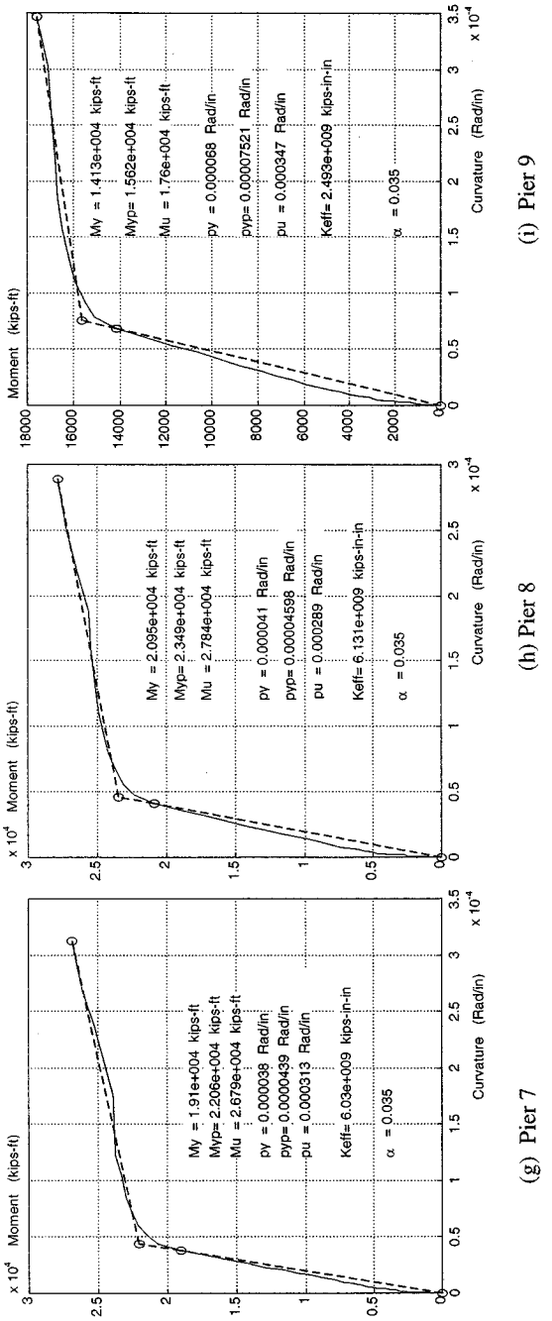

(i) Pier 9

(h) Pier 8

(g) Pier 7

FIGURE 3-14 (cont'd) Moment-Curvature Relationships for the Piers of the SR14/I5 Viaduct, Resulting from the COLx Column Ductility Program (Caltrans 1993).

TABLE 3-10

The 15 Scenario Earthquakes Considered in the Comparative Study of Eight Bridges

Scenario No.	Velocity v (m/sec)	Random Case
1	1,000	1
2	1,000	2
3	1,000	3
4	1,000	4
5	1,000	5
6	1,500	1
7	1,500	2
8	1,500	3
9	1,500	4
10	1,500	5
11	2,000	1
12	2,000	2
13	2,000	3
14	2,000	4
15	2,000	5

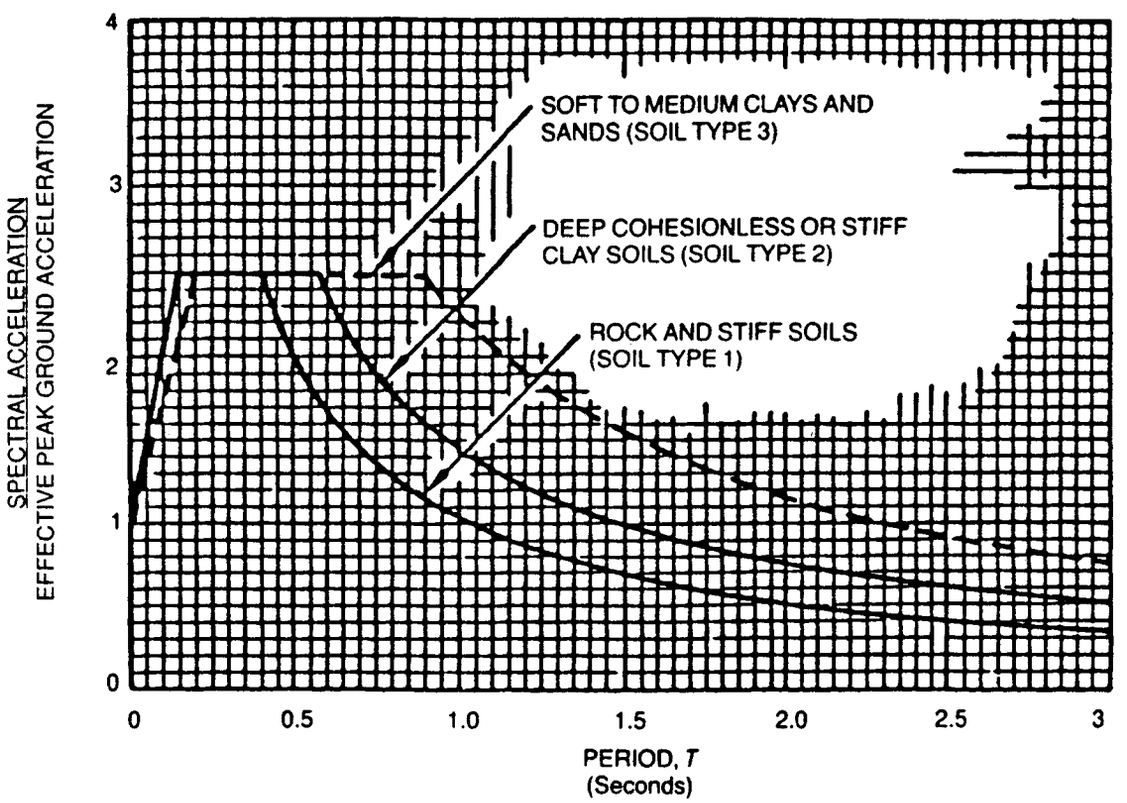

FIGURE 3-15 Uniform Building Code (International Conference of Building Officials 1994) Normalized Acceleration Response Spectra for Type I, II, and III soils and 5% Damping.

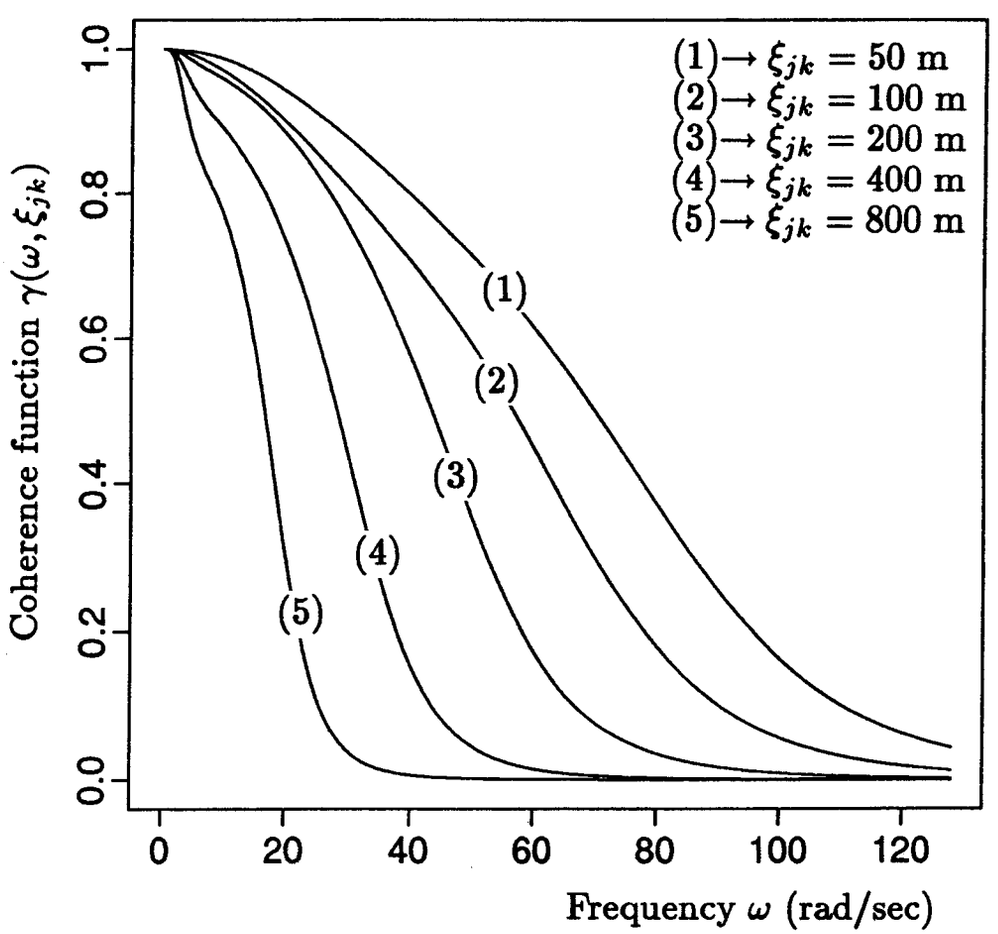

FIGURE 3-16 Abrahamson's Model for the Coherence Function $\gamma(\omega, \xi_{jk})$, where ω is the frequency and ξ_{jk} is the distance between points j and k.

other supports.

3.2.5 Dynamic Analyses and Conclusions

For each of the 15 scenario earthquakes considered (refer to Table 3-10), each one of the eight bridges in Table 3-1 was analyzed dynamically using differential and the corresponding identical support ground motion. Linear as well as nonlinear dynamic analyses were carried out for all bridges, with the exception of the Aptos Creek bridge for which only linear analyses were carried out. The computer code SAP90 beta version was used to perform these dynamic time history analyses.

The ratio defined in Eq. (3-1) was then computed for each one of the eight bridges and for each of the 15 scenario earthquakes, for the following response quantities:

Linear Analysis

It is reminded that linear analyses are performed for all eight bridges in this group. Values of ρ in Eq. (3-1) are computed for M/M_y at each one of the piers of each bridge, and for the opening and closing of each one of the expansion joints (hinges) of the five bridges that have at least one hinge (the Aptos Creek, TY1H, TY2H, Gavin Canyon, and SR14/I5 bridges). It should be noted that M is the bending moment at a specific cross-section, and M_y is the yield moment of the same cross-section.

Nonlinear Analysis

It is reminded that nonlinear analyses are performed for seven of the eight bridges in this group (the Aptos Creek bridge is only analyzed linearly). Values of ρ in Eq. (3-1) are computed for θ/θ_y at each one of the piers of the seven bridges, and for the opening and closing of each one of the expansion joints (hinges) of the four bridges that have at least one hinge (the TY1H, TY2H, Gavin Canyon, and SR14/I5 bridges). It should be noted that θ is the rotation of the nonlinear spring used to model the plastic zone at each end of every pier, and θ_y is the corresponding rotation at the yield point. The ratio θ/θ_y is therefore the ductility demand of the plastic zone.

Conclusions

Text Example Bridge

Statistical analysis of the ρ values for M/M_y for the two piers of the bridge resulting from linear dynamic analyses provides an overall mean value of 1.007, a standard deviation of 0.0251, and a corresponding coefficient of variation of 2.5%. The maximum value for ρ is $\rho_{\max} = 1.063$ observed at Pier 1 for a wave velocity of 1,000 m/sec. The wave velocity does not have any significant effect on the ρ values.

Statistical analysis of the ρ values for θ/θ_y for the two piers of the bridge resulting from nonlinear dynamic analyses provides an overall mean value of 0.997, a standard deviation of 0.0277, and a corresponding coefficient of variation of 2.8%. The maximum value for ρ is $\rho_{\max} = 1.034$ observed at Pier 1 for a wave velocity of 1,000 m/sec. The wave velocity does not have again any significant effect on the ρ values.

There is no considerable difference in the statistics of the ρ values resulting from linear (M/M_y) and nonlinear (θ/θ_y) analysis as indicated above.

Aptos Creek Bridge
Statistical analysis of the ρ values for M/M_y for the four piers of the bridge resulting from linear dynamic analyses provides an overall mean value of 1.002, a standard deviation of 0.0330, and a corresponding coefficient of variation of 3.3%. The maximum value for ρ is $\rho_{\max} = 1.078$ observed at Pier 3 for a wave velocity of 2,000 m/sec. The wave velocity does not have any significant effect on the ρ values. It is reminded that the Aptos Creek bridge is analyzed only linearly.

Statistical analysis of the ρ values for the opening and the closing of the single expansion joint of the bridge resulting from linear dynamic analyses provides an overall mean value of 1.019, a standard deviation of 0.0591, and a corresponding coefficient of variation of 5.8%. The maximum value for ρ is $\rho_{\max} = 1.141$ observed for the opening of the joint for a wave velocity of 1,000 m/sec. It should be pointed out that the aforementioned statistics for the ρ values of the opening and closing of the expansion joint of the bridge (linear analysis) are not as important as the corresponding statistics for the ρ values of M/M_y, as the opening and the closing of an expansion joint can not be used readily for design, and as the model used for the expansion joint of this bridge is a rather simple one.

FHWA-No.2 Example Bridge
Statistical analysis of the ρ values for M/M_y for the two piers of the bridge resulting from linear dynamic analyses provides an overall mean value of 0.987, a standard deviation of 0.0333, and a corresponding coefficient of variation of 3.4%. The maximum value for ρ is $\rho_{\max} = 1.067$ observed at Pier 2 for a wave velocity of 2,000 m/sec. It appears that the wave velocity of $v = 2,000$ m/sec produces higher ρ values.

Statistical analysis of the ρ values for θ/θ_y for the two piers of the bridge resulting from nonlinear dynamic analyses provides an overall mean value of 1.040, a standard deviation of 0.0727, and a corresponding coefficient of variation of 7.0%. The maximum value for ρ is $\rho_{\max} = 1.247$ observed at Pier 2 for a wave velocity of 2,000 m/sec. It appears that the wave velocity of $v = 2,000$ m/sec produces higher ρ values.

Although there is no considerable difference in the statistics of the ρ values resulting from linear (M/M_y) and nonlinear (θ/θ_y) analysis as indicated above, it appears that there is a slight increase in the overall mean value, standard deviation, coefficient of variation, and maximum ρ value for the nonlinear case, when compared to the linear case. Specifically, the overall mean value increases from 0.987 to 1.040, the standard deviation from 0.0333 to 0.0727, the coefficient of variation from 3.4% to 7.0%, and the maximum ρ value from 1.067 to 1.247.

TY0H Example Bridge
Statistical analysis of the ρ values for M/M_y for the four piers of the bridge resulting from linear dynamic analyses provides an overall mean value of 0.948, a standard deviation of 0.0778, and a corresponding coefficient of variation of 8.2%. The maximum value for ρ is

$\rho_{\max} = 1.116$

observed at Pier 1 for a wave velocity of 2,000 m/sec. It appears that the wave velocity of $v = 2,000$ m/sec produces higher ρ values.

Statistical analysis of the ρ values for θ/θ_y for the four piers of the bridge resulting from nonlinear dynamic analyses provides an overall mean value of 0.978, a standard deviation of 0.112, and a corresponding coefficient of variation of 11.5%. The maximum value for ρ is $\rho_{\max} = 1.176$ observed at Pier 1 for a wave velocity of 2,000 m/sec. It appears that the wave velocity of $v = 2,000$ m/sec produces higher ρ values.

Although there is no considerable difference in the statistics of the ρ values resulting from linear (M/M_y) and nonlinear (θ/θ_y) analysis as indicated above, it appears that there is a slight increase in the overall mean value, standard deviation, coefficient of variation, and maximum ρ value for the nonlinear case, when compared to the linear case. Specifically, the overall mean value increases from 0.948 to 0.978, the standard deviation from 0.0778 to 0.112, the coefficient of variation from 8.2% to 11.5%, and the maximum ρ value from 1.116 to 1.176.

TY1H Example Bridge

Statistical analysis of the ρ values for M/M_y for the four piers of the bridge resulting from linear dynamic analyses provides an overall mean value of 0.971, a standard deviation of 0.0521, and a corresponding coefficient of variation of 5.4%. The maximum value for ρ is $\rho_{\max} = 1.101$ observed at Pier 1 for a wave velocity of 1,000 m/sec. The wave velocity does not have any significant effect on the ρ values.

Statistical analysis of the ρ values for θ/θ_y for the four piers of the bridge resulting from nonlinear dynamic analyses provides an overall mean value of 1.003, a standard deviation of 0.0710, and a corresponding coefficient of variation of 7.1%. The maximum value for ρ is $\rho_{\max} = 1.160$ observed at Pier 3 for a wave velocity of 1,000 m/sec. The wave velocity does not have again any significant effect on the ρ values.

Although there is no considerable difference in the statistics of the ρ values resulting from linear (M/M_y) and nonlinear (θ/θ_y) analysis as indicated above, it appears that there is a slight increase in the overall mean value, standard deviation, coefficient of variation, and maximum ρ value for the nonlinear case, when compared to the linear case. Specifically, the overall mean value increases from 0.971 to 1.003, the standard deviation from 0.0521 to 0.0710, the coefficient of variation from 5.4% to 7.1%, and the maximum ρ value from 1.101 to 1.160.

Statistical analysis of the ρ values for the opening and the closing of the expansion joint of the bridge resulting from linear dynamic analyses provides an overall mean value of 1.446, a standard deviation of 0.187, and a corresponding coefficient of variation of 12.9%. The maximum value for ρ is $\rho_{\max} = 1.894$ observed for the closing of the joint for a wave velocity of 1,000 m/sec.

Statistical analysis of the ρ values for the opening and the closing of the expansion joint of the bridge resulting from nonlinear dynamic analyses provides an overall mean value of

1.562, a standard deviation of 0.251, and a corresponding coefficient of variation of 16.1%. The maximum value for ρ is $\rho_{\max} = 2.162$ observed for the opening of the joint for a wave velocity of 1,000 m/sec.

It should be pointed out that the aforementioned statistics for the ρ values of the opening and closing of the expansion joint of the bridge (linear and nonlinear analysis) are not as important as the corresponding statistics for the ρ values of M/M_y and θ/θ_y, as the opening and the closing of an expansion joint can not be used readily for design, and as the model used for the expansion joint of this bridge is a rather simple one.

TY2H Example Bridge

Statistical analysis of the ρ values for M/M_y for the four piers of the bridge resulting from linear dynamic analyses provides an overall mean value of 1.008, a standard deviation of 0.0443, and a corresponding coefficient of variation of 4.4%. The maximum value for ρ is $\rho_{\max} = 1.097$ observed at Pier 2 for a wave velocity of 1,000 m/sec. The wave velocity does not have any significant effect on the ρ values.

Statistical analysis of the ρ values for θ/θ_y for the four piers of the bridge resulting from nonlinear dynamic analyses provides an overall mean value of 0.979, a standard deviation of 0.0605, and a corresponding coefficient of variation of 6.2%. The maximum value for ρ is $\rho_{\max} = 1.204$ observed at Pier 2 for a wave velocity of 2,000 m/sec. The wave velocity does not have again any significant effect on the ρ values.

Although there is no considerable difference in the statistics of the ρ values resulting from linear (M/M_y) and nonlinear (θ/θ_y) analysis as indicated above, it appears that there is a slight increase in the overall standard deviation, coefficient of variation, and maximum ρ value for the nonlinear case, when compared to the linear case. Specifically, the overall standard deviation increases from 0.0443 to 0.0605, the coefficient of variation from 4.4% to 6.2%, and the maximum ρ value from 1.097 to 1.204. The overall mean value, however, decreases from 1.008 to 0.979.

Statistical analysis of the ρ values for the opening and the closing of the two expansion joints of the bridge resulting from linear dynamic analyses provides an overall mean value of 1.044, a standard deviation of 0.169, and a corresponding coefficient of variation of 16.2%. The maximum value for ρ is $\rho_{\max} = 1.481$ observed for the opening of joint 2 for a wave velocity of 1,500 m/sec.

Statistical analysis of the ρ values for the opening and the closing of the two expansion joints of the bridge resulting from nonlinear dynamic analyses provides an overall mean value of 1.014, a standard deviation of 0.150, and a corresponding coefficient of variation of 14.8%. The maximum value for ρ is $\rho_{\max} = 1.380$ observed for the opening of joint 2 for a wave velocity of 1,000 m/sec.

It should be pointed out that the aforementioned statistics for the ρ values of the opening and closing of the expansion joints of the bridge (linear and nonlinear analysis) are not as important as the corresponding statistics for the ρ values of M/M_y and θ/θ_y, as the opening and the closing of an expansion joint can not be used readily for design, and as

the model used for the expansion joints of this bridge is a rather simple one.

Gavin Canyon Bridge

Statistical analysis of the ρ values for M/M_y for the four piers of the bridge resulting from linear dynamic analyses provides an overall mean value of 0.989, a standard deviation of 0.0477, and a corresponding coefficient of variation of 4.8%. The maximum value for ρ is $\rho_{\max} = 1.083$ observed at Pier 3 for a wave velocity of 1,500 m/sec. The wave velocity does not have any significant effect on the ρ values.

Statistical analysis of the ρ values for θ/θ_y for the four piers of the bridge resulting from nonlinear dynamic analyses provides an overall mean value of 1.005, a standard deviation of 0.0634, and a corresponding coefficient of variation of 6.3%. The maximum value for ρ is $\rho_{\max} = 1.198$ observed at Pier 2 for a wave velocity of 2,000 m/sec. The wave velocity does not have again any significant effect on the ρ values.

Although there is no considerable difference in the statistics of the ρ values resulting from linear (M/M_y) and nonlinear (θ/θ_y) analysis as indicated above, it appears that there is a slight increase in the overall mean value, standard deviation, coefficient of variation, and maximum ρ value for the nonlinear case, when compared to the linear case. Specifically, the overall mean value increases from 0.989 to 1.005, the standard deviation from 0.0477 to 0.0634, the coefficient of variation from 4.8% to 6.3%, and the maximum ρ value from 1.083 to 1.198.

Statistical analysis of the ρ values for the opening and the closing of the two expansion joints of the bridge resulting from linear dynamic analyses provides an overall mean value of 1.079, a standard deviation of 0.159, and a corresponding coefficient of variation of 14.7%. The maximum value for ρ is $\rho_{\max} = 1.402$ observed for the opening of joint 1 for a wave velocity of 1,000 m/sec.

Statistical analysis of the ρ values for the opening and the closing of the two expansion joints of the bridge resulting from nonlinear dynamic analyses provides an overall mean value of 1.054, a standard deviation of 0.144, and a corresponding coefficient of variation of 13.7%. The maximum value for ρ is $\rho_{\max} = 1.370$ observed for the opening of joint 1 for a wave velocity of 1,000 m/sec.

It should be pointed out that the aforementioned statistics for the ρ values of the opening and closing of the expansion joints of the bridge (linear and nonlinear analysis) are not as important as the corresponding statistics for the ρ values of M/M_y and θ/θ_y, as the opening and the closing of an expansion joint can not be used readily for design, and as the model used for the expansion joints of this bridge is a rather simple one.

SR14/I5 Bridge

Statistical analysis of the ρ values for M/M_y for the nine piers of the bridge resulting from linear dynamic analyses provides an overall mean value of 0.974, a standard deviation of 0.147, and a corresponding coefficient of variation of 15.1%. The maximum value for ρ is $\rho_{\max} = 1.413$ observed at Pier 9 for a wave velocity of 1,000 m/sec. The wave velocity does not have any significant effect on the ρ values.

Statistical analysis of the ρ values for θ/θ_y for the nine piers of the bridge resulting from nonlinear dynamic analyses provides an overall mean value of 0.999, a standard deviation of 0.167, and a corresponding coefficient of variation of 16.8%. The maximum value for ρ is $\rho_{\max} = 1.551$ observed at Pier 7 for a wave velocity of 1,500 m/sec. The wave velocity does not have again any significant effect on the ρ values.

Although there is no considerable difference in the statistics of the ρ values resulting from linear (M/M_y) and nonlinear (θ/θ_y) analysis as indicated above, it appears that there is a slight increase in the overall mean value, standard deviation, coefficient of variation, and maximum ρ value for the nonlinear case, when compared to the linear case. Specifically, the overall mean value increases from 0.974 to 0.999, the standard deviation from 0.147 to 0.167, the coefficient of variation from 15.1% to 16.8%, and the maximum ρ value from 1.413 to 1.551.

Statistical analysis of the ρ values for the opening and the closing of the four expansion joints of the bridge resulting from linear dynamic analyses provides an overall mean value of 1.095, a standard deviation of 0.227, and a corresponding coefficient of variation of 20.7%. The maximum value for ρ is $\rho_{\max} = 2.142$ observed for the closing of joint 4 for a wave velocity of 1,000 m/sec.

Statistical analysis of the ρ values for the opening and the closing of the four expansion joints of the bridge resulting from nonlinear dynamic analyses provides an overall mean value of 1.291, a standard deviation of 0.530, and a corresponding coefficient of variation of 41.1%. The maximum value for ρ is $\rho_{\max} = 3.027$ observed for the closing of joint 4 for a wave velocity of 1,000 m/sec.

It should be pointed out that the aforementioned statistics for the ρ values of the opening and closing of the expansion joints of the bridge (linear and nonlinear analysis) are not as important as the corresponding statistics for the ρ values of M/M_y and θ/θ_y, as the opening and the closing of an expansion joint can not be used readily for design, and as the model used for the expansion joints of this bridge is a rather simple one.

General Conclusions from All Eight Bridges

Figure 3-17 plots the maximum ρ values for M/M_y at the piers (linear dynamic analysis) as a function of the largest span of the bridge, while Fig. 3-18 plots the maximum ρ values for M/M_y at the piers (linear dynamic analysis) as a function of the total length of the bridge. Figure 3-19 plots the maximum ρ values for ductility demand at the piers (nonlinear dynamic analysis) as a function of the largest span of the bridge, while Fig. 3-20 plots the maximum ρ values for ductility demand at the piers (nonlinear dynamic analysis) as a function of the total length of the bridge. It is reminded that ductility demand is the ratio θ/θ_y.

Figure 3-18 plots the maximum ρ values for M/M_y at the piers resulting from linear dynamic analysis, as a function of the total length of the bridge. Figure 3-18 provides the following indication: it appears that for bridges similar in form and configuration to the eight bridges considered in this part of the report and having a total length less than approximately 1,000 ft, the expected maximum ρ value for M/M_y at the piers resulting

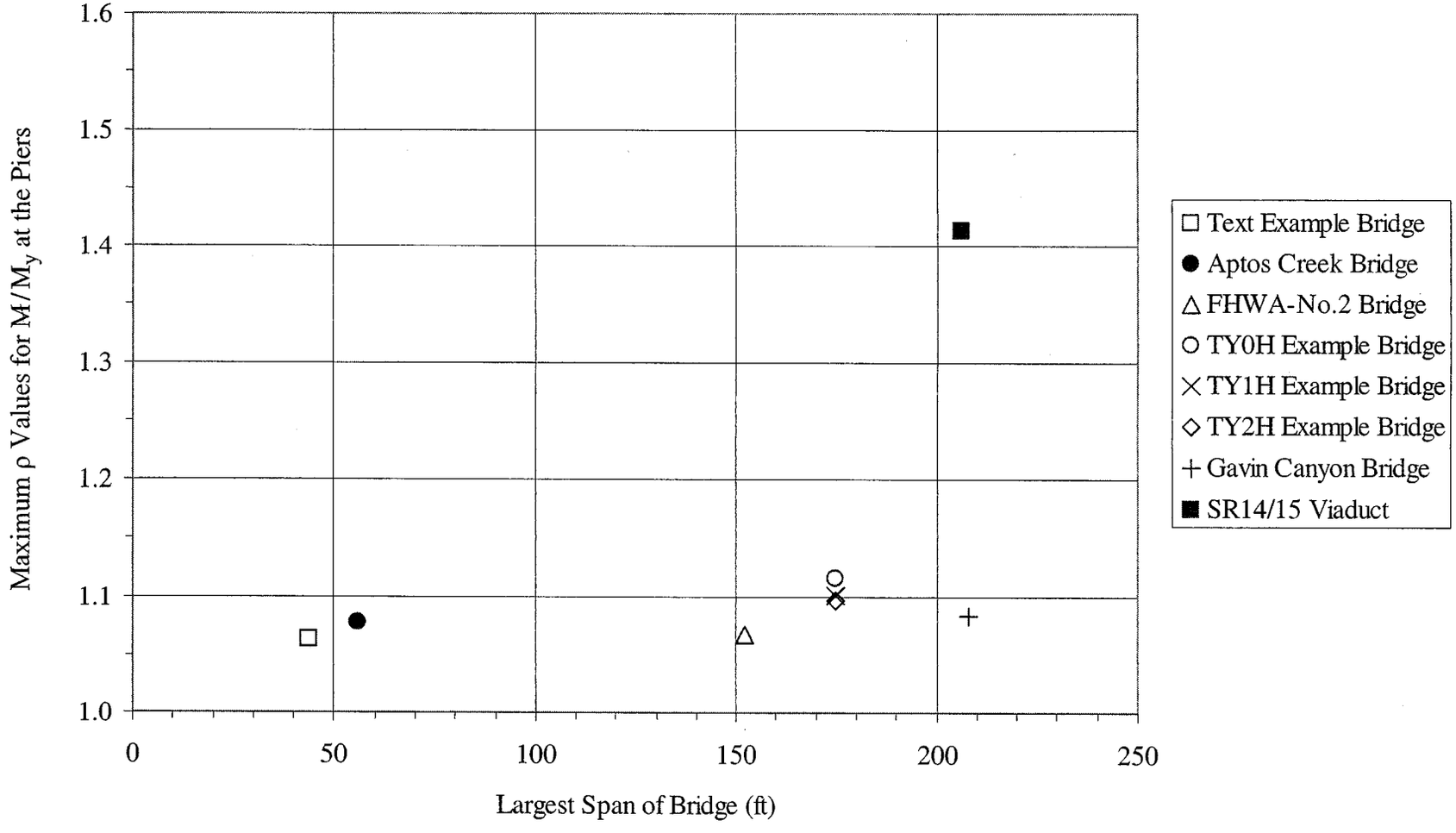

FIGURE 3-17 Maximum ρ Values for M / M_y at the Piers as a Function of the Largest Span of the Bridge (Linear Analysis).

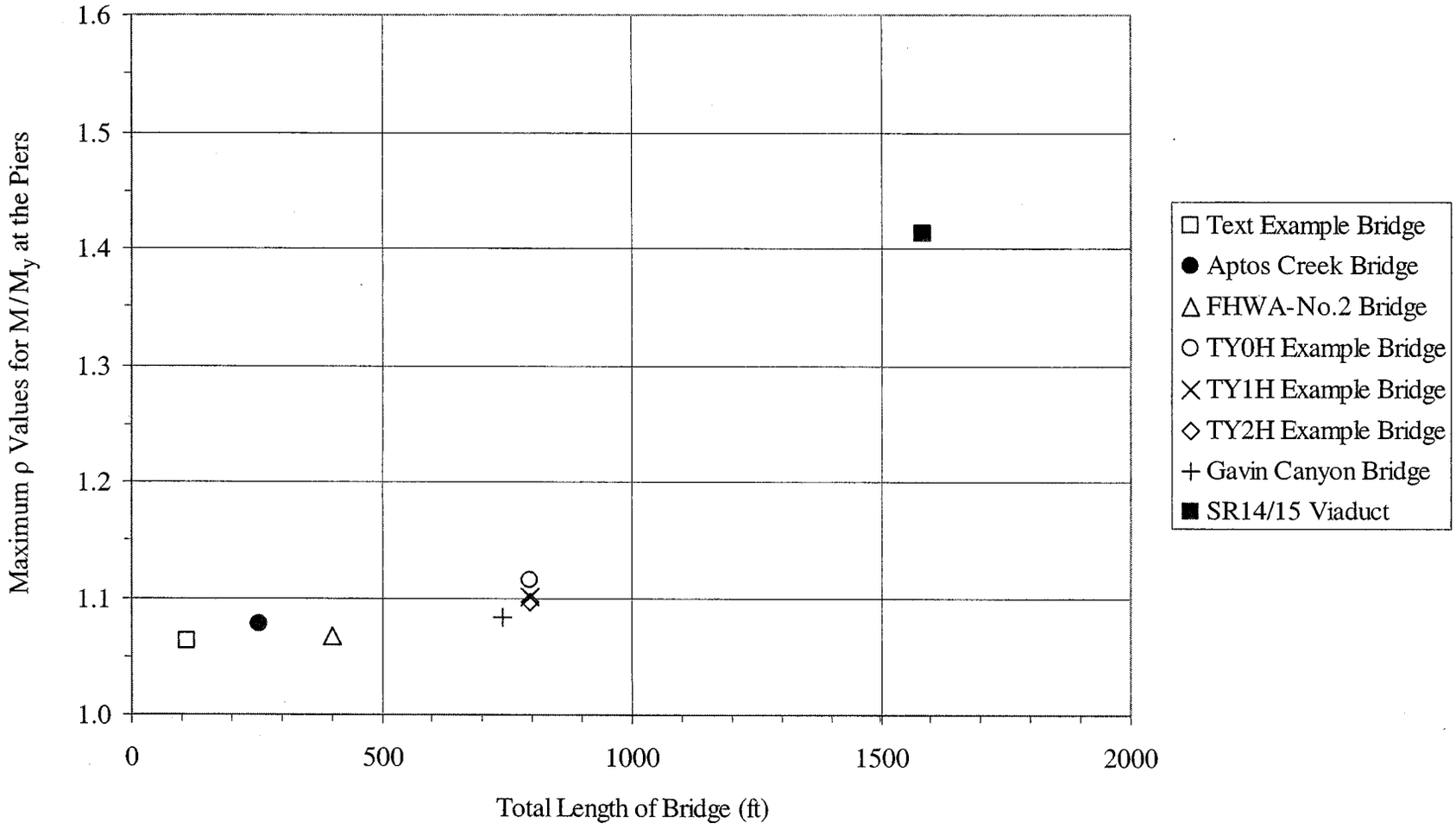

FIGURE 3-18 Maximum ρ Values for M / M_y at the Piers as a Function of the Total Length of the Bridge (Linear Analysis).

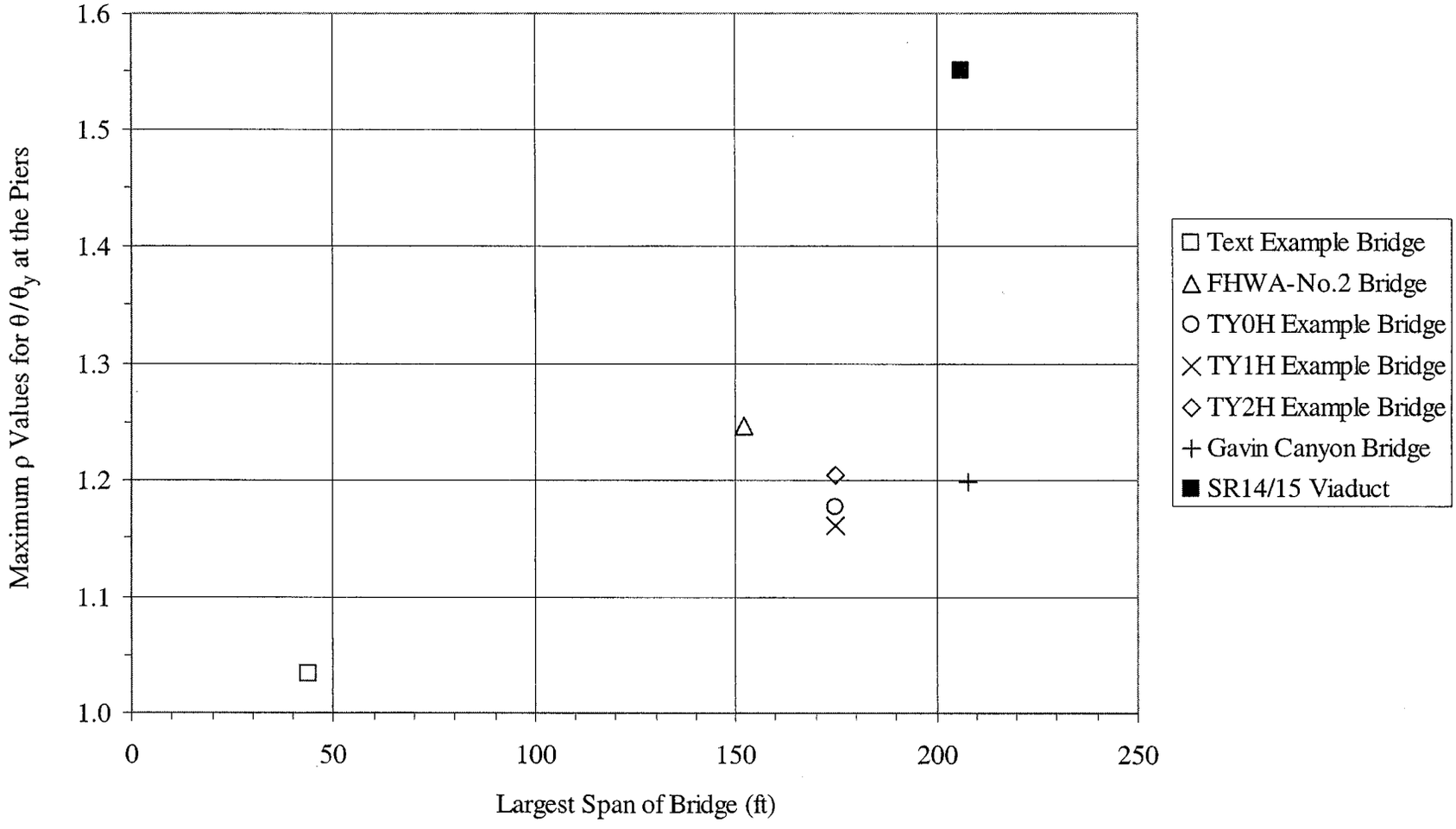

FIGURE 3-19 Maximum ρ Values for the Ductility Demand θ / θ_y at the Piers as a Function of the Largest Span of the Bridge (Nonlinear Analysis).

from linear dynamic analysis is going to be close to 1.10. For bridges larger than 1,000 ft, it is difficult to provide a general rule because there is only one data point as can be seen from Fig. 3-18, but it appears that the expected maximum ρ value for M/M_y can be much higher than 1.10.

Figure 3-20 plots the maximum ρ values for θ/θ_y at the piers resulting from nonlinear dynamic analysis, as a function of the total length of the bridge. Figure 3-20 provides the following indication: it appears that for bridges similar in form and configuration to the eight bridges considered in this part of the report and having a total length less than approximately 1,000 ft, the expected maximum ρ value for θ/θ_y at the piers resulting from nonlinear dynamic analysis is going to be close to 1.20-1.25. For bridges larger than 1,000 ft, it is difficult to provide a general rule because there is only one data point as can be seen from Fig. 3-20, but it appears that the expected maximum ρ value for θ/θ_y can be much higher than 1.20-1.25.

3.3 Effect of Different Local Soil Conditions

3.3.1 Introduction

In the preceding comparative analysis of the set of eight bridges, it has been assumed that all the supports of each bridge were on the same local soil conditions. In order to examine the very important case of bridges with supports on different local soil conditions, the Gavin Canyon bridge from the previous set of eight bridges is chosen for further analysis in this part of the report. Specifically, it will be assumed that one or two of the supports of this bridge can be in different (softer) local soil conditions than the rest. Such cases can be encountered in practice in bridges over small valleys where the abutments and some of the supports close to the abutments can be in harder soil conditions, while some of the supports around the center of the bridge can be in softer soil conditions.

3.3.2 Description of the Gavin Canyon Bridge

The description of the Gavin Canyon bridge that is considered in this part of the report can be found in the "Comparative Analysis of Eight Bridges" section.

3.3.3 Finite Element Model of the Gavin Canyon Bridge

The model developed in the "Comparative Analysis of Eight Bridges" section is used again here for the Gavin Canyon bridge. The only difference is that now the SAP2000 computer code is selected to perform the dynamic time history analyses, and only nonlinear dynamic analyses are considered.

3.3.4 Ground Motion

As mentioned earlier, in this part of the report it is assumed that the Gavin Canyon bridge has one or two of its four piers on softer soil than the rest of the piers and the abutments. The methodology presented in Chapter 2 of this report is used again to generate the ground motion time histories.

The following 40 scenario earthquakes have been considered: five different scenario earth-

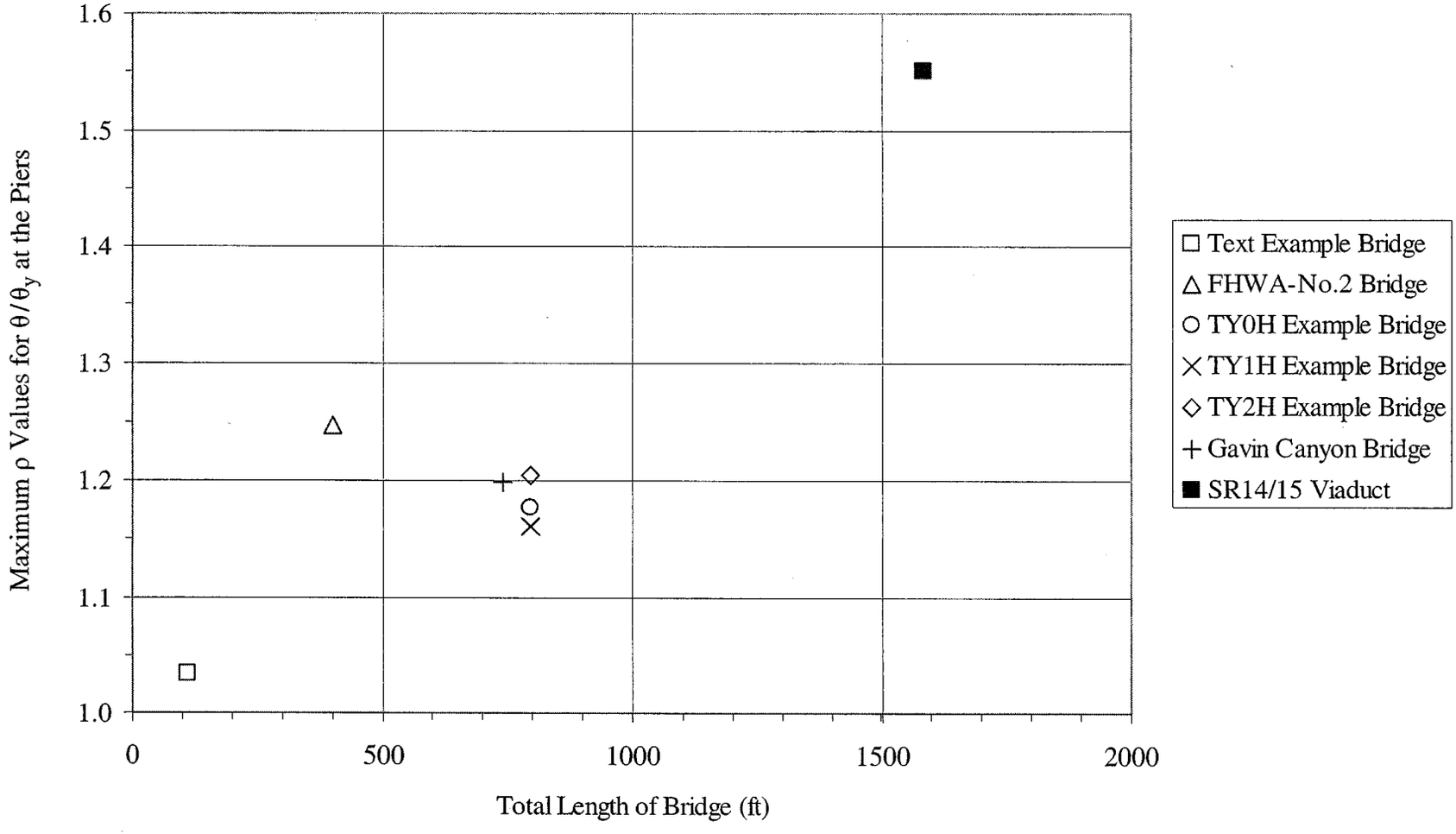

FIGURE 3-20 Maximum ρ Values for the Ductility Demand θ / θ_y at the Piers as a Function of the Total Length of the Bridge (Nonlinear Analysis).

quakes assuming that all four piers of the bridge are on hard soil (denoted by hhhh1 – hhhh5), five different scenario earthquakes assuming that the first pier of the bridge is on hard soil, the next two on medium soil, and the fourth on hard soil (denoted by hmmh1 – hmmh5), five different scenario earthquakes assuming that the first pier of the bridge is on hard soil, the next two on soft soil, and the fourth on hard soil (denoted by hssh1 – hssh5), five different scenario earthquakes assuming that the first pier of the bridge is on medium soil, the next two on soft soil, and the fourth on medium soil (denoted by mssm1 – mssm5), and finally twenty different scenario earthquakes assuming that the first two piers of the bridge are on medium soil, the third one on soft soil, and the fourth one on medium soil (denoted by mmsm1 – mmsm20). One of the reasons for considering the twenty scenario earthquakes mmsm1 – mmsm20 is to examine the variation in the ρ values (Eq. (3-1)) resulting from the Monte Carlo simulation procedure that was followed.

For all forty of the above scenario earthquakes, the apparent velocity of wave propagation was set equal to 1,000 m/sec, and the different scenario earthquakes corresponding to the same set of local soil conditions were obtained by varying the seed for the random number generator. These 40 cases are described in Table 3-11.

The Uniform Building Code (International Conference of Building Officials 1994) acceleration response spectrum for Type I soil, 5% damping, and 0.5g peak ground acceleration was selected to describe the ground motion at piers on hard soil, the UBC acceleration response spectrum for Type II soil, 5% damping, and 0.5g peak ground acceleration to describe the ground motion at piers on medium soil, and the UBC acceleration response spectrum for Type III soil, 5% damping, and 0.5g peak ground acceleration to describe the ground motion at piers on soft soil. These three response spectra are shown in Fig. 3-15.

Abrahamson's coherence law (Abrahamson 1993) was chosen again to describe the coherence loss between pairs of supports. The functional form of this law is provided in Eqs. (2-60)-(2-65) and is plotted in Fig. 3-16. Abrahamson's model for the coherence function has the advantage that it can be used for a broad range of soil conditions. This advantage is especially useful here as different supports of the bridge are on different local soil conditions. At this point, the reader is referred to an important note concerning the case of differential (asynchronous) support ground motion when the bridge supports are on different local soil conditions found in the second paragraph of Chapter 2 "Generation of Spatially Varying Seismic Ground Motion Time Histories" (this is before the "Introduction" section of Chapter 2).

Finally, the Jennings et al. envelope (Jennings et al. 1968) was used again to define the duration of strong ground motion with parameters shown in Fig. 2-4. It should be pointed out that as a two-dimensional model of the Gavin Canyon bridge was considered, only the horizontal component of ground motion parallel to the axis of the bridge has been generated.

For each set of differential (asynchronous) support ground motion time histories, the corresponding set of identical support ground motion time histories is obtained by considering that the acceleration time history at the first support of the bridge is applied at all the other supports.

TABLE 3-11

The 40 Scenario Earthquakes for the Study of
the Effect of Different Local Soil Conditions
Gavin Canyon Bridge

Scenario No.	Soil at Left Abutment	Soil at Pier 1	Soil at Pier 2	Soil at Pier 3	Soil at Pier 4	Soil at Right Abutment	Random Case
hhhh1	Hard	Hard	Hard	Hard	Hard	Hard	1
hhhh2	Hard	Hard	Hard	Hard	Hard	Hard	2
hhhh3	Hard	Hard	Hard	Hard	Hard	Hard	3
hhhh4	Hard	Hard	Hard	Hard	Hard	Hard	4
hhhh5	Hard	Hard	Hard	Hard	Hard	Hard	5
hmmh1	Hard	Hard	Medium	Medium	Hard	Hard	1
hmmh2	Hard	Hard	Medium	Medium	Hard	Hard	2
hmmh3	Hard	Hard	Medium	Medium	Hard	Hard	3
hmmh4	Hard	Hard	Medium	Medium	Hard	Hard	4
hmmh5	Hard	Hard	Medium	Medium	Hard	Hard	5
hssh1	Hard	Hard	Soft	Soft	Hard	Hard	1
hssh2	Hard	Hard	Soft	Soft	Hard	Hard	2
hssh3	Hard	Hard	Soft	Soft	Hard	Hard	3
hssh4	Hard	Hard	Soft	Soft	Hard	Hard	4
hssh5	Hard	Hard	Soft	Soft	Hard	Hard	5
mssm1	Medium	Medium	Soft	Soft	Medium	Medium	1
mssm2	Medium	Medium	Soft	Soft	Medium	Medium	2
mssm3	Medium	Medium	Soft	Soft	Medium	Medium	3
mssm4	Medium	Medium	Soft	Soft	Medium	Medium	4
mssm5	Medium	Medium	Soft	Soft	Medium	Medium	5

TABLE 3-11 (cont'd)

The 40 Scenario Earthquakes for the Study of
the Effect of Different Local Soil Conditions
Gavin Canyon Bridge

Scenario No.	Soil at Left Abutment	Soil at Pier 1	Soil at Pier 2	Soil at Pier 3	Soil at Pier 4	Soil at Right Abutment	Random Case
mmsm1	Medium	Medium	Medium	Soft	Medium	Medium	1
mmsm2	Medium	Medium	Medium	Soft	Medium	Medium	2
mmsm3	Medium	Medium	Medium	Soft	Medium	Medium	3
mmsm4	Medium	Medium	Medium	Soft	Medium	Medium	4
mmsm5	Medium	Medium	Medium	Soft	Medium	Medium	5
mmsm6	Medium	Medium	Medium	Soft	Medium	Medium	6
mmsm7	Medium	Medium	Medium	Soft	Medium	Medium	7
mmsm8	Medium	Medium	Medium	Soft	Medium	Medium	8
mmsm9	Medium	Medium	Medium	Soft	Medium	Medium	9
mmsm10	Medium	Medium	Medium	Soft	Medium	Medium	10
mmsm11	Medium	Medium	Medium	Soft	Medium	Medium	11
mmsm12	Medium	Medium	Medium	Soft	Medium	Medium	12
mmsm13	Medium	Medium	Medium	Soft	Medium	Medium	13
mmsm14	Medium	Medium	Medium	Soft	Medium	Medium	14
mmsm15	Medium	Medium	Medium	Soft	Medium	Medium	15
mmsm16	Medium	Medium	Medium	Soft	Medium	Medium	16
mmsm17	Medium	Medium	Medium	Soft	Medium	Medium	17
mmsm18	Medium	Medium	Medium	Soft	Medium	Medium	18
mmsm19	Medium	Medium	Medium	Soft	Medium	Medium	19
mmsm20	Medium	Medium	Medium	Soft	Medium	Medium	20

3.3.5 Dynamic Analyses and Conclusions

For each of the 40 scenario earthquakes considered (refer to Table 3-11), the Gavin Canyon bridge was analyzed dynamically using differential and the corresponding identical support ground motion. Only nonlinear dynamic analyses were carried out. The computer code SAP2000 was used to perform these dynamic time history analyses. Figure 3-21 displays a set of typical asynchronous displacement time histories at the four piers of the Gavin Canyon bridge, when Piers 1, 2, and 4 are on medium soil, and Pier 3 is on soft soil.

The ratio ρ defined in Eq. (3-1) was then computed for each of the forty scenario earthquakes, for the following response quantities: θ/θ_y at each one of the four piers of the bridge, and for the opening and closing of each one of the two expansion joints (hinges). It should be noted that θ is the rotation of the nonlinear spring used to model the plastic zone at each end of every pier, and θ_y is the corresponding rotation at the yield point. The ratio θ/θ_y is therefore the ductility demand of the plastic zone.

Conclusions

In order to estimate the effect of different local soil conditions on the ρ values of the Gavin Canyon bridge, Table 3-12 displays the statistics of ρ values for θ/θ_y for the 15 scenario earthquakes considered in the previous part of this report (same local soil conditions - refer to Table 3-10), and the corresponding statistics for the 20 scenario earthquakes: mmsm1-mmsm20 considered in this part of the report (different local soil conditions - refer to Table 3-11). Note that Table 3-12 is constructed from results of nonlinear analyses.

The most important conclusion from Table 3-12 is the very significant increase in the mean value, standard deviation, coefficient of variation, and maximum value of ρ for the case of different local soil conditions, when compared to the case of same local soil conditions, at Piers 2 and 3. Specifically, at Pier 2, the mean value of ρ increases from 1.008 to 1.635, the standard deviation of ρ from 0.086 to 0.236, the coefficient of variation of ρ from 8.6% to 14.4%, and the maximum ρ value from 1.20 to 2.27. At Pier 3, the mean value of ρ increases from 0.999 to 1.293, the standard deviation of ρ from 0.057 to 0.203, the coefficient of variation of ρ from 5.7% to 15.7%, and the maximum ρ value from 1.07 to 1.78.

It should be mentioned that Piers 1 and 4 do not show increases in the ρ values for θ/θ_y as dramatic as Piers 2 and 3 for the case of different local soil conditions, as can be easily observed in Table 3-12. This different behavior of Piers 1 and 4 can be easily explained from the model used for the two expansion joints of the Gavin Canyon bridge. It is reminded that the model used allows the two sections of the bridge converging to the joint to move independently in the horizontal direction and to rotate independently, and constrains them to move by the same amount in the vertical direction. Such a model is rather simple and is the main reason for this different behavior. If a gap-spring-type element was used to model the expansion joints in the horizontal direction, it is expected that Piers 1 and 4 would behave more similarly to Piers 2 and 3.

The general conclusion of this part of the report is therefore the following: when a bridge similar in type and configuration as the Gavin Canyon bridge has supports on different

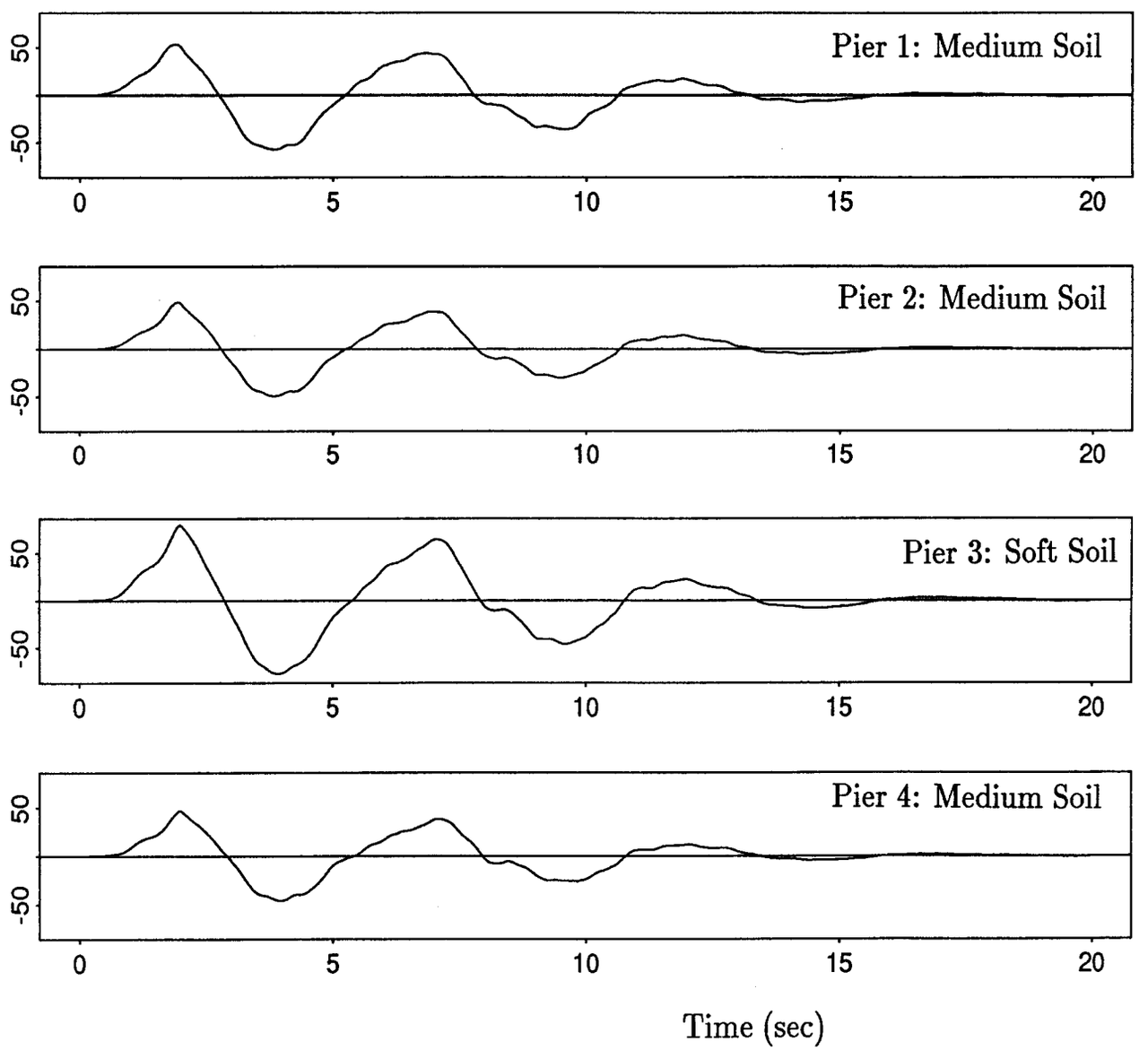

FIGURE 3-21 Typical Asynchronous Displacement Time Histories in cm at the Four Piers of the Gavin Canyon Bridge (Pier 1: Medium Soil, Pier 2: Medium Soil, Pier 3: Soft Soil, Pier 4: Medium Soil).

TABLE 3-12

Statistics of ρ Values for θ/θ_y
Gavin Canyon Bridge (Nonlinear Analysis)

Same Local Soil Conditions
Statistics of ρ Values for θ/θ_y for the
15 Scenario Earthquakes in Table 11

	Pier 1	**Pier 2**	**Pier 3**	**Pier 4**
Average of ρ values	1.013	1.008	0.999	1.002
Standard Deviation of ρ values	0.015	0.086	0.057	0.077
COV of ρ values	1.5%	8.6%	5.7%	7.7%
Maximum ρ value	1.04	1.20	1.07	1.14

Different Local Soil Conditions
Statistics of ρ Values for θ/θ_y for the
20 Scenario Earthquakes: mmsm1 – mmsm20 in Table 65

	Pier 1	**Pier 2**	**Pier 3**	**Pier 4**
Average of ρ values	0.986	1.635	1.293	1.009
Standard Deviation of ρ values	0.061	0.236	0.203	0.134
COV of ρ values	6.2%	14.4%	15.7%	13.3%
Maximum ρ value	1.04	2.27	1.78	1.24

local soil conditions, the expected maximum values of ρ for the ductility demand (θ/θ_y) at the piers can become much larger than unity, and certainly much larger than corresponding values resulting from all supports being considered on the same local soil conditions.

3.4 Effect of Modeling the Bridge in Three Dimensions

3.4.1 Introduction

In all the analyses considered so far, the finite element models used for the bridges were two-dimensional, and the only component of ground motion considered was the horizontal one along the axis of the bridge. In order to study the effect of different angles of incidence of the seismic waves with respect to the axis of the bridge and to examine the effect of the vertical component of ground motion, two bridges were modeled linearly in three dimensions in this part of the report. It was assumed that all the supports of these two bridges were on the same local soil conditions. In addition, a detailed sensitivity analysis with respect to the value of the apparent velocity of wave propagation was carried out for one of these two bridges.

The two bridges modeled in three dimensions in this part of the report are the SR14/I5 Interchange and a typical three-span concrete bridge designed by BERGER/ABAM Engineers Inc. for the Federal Highway Administration.

3.4.2 The SR14/I5 Interchange in Three Dimensions

This section of the report is based on the senior thesis of Sanjay Arwade entitled "Analysis of the Effect of Differential Support Motion on a Typical Reinforced Concrete Highway Bridge," presented at Princeton University in 1996.

Description of SR14/I5 Viaduct

The southbound SR14/I5 separation and overhead structure (that was also analyzed in two-dimensions in the "Comparative Analysis of Eight Bridges" section) is located at mile post 24.5 on Route 5 in Los Angeles County approximately 24 miles northwest of downtown Los Angeles and is generally aligned in the north-south direction. The bridge is a ten-span structure divided into five frames by four expansion joints. It has seat-type abutments and single column bents. The total length is 1,582 ft with an overall width of 55 ft. The structure is curved to a radius of 2,235 ft. Figure 3-22 taken from Buckle (1994) shows elevation, plan and section views of the viaduct.

The viaduct failed spectacularly on January 17, 1994. The entire frame 1 from abutment 1 to the hinge in span 3-4 collapsed, with total disintegration of the column at pier 2, and an apparent punching through the superstructure of pier 3. The bridge unseated off abutment 1, moving about 5 ft north, and also unseated off the hinge adjacent to pier 4, again ending up in a final position some distance north of its original plan position. The right exterior shear key at abutment 1 was damaged. However, the left shear key had little visual damage. The pier 3 bent cap was inclined towards pier 4 and the measured ground separation from the column at pier 4 was approximately six inches north-south and four inches east-west. The predominant motion of the structure appeared to be in the

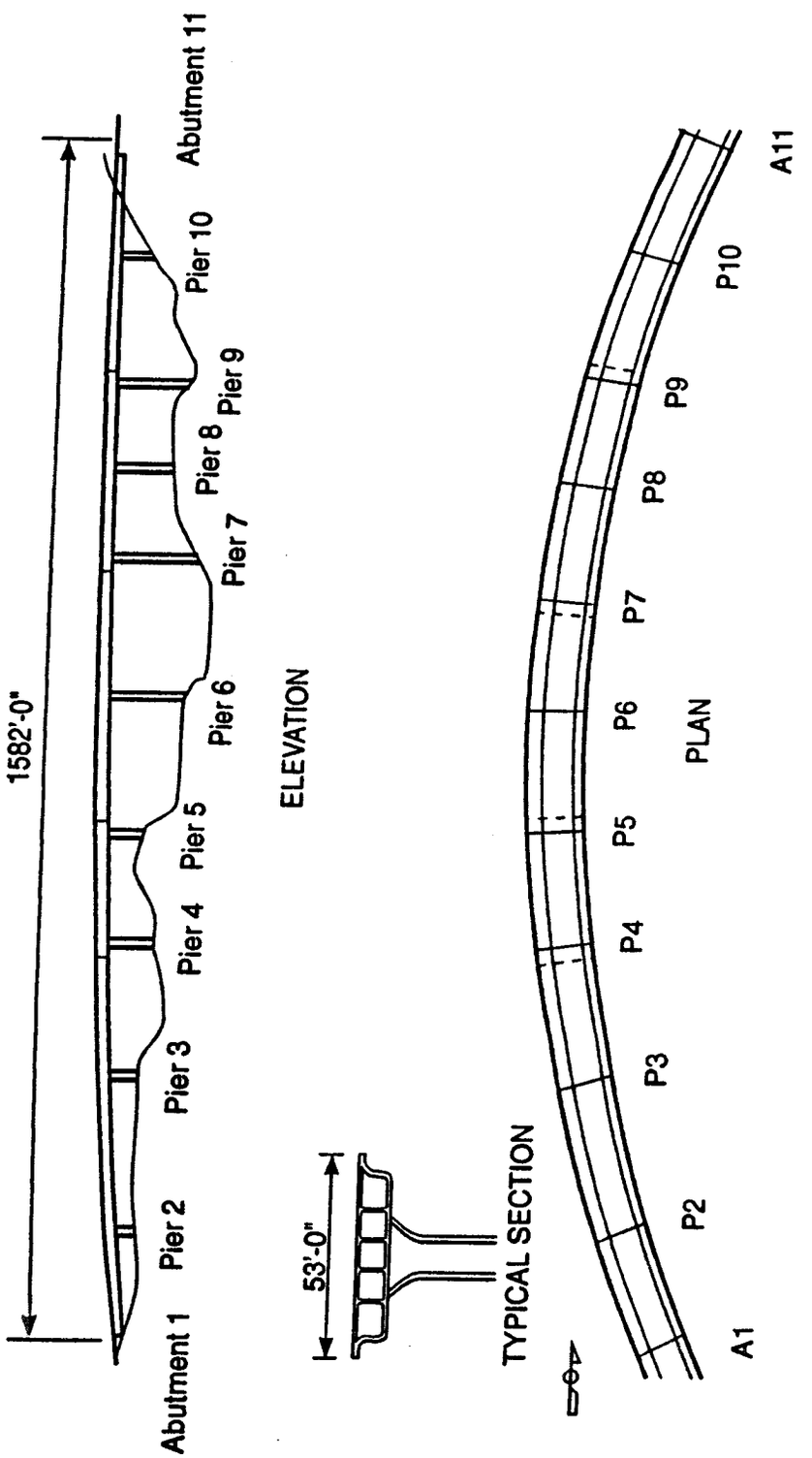

FIGURE 3-22 Elevation, Plan and Section Views of the Southbound SR14/I5 Separation and Overhead Taken from Buckle (1994).

north-south direction.

Finite Element Model of the SR14/I5 Viaduct

A linear three-dimensional finite element model of the SR14/I5 viaduct was constructed based on the "as built plans" of the structure. The motion of interest is the motion of the center axis of the bridge. For this reason, the structure is modeled in three dimensions using frame elements running along the neutral axis of the superstructure box girder. The section properties of these elements are chosen to represent the full width and depth of the box girder. The ANSYS computer code was selected for the dynamic time history analyses.

Ground Motion

The three-dimensional model of the SR14/I5 interchange was subjected to response spectrum compatible, spatially varying ground motions to examine whether differential support ground motion can lead to increased bridge response, when compared to the case of identical support ground motion. The methodology described in Chapter 2 of this report is used again to generate the ground motion time histories.

A total of 18 scenario earthquakes were considered by varying the velocity of seismic wave propagation v, the angle of incidence of seismic waves with respect to the axis of the bridge θ ($\theta = 0$ when seismic waves propagate parallel to the axis of the bridge, and $\theta = 90^o$ when seismic waves propagate at an angle of 90^o with respect to the axis of the bridge), and by considering combinations of horizontal and vertical components of ground motion. These 18 cases are described in Table 3-13a.

The Caltrans acceleration design response spectrum for 80-150 ft alluvium, 5% damping, and 0.5g peak ground acceleration was selected for all supports of the bridge (see Fig. 3-23). Abrahamson's coherence law (Abrahamson 1993) was chosen again to describe the coherence loss between pairs of supports. The functional form of this law is provided in Eqs. (2-60)-(2-65) and is plotted in Fig. 3-16. Finally, the Jennings et al. envelope (Jennings et al. 1968) was used to define the duration of strong ground motion (see Fig. 2-4).

The generated asynchronous displacement time histories at abutments 1 and 11 of the bridge are plotted in Fig. 3-24 for Case #6 in Table 3-13a, for demonstration purposes. The corresponding set of identical support ground motion time histories is again obtained by considering that the acceleration time history at the first support of the bridge is applied at all the other supports.

Dynamic Analysis and Conclusions

For each of the 18 scenario earthquakes considered (refer to Table 3-13a), the three-dimensional model of the SR14/I5 interchange was analyzed using differential and the corresponding identical support ground motion. Only linear dynamic analyses were carried out. The computer code ANSYS was used to perform these dynamic time history analyses.

TABLE 3-13a

The 18 Scenario Earthquakes Considered in the
Three-Dimensional Analysis of the SR14/I5 Viaduct

Case #	**Velocity v** (m/sec)	**Angle θ** (degrees)	**Ground Motion Components**
1	1,000	0	Horizontal only
2	1,200	0	Horizontal only
3	1,400	0	Horizontal only
4	1,600	0	Horizontal only
5	1,800	0	Horizontal only
6	2,000	0	Horizontal only
7	2,200	0	Horizontal only
8	2,400	0	Horizontal only
9	2,600	0	Horizontal only
10	2,800	0	Horizontal only
11	2,000	10	Horizontal only
12	2,000	20	Horizontal only
13	2,000	30	Horizontal only
14	2,000	40	Horizontal only
15	2,000	60	Horizontal only
16	2,000	90	Horizontal only
17	2,000	0	Horizontal + Vertical
18	2,000	30	Horizontal + Vertical

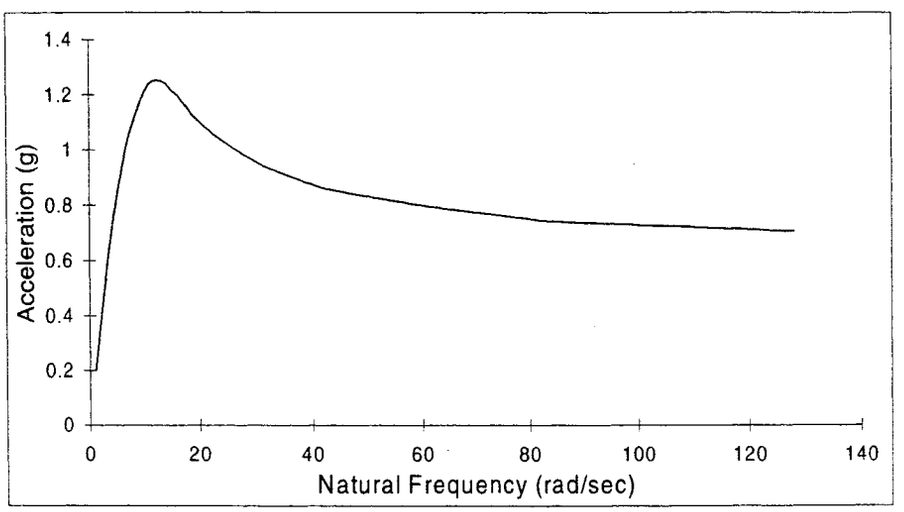

FIGURE 3-23 Caltrans Acceleration Design Response Spectrum for 80-150 ft Alluvium, 5% Damping, and 0.5g Peak Ground Acceleration.

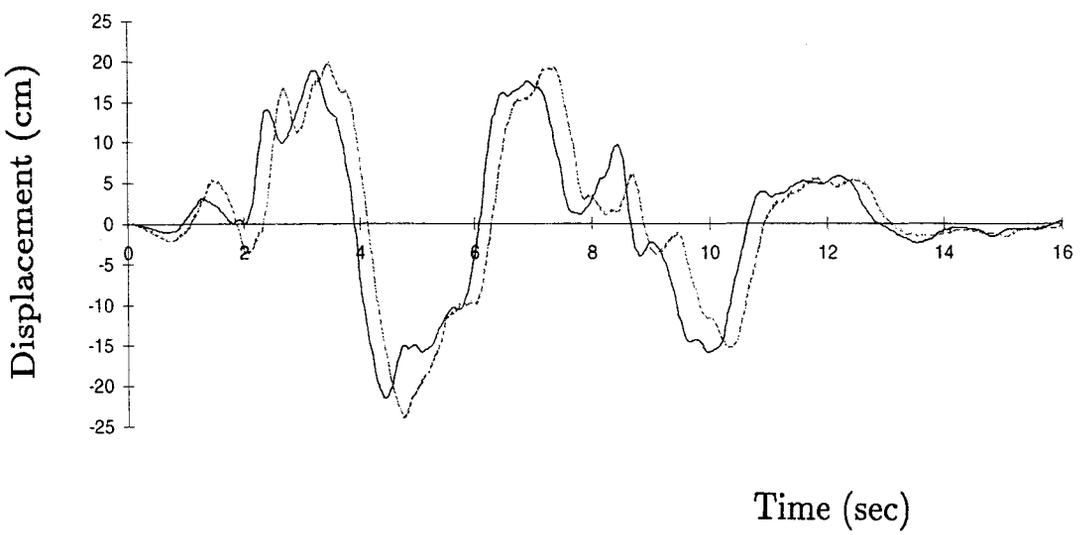

FIGURE 3-24 Generated Asynchronous Displacement Time Histories at Abutments 1 (continuous line) and 11 (dotted line) of the SR14/I5 Viaduct, for Case #6 in Table 75.

The ratio ρ defined in Eq. (3-1) was then computed for each of the 18 scenario earthquakes, for the following response quantity: the combined axial and bending stress at each one of the five segments of the deck. The computed values of ρ are provided in Table 3-13b for the five segments of the deck. It should be mentioned at this point that the linear three-dimensional study of the SR14/I5 viaduct presented here is not as detailed as the analyses performed earlier in this report, as there is only one random case considered for each combination of velocity v and angle of incidence θ (refer to Table 3-13a). The results presented in Table 3-13b for the ρ values of the combined axial and bending stress at each one of the five segments of the deck can serve therefore only as an indication of the effect of the angle of incidence of the seismic waves with respect to the axis of the bridge and of the vertical component of ground motion. Table 3-13b indicates a maximum ρ value of 1.18 occurring at segment 1 of the deck for scenario earthquake #1.

3.4.3 A Typical Three-Span Bridge in Three Dimensions

This section of the report is based on the senior thesis of Winnie Kwan entitled "The Effect of Spatially Differential Seismic Ground Motion on a Typical Three-Span Concrete Bridge," presented at Princeton University in 1997.

Description of the Typical Three-Span Bridge

This bridge involves a typical three-span continuous cast-in-place concrete box girder that was designed by BERGER/ABAM Engineers Inc. for the Federal Highway Administration (FHWA 1996). The total span of the bridge is 320 ft, with the individual spans being equal to 100, 120 and 100 ft as indicated in Fig. 3-25, with a skew of 30^o. The superstructure consists of a cast-in-place concrete box girder supported by two piers, each consisting of two circular cast-in-place concrete columns. For details about the geometry and materials of the bridge, the reader is referred to FHWA (1996).

Finite Element Model of the Typical Three-Span Bridge

The linear finite element model of the bridge developed by BERGER/ABAM Engineers (FHWA 1996) was used for the analysis. The computer code SAP2000 was selected to perform the linear dynamic time history analyses.

Ground Motion

The model of the typical three-span bridge was then subjected to response spectrum compatible, spatially varying ground motions to examine whether differential support ground motion can lead to increased bridge response, when compared to the case of identical support ground motion. The methodology described in Chapter 2 of this report is used again to generate the ground motion time histories.

A total of 36 scenario earthquakes were examined by considering four different apparent velocities of seismic wave propagation v (1,000, 1,500, 2,000, and 2,500 m/sec), three different angles of incidence of the seismic waves with respect to the axis of the bridge θ (0^o, 45^o, and 90^o), and by considering three different scenario earthquakes for each of the aforementioned $4\times3=12$ cases, by varying the seed for the random number generator. These 36 cases are described in Table 3-14.

TABLE 3-13b

The ρ Values for the Combined Axial and Bending Stress
in the Five Segments of the Deck for the
18 Scenario Earthquakes Considered in the
Three-Dimensional Analysis of the SR14/I5 Viaduct

Case #	ρ for segment 1	ρ for segment 2	ρ for segment 3	ρ for segment 4	ρ for segment 5
1	1.18	0.98	0.96	1.05	1.06
2	1.14	0.98	0.97	1.06	1.05
3	1.13	1.00	0.98	1.07	1.03
4	1.13	1.00	0.99	1.07	1.04
5	1.13	1.00	0.99	1.06	1.04
6	1.12	1.01	0.99	1.05	1.04
7	1.12	1.02	1.00	1.05	1.04
8	1.11	1.02	1.00	1.05	1.03
9	1.11	1.02	1.00	1.05	1.03
10	1.12	1.01	0.99	1.05	1.04
11	1.12	1.02	0.99	1.06	1.05
12	1.12	1.02	1.00	1.06	1.05
13	1.10	1.03	1.00	1.06	1.04
14	1.09	1.05	1.00	1.05	1.05
15	1.05	1.06	0.99	0.99	1.03
16	1.00	0.96	0.99	0.99	0.99
17	0.70	1.10	1.04	1.16	0.65
18	1.07	1.07	1.03	1.01	1.09

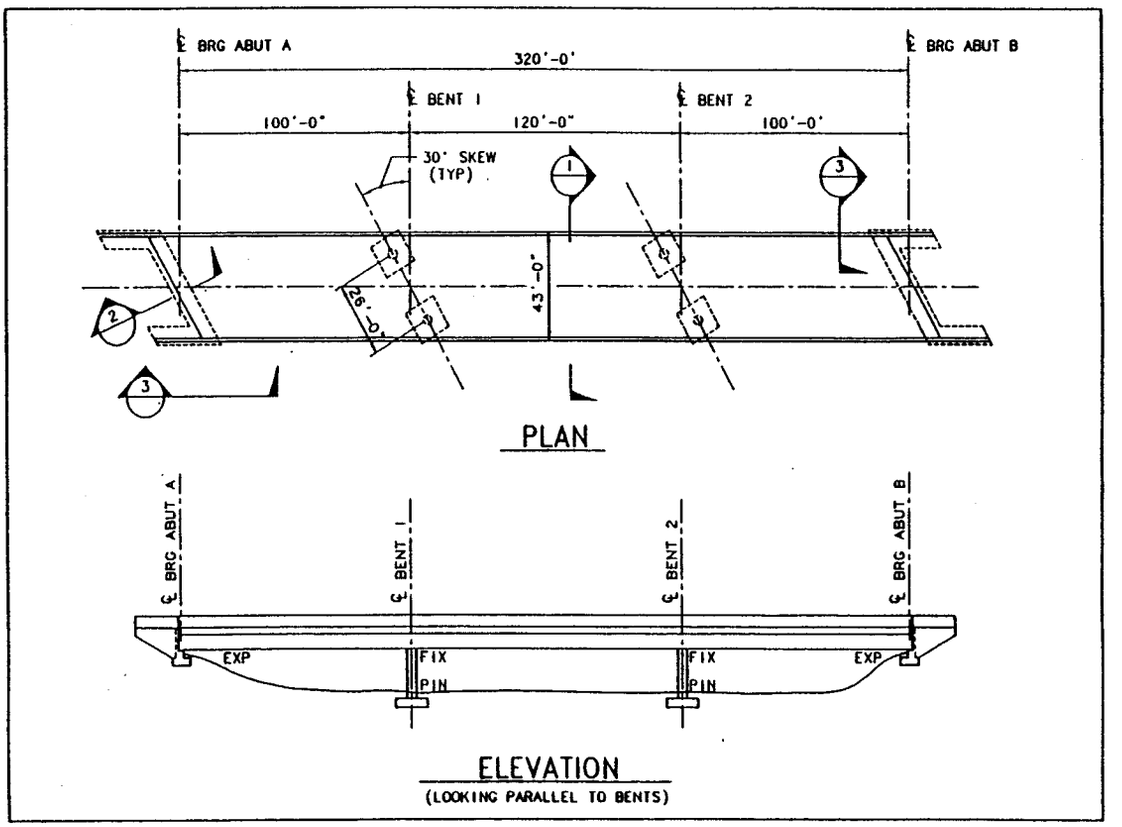

FIGURE 3-25 Elevation and Plan Views of the Typical Three-Span Continuous Concrete Bridge Taken from FHWA (1996).

The Uniform Building Code (International Conference of Building Officials 1994) acceleration response spectrum for Type II soil, 5% damping, and 0.3g peak ground acceleration was selected for all supports of the bridge (see Fig. 3-15). Abrahamson's coherence law (Abrahamson 1993) was chosen to describe the coherence loss between pairs of supports. The functional form of this law is provided in Eqs. (2-60)-(2-65) and is plotted in Fig. 3-16. Finally, the Jennings et al. envelope (Jennings et al. 1968) was used to define the duration of strong ground motion (see Fig. 2-4).

Typical generated asynchronous displacement time histories at supports 1 and 4 of the bridge are plotted in Fig. 3-26, for demonstration purposes. The corresponding set of identical support ground motion time histories is again obtained by considering that the acceleration time history at the first support of the bridge is applied at all the other supports.

Dynamic Analysis and Conclusions

For each of the 36 scenario earthquakes considered (refer to Table 3-14), the typical three-span bridge was analyzed using differential and the corresponding identical support ground motion. Only linear dynamic analyses were carried out. The computer code SAP2000 was used to perform these dynamic time history analyses.

The ratio ρ defined in Eq. (3-1) was then computed for each of the 36 scenario earthquakes, for the following response quantity: the combined axial and bending stress at the columns and the deck of the bridge. The computed values of ρ are provided in Table 3-14. It should be mentioned at this point that the linear three-dimensional study of the bridge developed by BERGER/ABAM Engineers presented here is not as detailed as the analyses performed earlier in this report, as there are only three random cases considered for each combination of velocity v and angle of incidence θ (refer to Table 3-14). The results presented in Table 3-14 for the ρ values of the combined axial and bending stress at the deck and the columns of the bridge can serve therefore only as an indication of the effect of the angle of incidence of the seismic waves with respect to the axis of the bridge and of the apparent velocity of wave propagation. Table 3-14 indicates a maximum ρ value of 1.072 for the columns (occurring for scenario earthquake #7) and 1.044 for the deck (occurring for scenario earthquake #35).

3.5 General Conclusions

There are very interesting conclusions that can be drawn from the case studies considered in Chapter 3. These conclusions will be used to determine which set of bridges and which cases of spatially varying ground motion deserve a more detailed study, in order to establish guidelines for the analysis and design of highway bridges to account for the effect of spatial variability of ground motion.

Figures 3-18 and 3-20 plot the most important results of the comparative analysis of the eight bridges. Specifically, Fig. 3-18 plots the maximum ρ values (defined in Eq. 3-1) for M/M_y (M being the bending moment and M_y being the yield moment) at the piers resulting from linear dynamic analysis, as a function of the total length of the bridge. Figure 3-18 provides the following indication: it appears that for bridges similar in form

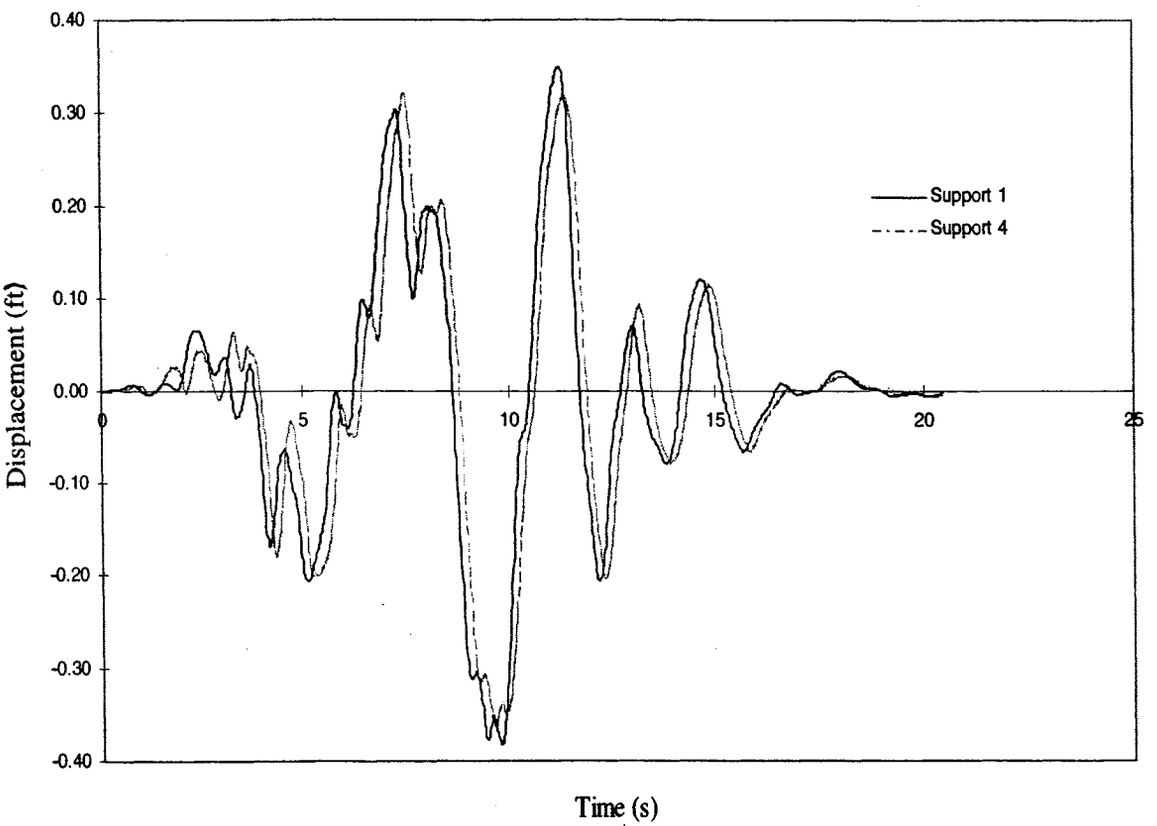

FIGURE 3-26 Typical Generated Asynchronous Displacement Time Histories at Supports 1 and 4 of the Typical Three-Span Continuous Concrete Bridge (FHWA 1996).

TABLE 3-14

The 36 Scenario Earthquakes Considered in the Three-Dimensional Analysis of the Typical Three-Span Continuous Concrete Bridge and the Corresponding ρ Values for the Combined Axial and Bending Stress in the Deck and the Columns

Scenario #	Velocity v (m/sec)	Angle θ (degrees)	Random case	ρ for deck	ρ for column
1	1,000	0	1	0.963	1.043
2	1,000	0	2	0.966	0.999
3	1,000	0	3	1.005	1.000
4	1,000	45	1	0.931	1.016
5	1,000	45	2	0.997	0.968
6	1,000	45	3	0.974	0.942
7	1,000	90	1	1.012	1.072
8	1,000	90	2	0.921	0.975
9	1,000	90	3	0.940	0.948
10	1,500	0	1	0.952	1.022
11	1,500	0	2	0.966	0.999
12	1,500	0	3	1.001	0.992
13	1,500	45	1	0.919	1.014
14	1,500	45	2	1.038	0.931
15	1,500	45	3	0.978	0.976
16	1,500	90	1	1.009	1.046
17	1,500	90	2	0.910	0.913
18	1,500	90	3	0.943	0.983
19	2,000	0	1	1.027	0.993
20	2,000	0	2	1.003	0.994
21	2,000	0	3	1.027	0.999
22	2,000	45	1	1.032	0.986
23	2,000	45	2	1.029	0.954
24	2,000	45	3	1.002	0.960
25	2,000	90	1	0.977	0.993
26	2,000	90	2	0.943	0.942
27	2,000	90	3	0.937	1.016
28	2,500	0	1	1.000	1.022
29	2,500	0	2	0.971	0.981
30	2,500	0	3	1.005	0.991
31	2,500	45	1	0.977	1.042
32	2,500	45	2	1.039	0.952
33	2,500	45	3	0.999	0.993
34	2,500	90	1	1.019	1.059
35	2,500	90	2	1.044	0.941
36	2,500	90	3	0.987	1.005

and configuration to the eight bridges considered in this comparative analysis and having a total length less than approximately 1,000 ft, the expected maximum ρ value for M/M_y at the piers resulting from linear dynamic analysis is going to be close to 1.10. For bridges larger than 1,000 ft, it is difficult to provide a general rule because there is only one data point as can be seen from Fig. 3-18, but it appears that the expected maximum ρ value for M/M_y can be much higher than 1.10. Figure 3-20 plots the maximum ρ values for θ/θ_y (ductility demand) at the piers resulting from nonlinear dynamic analysis, as a function of the total length of the bridge. Figure 3-20 provides the following indication: it appears that for bridges similar in form and configuration to the eight bridges considered in this comparative analysis and having a total length less than approximately 1,000 ft, the expected maximum ρ value for θ/θ_y at the piers resulting from nonlinear dynamic analysis is going to be close to 1.20-1.25. For bridges larger than 1,000 ft, it is difficult to provide a general rule because there is only one data point as can be seen from Fig. 3-20, but it appears that the expected maximum ρ value for θ/θ_y can be much higher than 1.20-1.25.

Table 3-12 displays the most important results of the analysis of the Gavin Canyon bridge when considered to have supports on different local soil conditions. Specifically, Table 3-12 displays the statistics of ρ values for θ/θ_y (ductility demand) for the 15 scenario earthquakes considered in Table 3-10 (same local soil conditions), and the corresponding statistics for the 20 scenario earthquakes: mmsm1-mmsm20 considered in Table 3-11 (different local soil conditions). Note that Table 3-12 is constructed from results of nonlinear analyses. The most important conclusion from Table 3-12 is the very significant increase in the mean value, standard deviation, coefficient of variation, and maximum value of ρ for the case of different local soil conditions, when compared to the case of same local soil conditions, at Piers 2 and 3. Specifically, at Pier 2, the mean value of ρ increases from 1.008 to 1.635, the standard deviation of ρ from 0.086 to 0.236, the coefficient of variation of ρ from 8.6% to 14.4%, and the maximum ρ value from 1.20 to 2.27. At Pier 3, the mean value of ρ increases from 0.999 to 1.293, the standard deviation of ρ from 0.057 to 0.203, the coefficient of variation of ρ from 5.7% to 15.7%, and the maximum ρ value from 1.07 to 1.78. The reason that Piers 1 and 4 do not show increases in the ρ values for θ/θ_y as dramatic as Piers 2 and 3 for the case of different local soil conditions is explained in detail earlier in this report. The general conclusion of Table 3-12 is therefore the following: when a bridge similar in type and configuration as the Gavin Canyon bridge has supports on different local soil conditions, the expected maximum values of ρ for the ductility demand (θ/θ_y) at the piers can become much larger than unity, and certainly much larger than corresponding values resulting from all supports being considered on the same local soil conditions.

The preliminary results obtained in Chapter 3 indicate that relatively longer bridges like the SR14/I5 viaduct (with overall length more than 1000′) are expected to show considerable increases in their structural response when analyzed using differential support ground motion, compared to the case of identical support ground motion. On the other hand, relatively shorter bridges (with overall length less than 1000′) appear to show only minor increases in their structural response when analyzed using differential support ground motion, compared to the case of identical support ground motion. The aforementioned

two statements about relatively longer and relatively shorter bridges are valid for bridges that have all their supports on the same type of local soil conditions. For the case when different supports of a bridge are on different local soil conditions, even relatively shorter bridges can show a significant increase in their structural response when analyzed using differential support ground motion, compared to the case of identical support ground motion. One of the major objectives of Chapter 4 is going to be, therefore, to verify the validity of the important preliminary conclusions mentioned above, by performing a more detailed analysis of a set of bridges. Such an analysis will involve a number of samples large enough to determine with adequate accuracy the statistics of the structural response through a Monte Carlo simulation approach.

SECTION 4
RIGOROUS ANALYSIS OF A SET OF HIGHWAY BRIDGES TO ESTIMATE THE EFFECT OF SPATIAL VARIATION OF SEISMIC GROUND MOTION

4.1 Introduction

The extensive but preliminary studies conducted in Chapter 3, have clearly indicated that there are several cases where differential (asynchronous) support ground motion can produce significantly higher structural response to multi-supported highway bridges, when compared to the case of identical support ground motion.

The studies performed on the set of bridges in Chapter 3 have followed a Monte Carlo simulation approach. Specifically, ground motion time histories have been modeled as stochastic vector processes, and the selected bridges have been analyzed linearly and nonlinearly in the time domain (time history analysis). The main reason that the Chapter 3 studies were considered preliminary is the fact that only a small number of time history analyses have been performed for each case (in the majority of cases less than five). It is believed that this relatively small number of samples considered is not enough to provide reliable estimates for the statistics of structural response. The reason that only a relatively small number of samples has been considered in Chapter 3 is that the main objectives at that stage were to establish whether spatial variability of ground motion necessitated further study, and if the answer to that question was positive, to determine which were the specific cases that required further study. The answer to the first question was positive, while as far as the second question is concerned, it was found that the case that could potentially pose the greatest risk to highway bridges was the case of multi-supported structures with supports on different local soil conditions. In addition, relatively longer bridges were found to be in higher risk than relatively shorter bridges when subjected to differential support ground motion. It should be noted that another reason that the studies in Chapter 3 were considered preliminary was the use of an earlier version of the SAP2000 software that presented some problems when performing dynamic time history analyses using spatially varying seismic ground motion. In Chapter 4, all analyses were done using the latest version of SAP2000 that has eliminated these early problems.

A Monte Carlo simulation approach is also followed in Chapter 4. Seismic ground motion time histories are again modeled as a non-stationary stochastic vector process. Generated ground motion time histories at the different supports of a bridge are made compatible with prescribed design response spectra, and reflect a given apparent velocity of wave propagation, coherence function, and duration of strong ground motion. It has been mentioned earlier that spatial variability of seismic ground motion can be attributed to the following three mechanisms: 1) the difference in arrival times of the seismic waves at different locations, commonly known as the "wave passage effect," 2) the change in shape of the propagating waveform due to multiple scatterings of the seismic waves in the highly inhomogeneous soil medium, referred to as the "incoherence effect," and 3) the change in amplitude and frequency content of ground motion at different locations on the ground surface due to different local soil conditions, known as the "local site effect." In the methodology developed in Chapter 2 to generate sample functions of spatially correlated ground motion time histories, the wave passage effect is described by the apparent velocity of wave propagation, the incoherence effect is described by assigning a

coherence function, and the local site effect is described by prescribing different response spectra at locations with different local soil conditions.

4.2 The Seven Bridges Selected

Based on the preliminary studies of the set of bridges in Chapter 3, the following set of seven representative bridges has been selected to perform a more detailed and rigorous analysis in Chapter 4: the "Text Example" bridge, the "FHWA-No.2" bridge, the "TY0H" bridge, the "TY1H" bridge, the "TY2H" bridge, the "Gavin Canyon" bridge, and the "Santa Clara" bridge. Detailed descriptions of the first six bridges can be found in Chapter 3, while a description of the twelve-span Santa Clara bridge is provided later in this section. For the first six bridges, plots of their elevation and cross-sectional information can be found in Figures 3-1 and 3-3 – 3-7, while Table 3-1 provides information about their total length and number of spans and Tables 3-2 and 3-4 – 3-8 provide information about the moment of inertia, cross-sectional area, mass density, and elastic modulus of the girders and the columns of each bridge. The seven bridges selected for this comparative study represent a wide range of number of spans and total lengths. The reason for this selection is to study the response of bridges in relation to their length. The total lengths of these seven bridges range from 111 ft to 1,641 ft. The number of spans ranges from 3 to 12.

In Chapter 3, the selected bridges were studied by performing both linear and nonlinear dynamic analyses. In this chapter, it was decided to carry out exclusively nonlinear dynamic analyses, because the bridge response under strong ground motion that can cause severe damage to the structure is nonlinear in most cases of practical interest. Along the lines of a Monte Carlo simulation approach, a number of samples of spatially varying ground motion time histories are generated at the structural supports using the methodology developed in Chapter 2. The statistics of the maximum structural response (mean, standard deviation, and coefficient of variation) for each one of the seven bridges are then calculated in terms of the ductility demand at the piers from an ensemble of 20 (twenty) sample time history analyses. The number of twenty samples was determined after estimating the maximum response statistics in a typical case using ten, twenty, forty, and eighty samples, and observing that the aforementioned statistics could be estimated with adequate accuracy using only twenty samples.

Two general types of support ground motions were considered: 1) all structural supports on same local soil conditions, and 2) different structural supports on different local soil conditions. For comparison purposes each bridge was also subjected to identical support ground motion. In addition, the relative significance of the effects of incoherence, wave passage, and variable local soil conditions at different supports of the bridge were examined for different apparent velocities of wave propagation. A detailed description of the ground motion cases considered follows in section 4.3. It should be pointed out that all seven bridges in this group were subjected to the same cases of ground motion for comparison purposes.

4.2.1 Description of the Santa Clara Bridge

The elevation and sectional views of the Santa Clara bridge are displayed in Figs. 4-1 – 4-2. Table 4-1 provides information about the moment of inertia, cross-sectional area, mass density, and elastic modulus of the girders and the columns of the bridge. It is a twelve span reinforced concrete bridge with interior spans of 143 ft., exterior spans of 105.25 ft., and a total length of 1640.5 ft. The superstructure consists of a 49-ft. wide, 4-cell concrete box-girder, which is

TABLE 4-1 Material and Cross Sectional Properties of Analysis Model for Santa Clara Bridge Using SAP2000

Structural Component	Moment of Inertia (ft^4)	Cross Sectional Area (ft^2)	Mass Density (pcf)	Young's Modulus (Ksi)
RC Girders	392.87	74.72	150	3605
Pier Section at A	83.67	62.75	150	3250
Pier Section at B	60.00	45.00	150	3250
Pier Section at C	54.67	41.00	150	3250

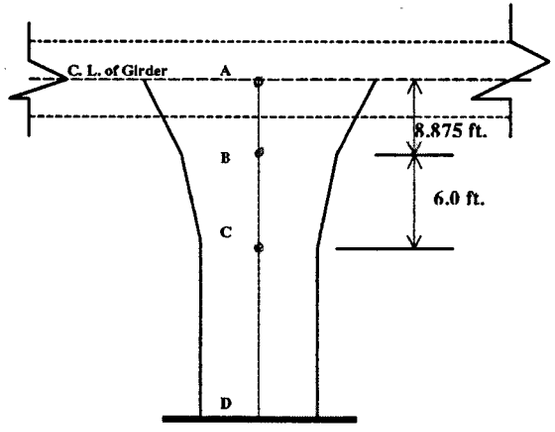

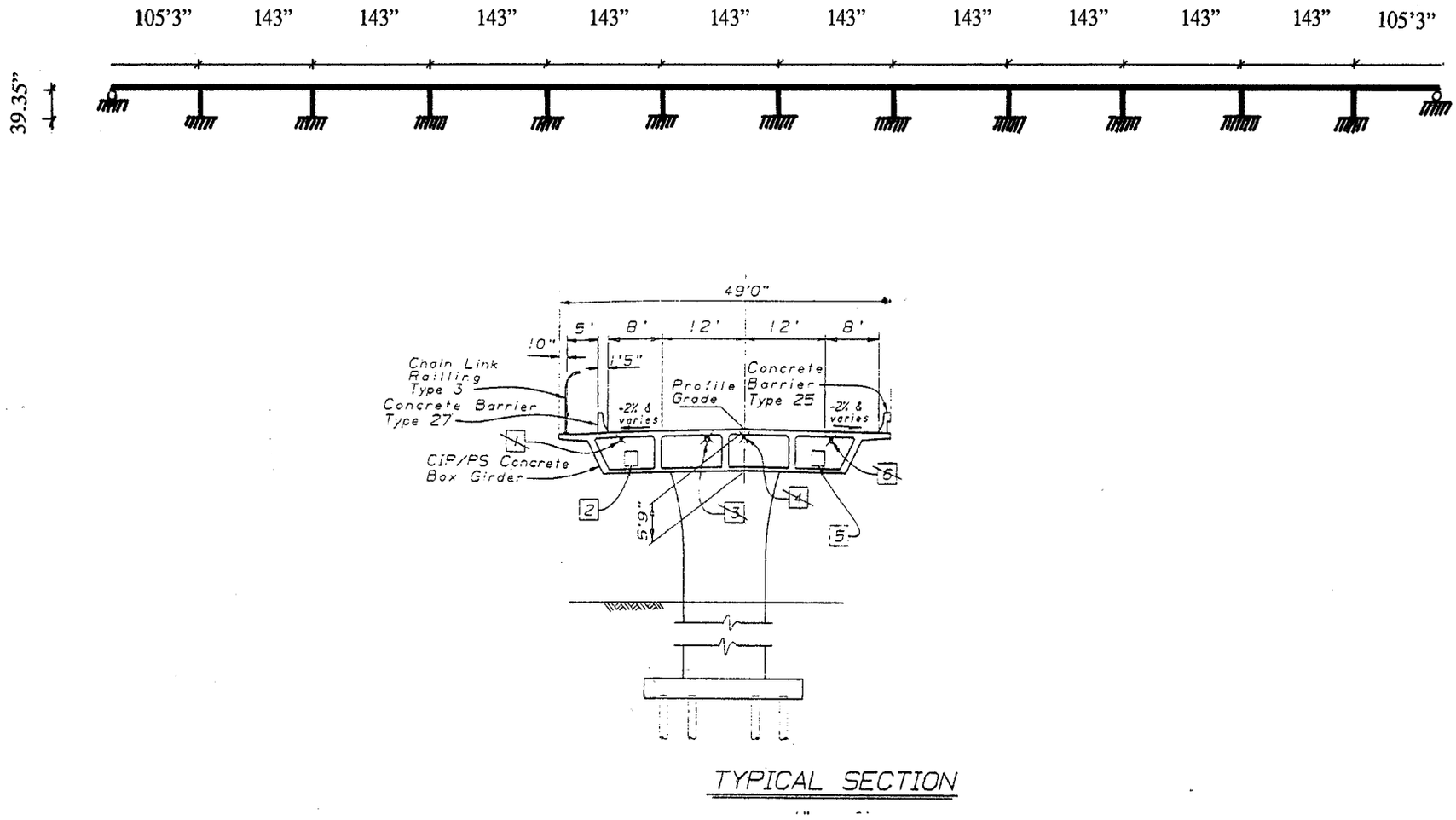

FIGURE 4-1 Elevation and Sectional View of Santa Clara Bridge

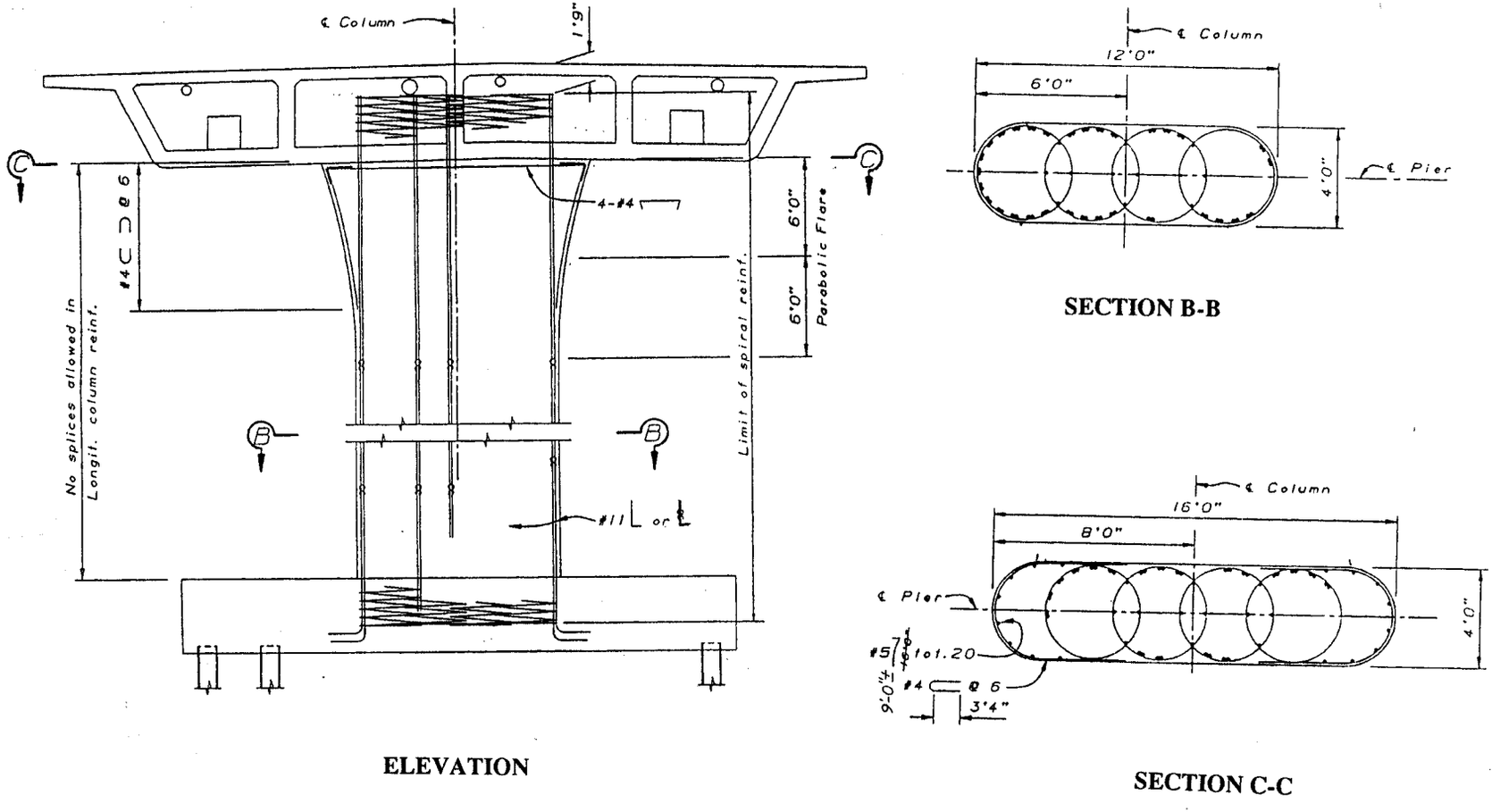

FIGURE 4-2a Elevation and Section of Piers of Santa Clara Bridge.

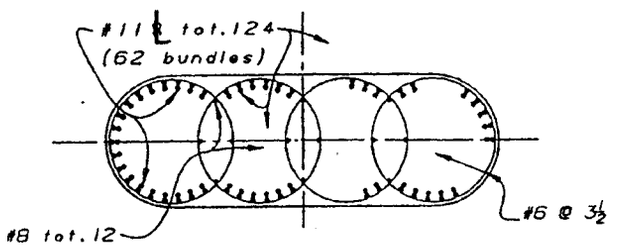

PIER 1

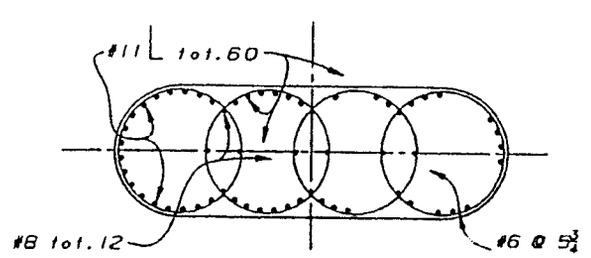

PIER 2

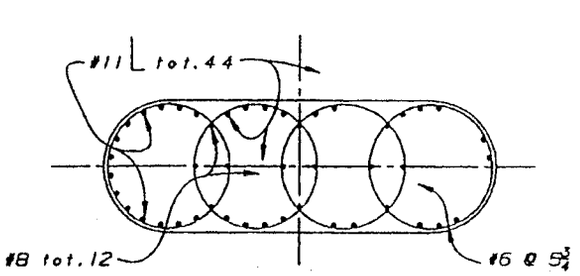

PIER 3, 4, 8 and 9

FIGURE 4-2b Cross – Section of Piers of Santa Clara Bridge.

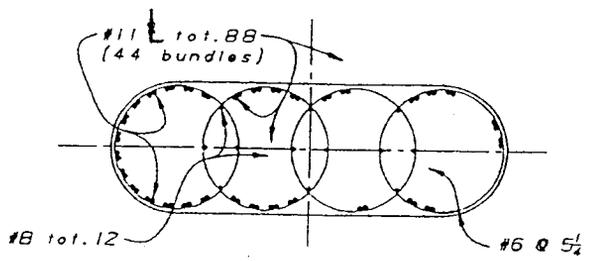

PIER 5

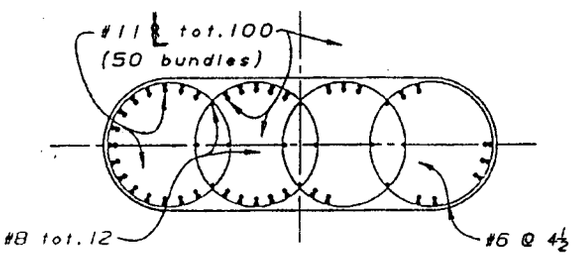

PIER 6

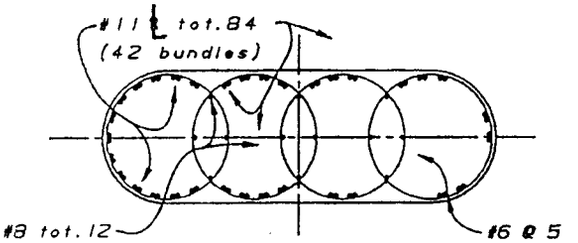

PIER 7 and 11

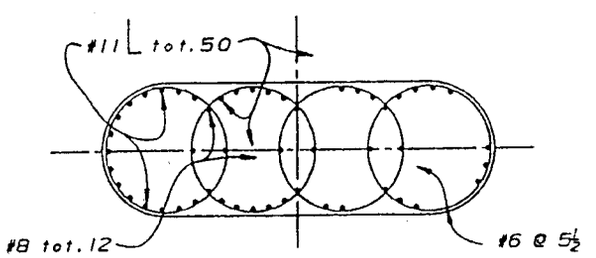

PIER 10

FIGURE 4-2c Cross – Section of Piers of Santa Clara Bridge.

supported on single column piers and at the two ends supported on abutments. The columns are flared at the top, oblong in shape, with typical cross sectional dimensions of 12 ft x 4 ft and a height of 39.35 ft. The reinforcement details for all piers are displayed in Figs. 4-2a, 4-2b and 4-2c.

4.2.2 Finite Element Models of the Seven Bridges

One of the important decisions that had to be made in Chapter 4 was to determine the number of ground motion cases to consider. There were cases of differential (asynchronous) support ground motion where all the bridge supports were assumed to be on the same type of local soil conditions, cases where different supports were assumed to be on different types of local soil conditions, and cases where all supports were subjected to identical support ground motion. In addition, there were sub-cases where only the wave passage effect was considered, sub-cases where only the incoherence effect was considered, and sub-cases with different apparent velocities of wave propagation (all these cases are described in detail in section 4.3). One of the main concerns was therefore whether to consider seismic waves arriving at some angle with respect to the axis of the bridge. Preliminary studies in Chapter 3 using an essentially two-dimensional model of the SR14/I5 viaduct have indicated that when seismic waves arrive at an angle with respect to the axis of the bridge, it is possible in some cases to have structural response higher than the corresponding one for longitudinal seismic loading. However, in Chapter 4, it was decided to consider only the case of longitudinal seismic loading (seismic waves propagating parallel to the axis of the bridge). There were two reasons for this decision. The first one was that in order to have a definite answer about the importance of the angle of incidence, an enormous number of case studies would have to be considered. The second reason was that the relatively simple two-dimensional models of the bridges using frame elements are not capable of capturing the complex three-dimensional behavior of the bridges when the seismic waves arrive at a certain angle with respect to the axis of the structure.

It was decided therefore that the motion of interest in this comparative study of the seven bridges would be the longitudinal motion of the center axis of each bridge. For this reason, each bridge is modeled in two dimensions using frame elements. The section properties of these elements are chosen to represent the actual cross-sections of the bridge and the effective column length is measured from the mid-point of the deck to the foundation. Information about the cross-sectional area and moment of inertia of the different sections of each bridge, along with basic information about the finite element discretization is provided in Tables 3-2, 3-4 – 3-9 and 4-1.

The computer code SAP2000 is selected to perform the nonlinear dynamic time history analyses. This program has the capability to evaluate the nonlinear dynamic response of a bridge model subjected to differential (asynchronous) support excitation. A relatively simple model is used to perform the nonlinear dynamic analyses. This appears quite appropriate considering the various types of approximation in modeling the bridge structures, and the high level of uncertainty involved in determining the input seismic ground motion.

The model used to describe the potentially nonlinear behavior of the piers of all seven bridges (the only members considered to exhibit nonlinear behavior in this study) is depicted in Fig. 3-9a. According to this model, a pier is modeled as an elastic column of length $2H_e$, with a pair of plastic zones of length L_p at each end of the column, as shown in Fig. 3-9a. The total length H of

the pier from the ground to the soffit of the girder is therefore equal to $2(H_e+L_p)$. Each plastic zone is then modeled to consist of a nonlinear rotational spring and a rigid element of length L_p as shown in Fig. 3-9b. The typical moment-rotation relationship used in this study for the nonlinear springs is the bilinear one shown in Fig. 3-9c. Its parameters are established using the *Column Ductility Program* COLx (Caltrans 1993). The specific moment-curvature relationships resulting from the COLx program are displayed in Figs. 3-10 – 3-13 for the first six bridges in this study and in Fig. 4-3a – 4-3d for the piers of the Santa Clara bridge. The various parameters shown in Figs. 3-9 – 3-13 and in Fig. 4-3a – 4-3d are defined as follows:

M_y = Yield moment
p_y = Curvature at yield
M_{yp} = Moment at idealized yield point
p_{yp} = Curvature at idealized yield point
M_u = Ultimate moment
p_u = Maximum curvature
K_{eff} or K_s = Elastic or initial stiffness (before yielding)
α = Coefficient that determines the post yield stiffness (i.e. αK_{eff} is the stiffness of the bilinear curve after yielding)
θ_y = Yield rotation of the nonlinear spring ($\theta_y = p_{yp} \times L_p$ where L_p is the length of the plastic zone)

The resulting curvature values are then multiplied by the length of the plastic zone (given by the COLx computer program) to obtain the moment-rotation relationship for the nonlinear springs. The yield point is obtained by approximating the actual curve as a bilinear one.

For those bridges with expansion joints, the joints are modeled by allowing the two sections of the bridge converging to the joint to move independently in the horizontal direction and to rotate independently, and by constraining them to move by the same amount in the vertical direction.

4.3 Ground Motion Cases Considered for the Seven Bridges

As mentioned earlier, all seven bridges were subjected to response spectrum compatible, spatially varying ground motions to determine whether differential support ground motion can lead to increased bridge response, when compared to the case of identical support ground motion.

In the remaining part of this chapter, the following definitions are used for the terms: "Differential Support Ground Motion", "Different Local Soil Conditions", "Same Local Soil Conditions", and "Identical Support Ground Motion".

Differential Support Ground Motion: For elongated structures on multiple supports, different supports are considered to experience different ground motion time histories. This is due to the effect of wave passage, loss of coherence and (possibly) different supports being on different types of local soil conditions.

Different Local Soil Conditions: This is the case of differential support ground motion where different supports of the bridge are on different local soil conditions.

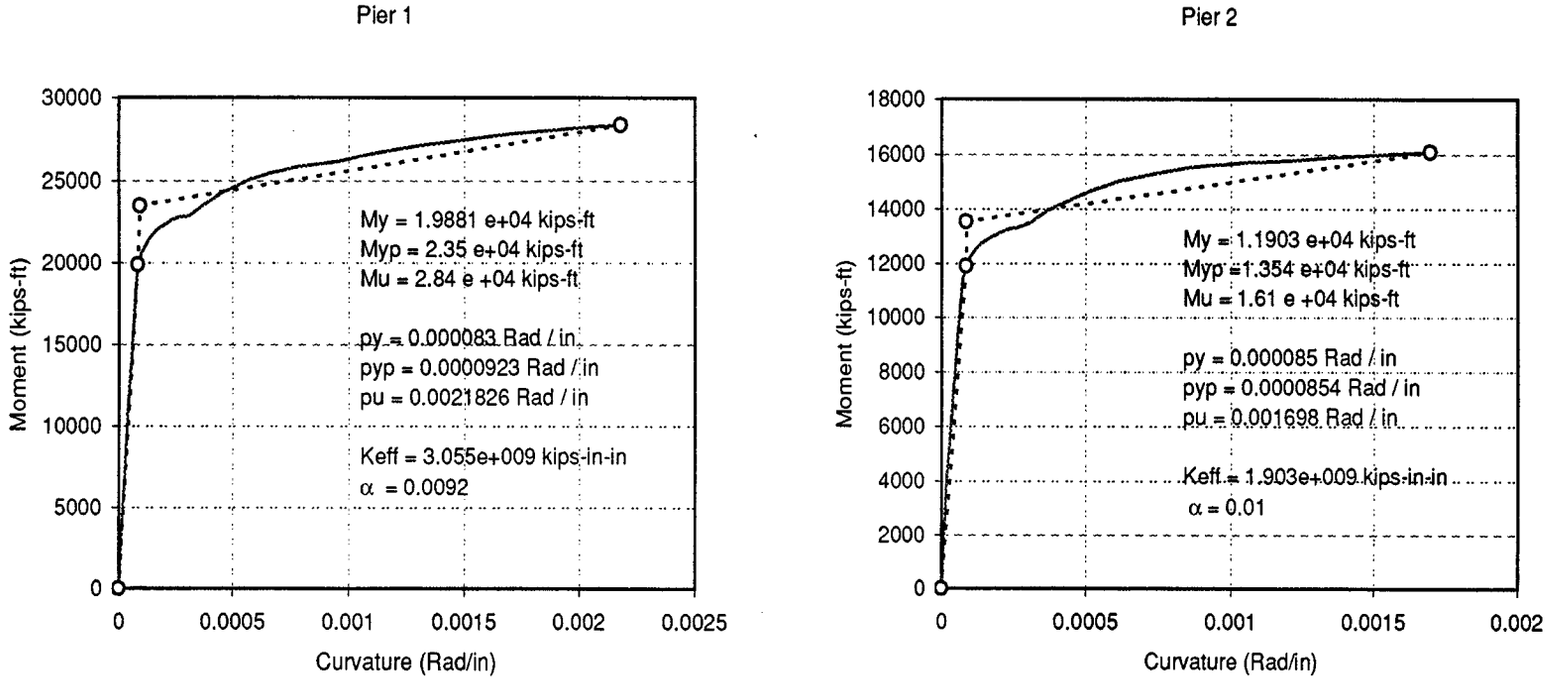

FIGURE 4-3a Moment - Curvature Relationships for the Piers of Santa Clara bridge resulting from the COLx Column Ductility Program (Caltrans 1993)

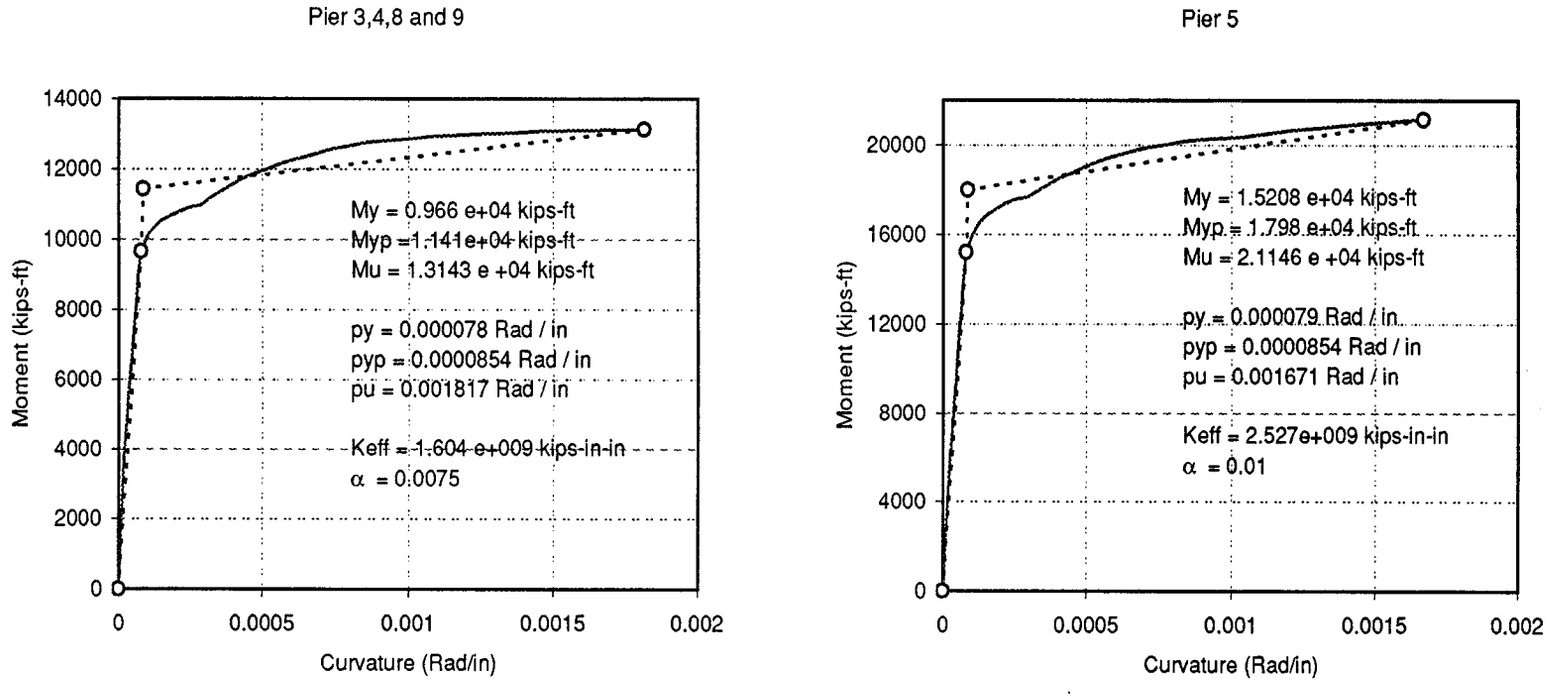

FIGURE 4-3b Moment - Curvature Relationships for the Piers of Santa Clara bridge resulting from the COLx Column Ductility Program (Caltrans 1993)

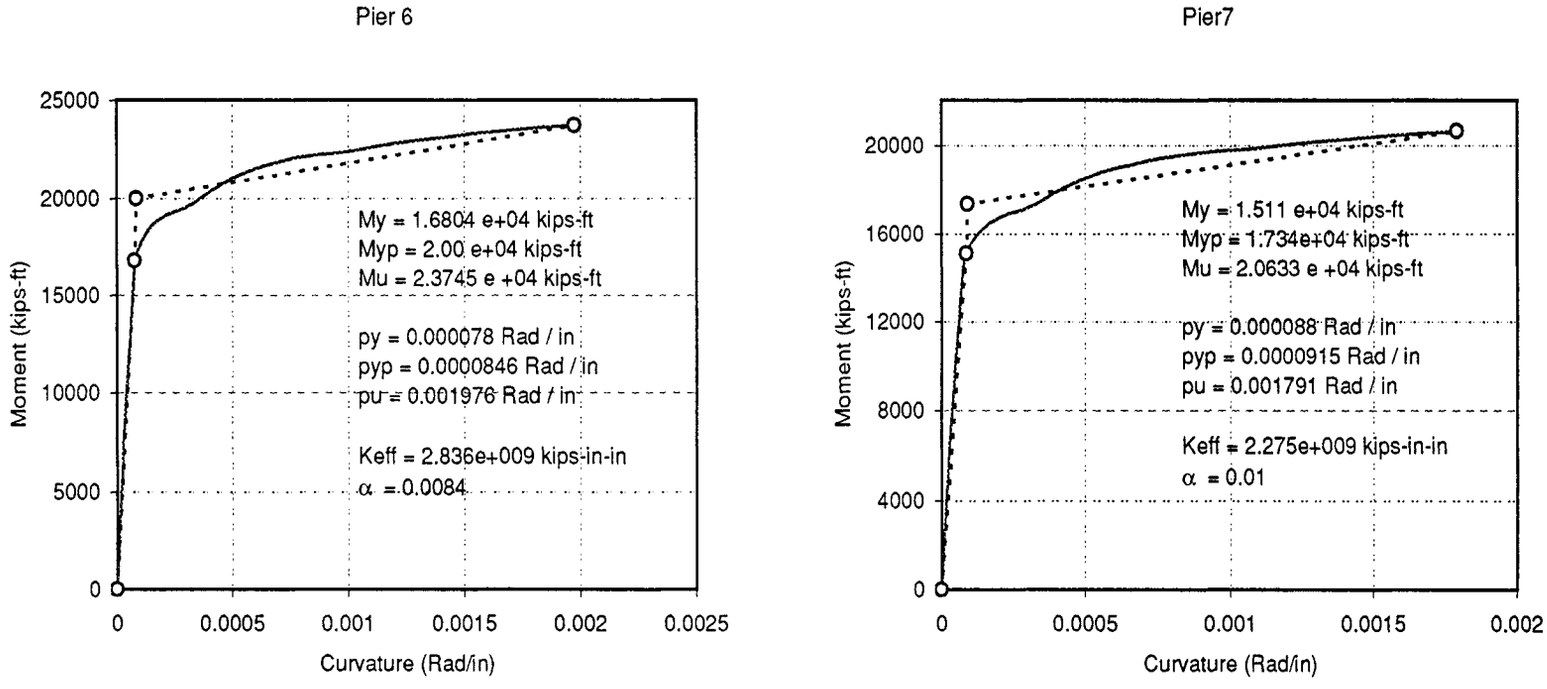

FIGURE 4-3c Moment - Curvature Relationships for the Piers of Santa Clara bridge resulting from the COLx Column Ductility Program (Caltrans 1993)

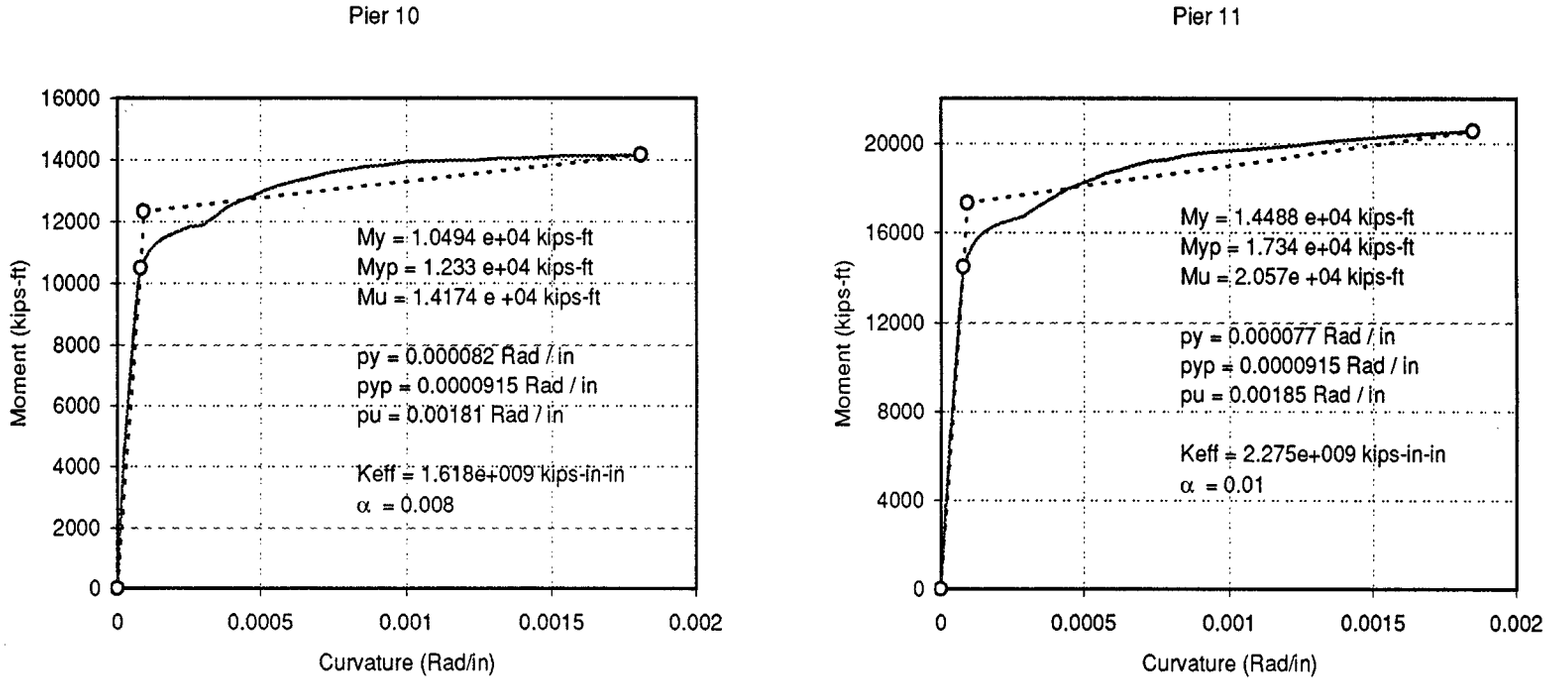

FIGURE 4-3d Moment - Curvature Relationships for the Piers of Santa Clara bridge resulting from the COLx Column Ductility Program (Caltrans 1993)

Same Local Soil Conditions: This is the case of differential support ground motion where all the supports of the bridge are on the same local soil conditions.

Identical Support Ground Motion: For elongated structures on multiple supports, all supports are assumed to be subjected to identical support ground motion time histories. For the purposes of this study, the ground motion time history at the first support of the bridge is applied at all the other supports in order to check the validity of this assumption used in engineering practice when performing dynamic analysis of multi-span bridges.

The methodology developed in Chapter 2 of this report is used to generate the spatially varying ground motion time histories that are used as input excitations for the nonlinear dynamic analyses of the seven bridges. According to this methodology, the generated ground motion time histories at the different supports of a bridge are made compatible with prescribed design response spectra, and reflect a given apparent velocity of wave propagation, coherence function, and duration of strong ground motion.

In order to determine the relative importance of the wave passage and incoherence effects to the nonlinear dynamic structural response, the following three cases were considered:

CASE 1: Both the wave passage and incoherence effects are considered (loss of coherence and wave propagation considered).

CASE 2: Only the incoherence effect is considered (loss of coherence but no wave propagation considered).

CASE 3: Only the wave passage effect is considered (wave propagation considered, but seismic waves are perfectly coherent - no loss of coherence).

Table 4-2 describes the three cases in more detail indicating that within each case it is possible to have two sub-cases of differential support ground motion: different local soil conditions and same local soil conditions. Table 4-2 also indicates the two values considered for the apparent velocity of wave propagation: 300 m/sec and 1,000 m/sec.

In order to study the very important case of bridges with supports on different local soil conditions, certain supports of each bridge were assumed to be in different (softer) local soil conditions than the rest. Such cases can be encountered in practice in bridges over small (or larger) valleys where the abutments and some of the supports close to the abutments can be in harder soil conditions, while some of the supports around the center of the bridge can be in softer local soil conditions. Table 4-3 describes the different local soil conditions assumed for the piers of each one of the seven bridges.

From the above, it is obvious that there is a very large number of different cases of ground motions that were considered for each bridge. It has to be pointed out that for each one of these

TABLE 4-2 Detailed Description of Cases Considered

SPATIAL VARIABILITY EFFFECTS CONSIDERED	CONDITIONS AT SUPPORTS AND INFORMATION ABOUT APPARENT VELOCITY OF WAVE PROPAGATION
CASE 1 Both the wave passage and incoherence effects considered.	1) All supports on same local soil conditions with velocity of 1000 m/s. 2) All supports on same local soil conditions with velocity of 300 m/s. 3) Different supports on different local soil conditions with velocity of 1000 m/s.
CASE 2 Only the incoherence effect considered. (no wave passage effect)	1) All supports on same local soil conditions with velocity approaching infinity. 2) Different supports on different local soil conditions with velocity approaching infinity.
CASE 3 Only the wave passage effect considered. (no incoherence effect)	1) All supports on same local soil conditions with velocity of 1000 m/s. 2) All supports on same local soil conditions with velocity of 300 m/s. 3) DIFFERENT supports on different local soil conditions with velocity of 1000 m/s.

TABLE 4-3 Description of Different Local Soil Conditions for Various Bridges

	Bridge	Total No. of Spans	Total No. of Piers	Soil at Left Abutment	UBC Soil Type II (medium) at Piers	UBC Soil Type III (soft) at Piers	Soil at Right Abutment
1	TEXT BRIDGE	3	2	medium	Pier 1	Pier 2	medium
2	FHWA BRIDGE	3	2	medium	-	Pier 1, Pier 2	medium
3	GAVIN CANYON	5	4	medium	Pier 1 , Pier 4	Pier 2, Pier 3	medium
4	TYOH BRIDGE	5	4	medium	Pier 1 , Pier 4	Pier 2, Pier 3	medium
5	TY1H BRIDGE	5	4	medium	Pier 1 , Pier 4	Pier 2, Pier 3	medium
6	TY2H BRIDGE	5	4	medium	Pier 1 , Pier 4	Pier 2, Pier 3	medium
7	SANTA CLARA	12	11	medium	Pier 1-4 , Pier 8-11	Pier 5-7	medium

cases and for each bridge, there are twenty nonlinear dynamic analyses that are performed in order to estimate the statistics of the maximum response.

4.3.1 Design Response Spectrum

The acceleration response spectra for Type I, II, and III soils as specified by the Uniform Building Code (International Conference of Building Officials, 1994) for 5% damping and 0.5g peak ground acceleration were selected for the different supports of each one of the seven bridges, depending on the different local soil conditions at each support. Plots of these three response spectra are displayed in Fig. 4-4.

4.3.2 Coherence Function

Although in Chapter 3 both the Abrahamson (1993) and the Harichandran and Vanmarcke (1986) models for the coherence function were used, in this chapter it is only the Harichandran and Vanmarcke model that is used. There are two reasons for this decision. The first one is that the Harichandran and Vanmarcke model with its larger coherence loss at low frequencies is considered to provide generally conservative results for the structural response in the majority of cases. (Zerva (1994), Kareem, Deodatis and Shinozuka (1997)). The second reason is that the Abrahamson model sometimes created some numerical difficulties with the Cholesky decomposition of the cross-spectral density matrix of the stochastic vector process modeling the ground motion.

The Harichandran and Vanmarcke model for the coherence function $\gamma_{jk}(\omega)$ has the following form:

$$\gamma_{jk}(\omega) = A\exp\left[-\frac{2\xi_{jk}}{\alpha\theta(\omega)}(1-A+\alpha A)\right] + (1-A)\exp\left[-\frac{2\xi_{jk}}{\theta(\omega)}(1-A+\alpha A)\right] \tag{4-1}$$

where ξ_{jk} is the distance between points j and k, $\theta(\omega)$ is the frequency - dependent correlation distance:

$$\theta(\omega) = k\left[1+\left(\frac{\omega}{\omega_0}\right)^b\right]^{-1/2} \tag{4-2}$$

and A, α, k, ω_0 and b are model parameters.

For the purpose of this study the model parameters are chosen as follows:

$A = 0.626, \alpha = 0.022$, $k = 19700$ m, $\omega_0 = 12.692$ rad/sec, $b = 3.47$

The functional forms of the Harichandran-Vanmarcke model for the coherence function are plotted in Fig. 4-5 as a function of frequency, for different values of the separation distance. It becomes quite obvious when comparing Fig. 4-5 with Fig. 2-15 depicting the Abrahamson

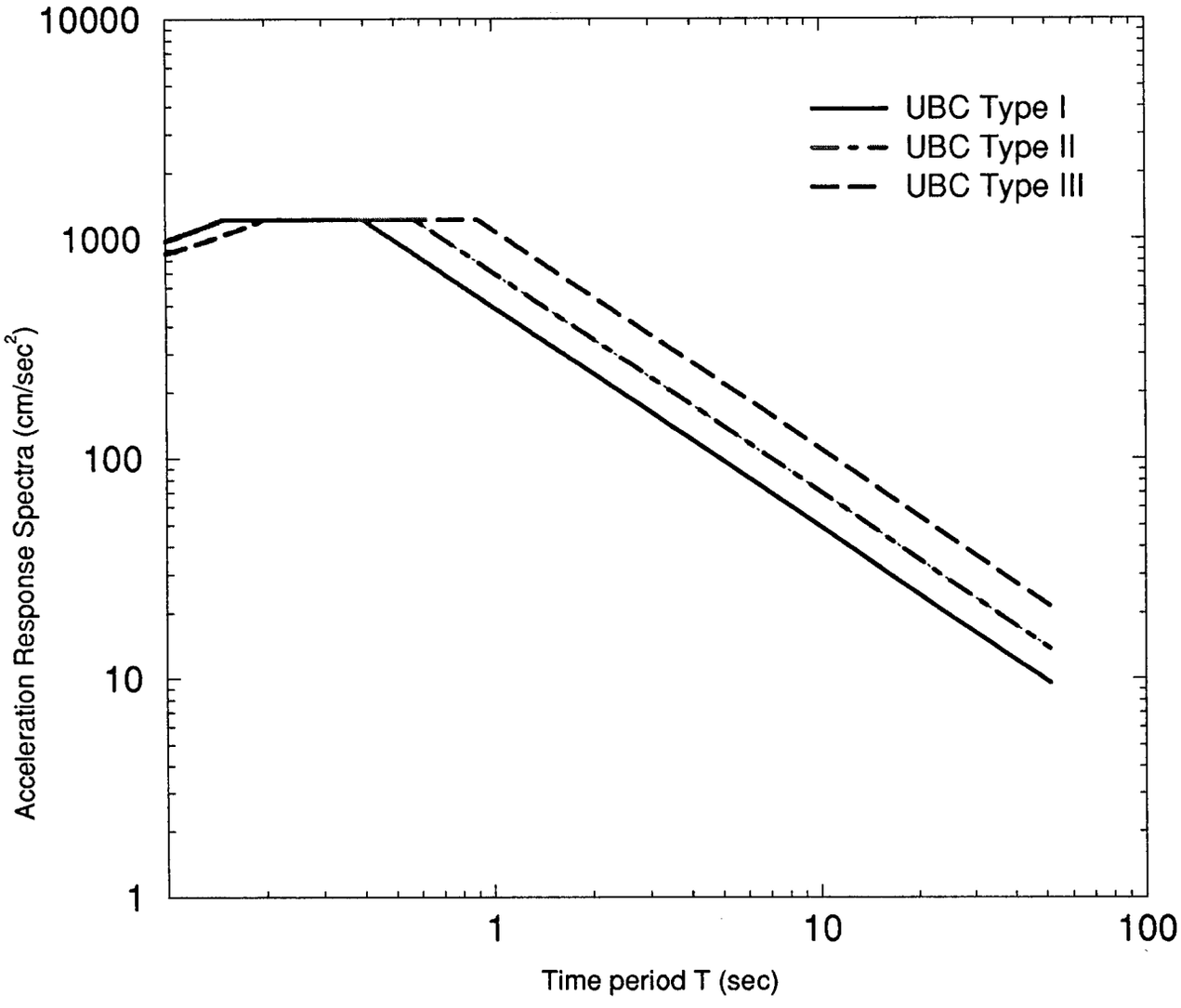

FIGURE 4-4 Uniform Building Code Acceleration Response Spectra for Type I (Rock and Stiff soils), Type II (Deep Cohesionless or Stiff Clay soils) and Type III (Soft to Medium Clays and Sands) for 5% damping.

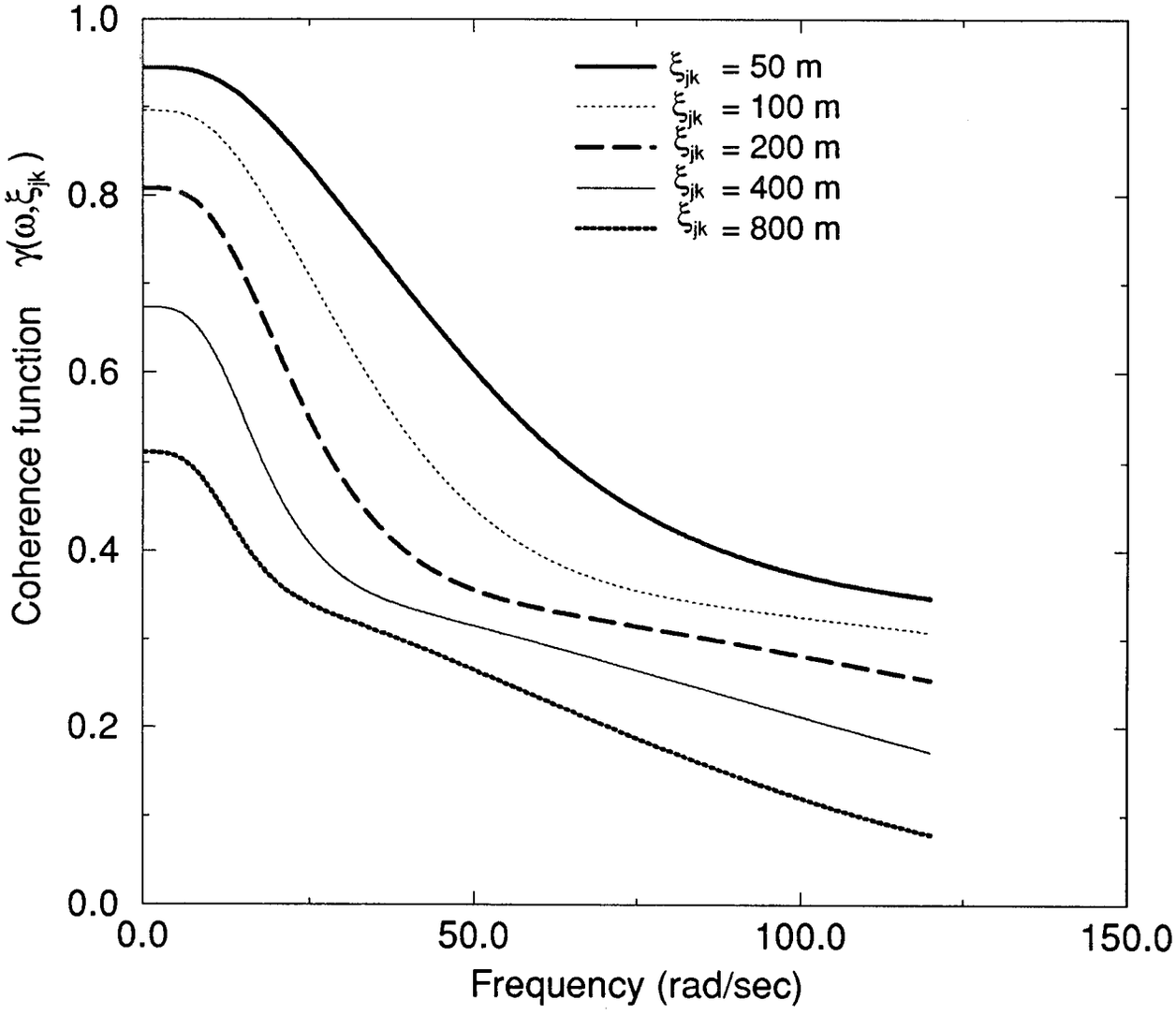

FIGURE 4-5 Harichandran and Vanmarcke Model for coherence function $\gamma(\omega,\xi_{jk})$, where ω is the frequency and ξ_{jk} is the separation distance between points j and k.

model for the coherence function that the Harichandran and Vanmarcke model allows for imperfect coherence (coherence less than unity) even for frequencies very close to zero.

4.3.3 Apparent Velocity of Wave Propagation

Two values are selected for the apparent velocity of wave propagation as indicated in Table 4-2. A low value of 300 m/sec, and a higher value of 1,000 m/sec.

4.3.4 Envelope Function

Finally, in order to introduce the non-stationary characteristics of seismic ground motion, the Jennings et al. envelope (Jennings et al. 1968) was used to define the duration of strong ground motion with parameters shown in Fig. 2-4.

4.3.5 Generated Ground Motion Time Histories for the Case of Different Local Soil Conditions

At this point, the following important note has to be made concerning the case of differential (asynchronous) support ground motion when the bridge supports are on different local soil conditions. As mentioned earlier, the way to approach such a case is by assigning different response (or power) spectra to the various bridge supports according to the corresponding local soil conditions. Such an approach makes necessary the use of a coherence function between bridge supports on different local soil conditions that would account for this change in local soil conditions. Unfortunately, such a coherence function is not currently available, as every model for the coherence in the literature has been established for uniform (homogeneous) soil conditions. Consequently, throughout this report, coherence functions for uniform (homogeneous) soil conditions are used for the cases involving different local soil conditions. Although this is definitely an approximation, it has been determined to be a reasonable one, as in such cases the effect from the difference in amplitude and frequency content is the dominant one (compared to loss of coherence and wave passage). A similar argument can be made for the apparent velocity of wave propagation (although in this case it is possible to assign equivalent "average" velocities between points).

4.4 Nonlinear Dynamic Analysis of the Seven Bridges

As mentioned earlier, nonlinear dynamic analyses were performed for the seven bridges selected using the SAP2000 computer code. A large number of cases of differential support ground motions have been considered as described in detail in section 4.3. For each one of these cases, the structural response was measured in terms of the peak ductility demand at each pier of each of the seven bridges. Statistics of the peak ductility demand (mean value and standard deviation) were obtained by ensemble averaging from 20 time history analyses for each case.

As mentioned in the previous paragraph, the parameter used to describe the (nonlinear) structural response is the *ductility demand*. The ductility demand is defined as follows: denoting by θ the rotation of the nonlinear spring used to model the plastic zone at each end of every pier, and by θ_y the corresponding rotation at the yield point, the ratio θ/θ_y is defined as the *ductility demand* of the plastic zone.

4.4.1 Presentation of Results of Nonlinear Dynamic Analyses

As mentioned in section 4.3, there is a large number of cases of differential support ground motion that have been considered. The three basic cases are the following:

CASE 1: Both the wave passage and incoherence effects are considered (loss of coherence and wave propagation considered).

CASE 2: Only the incoherence effect is considered (loss of coherence but no wave propagation considered).

CASE 3: Only the wave passage effect is considered (wave propagation considered, but seismic waves are perfectly coherent - no loss of coherence).

Within each one of the above three cases, there are two sub-cases of differential support ground motion: different local soil conditions and same local soil conditions. There are also two values considered for the apparent velocity of wave propagation: 300 m/sec and 1,000 m/sec. In addition, each bridge was also analyzed using identical support ground motion for comparison purposes. The aforementioned cases are described in Tables 4-2 and 4-3.

For each of the cases, 20 different nonlinear dynamic time history analyses were performed along the lines of a Monte Carlo simulation approach, in order to determine the statistics (mean and standard deviation) of the peak ductility demand at each of the piers.

A series of figures are provided displaying information about the statistics of the peak ductility demand. These are Figs. 4-6 – 4-61. As there is a similar set of figures provided for each bridge, the contents of these figures will be described using as an example the complete set of figures for the FHWA-No.2 bridge (Figs. 4-6 – 4-13).

Figures 4-6 – 4-9 display information about the mean value (denoted by a black square) and the mean value plus/minus one standard deviation (denoted by a vertical line above and below the black square) for the peak ductility demand of the two piers of the FHWA-No. 2 bridge (obtained by ensemble averaging from 20 time history analyses). The 8 graphs in Figs. 4-6 – 4-9 correspond to the following eight cases of differential support ground motion considered:

1. Case 1 (both the wave passage and incoherence effects considered) with same local soil conditions and apparent velocity of wave propagation equal to 1,000 m/sec (top graph in Fig. 4-6).

2. Case 1 (both the wave passage and incoherence effects considered) with different local soil conditions and apparent velocity of wave propagation equal to 1,000 m/sec (bottom graph in Fig. 4-6).

3. Case 2 (only the incoherence effect considered) with same local soil conditions and apparent velocity of wave propagation approaching infinity. (top graph in Fig. 4-7).

4. Case 2 (only the incoherence effect considered) with different local soil conditions and apparent velocity of wave propagation approaching infinity. (bottom graph in Fig. 4-7).

5. Case 3 (only the wave passage effect considered) with same local soil conditions and apparent velocity of wave propagation equal to 1,000 m/sec (top graph in Fig. 4-8).

6. Case 3 (only the wave passage effect considered) with different local soil conditions and apparent velocity of wave propagation equal to 1,000 m/sec (bottom graph in Fig. 4-8).

7. Case 1 (both the wave passage and incoherence effects considered) with same local soil conditions and apparent velocity of wave propagation equal to 300 m/sec (top graph in Fig. 4-9).

8. Case 3 (only the wave passage effect considered) with same local soil conditions and apparent velocity of wave propagation equal to 300 m/sec (bottom graph in Fig. 4-9).

Figures 4-10a and 4-10b present comparisons of the mean values for the peak ductility demand at the two piers of the FHWA-No.2 bridge for different cases examined. Results from Cases 1, 2, and 3 are compared to estimate the relative effect of loss of coherence and wave passage. In addition, the cases of different and same local soil conditions can be easily compared, and the effect of different apparent velocities of wave propagation can be assessed, by studying the bar charts in Figs. 4-10a and 4-10b. It should be mentioned that in these graphs, SAME denotes that all bridge supports are on the same type of local soil conditions, while DIFF denotes that different supports are on different local soil conditions.

Figure 4-11 is similar to Figs. 4-6 - 4-9, but in this case the mean value and the standard deviation for the peak ductility demand at the two piers of the FHWA-No.2 bridge are presented for the case of identical support ground motion.

Figure 4-12 presents a comparison of the mean values for the peak ductility demand at the two piers of the FHWA-No.2 bridge for the following three cases: differential support ground motion and different local soil conditions, differential support ground motion and same local soil conditions, and identical support ground motion. Note that IDENT denotes the case of identical support ground motion. The definitions of SAME and DIFF are provided in a previous paragraph.

Finally, Fig. 4-13 presents the same information as Fig. 4-12 but in the form of ratios rather than direct values. It should be noted that Figs. 4-12 and 4-13 make it easy to assess the differences in the mean values for the peak ductility demand between the two cases of differential support ground motion: different versus same local soil conditions. In addition, direct comparisons can be done with the reference case of identical support ground motion.

Every other bridge of the remaining six bridges is provided with a similar set of figures (Figs. 4-14 – 4-61). Based on the information provided in Figs. 4-6 – 4-61, it is possible to establish the following observations/conclusions for each one of the seven bridges considered.

4.4.2 Observations/Conclusions for FHWA-No.2 Bridge

1. *Effect of local soil conditions*: It was found that the peak ductility demand for every pier when considering different local soil conditions becomes almost *double* from the corresponding value when considering same local soil conditions. This indicates that it is very important to take into account the local soil effect when studying bridges similar to this one having supports on different local soil conditions.

2. *Effect of apparent velocity of wave propagation*: Comparing corresponding cases with apparent velocities of wave propagation of 300 m/sec and 1,000 m/sec, it was found that the velocity has *no significant effect* on the peak ductility demand of the piers. However, for Case 3 where there is only wave propagation (and no loss of coherence), it was observed that the peak ductility demand reduces at Pier 2 for velocity of 300 m/sec (when compared to the case of 1,000 m/sec).

3. *Relative effect of coherence and wave passage*:

   For same local soil conditions:
   For pier 1, the incoherence and wave passage effects are approximately equally important and they have a jointly reinforcing effect (this means that the peak ductility demand for Case 1 is larger than the peak ductility demand of either Case 2 or 3). For pier 2, it appears that the incoherence effect is more important than the wave passage effect, and the two effects have a jointly canceling effect (this means that the peak ductility demand for Case 1 is less than either the peak ductility demand of Case 2 or 3).

   For different local soil conditions:
   The relative effect of wave passage and incoherence on the peak ductility demand of the piers is identical to the case where all piers are on the same local soil conditions.

   For low velocity:
   At low apparent velocities of wave propagation, the effect of incoherence becomes more pronounced, especially for pier 2.

4. The assumption of identical support ground motion is *unconservative* and the peak ductility demand for both piers would be underestimated by a factor of approximately 2.6 (for bridge supports on different local soil conditions) or a factor of approximately 1.4 (for bridge supports on the same local soil conditions), if the bridge were to be analyzed using identical support ground motion, rather than differential support ground motion.

4.4.3 Observations/Conclusions for TEXT Bridge

1. *Effect of local soil conditions*: It was found that the peak ductility demand when considering different local soil conditions becomes 1.6 times (for Pier 1) the corresponding value when considering same local soil conditions. This indicates that it is very important to take into account the local soil effect when studying bridges similar to this one having supports on different local soil conditions.
2. *Effect of apparent velocity of wave propagation*: Comparing corresponding cases with apparent velocities of wave propagation of 300 m/sec and 1,000 m/sec, it was found that the

velocity has *no significant effect* on the peak ductility demand of the piers. However, for Case 3 where there is only wave propagation (and no loss of coherence), it was observed that the peak ductility demand reduces at Pier 2 for velocity of 300 m/sec (when compared to the case of 1,000 m/sec).

3. *Relative effect of coherence and wave passage*

   For same local soil conditions:
   For both Piers 1 and 2, the incoherence effect appears to be more important than the wave passage effect, and the two effects have a jointly reinforcing effect (this means that the peak ductility demand for Case 1 is larger than the peak ductility demand of either Case 2 or 3).

   For different local soil conditions:
   For Pier 1, the incoherence and wave passage effects are approximately equally important and they have a jointly reinforcing effect (this means that the peak ductility demand for Case 1 is larger than the peak ductility demand of either Case 2 or 3). For Pier 2, the incoherence effect is more important than the wave passage effect, and the two effects have a jointly reinforcing effect.

   For low velocity:
   At low apparent velocities of wave propagation, the effect of incoherence becomes more pronounced especially for Pier 2.

4. The assumption of identical support ground motion is unconservative and the peak ductility demand for the piers would be underestimated by a factor as high as 2.2 (for bridge supports on different local soil conditions) or by a factor as high as 1.3 (for bridge supports on same local soil conditions), if the bridge were to be analyzed using identical support ground motion, rather than differential support ground motion.

4.4.4 Observations/Conclusions for GC2D Bridge

1. *Effect of local soil conditions*: It was found that the peak ductility demand when considering different local soil conditions does not vary much for Piers 1 and 4 from the corresponding value when considering same local soil conditions. However, the peak ductility demand when considering different local soil conditions for Piers 2 and 3 becomes as much as 1.8 times higher than the corresponding value when considering same local soil conditions.

2. *Effect of apparent velocity of wave propagation*: Comparing corresponding cases with apparent velocities of wave propagation of 300 m/sec and 1,000 m/sec, it was found that the velocity has *no significant effect* on the peak ductility demand except for Pier 3. For Pier 3, the peak ductility demand reduces when the apparent velocity of wave propagation is 300 m/sec (as compared to the case of 1,000 m/s). Also for Case 3 where there is only wave propagation (and no loss of coherence), it was observed that the peak ductility demand reduces at Pier 3 for velocity of 300 m/sec (when compared to the case of 1,000 m/sec).

3. *Relative effect of coherence and wave passage*:

For same local soil conditions:
For Piers 1 and 2, the incoherence and wave passage effects are approximately equally important and provide values for the peak ductility demand almost equal to the corresponding value for Case 1 (both loss of coherence and wave passage). For Piers 3 and 4, it appears that the incoherence effect is slightly more important than the wave passage effect and the two effects have a jointly canceling effect.

For different local soil conditions:
For Pier 1, the incoherence and wave passage effects are approximately equally important and provide values for the peak ductility demand almost equal to the corresponding value for Case 1 (both loss of coherence and wave passage). For piers 2, 3 and 4, the incoherence effect is slightly more important than the wave passage effect, and the two effects have a jointly canceling effect for Piers 3 and 4 and a jointly reinforcing effect for Pier 2.

For low velocity:
At low velocities, the effect of wave passage reduces and that of incoherence increases for Pier 3. For Pier 4 the effect of incoherence becomes approximately equally important to that of wave passage.

4. The assumption of identical support ground motion is reasonable for Piers 1 and 4 (for bridge supports on same as well as different local soil conditions). For Piers 2 and 3, the assumption of identical support ground motion is unconservative and the peak ductility demand for Pier 2 would be underestimated by a factor of approximately 2.2 (for bridge supports on different local soil conditions) or by a factor of approximately 1.2 (for bridge supports on same local soil conditions), if the bridge were to be analyzed using identical support ground motion, rather than differential support ground motion.

4.4.5 Observations/Conclusions for TYOH Bridge

1. *Effect of local soil conditions*: It was found that the peak ductility demand for every pier when considering different local soil conditions becomes as much as 1.7 times the corresponding value when considering same local soil conditions. This indicates that it is very important to take into account the local soil effect when studying bridges similar to this one having supports on different local soil conditions.

2. *Effect of apparent velocity of wave propagation*: Comparing corresponding cases with apparent velocities of wave propagation of 300 m/sec and 1,000 m/sec, it was found that the peak ductility demand increases for Pier 1 and reduces for Piers 2, 3 and 4 when the apparent velocity of wave propagation is reduced to 300m/s (as compared to the case of 1,000m/s). For Case 3 where there is only wave propagation (and no loss of coherence), it was observed that the peak ductility demand increases for Pier 1 and reduces for Piers 2 and 3 for the case of velocity 300 m/sec (when compared to the case of 1,000 m/sec).

3. *Relative effect of coherence and wave passage*:

   For same local soil conditions:

For all the piers, the incoherence effect appears to be more important than the wave passage effect. The two effects have a jointly reinforcing effect for Pier 1 and a jointly canceling effect for Piers 2, 3 and 4.

For different local soil conditions:
For all the piers, the incoherence effect appears to be more important than the wave passage effect. The two effects have a jointly reinforcing effect for Piers 1 and 2 and a jointly canceling effect for Piers 3 and 4.

For low velocity:
At low apparent velocities of wave propagation, the effect of wave passage becomes more important than the incoherence effect for Pier 1 and reduces for Pier 3.

4. The assumption of identical support ground motion is unconservative and the peak ductility demand for the piers would be underestimated by a factor as high as 2.1 (for bridge supports on different local soil conditions) or by a factor as high as 1.6 (for bridge supports on the same local soil conditions), if the bridge were to be analyzed using identical support ground motion, rather than differential support ground motion.

4.4.6 Observations/Conclusions for TY1H Bridge

1. *Effect of local soil conditions*: It was found that the peak ductility demand for every pier when considering different local soil conditions becomes as much as 1.5 times the corresponding value when considering same local soil conditions. This indicates that it is very important to take into account the local soil effect when studying bridges similar to this one having supports on different local soil conditions.

2. *Effect of apparent velocity of wave propagation*: Comparing corresponding cases with apparent velocities of wave propagation of 300 m/sec and 1,000 m/sec, it was found that the peak ductility demand increases for Pier 1 and reduces for Piers 2 and 4 when the apparent velocity of wave propagation is reduced to 300 m/s (as compared to the case of 1,000 m/s). For Case 3 where there is only wave propagation (and no loss of coherence), it was observed that the peak ductility demand reduces for Piers 2 and 4 for the case of velocity 300 m/sec (when compared to the case of 1,000 m/sec).

3. *Relative effect of coherence and wave passage*:

For same local soil conditions:
For all four piers, the incoherence effect appears to be more important than the wave passage effect. The two effects have a jointly reinforcing effect for Piers 1 and 3 and a jointly canceling effect for Piers 2 and 4.

For different local soil conditions:
For all four piers, the incoherence effect appears to be more important than the wave passage effect, and the relative effect of wave passage and incoherence is similar to the case with same local soil conditions.

For low velocity:
At low apparent velocities of wave propagation, the effect of incoherence becomes more pronounced for Piers 2 and 4 whereas the effect of wave passage reduces for these piers. This results in a decrease in the peak ductility demands of Piers 2 and 4 for Case 1 (both wave passage and loss of coherence) and the two effects seem to have a jointly canceling effect.

4. The assumption of identical support ground motion is unconservative and the peak ductility demand for the piers would be underestimated by a factor as high as 2.1 (for bridge supports on different local soil conditions) or by a factor as high as 1.4 (for bridge supports on the same local soil conditions), if the bridge were to be analyzed using identical support ground motion, rather than differential support ground motion.

4.4.7 Observations/Conclusions for TY2H Bridge

1. *Effect of local soil conditions*: It was found that the peak ductility demand for every pier when considering different local soil conditions becomes as much as 1.7 times the corresponding value when considering same local soil conditions. This indicates that it is very important to take into account the local soil effect when studying bridges similar to this one having supports on different local soil conditions.

2. *Effect of apparent velocity of wave propagation*: Comparing corresponding cases with apparent velocities of wave propagation of 300 m/sec and 1,000 m/sec, it was found that the peak ductility demand reduces for Pier 3 when the apparent velocity of wave propagation is reduced to 300 m/s (as compared to the case of 1,000 m/s). For Case 3, where there is only wave propagation (and no loss of coherence), it was observed that the peak ductility demand slightly increases for Piers 1, 4 and reduces for Piers 2, 3 for the case of velocity 300 m/sec (when compared to the case of 1,000 m/sec).

3. *Relative effect of coherence and wave passage*:

   For same local soil conditions:
   For Pier 1, the incoherence and the wave passage effects are approximately equally important. For Piers 2, 3 and 4 the incoherence effect appears to be more important than the wave passage effect. The two effects have a jointly reinforcing effect for Piers 2 and 4 and a jointly canceling effect for Pier 3.

   For different local soil conditions:
   The relative effect of wave passage and incoherence for Piers 2 and 3 is similar to the case with same local soil conditions. For Pier 1 the wave passage effect becomes more important than the incoherence effect, whereas for Pier 4 the wave passage and incoherence effects become equally important.

   For low velocity:
   At low apparent velocities of wave propagation, the effect of incoherence becomes more pronounced for Pier 3 whereas the effect of wave passage reduces for this pier. This results in a decrease in the peak ductility demand in this pier for Case 1 (both wave passage and loss of coherence), and the two effects seem to have a jointly canceling effect. Moreover, for Pier 1,

the wave passage effect becomes more important the incoherence effect when the velocity is reduced to 300 m/s.

4. The assumption of identical support ground motion is unconservative and the peak ductility demand for the piers would be underestimated by a factor as high as 2.7 (for bridge supports on different local soil conditions) or by a factor as high as 1.7 (for bridge supports on the same local soil conditions), if the bridge were to be analyzed using identical support ground motion, rather than differential support ground motion.

4.4.8 Observations/Conclusions for Santa Clara Bridge

1. *Effect of local soil conditions*: It was found that the peak ductility demand when considering different local soil conditions becomes almost *twice* than the corresponding value when considering same local soil conditions for Piers 5, 6 and 7. For Piers 10 and 11, the peak ductility demand when considering different local soil conditions becomes *much less* (two-thirds *for Pier 10*, one-third for Pier 11) than the corresponding value when considering same local soil conditions. This indicates that when studying very long bridges similar to this one having supports on different local soil conditions, the peak ductility demand may increase or decrease by a large amount in different piers, depending on the structural properties and the configuration of the bridge.

2. *Effect of apparent velocity of wave propagation* Comparing corresponding cases with apparent velocities of wave propagation of 300 m/sec and 1,000 m/sec, it was found that the velocity has a very significant effect on the peak ductility demand of the piers. The peak ductility demand increases for Piers 1 to 9 and reduces for Piers 10 and 11, when the apparent velocity of wave propagation is reduced to 300 m/s (as compared to the case of 1,000 m/s).
   The most significant effect is observed for Case 3 (where there is only wave propagation and no loss of coherence), where the peak ductility demand increases for all piers for the velocity of 300 m/sec (when compared to the case of 1,000 m/sec).

3. *Relative effect of coherence and wave passage*:

   For same local soil conditions:
   For all eleven piers, the incoherence effect appears to be more important than the wave passage effect. The two effects have a jointly reinforcing effect for external piers (1, 2, 10 and 11) and a jointly canceling effect for Piers 3 to 9.

   For different local soil conditions:
   For all eleven piers, the incoherence effect appears to be more important than the wave passage effect and the relative effect is similar to the case with same local soil conditions, except for Piers 5 to 9. For these piers the effect of wave passage increases as compared to the case of same local soil conditions; however, the effect of incoherence still remains more important than the effect of wave passage.

   For low velocity:

At low apparent velocities of wave propagation, the effect of wave passage increases for all piers, as compared to the case with velocity 1000 m/s. This effect is most pronounced for Piers 1 to 5 where the wave passage effect becomes more important than the incoherence effect. This results in an increase in the peak ductility demand for Piers 1 to 5 for Case 1(both wave passage and loss of coherence), and the two effects seem to have a jointly canceling effect for Piers 1 to 3 and a jointly reinforcing effect for Piers 4 and 5.

4. The assumption of identical support ground motion *severely underestimates* the peak ductility demand in all the piers by a factor as high as 6.8, both for same as well as for different local soil conditions. Unlike the other six relatively shorter bridges where the same local soil conditions always yielded smaller values for peak ductility demand from the case of different local soil conditions, for this longer bridge higher peak ductility demands are obtained for Piers 10 and 11 in the case of same local soil conditions as compared to the case of different local soil conditions.

4.4.9 Observations/Conclusions from Other Researchers' Work

After presenting observations and conclusions for the seven bridges considered in this study, and before attempting to establish general conclusions and guidelines, some of the main results reached by other researchers having studied in the past the effect of spatial variability of seismic ground motion on the response of various structures are presented in this section. Specifically, work done by Der Kiureghian, Harichandran, Monti, Zerva and their associates is discussed in this section.

Der Kiureghian and his associates have studied the effect of spatial variability of seismic ground motion on the linear response of two multi-span bridges (one with 120 ft spans and the other with 240 ft spans) using the "Multiple Support Response Spectrum" method that they have developed (a linear random vibration approach). They have used a model for the coherence function that Der Kiureghian (1996) developed and they have considered all three spatial variability effects: the wave passage, the incoherence, and the local soil effects. They have modeled their multi-span bridges as frame structures. Their main conclusions were:

1) The spatial variability effect, consisting of the incoherence effect, the wave passage effect, and the site response (local soil) effect, can strongly influence the response of bridge structures. It could amplify or de-amplify the bridge response by as much as an order of magnitude or more.

2) For the bridge with the longer spans (240 ft), the wave passage effect had the largest influence, followed by the site response effect and the incoherence effect.

3) For the bridge with the shorter spans (120 ft), the site effect had the largest influence, followed by the wave passage effect and the incoherence effect.

Harichandran and his associates examined the response of single and multiple span continuous beams with different span lengths, subjected to spatially varying ground motions at their supports, using a linear random vibration approach. Their attention was mainly focused on the variance of various response quantities, as the expected maximum value of the response is

directly proportional to the variance and the duration of the response. They have used the model for the coherence function proposed by Harichandran and Vanmarcke (1986), and they have considered the following two spatial variability effects: the wave passage, and the incoherence effects. Their main conclusions were:

For single span beams:

1) The assumption of identical support ground motion provides a higher response in single span beams for all fundamental frequencies and is overly conservative.

2) Considering only the incoherence effect overestimates the response in all cases.

3) Considering only the wave passage effect underestimates the response in some cases.

For multiple span continuous beams:

1) For relatively stiffer beams, the pseudo-static response can induce significantly larger stresses - almost by an order of magnitude - when the incoherence effect is considered.

2) Deterministic or probabilistic analysis accounting for only the wave passage effect will seriously underestimate the response for stiff lifelines but should be adequate for flexible lifelines for which the dynamic response is dominant.

Zerva and her associates have studied the effect of spatial variation of ground motion on multiply supported structures modeled as continuous beams. Some of the commonly utilized spatial coherence models were chosen to study characteristics that affect the response of such structures. They have used a linear random vibration approach, and they have considered the following two spatial variability effects: the wave passage and the incoherence effects. Their main conclusions were:

1) The effect of spatial variation of ground motion is not critical for single-span simply supported beams, and the assumption of identical support ground motion seems to be a perfectly reasonable assumption for such bridges.

2) Comparing some of the commonly utilized spatial coherence models, it was found that models for the coherence function with partial correlation at low frequencies and with slow exponential decay as the frequency and separation distance increase would produce the highest response for lifelines.

3) For high apparent velocities of wave propagation, the incoherence effect is more important than the wave passage effect, while for relatively lower velocities the wave passage effect can become more significant.

4) One of the most important effects of spatial incoherence on the response is the introduction of high quasi-static internal forces in the structure with the simultaneous reduction in the dynamic forces. The highest dynamic response is induced by identical support ground

motion. However, to estimate the total response (quasi-static and dynamic) it is recommended to incorporate both the wave passage and incoherence effects in the seismic analysis of such types of extended structures.

Monti and his associates performed a unique study, in the sense that they examined the nonlinear response of a bridge subjected to differential support ground motion. They modeled their multi-span bridge as a frame and performed a sensitivity analysis for different pier heights (or equivalently stiffnesses). As they had to perform nonlinear dynamic analyses, they followed a Monte Carlo simulation approach. They used the Luco and Wong (1986) model for the coherence function. They considered the following two spatial variability effects: the wave passage and the incoherence effects. Their main conclusions were:

1) The apparent velocity of wave propagation has a notable effect on the bridge response only for the case of zero coherence. When some amount of coherence is present its effect is reduced.

2) When high levels of incoherence are present, the response to differential support ground motion is not influenced significantly by the wave passage effect.

3) For firm soils there is a considerable reduction in the mean value of the response displacements for increasing levels of incoherence, but this behavior is not so evident for medium soils. However for both type of soils the standard deviation of the response increases with increasing levels of incoherence.

4) When the effect of wave passage alone is considered, there is a reduction of forces in the central piers and an increase of forces in the external ones. However if the apparent velocity of wave propagation is reduced, there is a substantial reduction of forces in every pier.

5) For very low levels of coherence, the wave passage effect decreases the response shear forces in the piers and increases the pseudo-static component. The reverse happens for high levels of coherence and low values of the apparent velocity of wave propagation.

6) One of the most important conclusions was that the assumption of incoherent motion leads to a decrease in design forces, when compared to the corresponding values obtained using identical support ground motion. Therefore the assumption of identical support ground motions is a globally conservative one for design purposes.

4.4.10 General Observations and Conclusions

Studying the results from past work of other researchers (described very briefly in section 4.4.9), it becomes very difficult to draw general conclusions concerning the effect of spatial variability of seismic ground motion on the response of elongated structures on multiple supports. First, it is quite difficult to make comparisons among the results of the different studies presented in section 4.4.9, as different researchers use different structures, different ways to model their structures, different models for the spatial variability of seismic ground motion, different approaches to analyze the structures, and different quantities to measure the response of the structure. Therefore some of the conclusions reached by different researchers might seem contradictory

because of differences in the cases that they have considered. There isn't even agreement about whether the assumption of spatial variability of seismic ground motion is beneficial or detrimental to the structural response (compared to the case of identical support ground motion). The only common conclusion is that the effect of spatial variability of ground motion on the response of the structure is a very complex one, depending on various parameters describing the structure and the characteristics of the ground motion.

Based on the results, observations and conclusions of the seven bridges examined in detail in Chapter 4, the following general conclusions can be drawn:

1. *The peak ductility demand at the piers can increase substantially when the bridge is analyzed using differential support ground motion and considering that different supports of the bridge are on different local soil conditions, compared to the case of identical support ground motion. Specifically, the ratio of the peak ductility demand at the piers using differential support ground motion and considering that different supports of the bridge are on different local soil conditions over the peak ductility demand using identical support ground motion is of the order of 2.0 - 2.5 for the six medium span bridges, and as high as 4.0 for the longer Santa Clara Bridge.*

2. *The peak ductility demand at the piers can increase by a smaller amount when the bridge is analyzed using differential support ground motion and considering that all supports of the bridge are on the same local soil conditions, compared to the case of identical support ground motion. Specifically, the ratio of the peak ductility demand at the piers using differential support ground motion and considering that all supports of the bridge are on the same local soil conditions over the peak ductility demand using identical support ground motion is of the order of 1.0 – 1.5 for the six medium span bridges, and as high as 4.0 for the longer Santa Clara Bridge.*

3. *Low apparent velocity of wave propagation might reduce in some cases the peak ductility demand of some of the piers, for the general case where both the wave propagation and loss of coherence effects are considered and all supports of the bridge are on the same type of local soil conditions. Further, a low value of the velocity might change the relative contribution of the wave passage and the incoherence effects in some of the piers.*

4. *The incoherence effect is in general more important than the wave passage effect. The wave passage effect becomes more important than the incoherence effect only for the relatively longer Santa Clara bridge and for low velocities of wave propagation. But even in cases where the incoherence effect is more important, the wave passage effect is still substantial and its interaction with the incoherence effect cannot be predicted a priori. Therefore neglecting either one of these two effects might produce inaccurate results.*

5. *The relative contribution of the wave passage and incoherence effects to the peak ductility demand of the piers does not seem to be affected to any considerable degree by the assumption of different versus same local soil conditions at the supports of the bridge.*

6. *The identical support ground motion assumption seems to be generally unconservative, but much more so in the case of different local soil conditions. However, for the relatively longer Santa Clara bridge, the identical support ground motion assumption severely underestimates the peak ductility demand at the piers by approximately the same amount for both same as well as different local soil conditions.*

FHWA BRIDGE

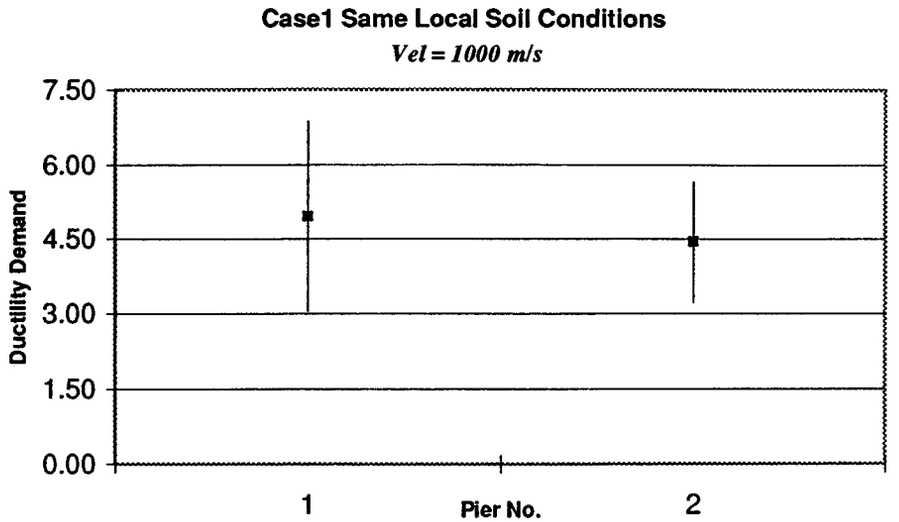

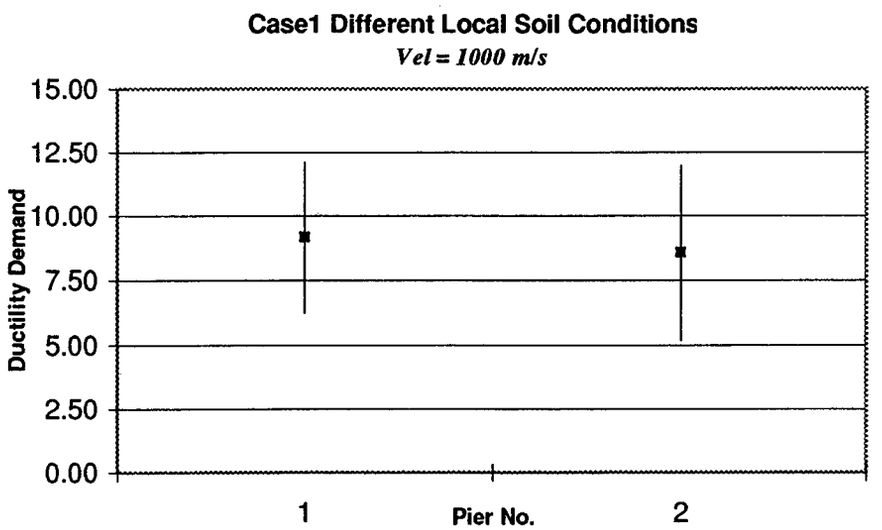

FIGURE 4-6 Mean value (denoted by block square) and mean value plus / minus one standard deviation (denoted by vertical line above and below square) for the peak ductility demand of the various piers of FHWA bridge, obtained by ensemble averaging from 20 time history analyses.

FHWA BRIDGE

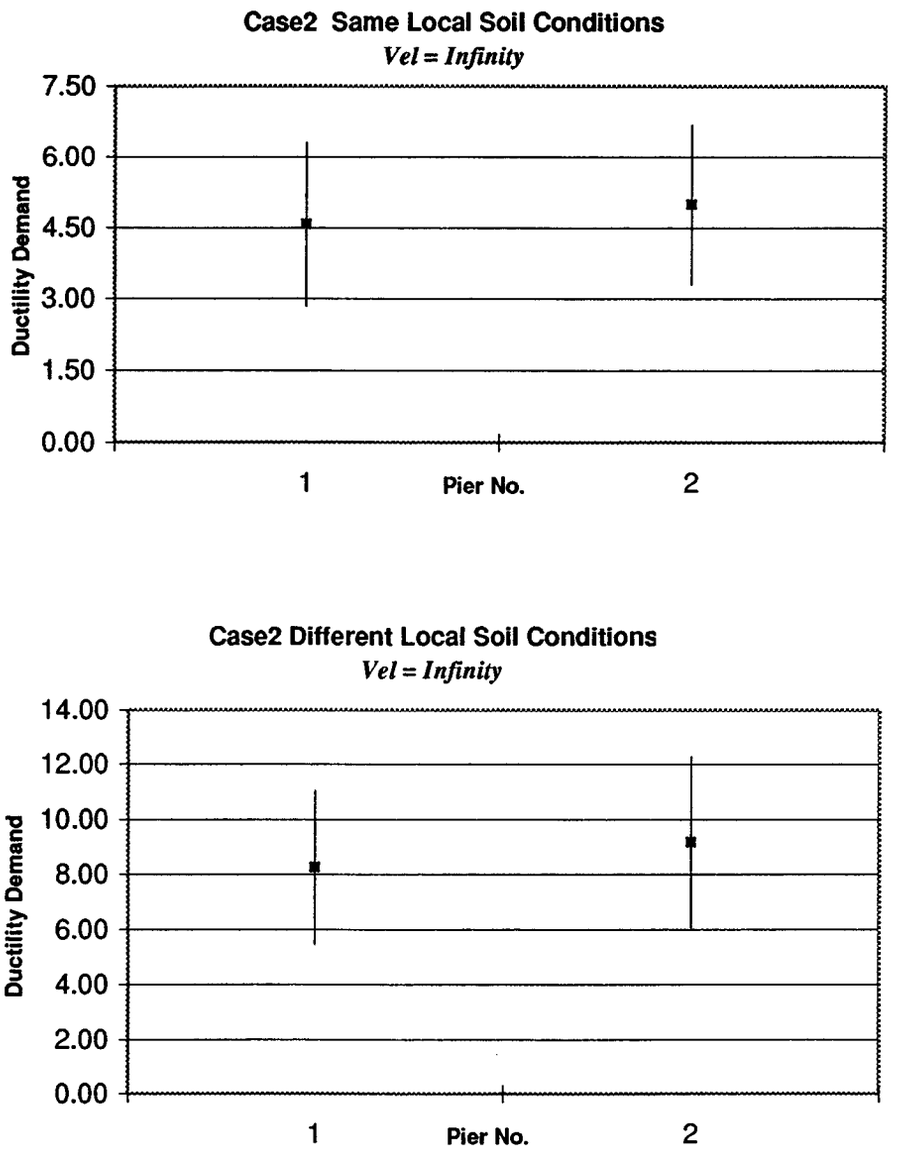

FIGURE 4-7 Mean value (denoted by block square) and mean value plus / minus one standard deviation (denoted by vertical line above and below square) for the peak ductility demand of the various piers of FHWA bridge, obtained by ensemble averaging from 20 time history analyses.

FHWA BRIDGE

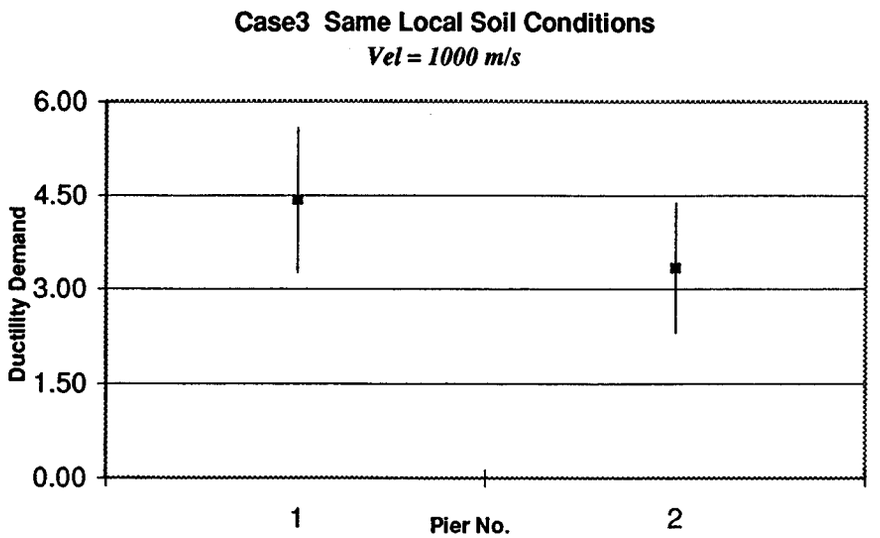

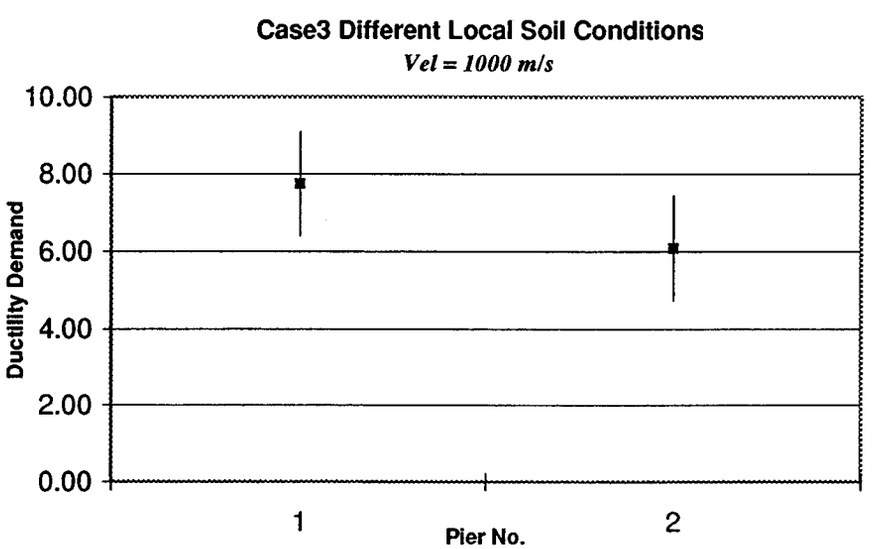

FIGURE 4-8 Mean value (denoted by block square) and mean value plus / minus one standard deviation (denoted by vertical line above and below square) for the peak ductility demand of the various piers of FHWA bridge, obtained by ensemble averaging from 20 time history analyses.

FHWA BRIDGE

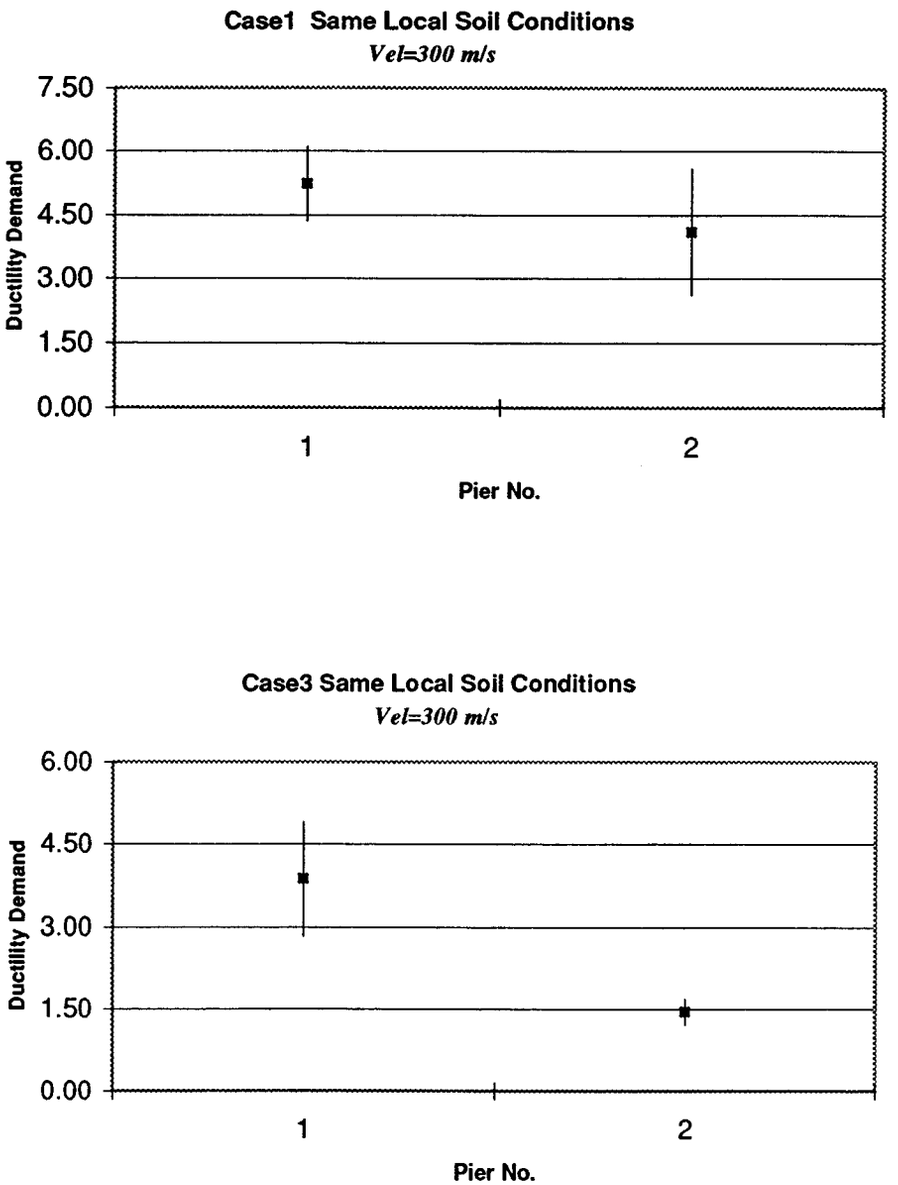

FIGURE 4-9 Mean value (denoted by block square) and mean value plus / minus one standard deviation (denoted by vertical line above and below square) for the peak ductility demand of the various piers of FHWA bridge, obtained by ensemble averaging from 20 time history analyses.

FHWA BRIDGE

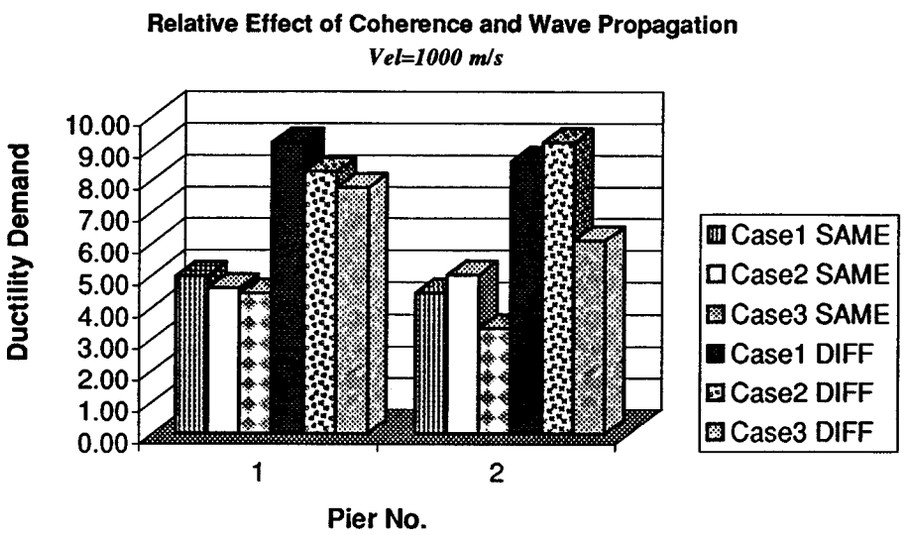

SAME denotes all supports on same local soil conditions
DIFF denotes supports on different local soil conditions

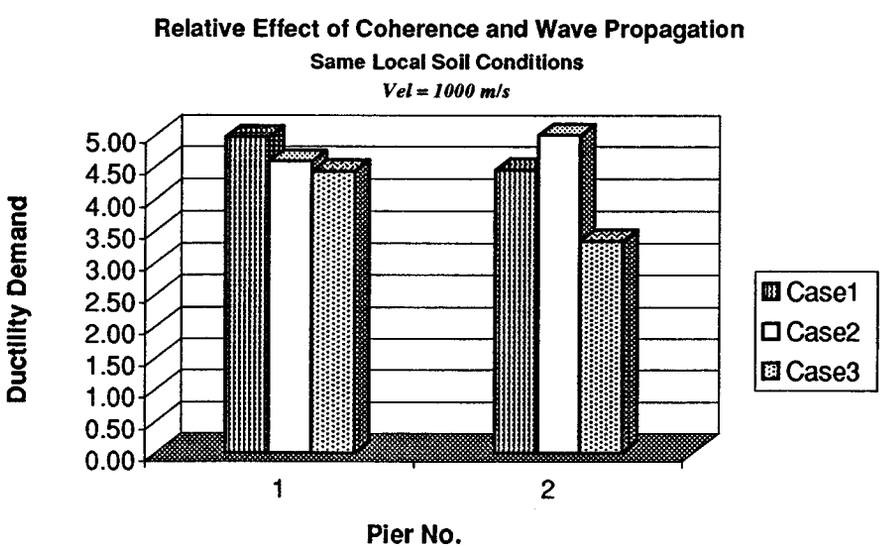

FIGURE 4-10a Bar chart depicting mean values for the peak ductility demand of the various piers of FHWA bridge, obtained from ensemble averaging from 20 time history analyses. Case 1, 2 and 3 are compared to estimate the relative effect of coherence and wave propagation. The effect of different local soil conditions and the effect of different velocities of wave propagation can also be assessed.

FHWA BRIDGE

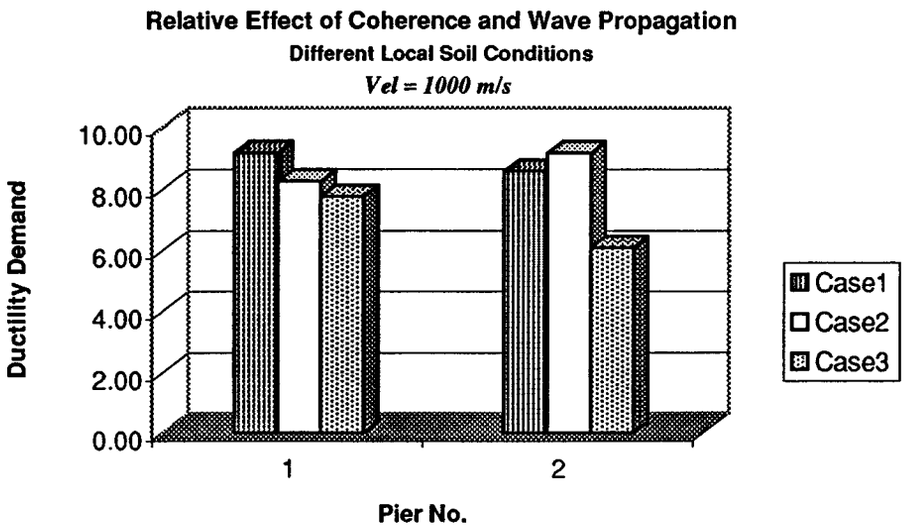

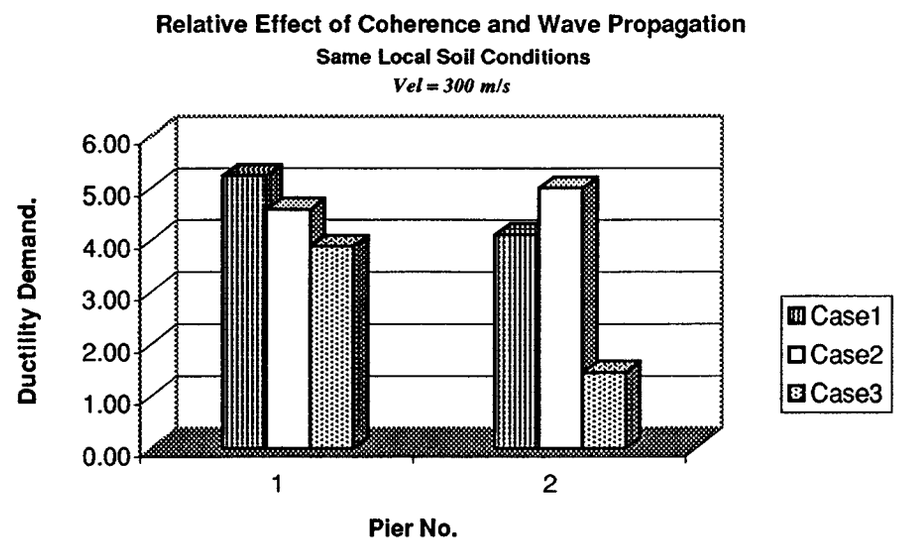

FIGURE 4-10b Bar chart depicting mean values for the peak ductility demand of the various piers of FHWA bridge, obtained from ensemble averaging from 20 time history analyses. Case 1, 2 and 3 are compared to estimate the relative effect of coherence and wave propagation. The effect of different local soil conditions and the effect of different velocities of wave propagation can also be assessed.

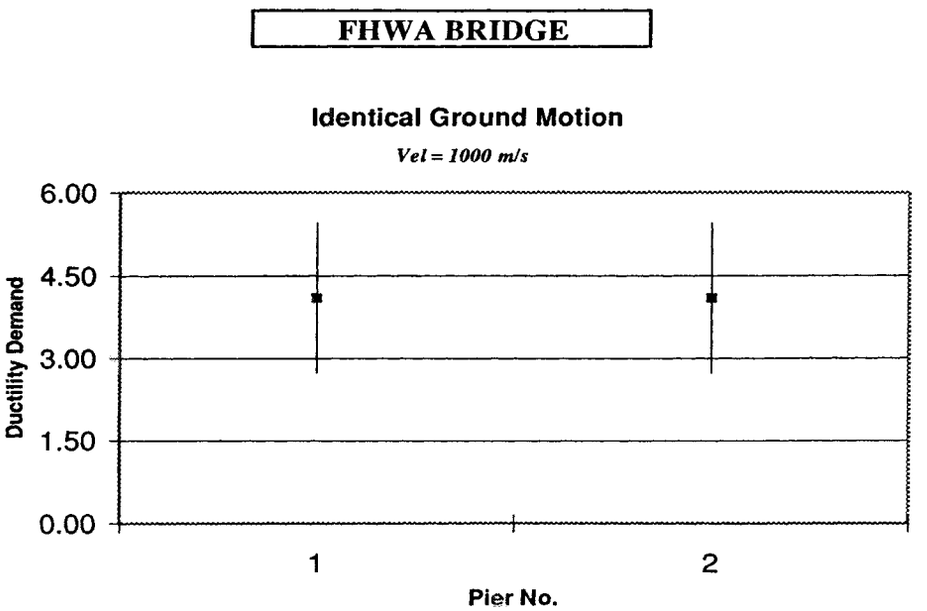

FIGURE 4-11 Mean value (denoted by block square) and mean value plus / minus one standard deviation (denoted by vertical line above and below square) for the peak ductility demand of the various piers of FHWA bridge, obtained by ensemble averaging from 20 time history analyses, for the case of identical support ground motion.

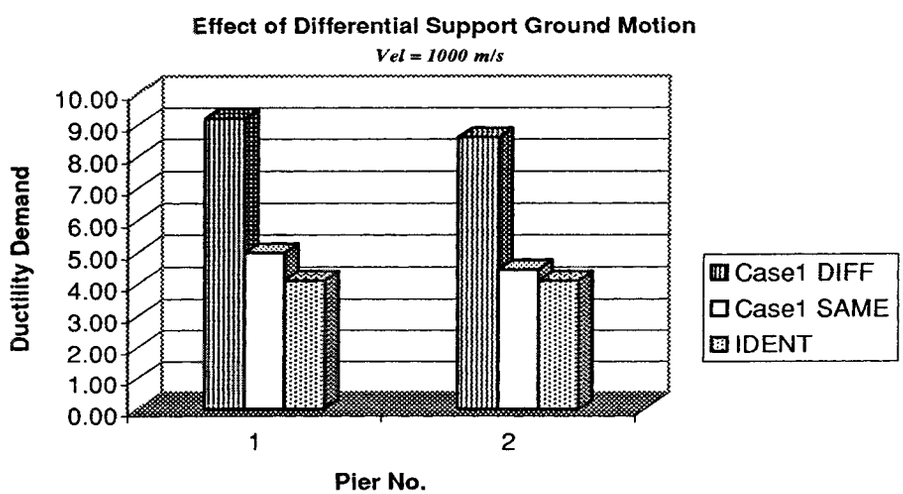

DIFF denotes supports on different local soil conditions
SAME denotes all supports on same local soil conditions
IDENT denotes identical support ground motion

FIGURE 4-12 Bar chart depicting mean values for the peak ductility demand of the various piers of FHWA bridge, obtained from ensemble averaging from 20 time history analyses. Comparison of cases with differential support ground motion and different local soil conditions, differential support ground motion and same local soil conditions, and identical support ground motion.

FHWA BRIDGE

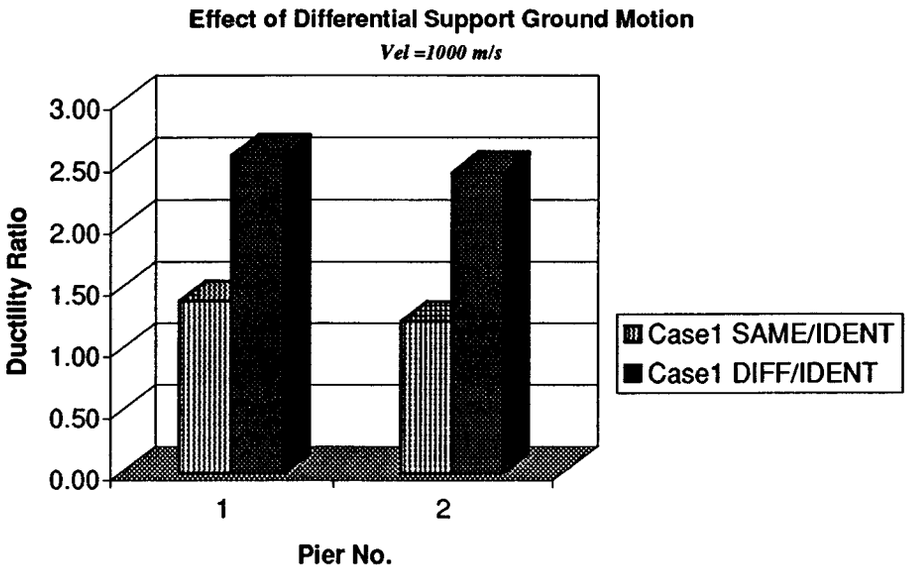

SAME/IDENT denotes the ratio of the peak ductility demand computed using differential support ground motion and same local soil conditions over the peak ductility demand computed using identical support ground motion.

DIFF/IDENT denotes the ratio of the peak ductility demand computed using differential support ground motion and different local soil conditions over the peak ductility demand computed using identical support ground motion.

FIGURE 4-13 Bar chart depicting ratios of mean values for the peak ductility demand of the various piers of FHWA bridge, obtained by ensemble averaging from 20 time history analyses The effect of differential support ground motion and different local soil conditions, differential support ground motion and same local soil conditions and identical support ground motion can be assessed.

TEXT BRIDGE

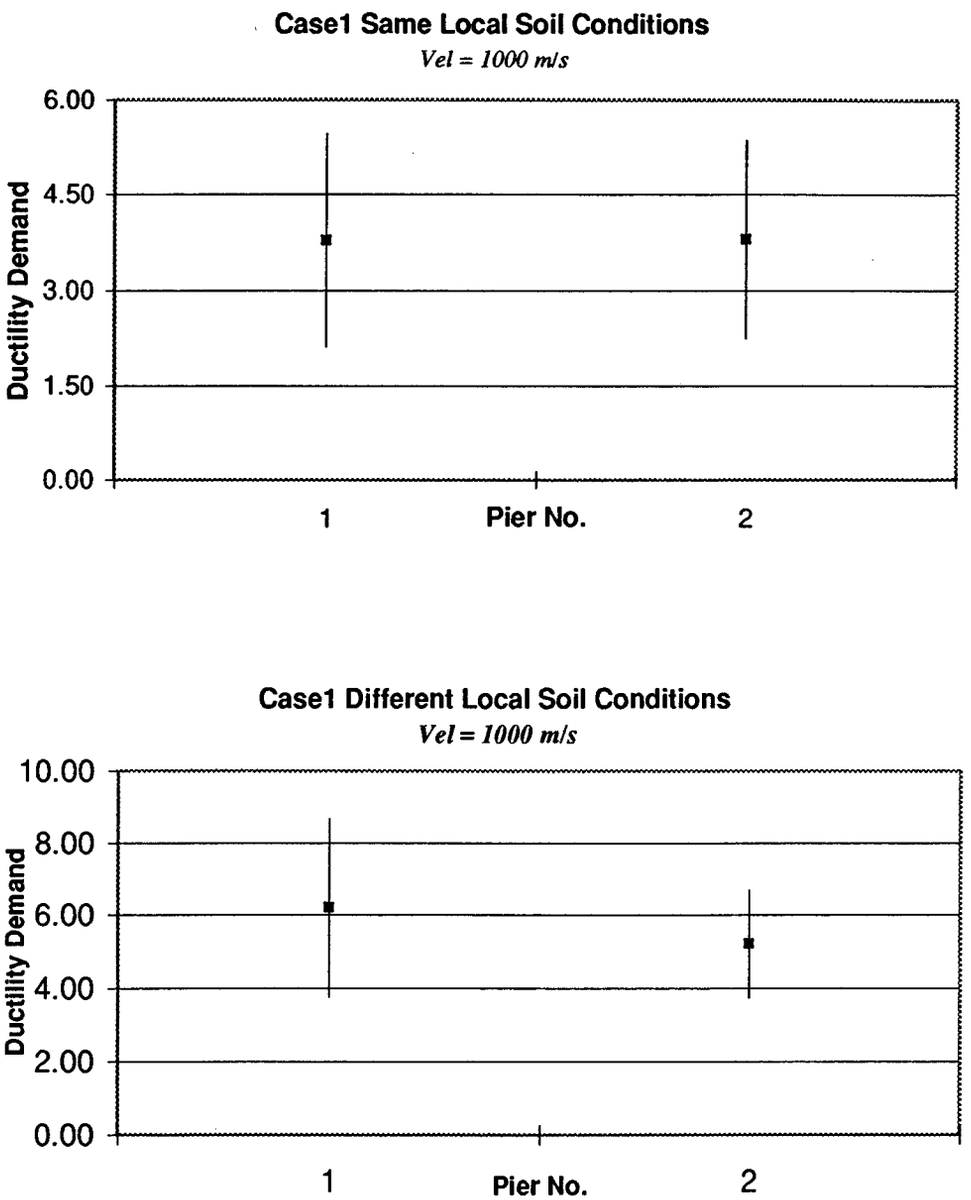

FIGURE 4-14 Mean value (denoted by block square) and mean value plus / minus one standard deviation (denoted by vertical line above and below square) for the peak ductility demand of the various piers of TEXT bridge, obtained by ensemble averaging from 20 time history analyses.

TEXT BRIDGE

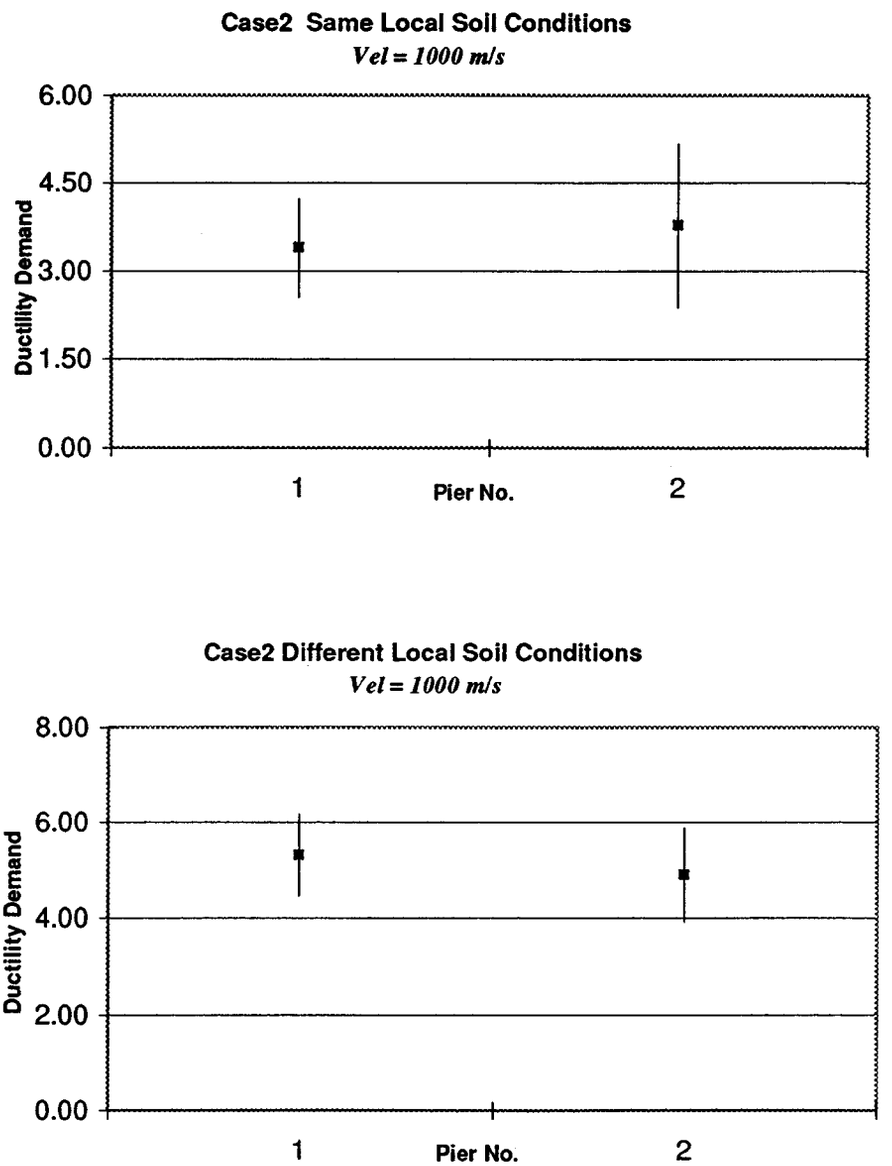

FIGURE 4-15 Mean value (denoted by block square) and mean value plus / minus one standard deviation (denoted by vertical line above and below square) for the peak ductility demand of the various piers of TEXT bridge, obtained by ensemble averaging from 20 time history analyses.

TEXT BRIDGE

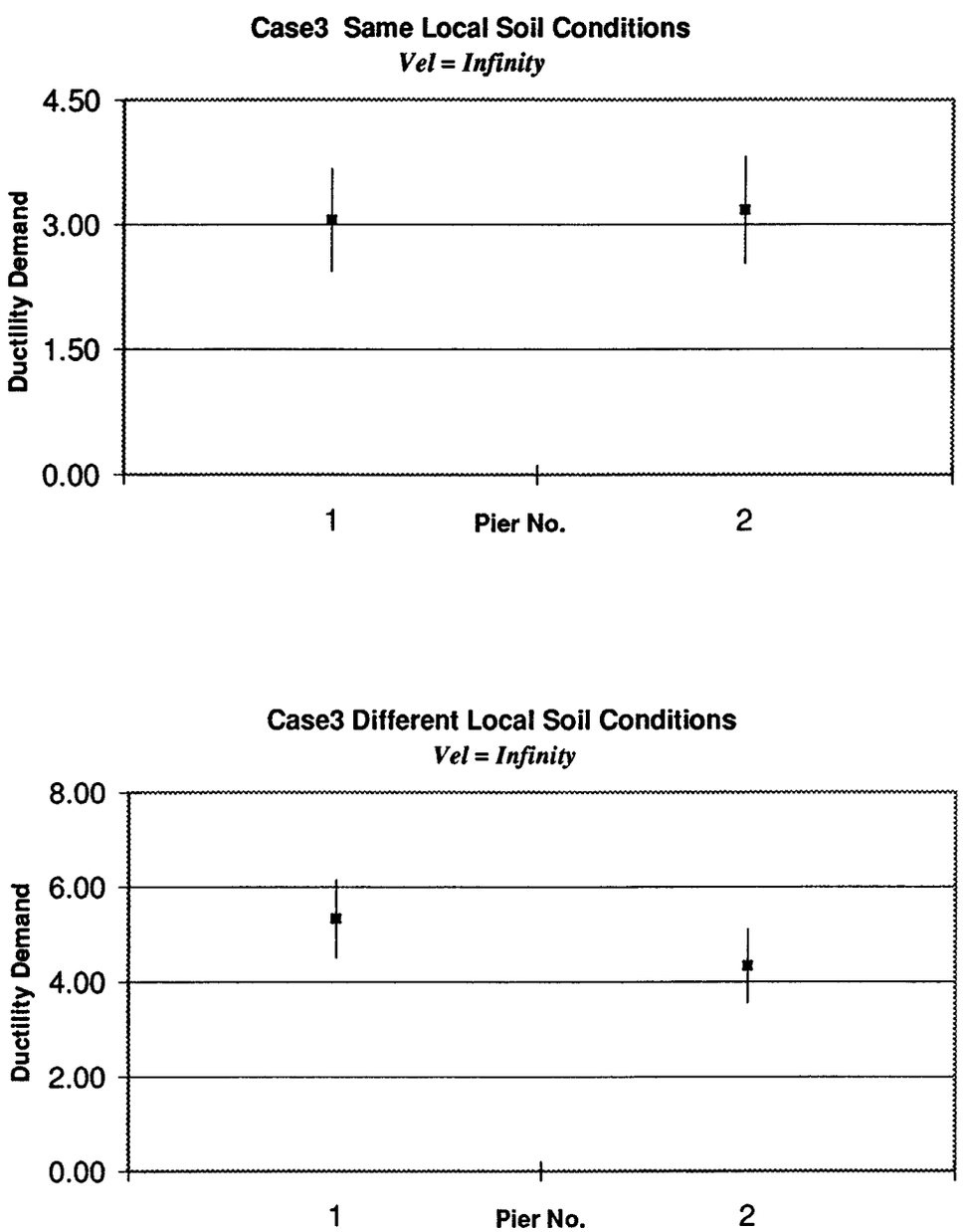

FIGURE 4-16 Mean value (denoted by block square) and mean value plus / minus one standard deviation (denoted by vertical line above and below square) for the peak ductility demand of the various piers of TEXT bridge, obtained by ensemble averaging from 20 time history analyses.

TEXT BRIDGE

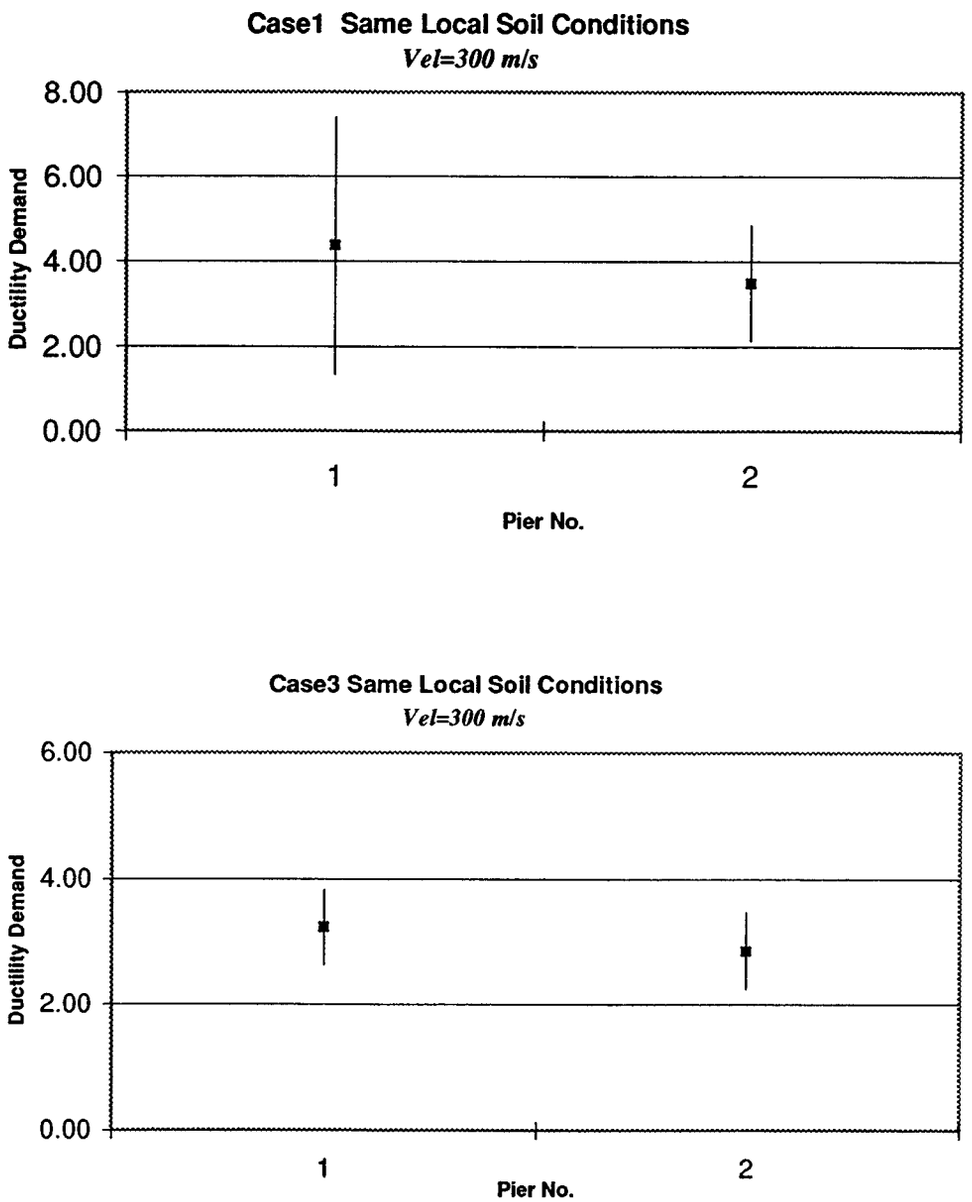

FIGURE 4-17 Mean value (denoted by block square) and mean value plus / minus one standard deviation (denoted by vertical line above and below square) for the peak ductility demand of the various piers of TEXT bridge, obtained by ensemble averaging from 20 time history analyses.

TEXT BRIDGE

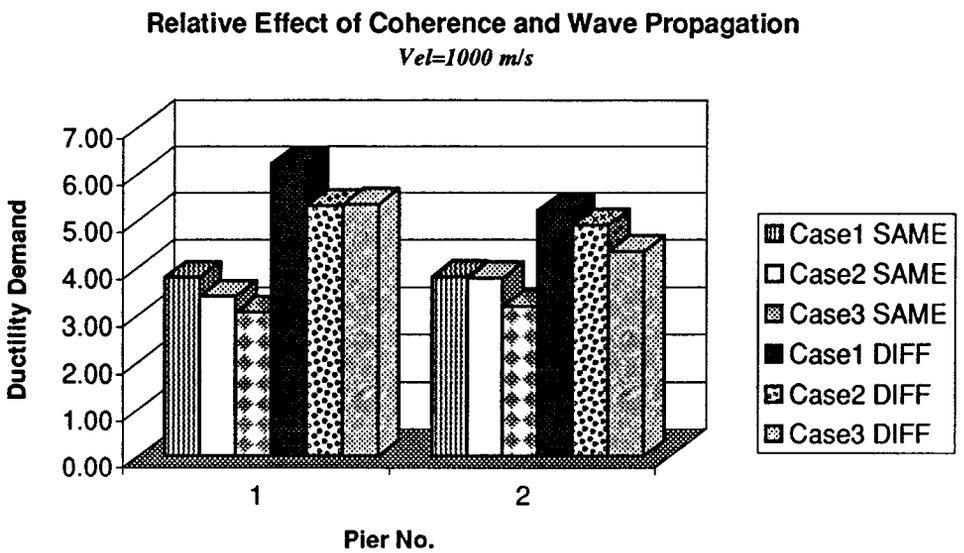

SAME denotes all supports on same local soil conditions
DIFF denotes supports on different local soil conditions

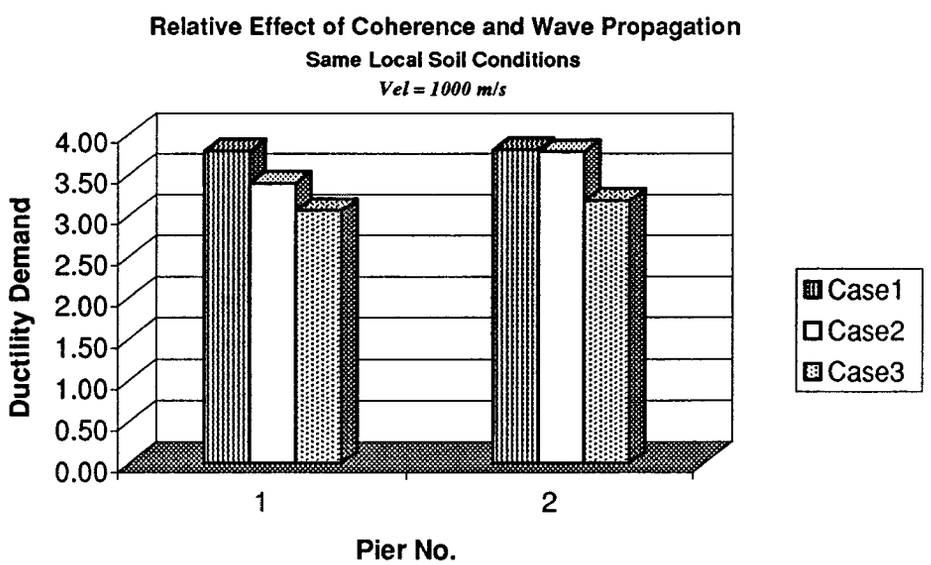

FIGURE 4-18a Bar chart depicting mean values for the peak ductility demand of the various piers of TEXT bridge, obtained from ensemble averaging from 20 time history analyses. Case 1, 2 and 3 are compared to estimate the relative effect of coherence and wave propagation. The effect of different local soil conditions and the effect of different velocities of wave propagation can also be assessed.

TEXT BRIDGE

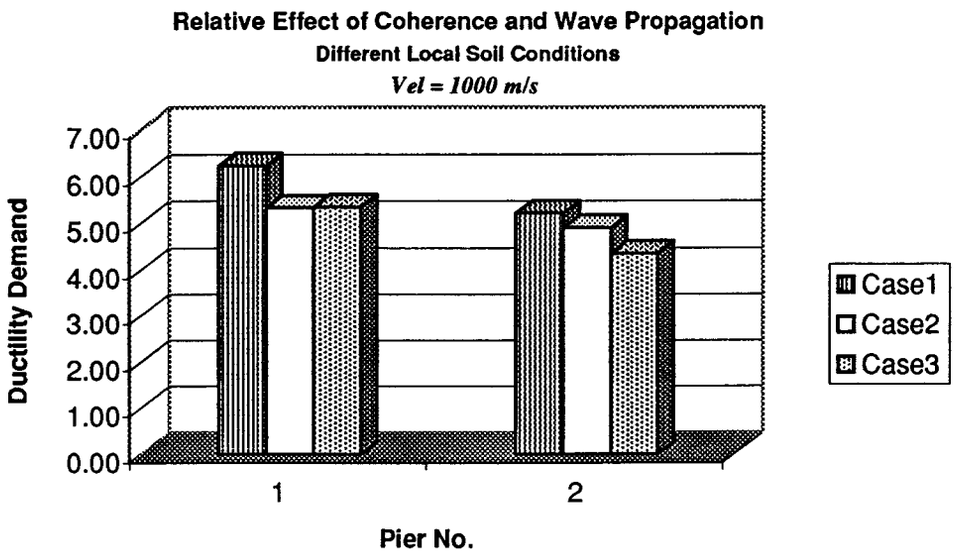

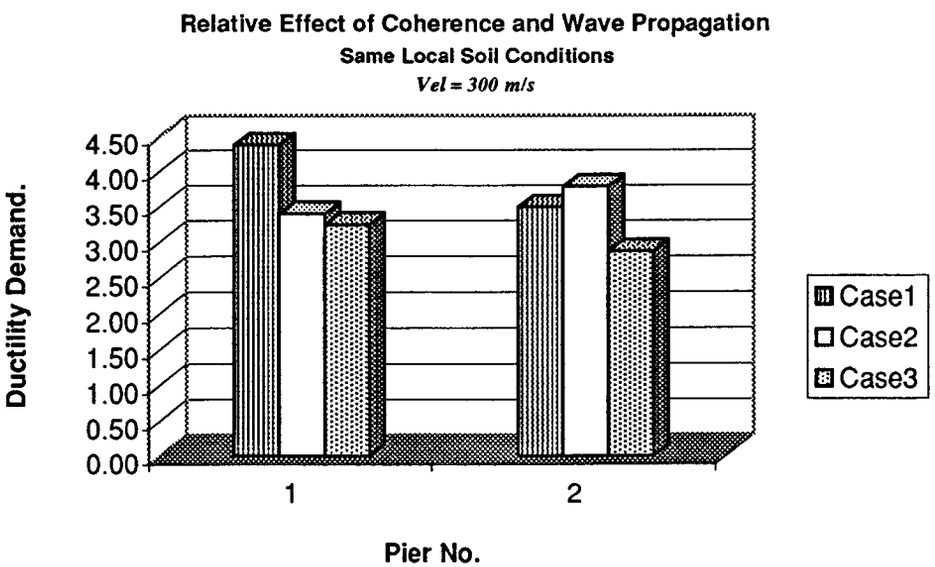

FIGURE 4-18b Bar chart depicting mean values for the peak ductility demand of the various piers of TEXT bridge, obtained from ensemble averaging from 20 time history analyses. Case 1, 2 and 3 are compared to estimate the relative effect of coherence and wave propagation. The effect of different local soil conditions and the effect of different velocities of wave propagation can also be assessed.

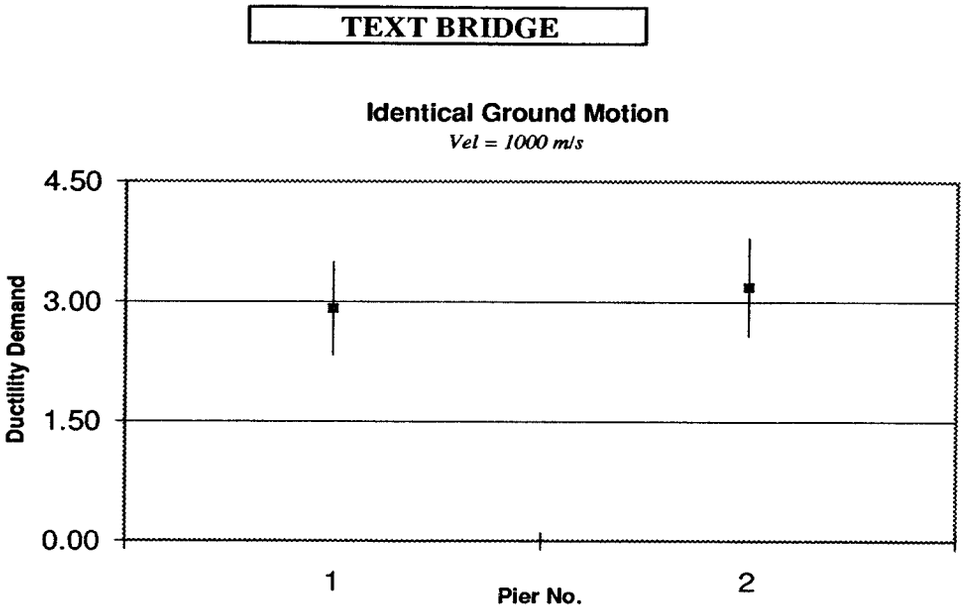

FIGURE 4-19 Mean value (denoted by block square) and mean value plus / minus one standard deviation (denoted by vertical line above and below square) for the peak ductility demand of the various piers of TEXT bridge, obtained by ensemble averaging from 20 time history analyses, for the case of identical support ground motion.

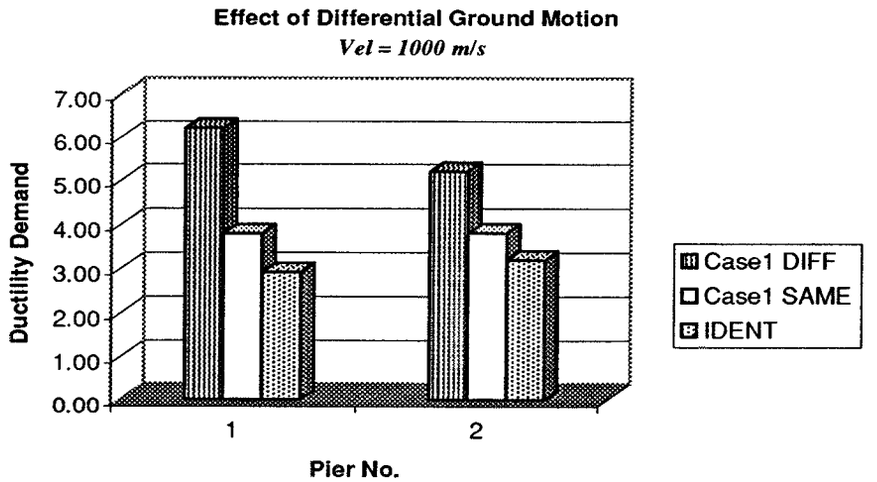

DIFF denotes supports on different local soil conditions
SAME denotes all supports on same local soil conditions
IDENT denotes identical support ground motion

FIGURE 4-20 Bar chart depicting mean values for the peak ductility demand of the various piers of TEXT bridge, obtained from ensemble averaging from 20 time history analyses. Comparison of cases with differential support ground motion and different local soil conditions, differential support ground motion and same local soil conditions, and identical support ground motion.

TEXT BRIDGE

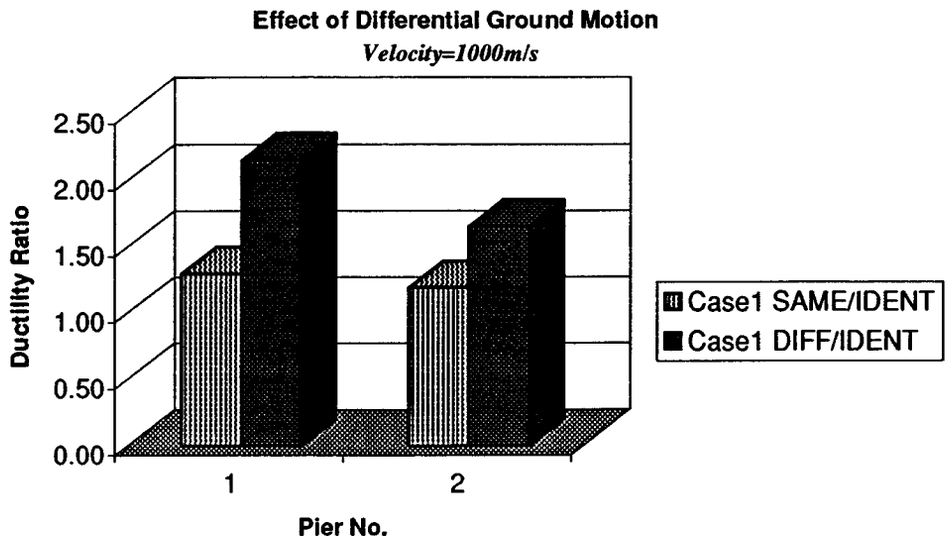

SAME/IDENT denotes the ratio of the peak ductility demand computed using differential support ground motion and same local soil conditions over the peak ductility demand computed using identical support ground motion.

DIFF/IDENT denotes the ratio of the peak ductility demand computed using differential support ground motion and different local soil conditions over the peak ductility demand computed using identical support ground motion.

FIGURE 4-21 Bar chart depicting ratios of mean values for the peak ductility demand of the various piers of TEXT bridge, obtained by ensemble averaging from 20 time history analyses The effect of differential support ground motion and different local soil conditions, differential support ground motion and same local soil conditions and identical support ground motion can be assessed.

GC2D BRIDGE

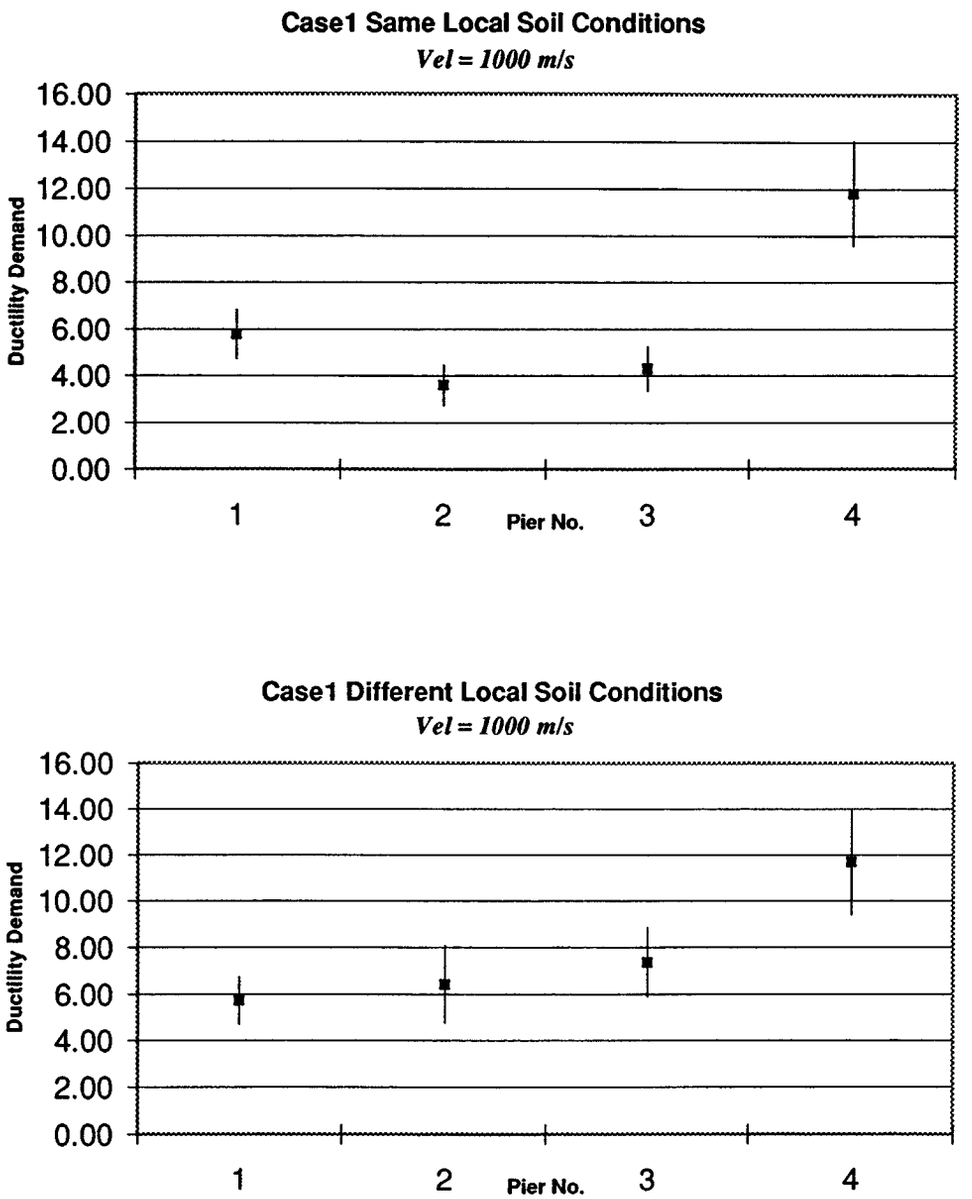

FIGURE 4-22 Mean value (denoted by block square) and mean value plus / minus one standard deviation (denoted by vertical line above and below square) for the peak ductility demand of the various piers of GC2D bridge, obtained by ensemble averaging from 20 time history analyses.

GC2D BRIDGE

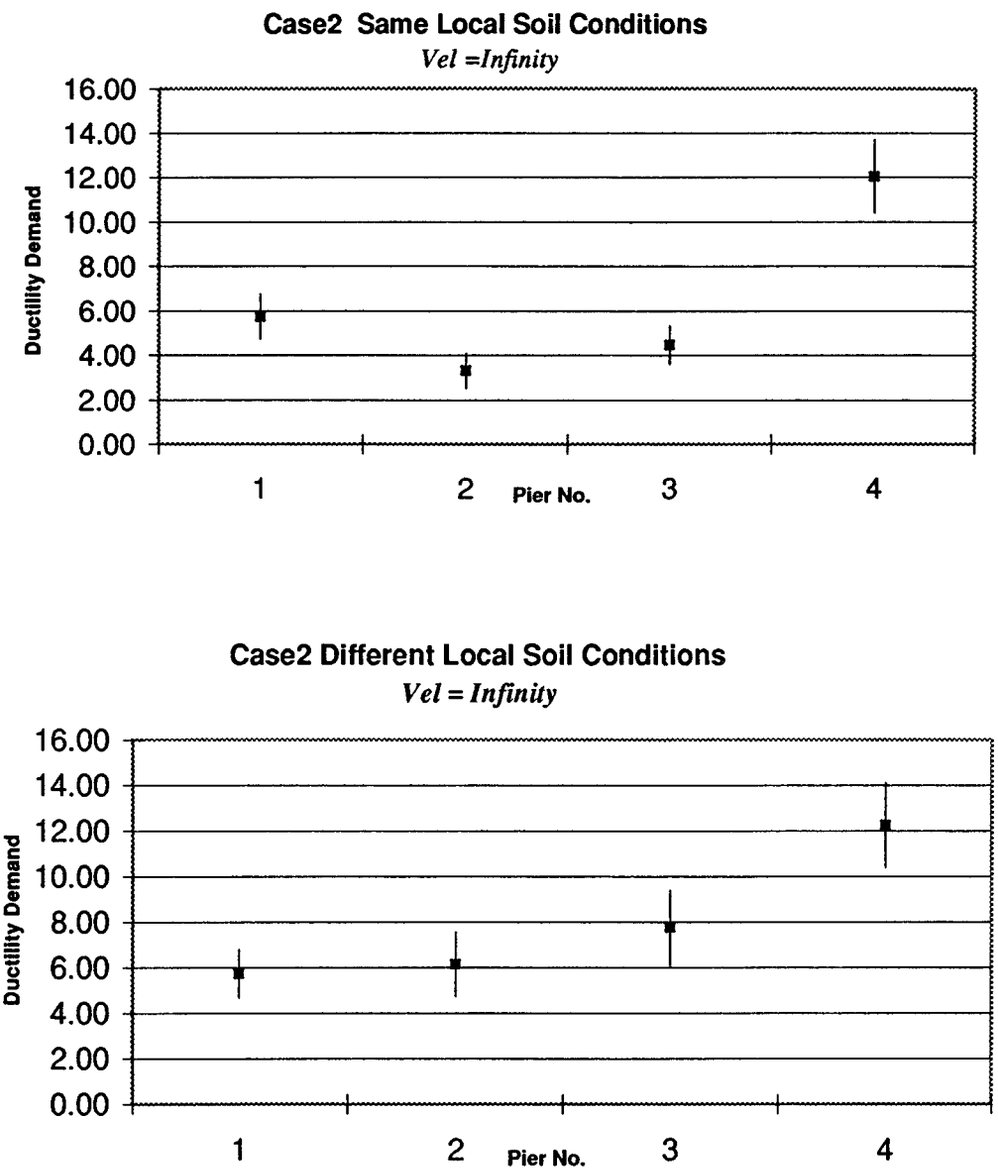

FIGURE 4-23 Mean value (denoted by block square) and mean value plus / minus one standard deviation (denoted by vertical line above and below square) for the peak ductility demand of the various piers of GC2D bridge, obtained by ensemble averaging from 20 time history analyses.

GC2D BRIDGE

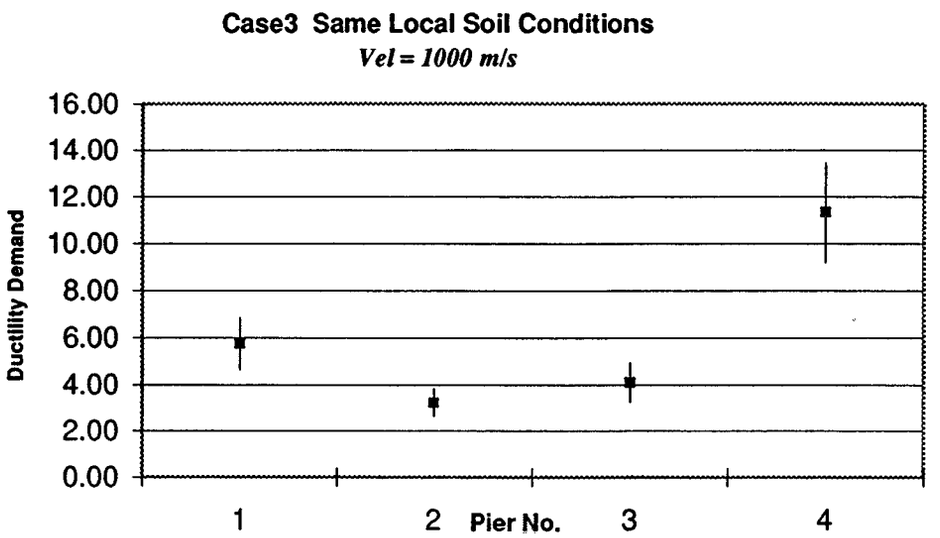

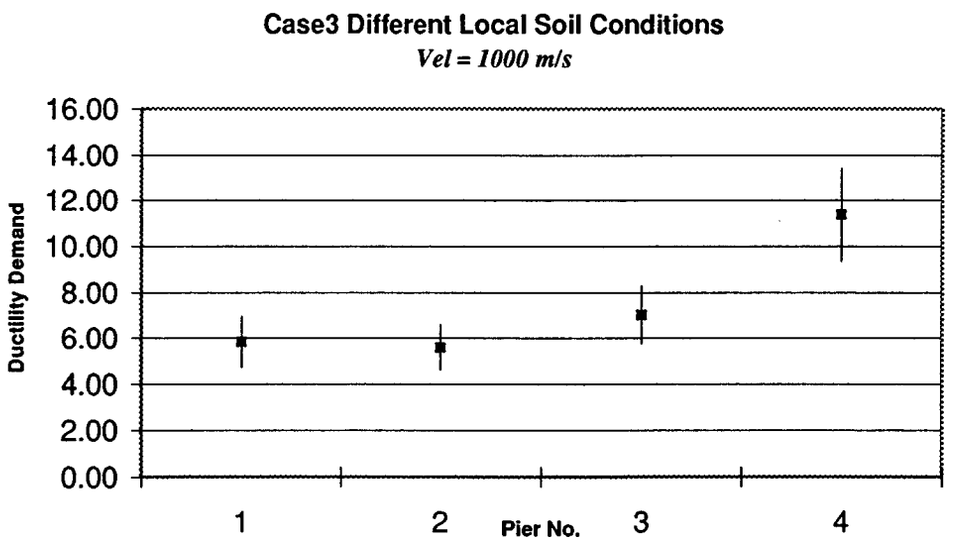

FIGURE 4-24 Mean value (denoted by block square) and mean value plus / minus one standard deviation (denoted by vertical line above and below square) for the peak ductility demand of the various piers of GC2D bridge, obtained by ensemble averaging from 20 time history analyses.

GC2D BRIDGE

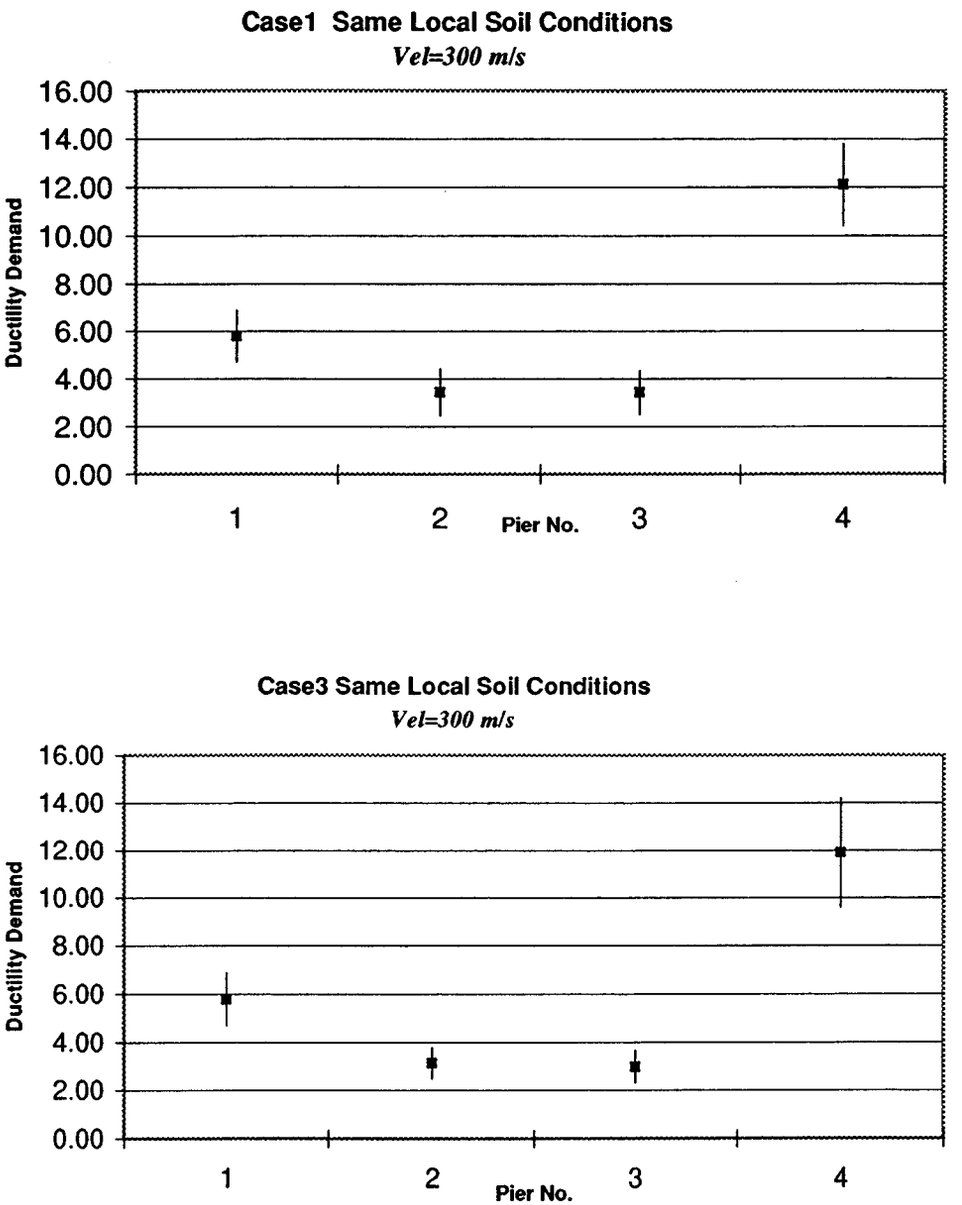

FIGURE 4-25 Mean value (denoted by block square) and mean value plus / minus one standard deviation (denoted by vertical line above and below square) for the peak ductility demand of the various piers of GC2D bridge, obtained by ensemble averaging from 20 time history analyses.

GC2D BRIDGE

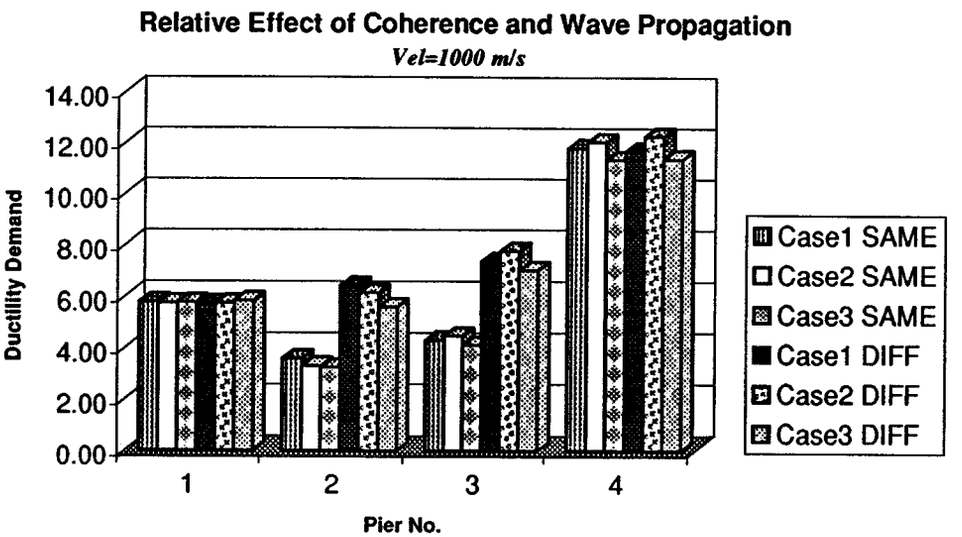

SAME denotes all supports on same local soil conditions
DIFF denotes supports on different local soil conditions

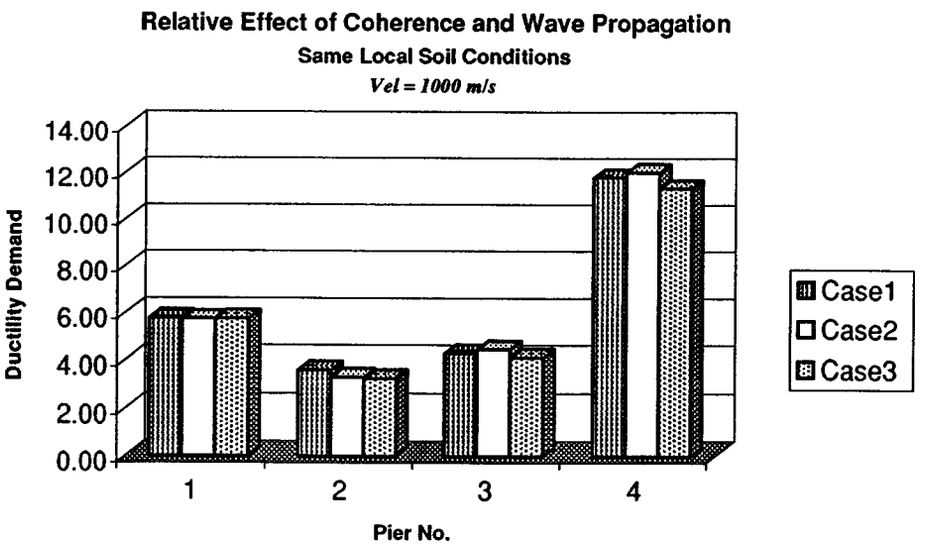

FIGURE 4-26a Bar chart depicting mean values for the peak ductility demand of the various piers of GC2D bridge, obtained from ensemble averaging from 20 time history analyses. Case 1, 2 and 3 are compared to estimate the relative effect of coherence and wave propagation. The effect of different local soil conditions and the effect of different velocities of wave propagation can also be assessed.

GC2D BRIDGE

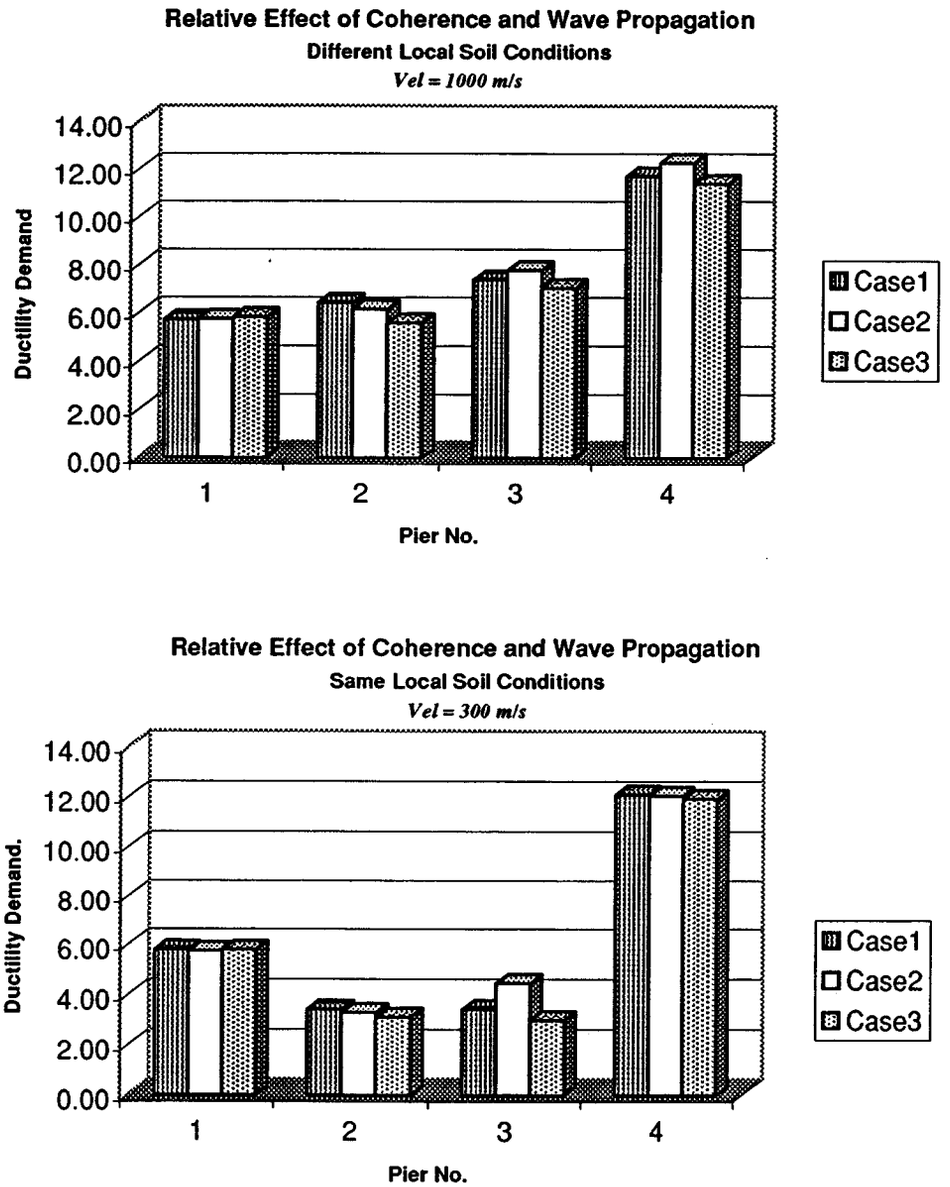

FIGURE 4-26b Bar chart depicting mean values for the peak ductility demand of the various piers of GC2D bridge, obtained from ensemble averaging from 20 time history analyses. Case 1, 2 and 3 are compared to estimate the relative effect of coherence and wave propagation. The effect of different local soil conditions and the effect of different velocities of wave propagation can also be assessed.

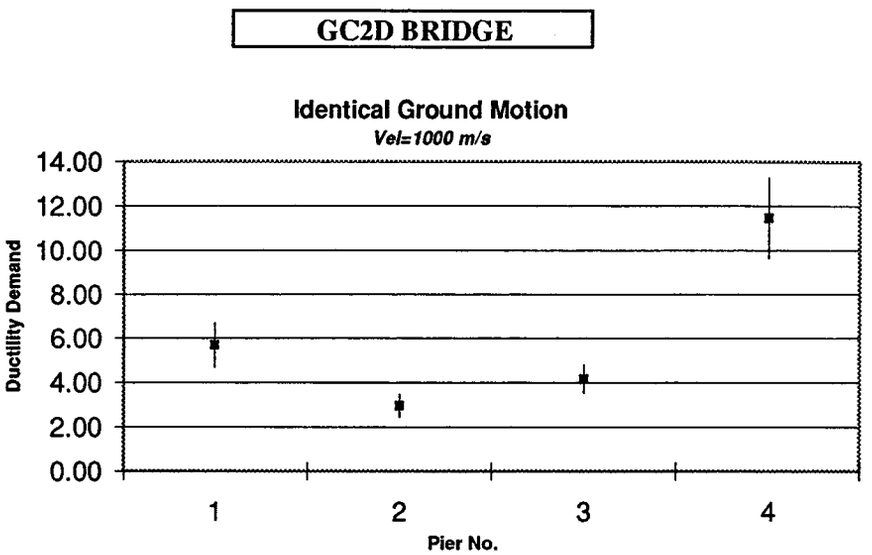

FIGURE 4-27 Mean value (denoted by block square) and mean value plus / minus one standard deviation (denoted by vertical line above and below square) for the peak ductility demand of the various piers of GC2D bridge, obtained by ensemble averaging from 20 time history analyses, for the case of identical support ground motion.

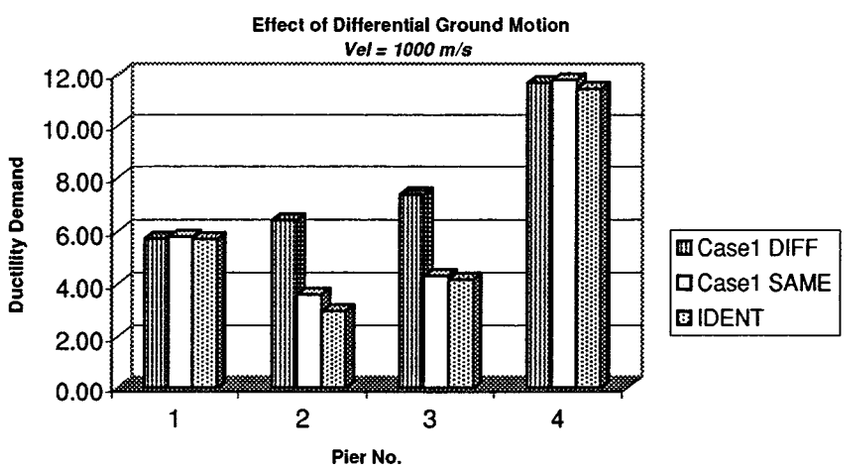

DIFF denotes supports on different local soil conditions
SAME denotes all supports on same local soil conditions
IDENT denotes identical support ground motion

FIGURE 4-28 Bar chart depicting mean values for the peak ductility demand of the various piers of GC2D bridge, obtained from ensemble averaging from 20 time history analyses. Comparison of cases with differential support ground motion and different local soil conditions, differential support ground motion and same local soil conditions, and identical support ground motion.

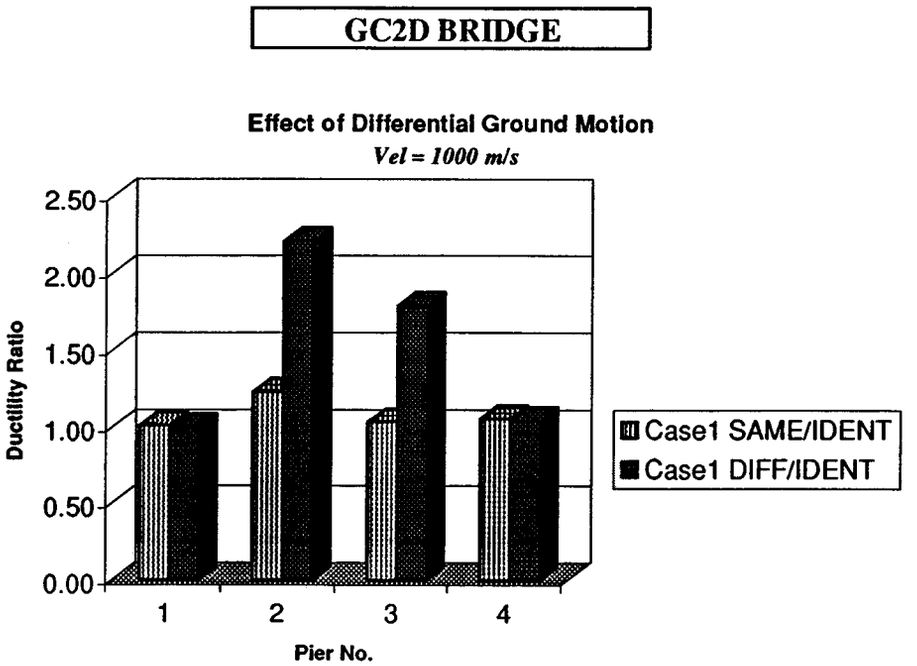

SAME/IDENT denotes the ratio of the peak ductility demand computed using differential support ground motion and same local soil conditions over the peak ductility demand computed using identical support ground motion.

DIFF/IDENT denotes the ratio of the peak ductility demand computed using differential support ground motion and different local soil conditions over the peak ductility demand computed using identical support ground motion.

FIGURE 4-29 Bar chart depicting ratios of mean values for the peak ductility demand of the various piers of FHWA bridge, obtained by ensemble averaging from 20 time history analyses The effect of differential support ground motion and different local soil conditions, differential support ground motion and same local soil conditions and identical support ground motion can be assessed.

TYOH BRIDGE

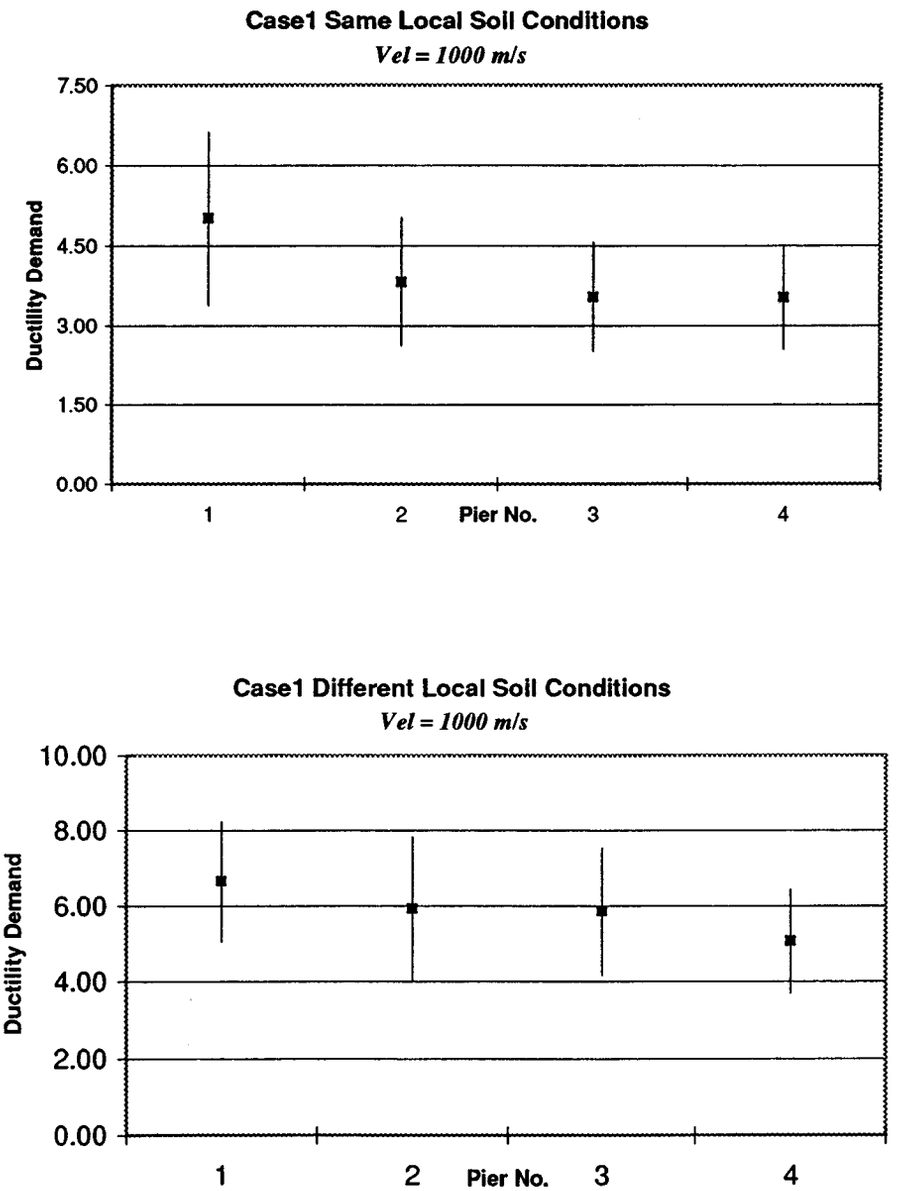

FIGURE 4-30 Mean value (denoted by block square) and mean value plus / minus one standard deviation (denoted by vertical line above and below square) for the peak ductility demand of the various piers of TYOH bridge, obtained by ensemble averaging from 20 time history analyses.

TYOH BRIDGE

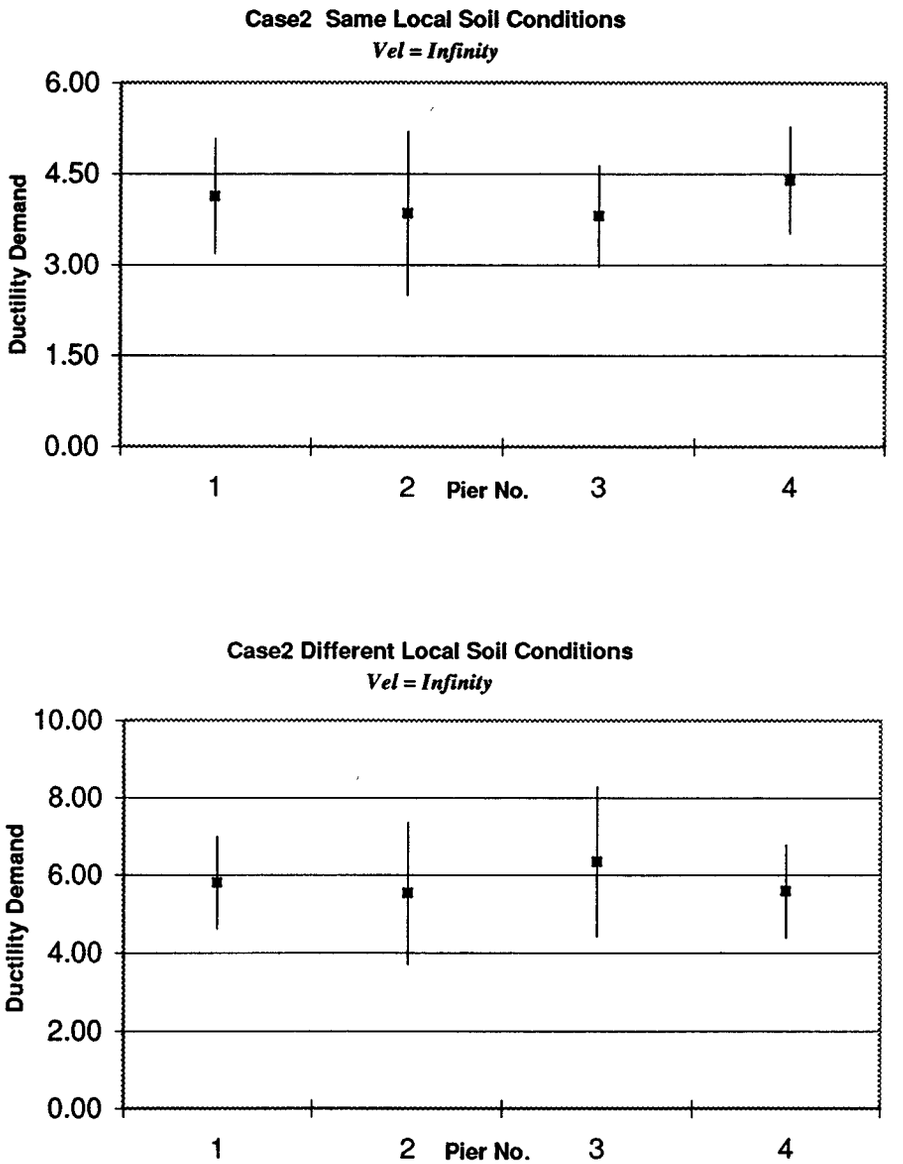

FIGURE 4-31 Mean value (denoted by block square) and mean value plus / minus one standard deviation (denoted by vertical line above and below square) for the peak ductility demand of the various piers of TYOH bridge, obtained by ensemble averaging from 20 time history analyses.

TYOH BRIDGE

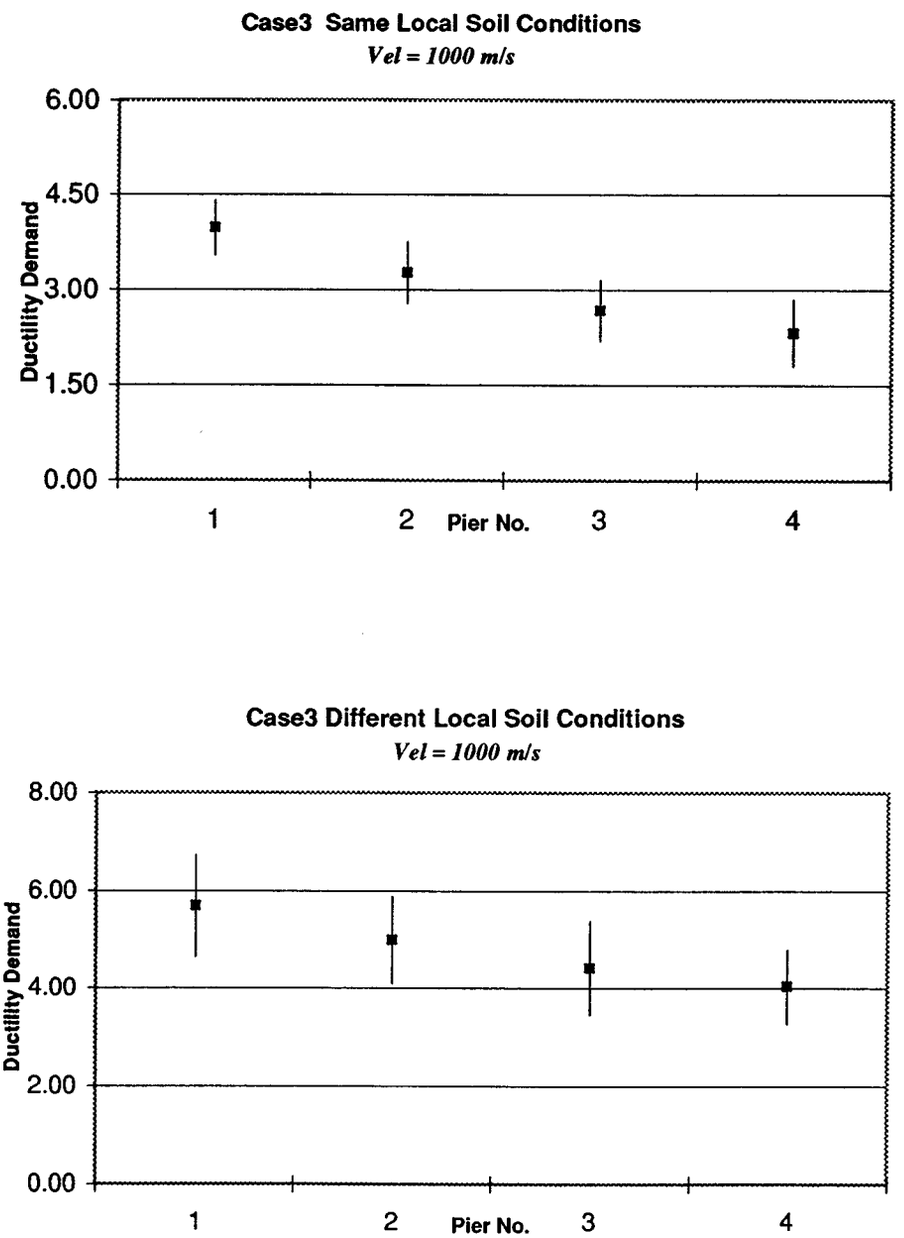

FIGURE 4-32 Mean value (denoted by block square) and mean value plus / minus one standard deviation (denoted by vertical line above and below square) for the peak ductility demand of the various piers of TYOH bridge, obtained by ensemble averaging from 20 time history analyses.

TYOH BRIDGE

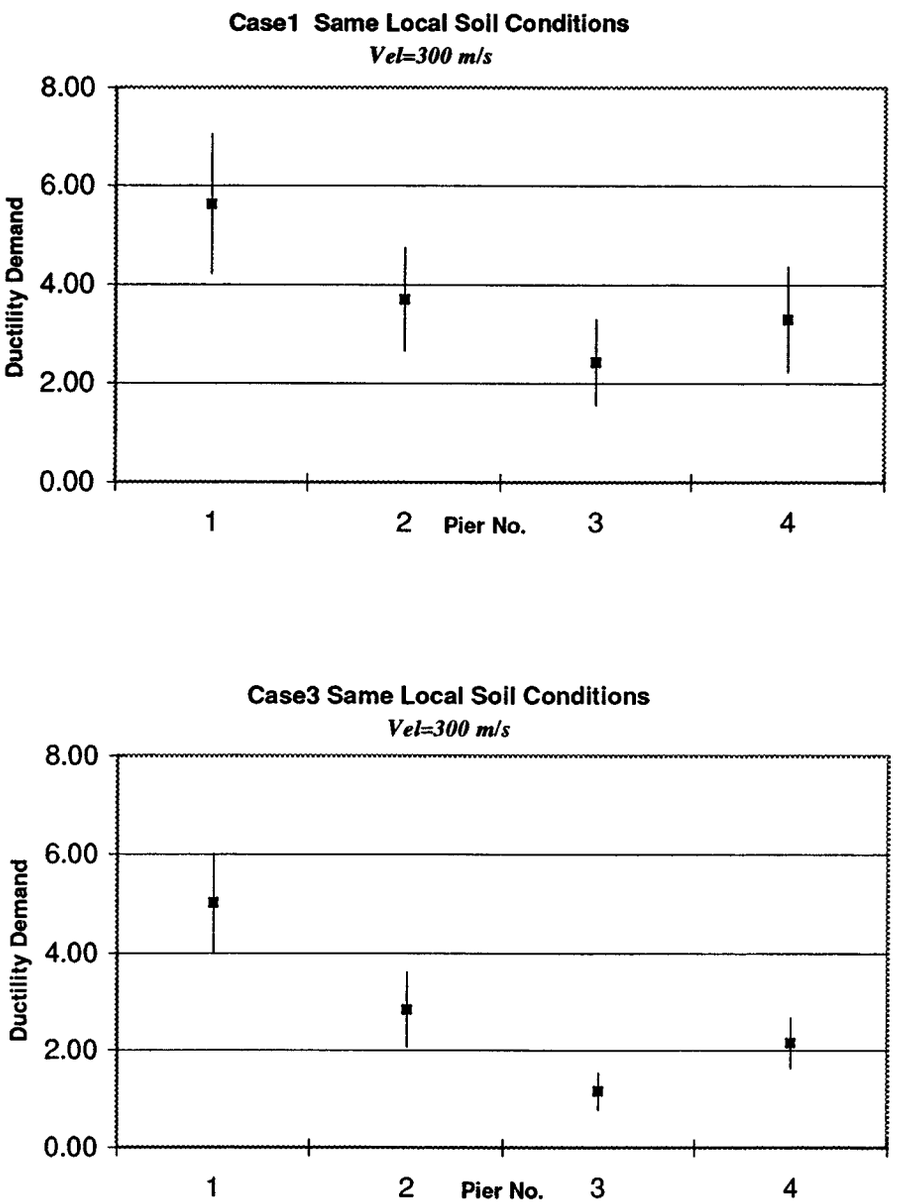

FIGURE 4-33 Mean value (denoted by block square) and mean value plus / minus one standard deviation (denoted by vertical line above and below square) for the peak ductility demand of the various piers of TYOH bridge, obtained by ensemble averaging from 20 time history analyses.

TYOH BRIDGE

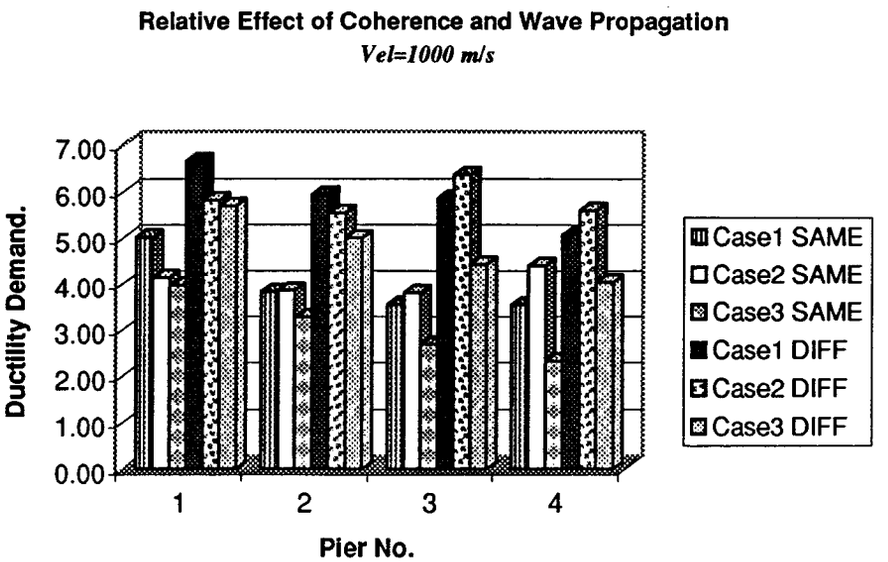

SAME denotes all supports on same local soil conditions
DIFF denotes supports on different local soil conditions

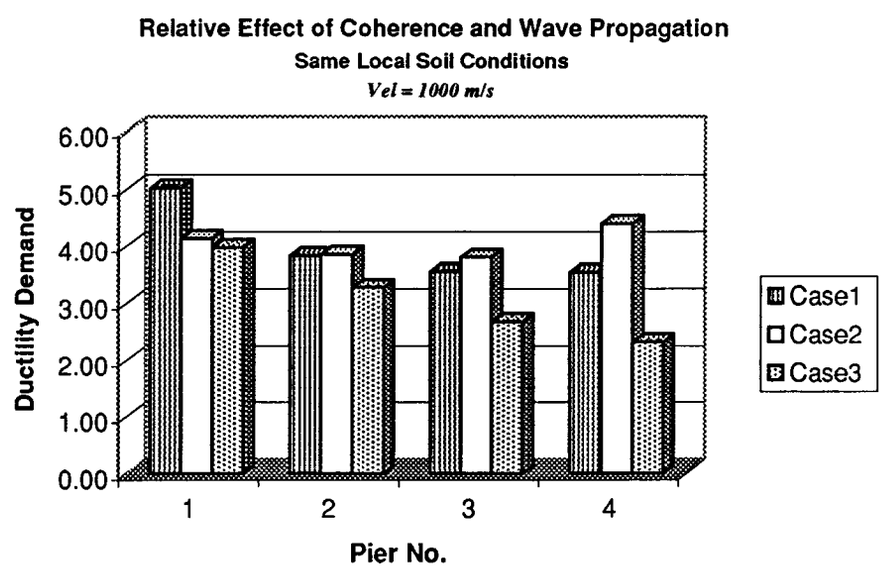

FIGURE 4-34a Bar chart depicting mean values for the peak ductility demand of the various piers of TYOH bridge, obtained from ensemble averaging from 20 time history analyses. Case 1, 2 and 3 are compared to estimate the relative effect of coherence and wave propagation. The effect of different local soil conditions and the effect of different velocities of wave propagation can also be assessed.

TYOH BRIDGE

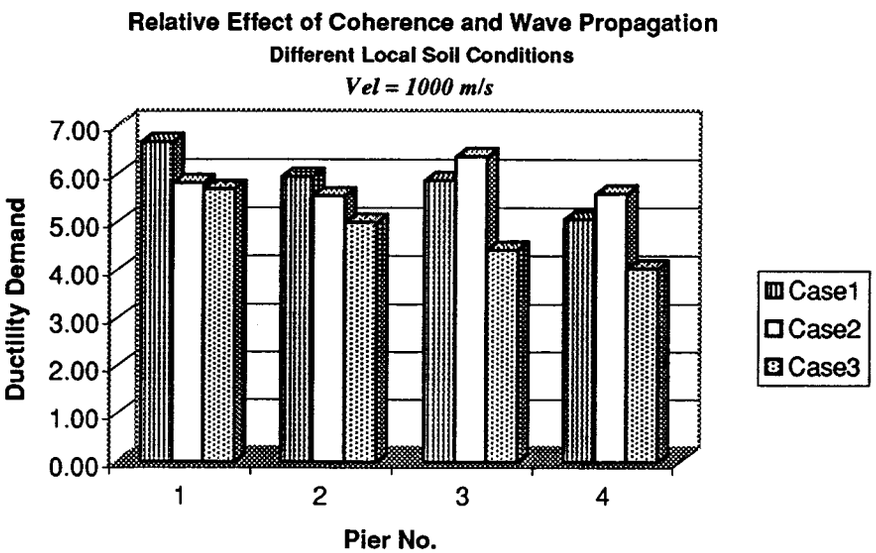

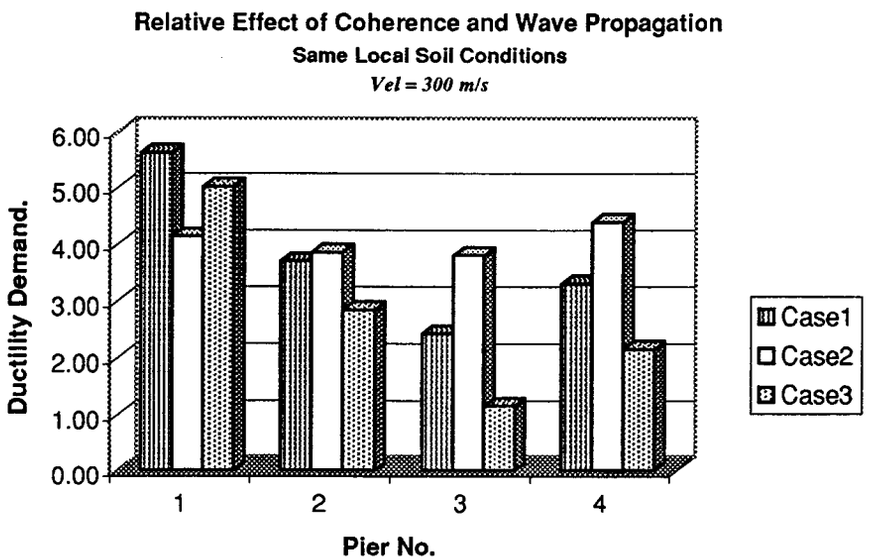

FIGURE 4-34b Bar chart depicting mean values for the peak ductility demand of the various piers of TYOH bridge, obtained from ensemble averaging from 20 time history analyses. Case 1, 2 and 3 are compared to estimate the relative effect of coherence and wave propagation. The effect of different local soil conditions and the effect of different velocities of wave propagation can also be assessed.

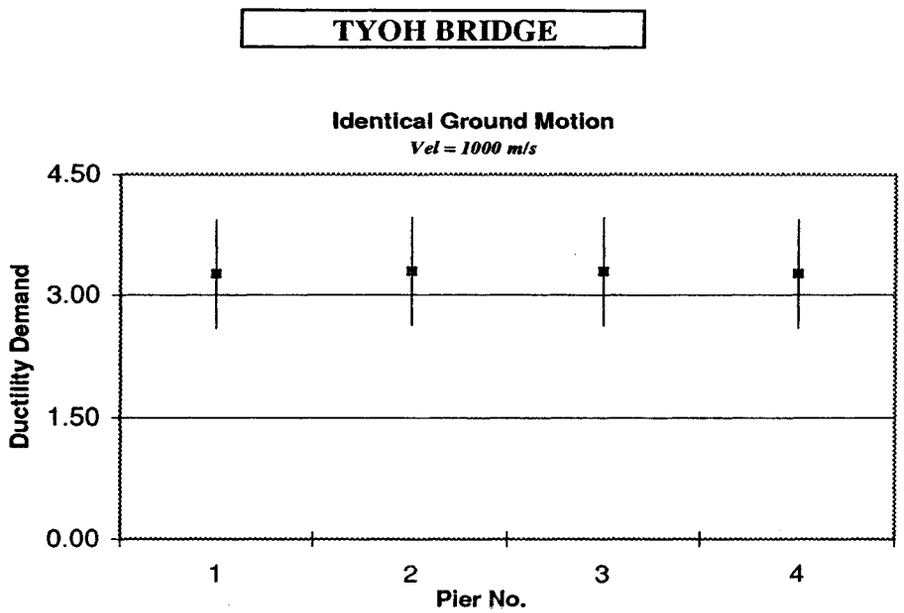

FIGURE 4-35 Mean value (denoted by block square) and mean value plus / minus one standard deviation (denoted by vertical line above and below square) for the peak ductility demand of the various piers of TYOH bridge, obtained by ensemble averaging from 20 time history analyses, for the case of identical support ground motion.

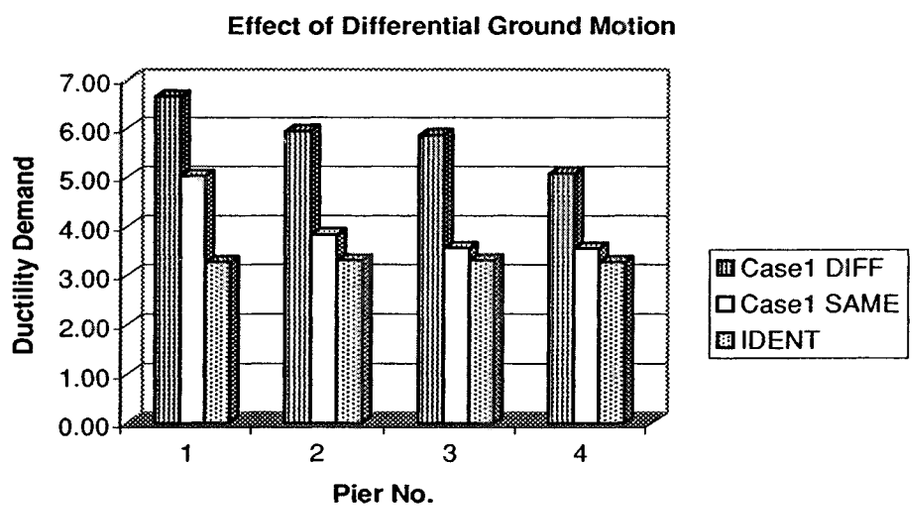

DIFF denotes supports on different local soil conditions
SAME denotes all supports on same local soil conditions
IDENT denotes identical support ground motion

FIGURE 4-36 Bar chart depicting mean values for the peak ductility demand of the various piers of TYOH bridge, obtained from ensemble averaging from 20 time history analyses. Comparison of cases with differential support ground motion and different local soil conditions, differential support ground motion and same local soil conditions, and identical support ground motion.

TYOH BRIDGE

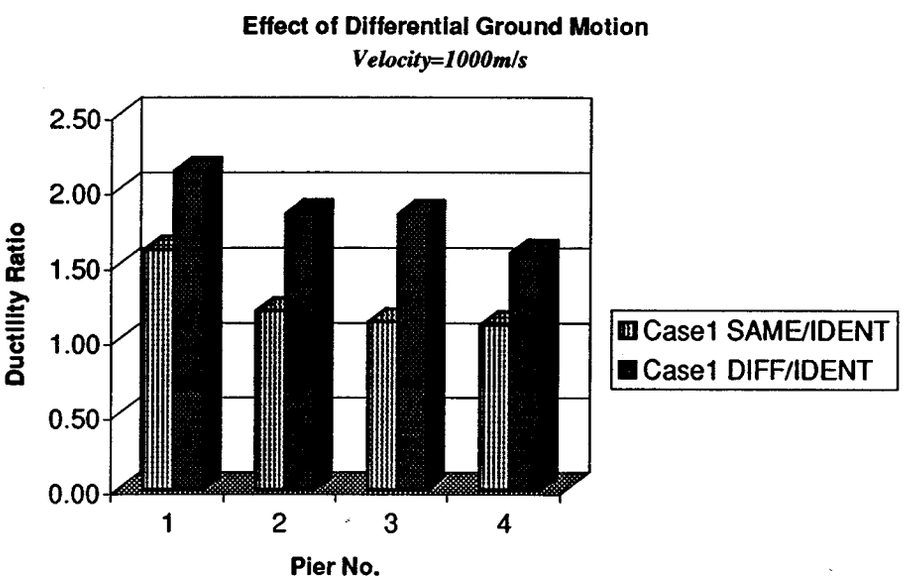

SAME/IDENT denotes the ratio of the peak ductility demand computed using differential support ground motion and same local soil conditions over the peak ductility demand computed using identical support ground motion.

DIFF/IDENT denotes the ratio of the peak ductility demand computed using differential support ground motion and different local soil conditions over the peak ductility demand computed using identical support ground motion.

FIGURE 4-37 Bar chart depicting ratios of mean values for the peak ductility demand of the various piers of TYOH bridge, obtained by ensemble averaging from 20 time history analyses The effect of differential support ground motion and different local soil conditions, differential support ground motion and same local soil conditions and identical support ground motion can be assessed.

TY1H BRIDGE

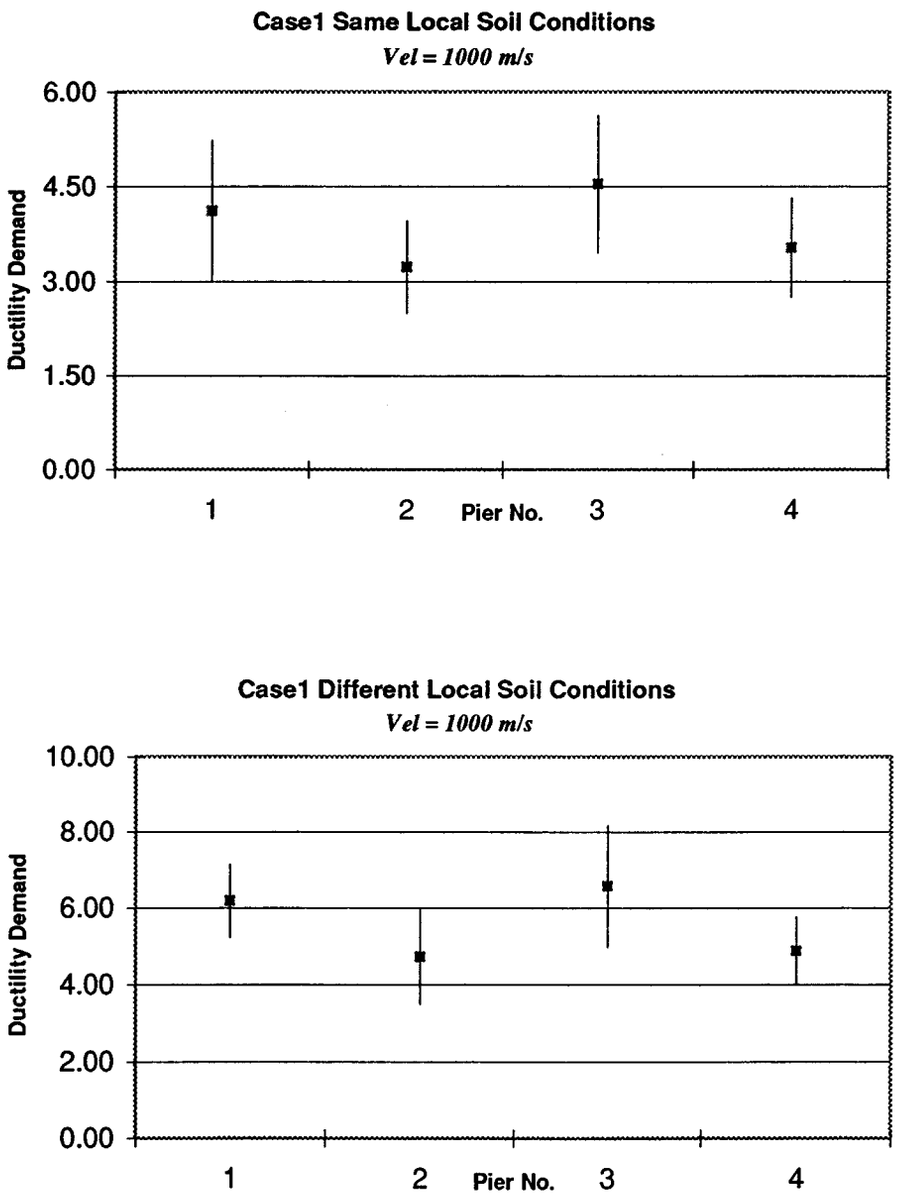

FIGURE 4-38 Mean value (denoted by block square) and mean value plus / minus one standard deviation (denoted by vertical line above and below square) for the peak ductility demand of the various piers of TY1H bridge, obtained by ensemble averaging from 20 time history analyses.

TY1H BRIDGE

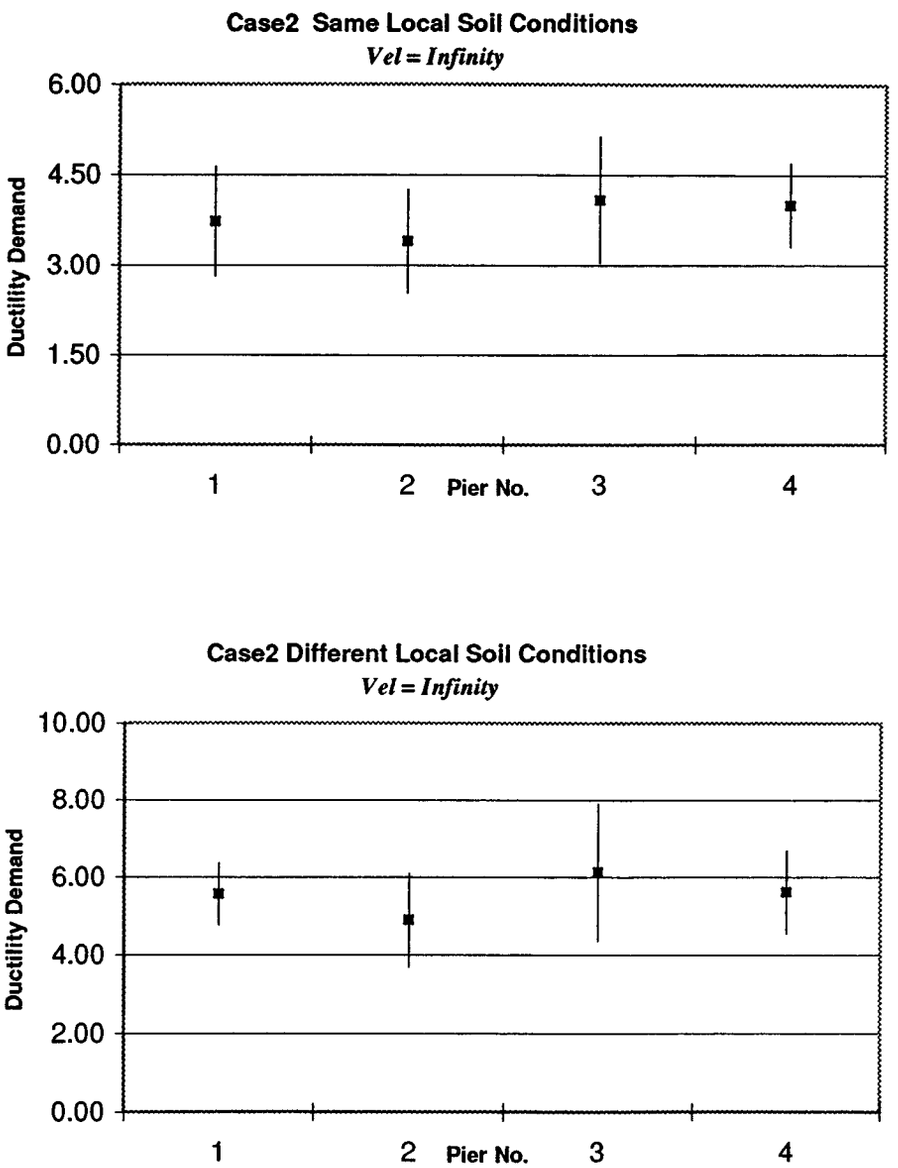

FIGURE 4-39 Mean value (denoted by block square) and mean value plus / minus one standard deviation (denoted by vertical line above and below square) for the peak ductility demand of the various piers of TY1H bridge, obtained by ensemble averaging from 20 time history analyses.

TY1H BRIDGE

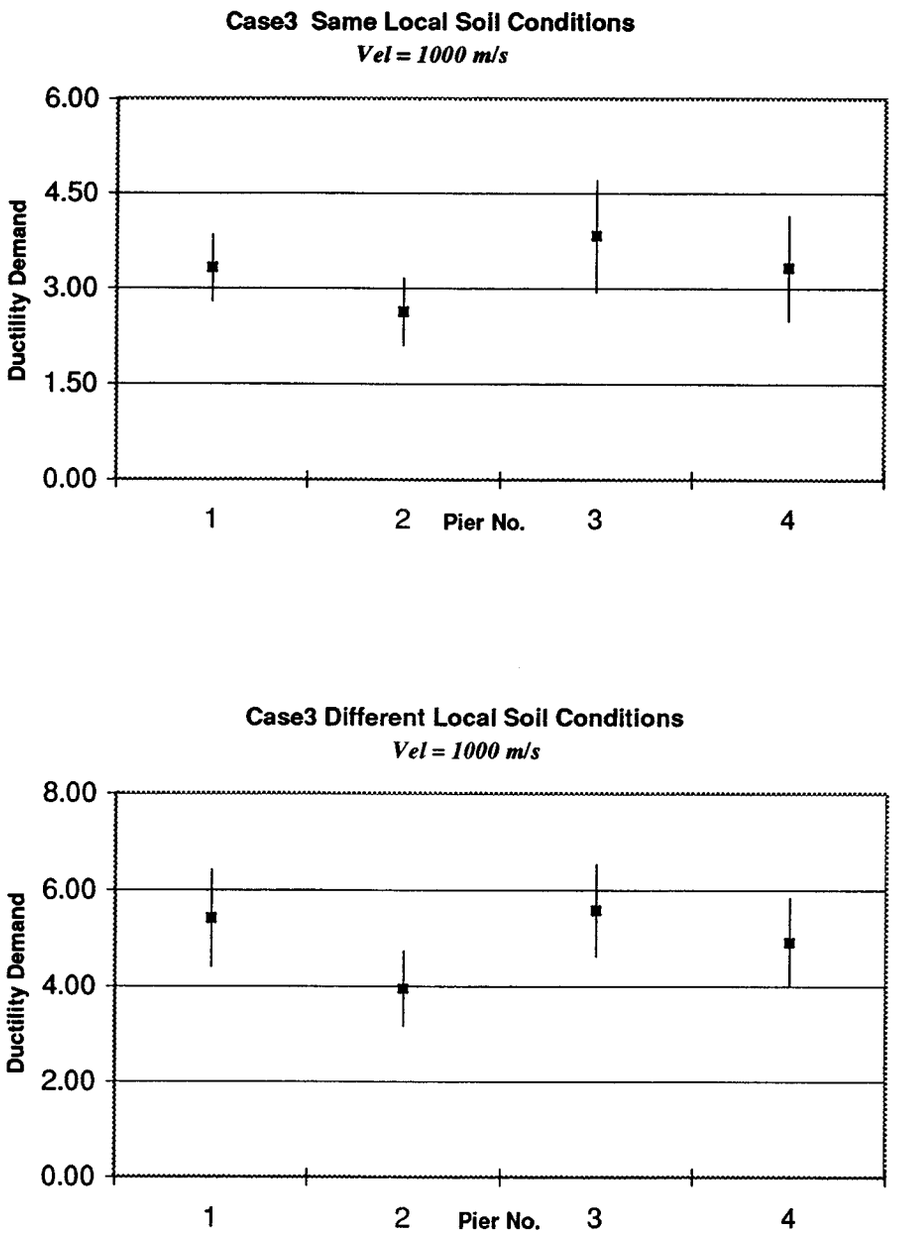

FIGURE 4-40 Mean value (denoted by block square) and mean value plus / minus one standard deviation (denoted by vertical line above and below square) for the peak ductility demand of the various piers of TY1H bridge, obtained by ensemble averaging from 20 time history analyses.

TY1H BRIDGE

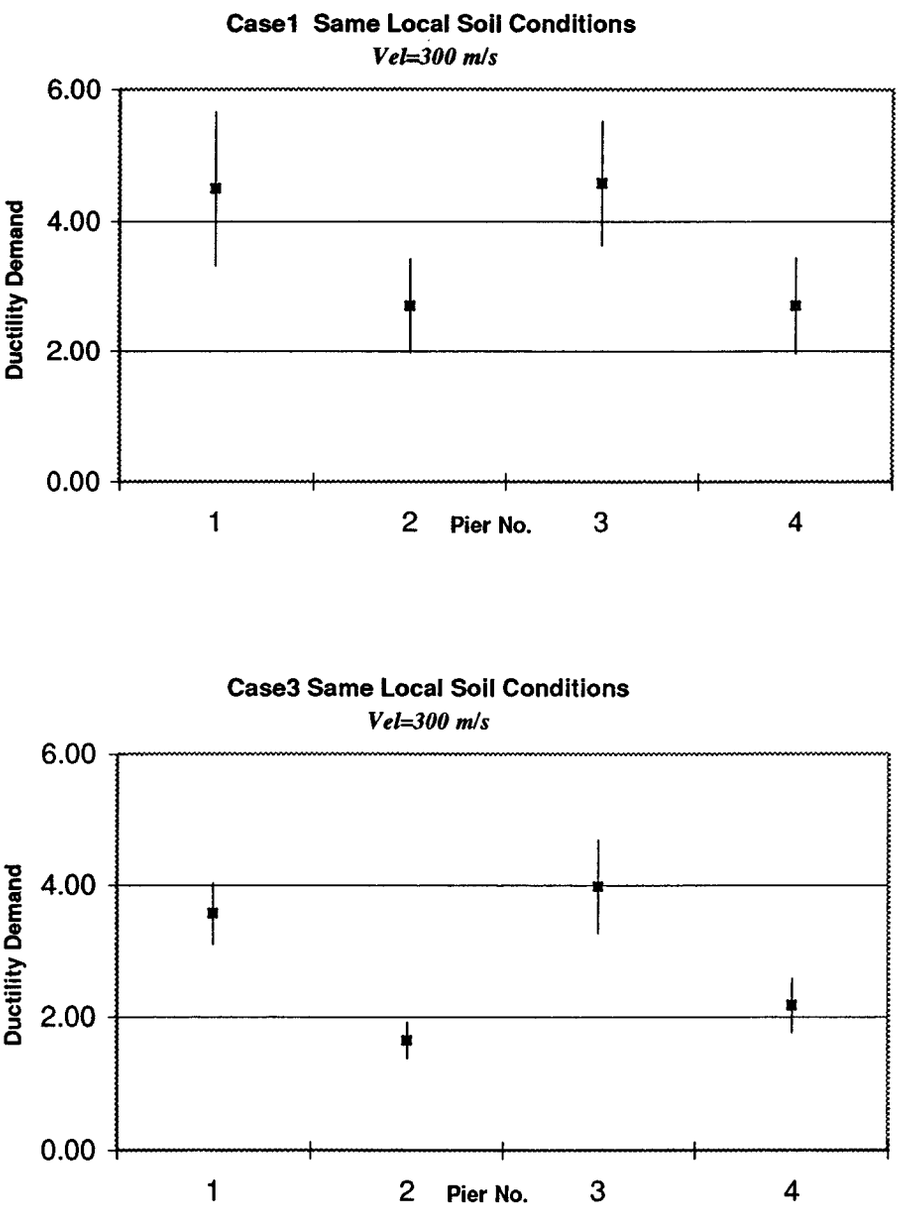

FIGURE 4-41 Mean value (denoted by block square) and mean value plus / minus one standard deviation (denoted by vertical line above and below square) for the peak ductility demand of the various piers of TY1H bridge, obtained by ensemble averaging from 20 time history analyses.

TY1H BRIDGE

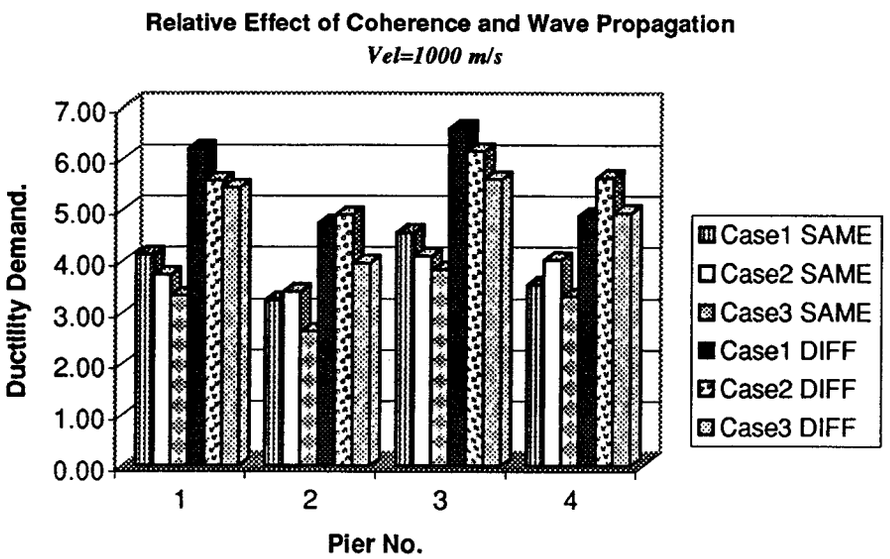

SAME denotes all supports on same local soil conditions
DIFF denotes supports on different local soil conditions

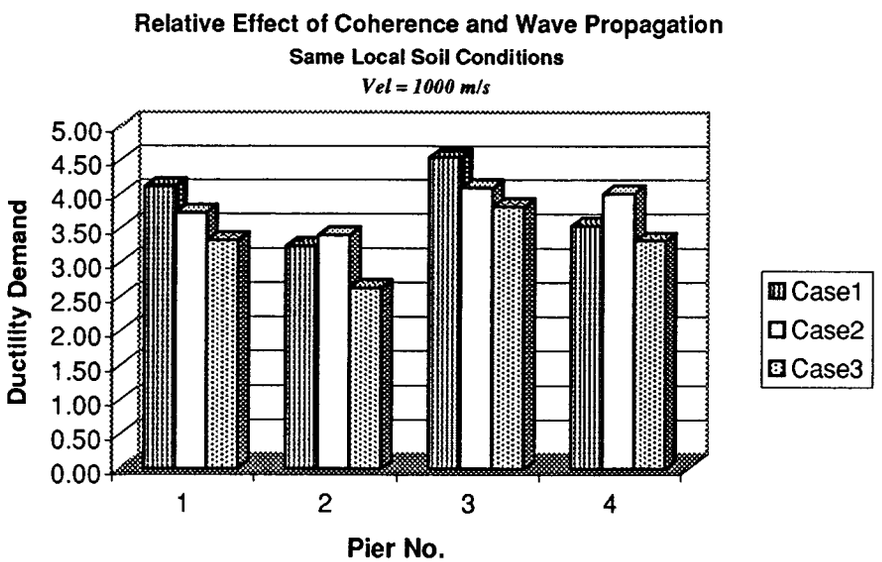

FIGURE 4-42a Bar chart depicting mean values for the peak ductility demand of the various piers of TY1H bridge, obtained from ensemble averaging from 20 time history analyses. Case 1, 2 and 3 are compared to estimate the relative effect of coherence and wave propagation. The effect of different local soil conditions and the effect of different velocities of wave propagation can also be assessed.

TY1H BRIDGE

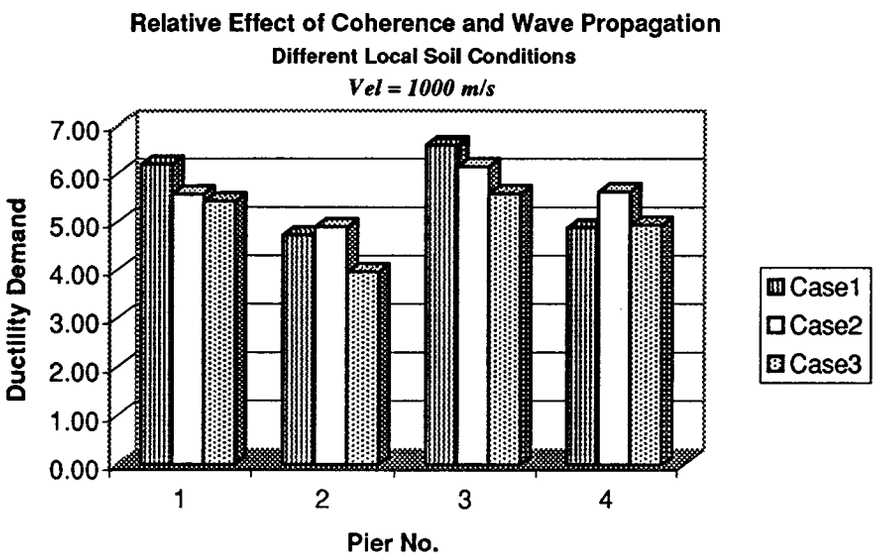

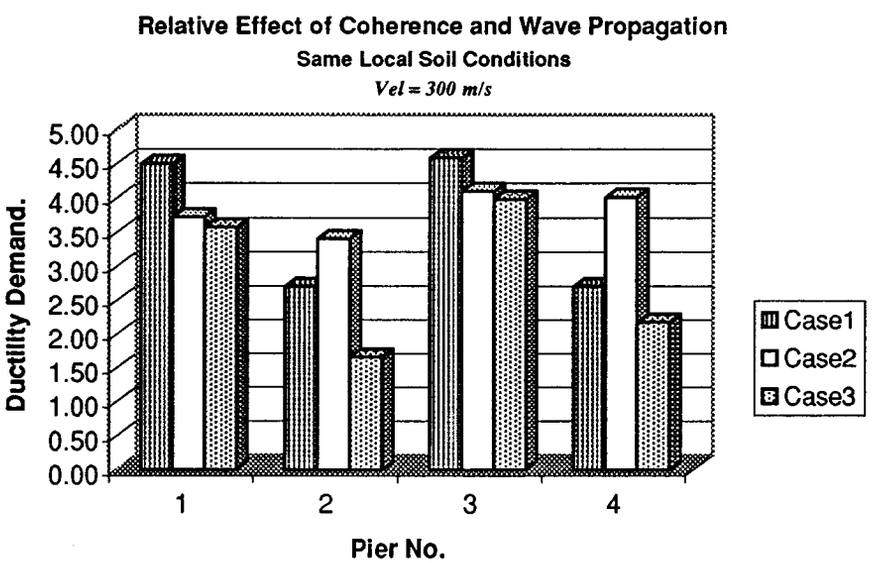

FIGURE 4-42b Bar chart depicting mean values for the peak ductility demand of the various piers of TY1H bridge, obtained from ensemble averaging from 20 time history analyses. Case 1, 2 and 3 are compared to estimate the relative effect of coherence and wave propagation. The effect of different local soil conditions and the effect of different velocities of wave propagation can also be assessed.

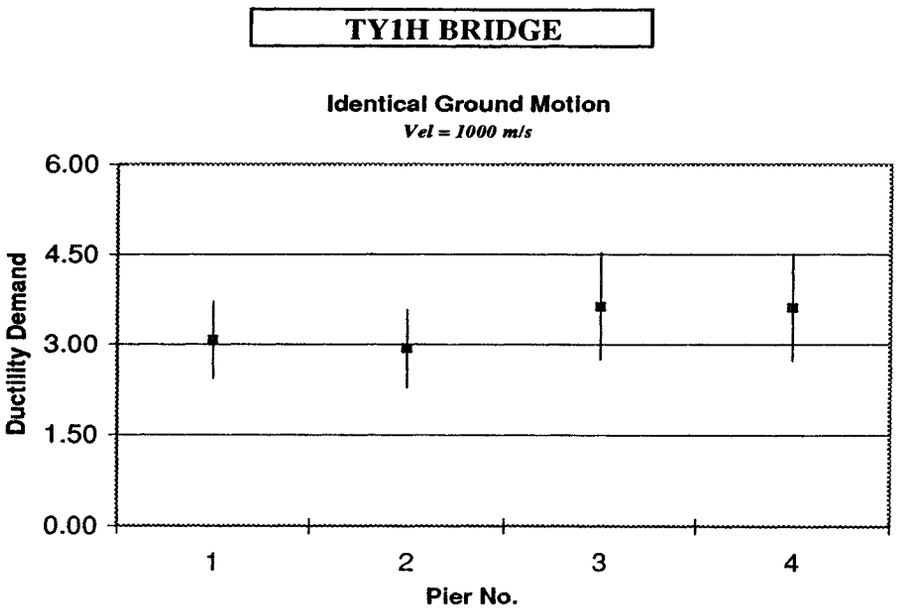

FIGURE 4-43 Mean value (denoted by block square) and mean value plus / minus one standard deviation (denoted by vertical line above and below square) for the peak ductility demand of the various piers of TY1H bridge, obtained by ensemble averaging from 20 time history analyses, for the case of identical support ground motion.

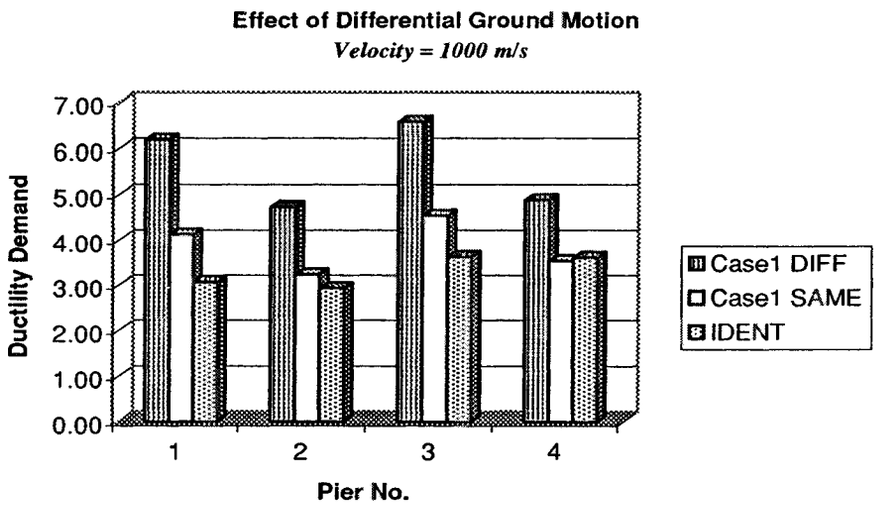

DIFF denotes supports on different local soil conditions
SAME denotes all supports on same local soil conditions
IDENT denotes identical support ground motion

FIGURE 4-44 Bar chart depicting mean values for the peak ductility demand of the various piers of TY1H bridge, obtained from ensemble averaging from 20 time history analyses. Comparison of cases with differential support ground motion and different local soil conditions, differential support ground motion and same local soil conditions, and identical support ground motion.

TY1H BRIDGE

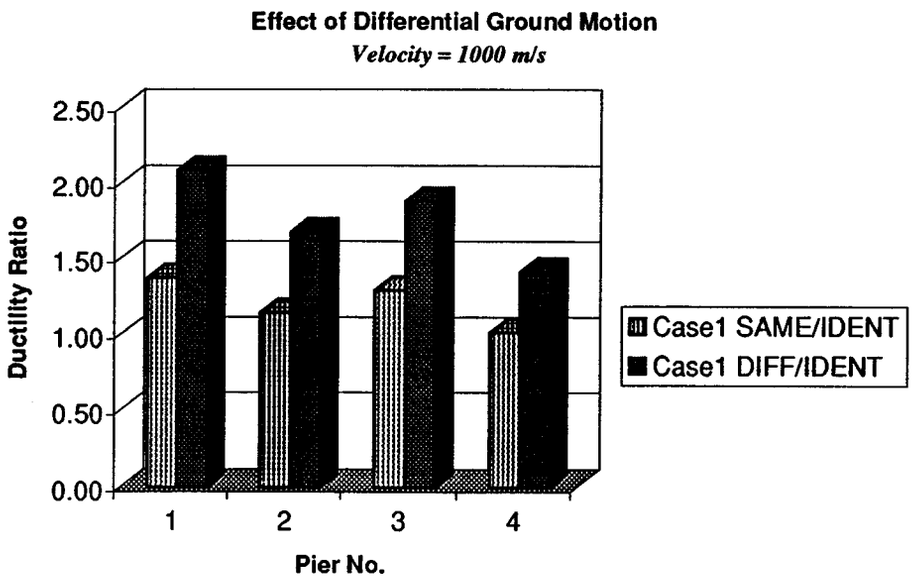

SAME/IDENT denotes the ratio of the peak ductility demand computed using differentia support ground motion and same local soil conditions over the peak ductility demand computed using identical support ground motion.

DIFF/IDENT denotes the ratio of the peak ductility demand computed using differential support ground motion and different local soil conditions over the peak ductility demand computed using identical support ground motion.

FIGURE 4-45 Bar chart depicting ratios of mean values for the peak ductility demand of the various piers of TY1H bridge, obtained by ensemble averaging from 20 time history analyses The effect of differential support ground motion and different local soil conditions, differential support ground motion and same local soil conditions and identical support ground motion can be assessed.

TY2H BRIDGE

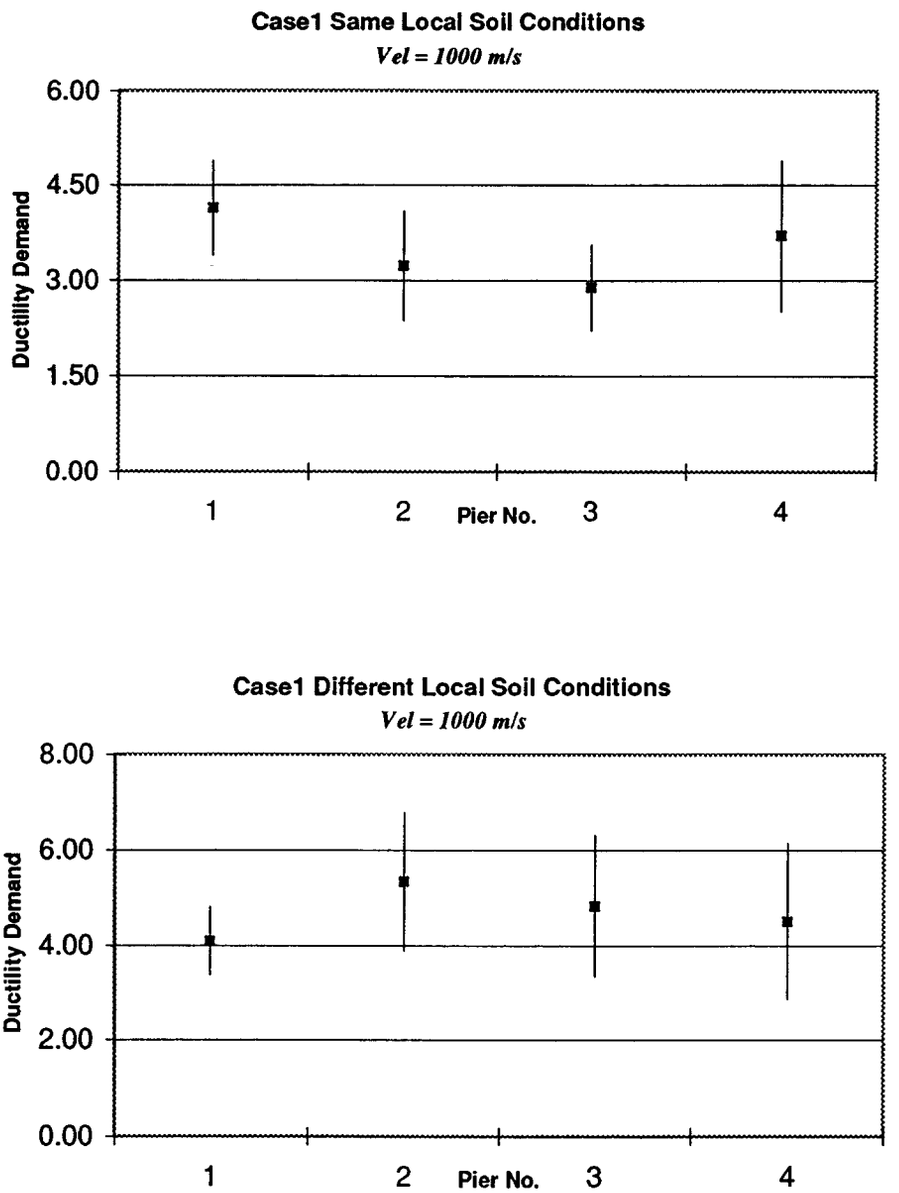

FIGURE 4-46 Mean value (denoted by block square) and mean value plus / minus one standard deviation (denoted by vertical line above and below square) for the peak ductility demand of the various piers of TY2H bridge, obtained by ensemble averaging from 20 time history analyses.

TY2H BRIDGE

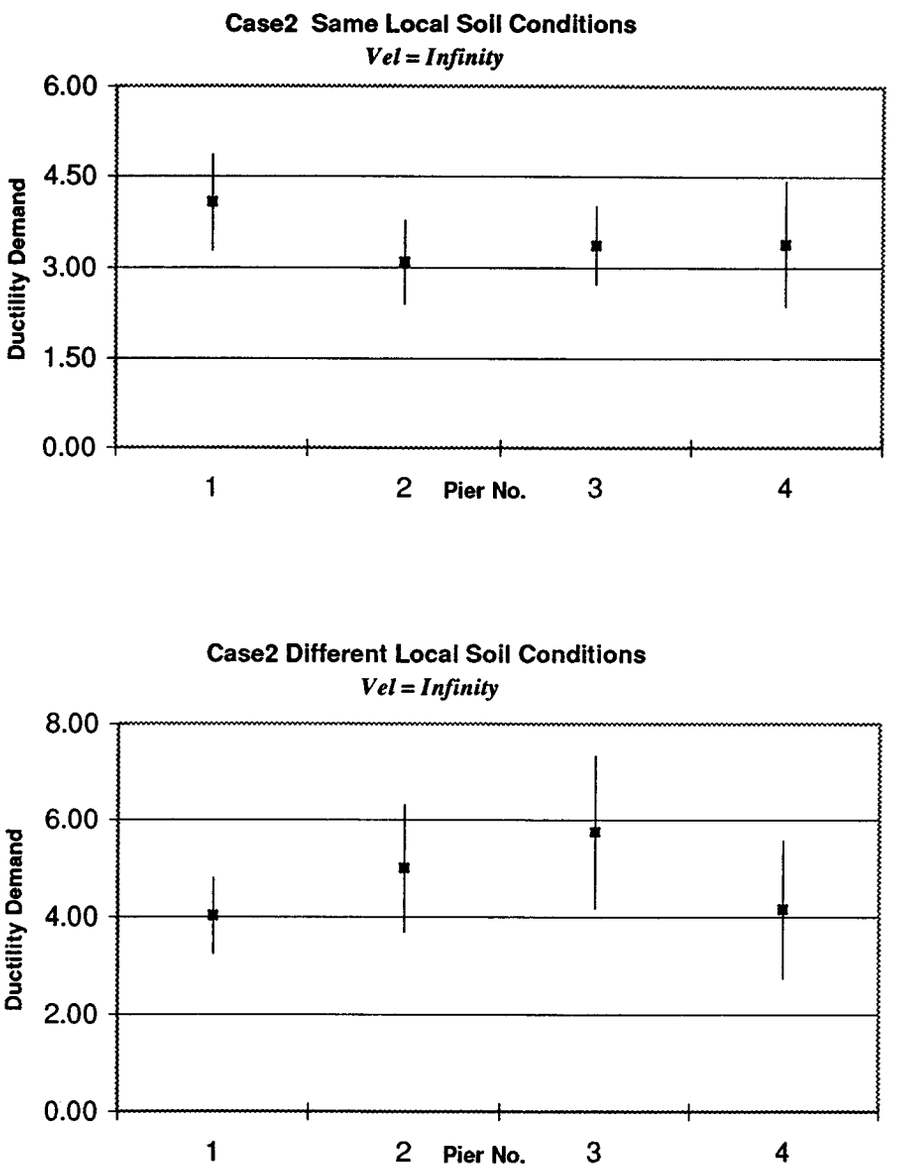

FIGURE 4-47 Mean value (denoted by block square) and mean value plus / minus one standard deviation (denoted by vertical line above and below square) for the peak ductility demand of the various piers of TY2H bridge, obtained by ensemble averaging from 20 time history analyses.

TY2H BRIDGE

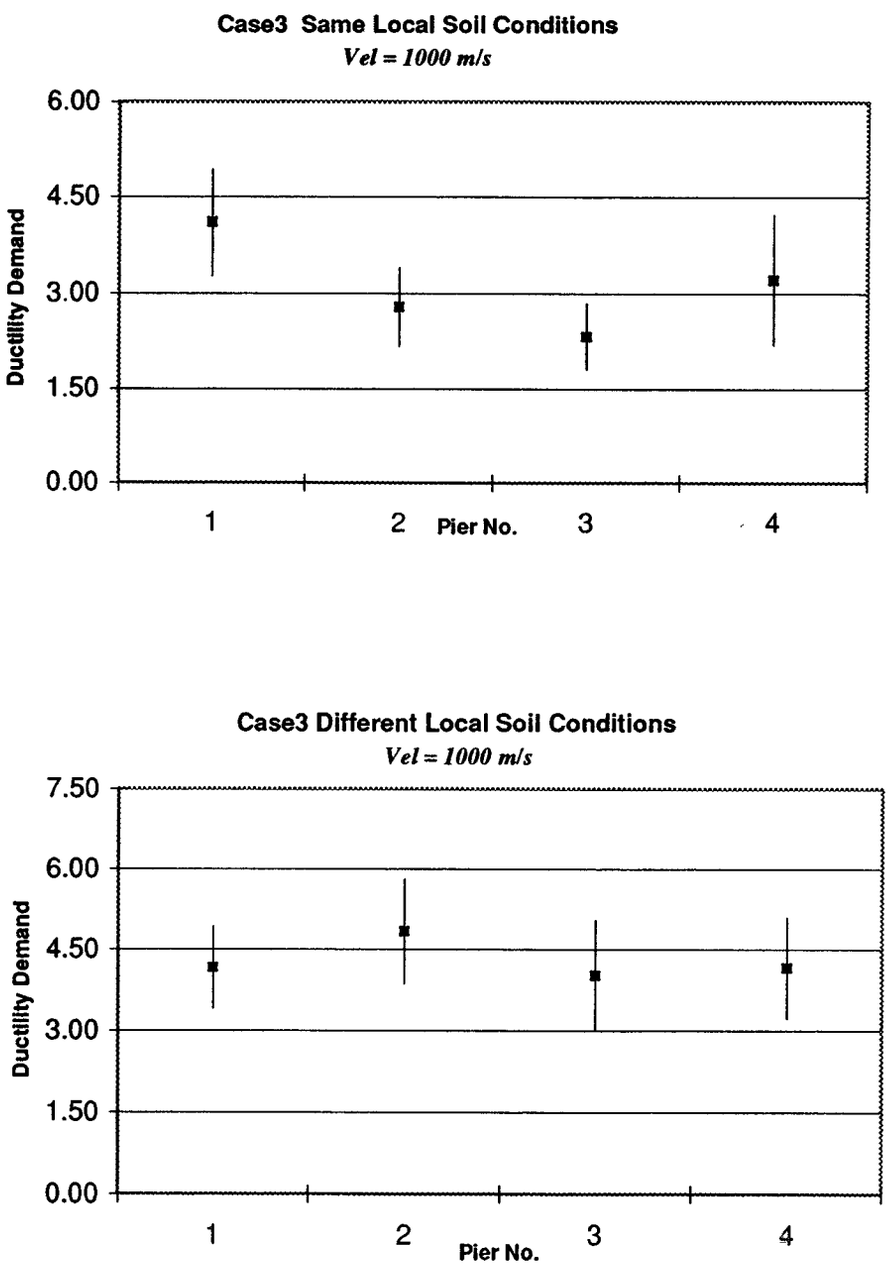

FIGURE 4-48 Mean value (denoted by block square) and mean value plus / minus one standard deviation (denoted by vertical line above and below square) for the peak ductility demand of the various piers of TY2H bridge, obtained by ensemble averaging from 20 time history analyses.

TY2H BRIDGE

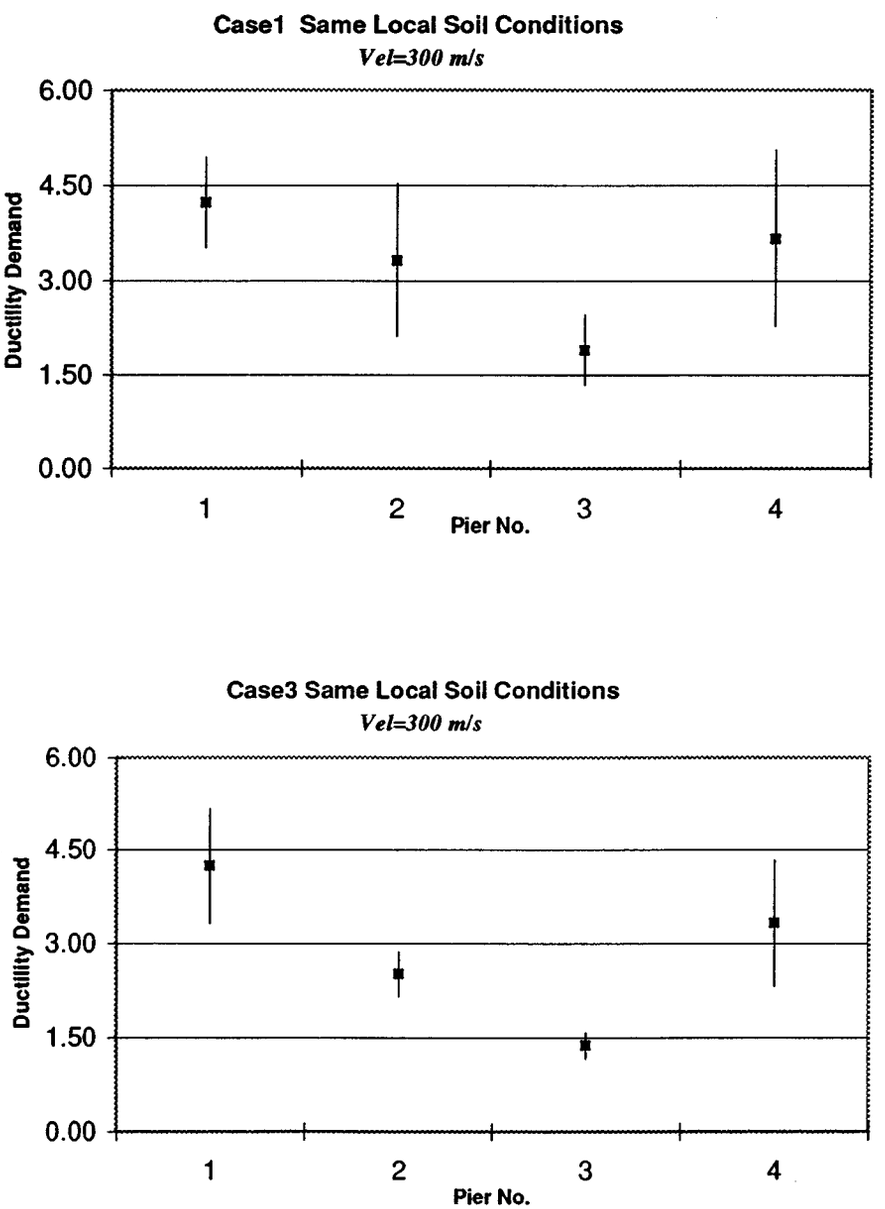

FIGURE 4-49 Mean value (denoted by block square) and mean value plus / minus one standard deviation (denoted by vertical line above and below square) for the peak ductility demand of the various piers of TY2H bridge, obtained by ensemble averaging from 20 time history analyses.

TY2H BRIDGE

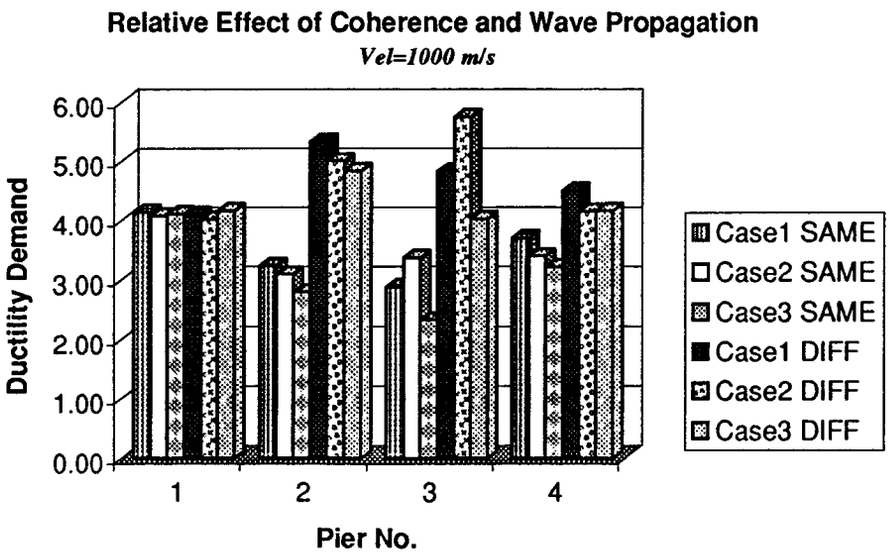

SAME denotes all supports on same local soil conditions
DIFF denotes supports on different local soil conditions

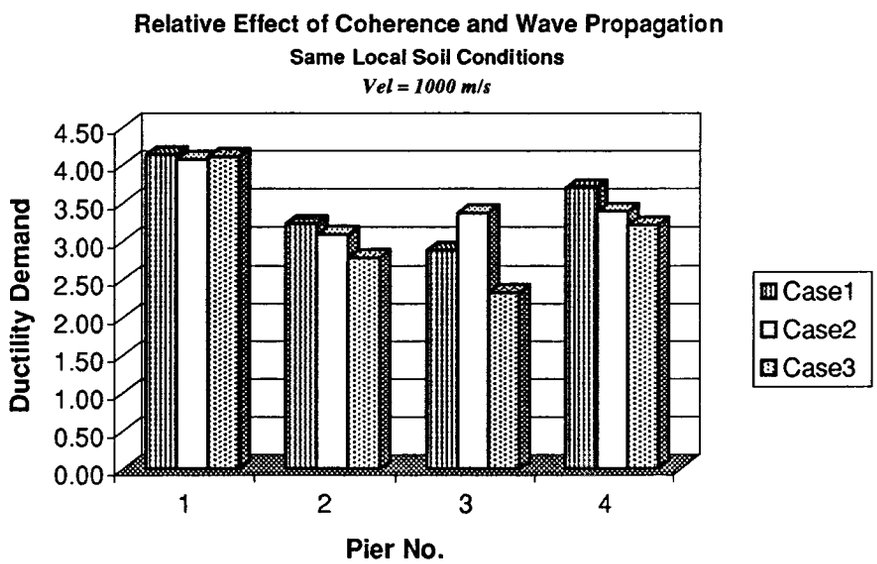

FIGURE 4-50a Bar chart depicting mean values for the peak ductility demand of the various piers of TY2H bridge, obtained from ensemble averaging from 20 time history analyses. Case 1, 2 and 3 are compared to estimate the relative effect of coherence and wave propagation. The effect of different local soil conditions and the effect of different velocities of wave propagation can also be assessed.

TY2H BRIDGE

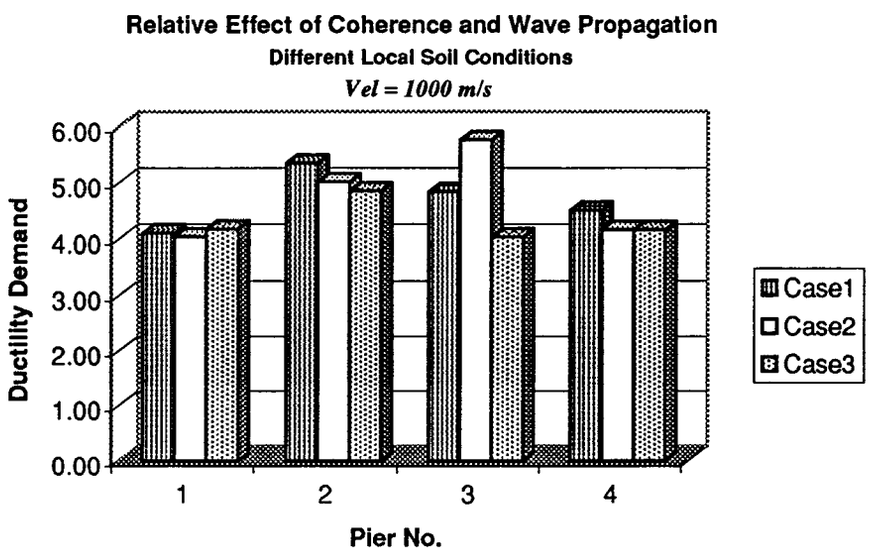

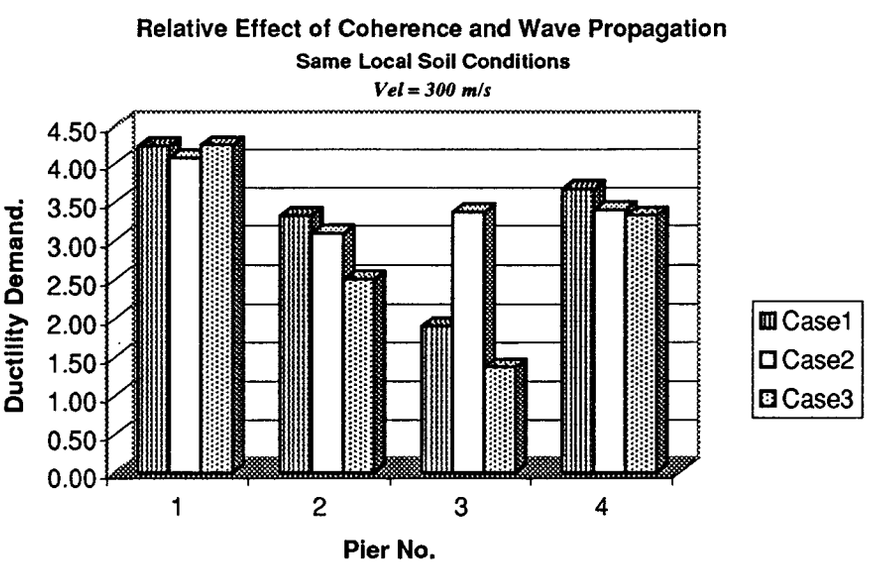

FIGURE 4-50b Bar chart depicting mean values for the peak ductility demand of the various piers of TY2H bridge, obtained from ensemble averaging from 20 time history analyses. Case 1, 2 and 3 are compared to estimate the relative effect of coherence and wave propagation. The effect of different local soil conditions and the effect of different velocities of wave propagation can also be assessed.

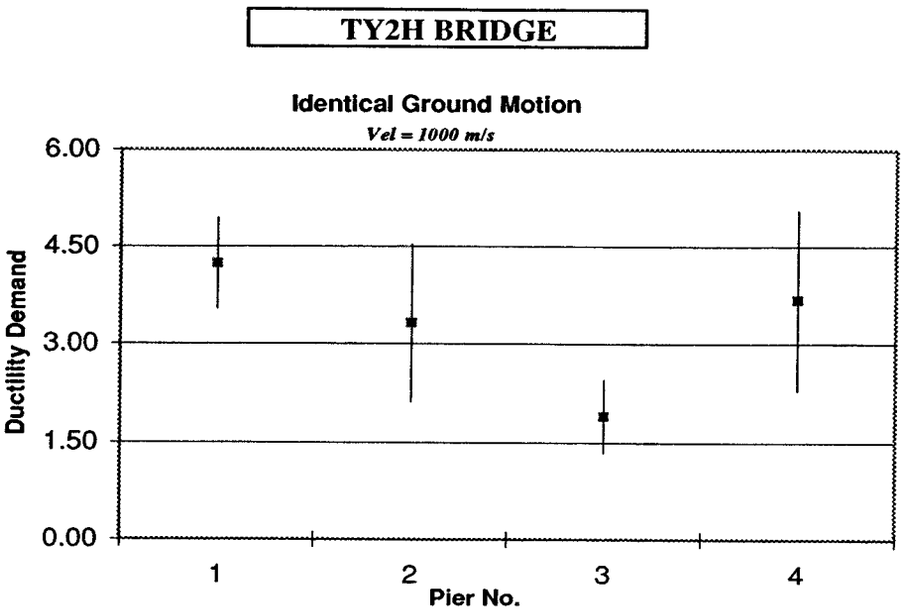

FIGURE 4-51 Mean value (denoted by block square) and mean value plus / minus one standard deviation (denoted by vertical line above and below square) for the peak ductility demand of the various piers of TY2H bridge, obtained by ensemble averaging from 20 time history analyses, for the case of identical support ground motion.

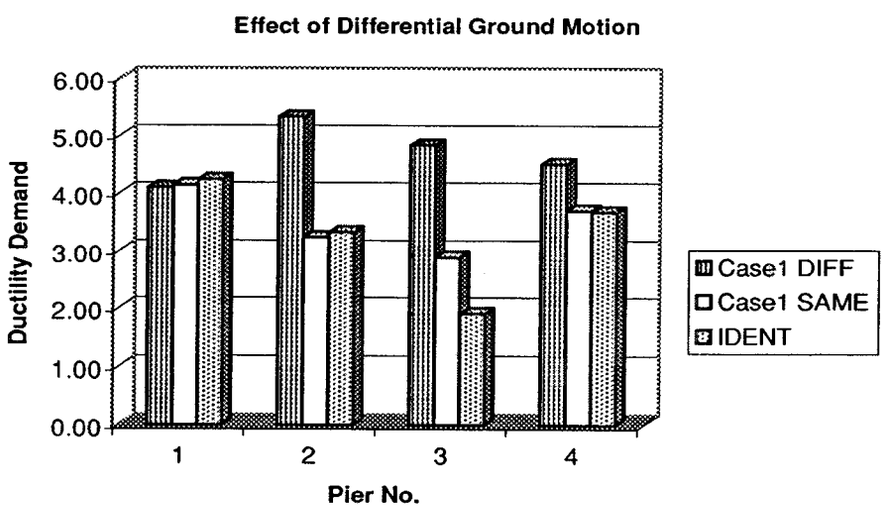

DIFF denotes supports on different local soil conditions
SAME denotes all supports on same local soil conditions
IDENT denotes identical support ground motion

FIGURE 4-52 Bar chart depicting mean values for the peak ductility demand of the various piers of TY2H bridge, obtained from ensemble averaging from 20 time history analyses. Comparison of cases with differential support ground motion and different local soil conditions, differential support ground motion and same local soil conditions, and identical support ground motion.

TY2H BRIDGE

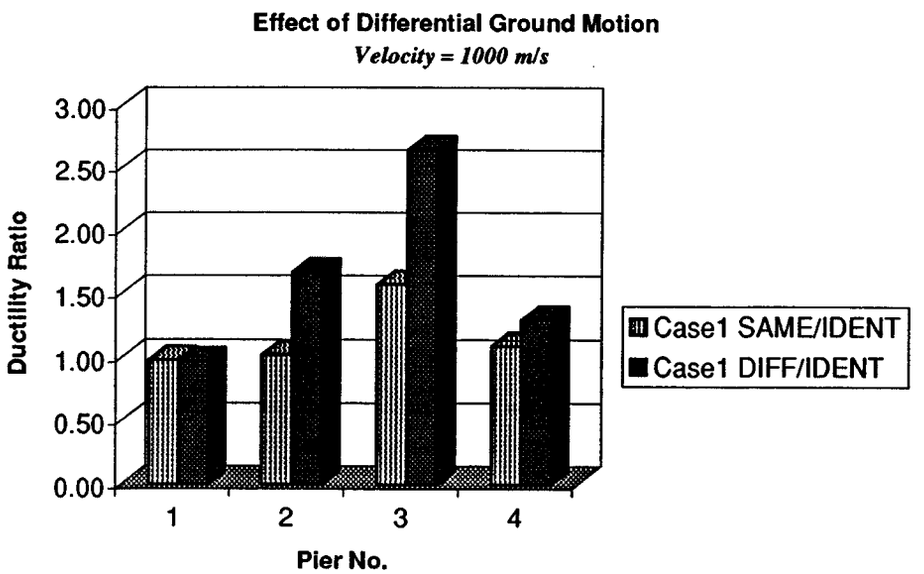

SAME/IDENT denotes the ratio of the peak ductility demand computed using differential support ground motion and same local soil conditions over the peak ductility demand computed using identical support ground motion.

DIFF/IDENT denotes the ratio of the peak ductility demand computed using differential support ground motion and different local soil conditions over the peak ductility demand computed using identical support ground motion.

FIGURE 4-53 Bar chart depicting ratios of mean values for the peak ductility demand of the various piers of TY2H bridge, obtained by ensemble averaging from 20 time history analyses The effect of differential support ground motion and different local soil conditions, differential support ground motion and same local soil conditions and identical support ground motion can be assessed.

SANTA CLARA BRIDGE

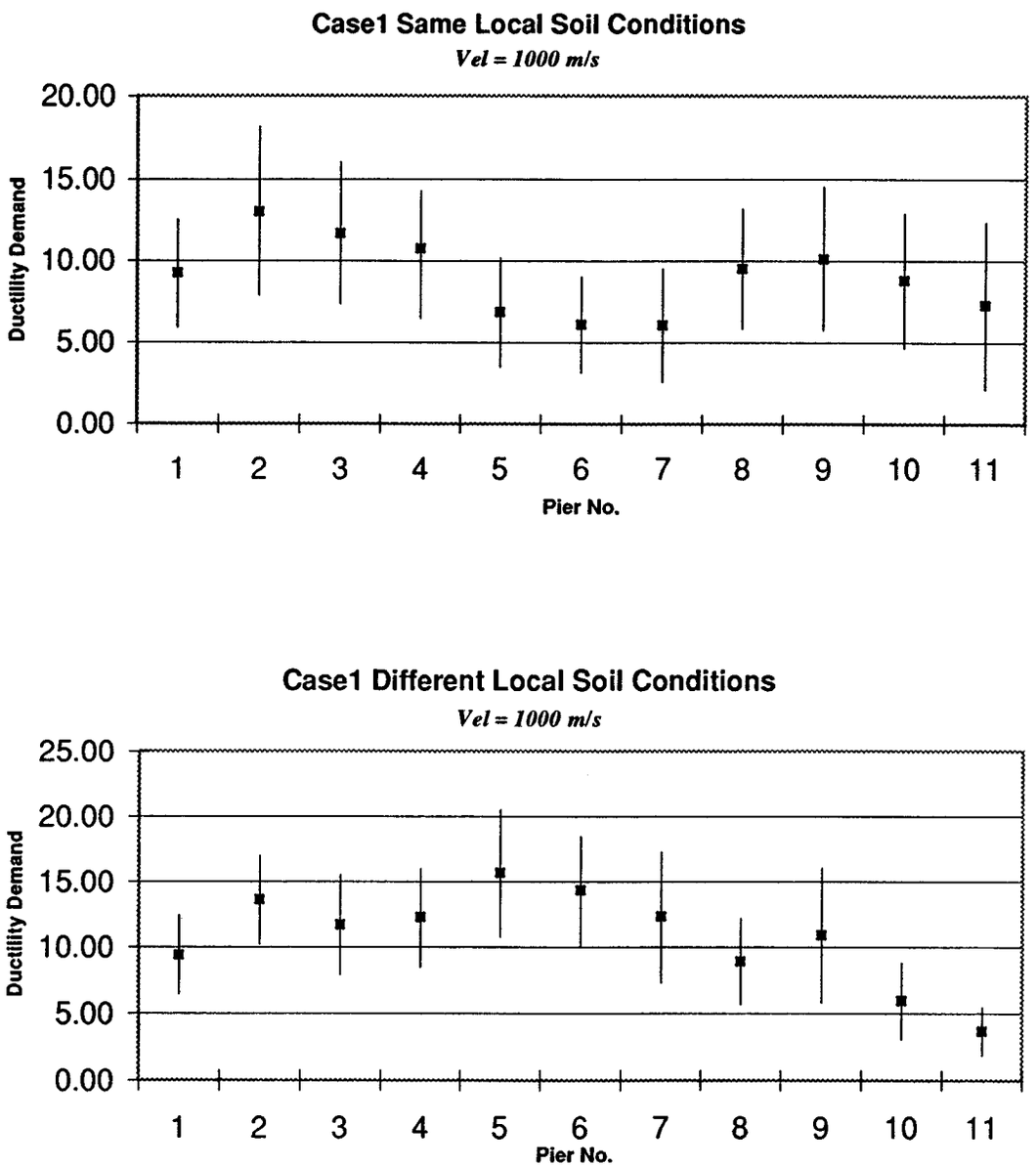

FIGURE 4-54 Mean value (denoted by block square) and mean value plus / minus one standard deviation (denoted by vertical line above and below square) for the peak ductility demand of the various piers of SANTA CLARA bridge, obtained by ensemble averaging from 20 time history analyses.

SANTA CLARA BRIDGE

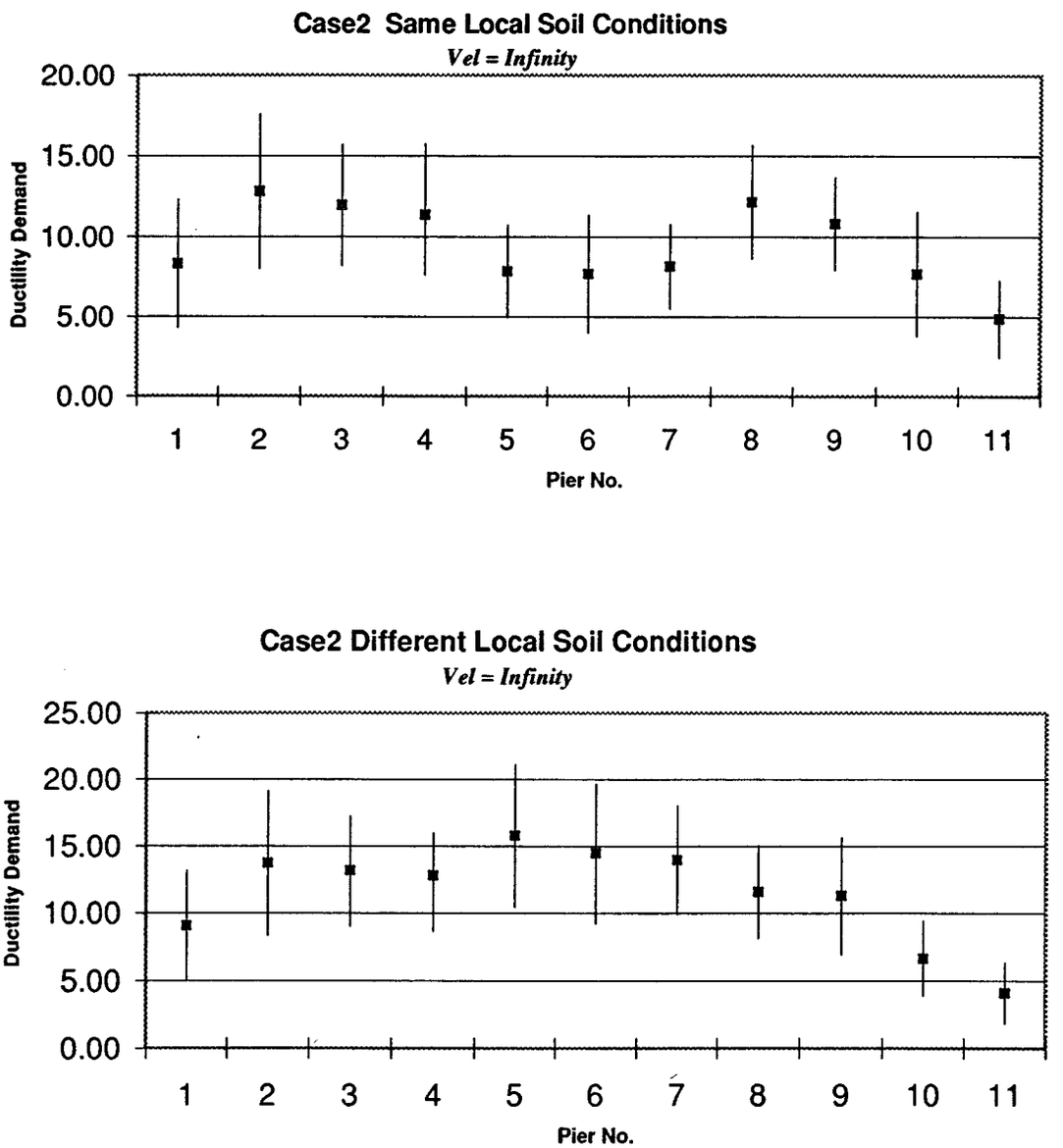

FIGURE 4-55 Mean value (denoted by block square) and mean value plus / minus one standard deviation (denoted by vertical line above and below square) for the peak ductility demand of the various piers of SANTA CLARA bridge, obtained by ensemble averaging from 20 time history analyses.

SANTA CLARA BRIDGE

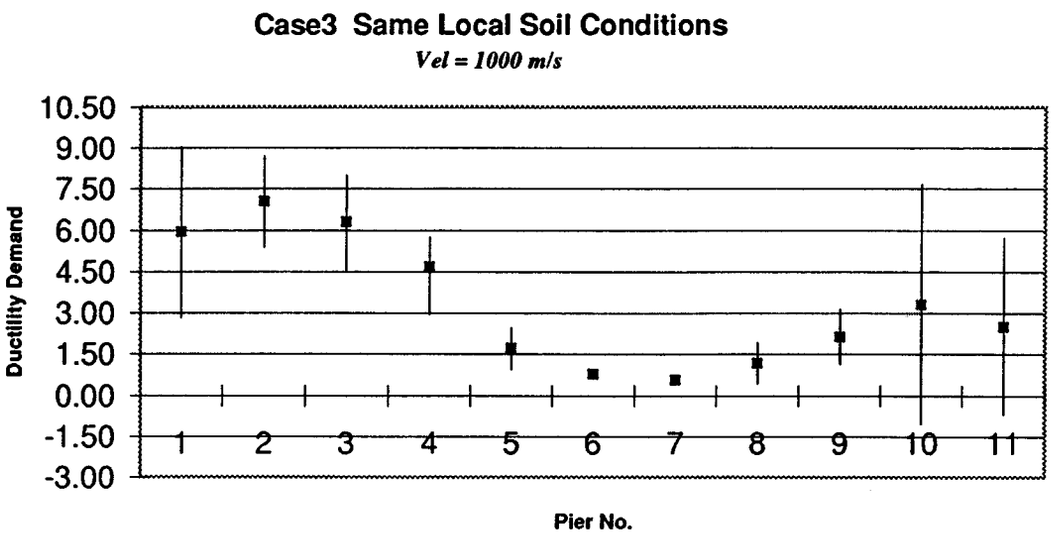

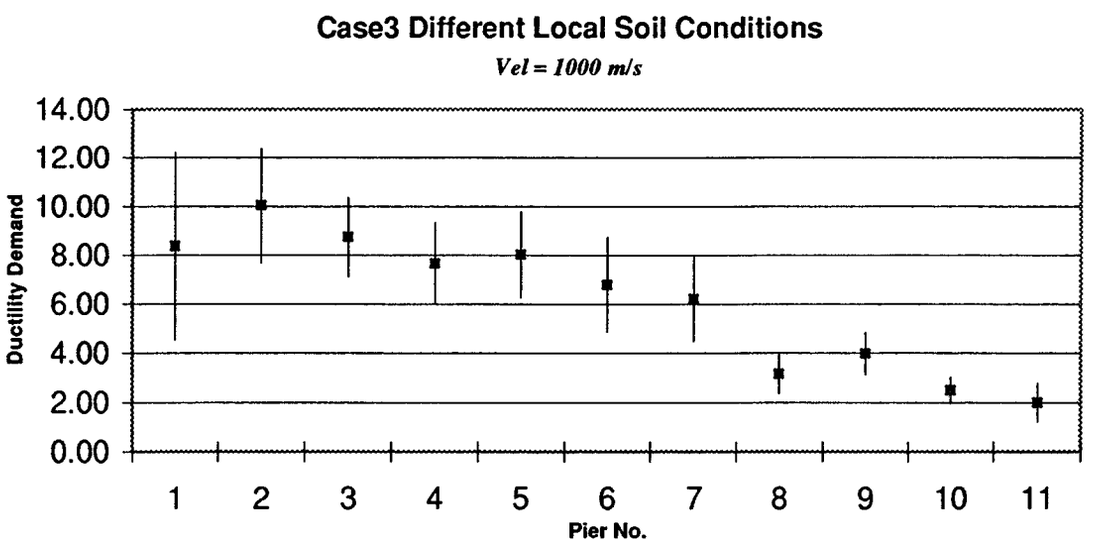

FIGURE 4-56 Mean value (denoted by block square) and mean value plus / minus one standard deviation (denoted by vertical line above and below square) for the peak ductility demand of the various piers of SANTA CLARA bridge, obtained by ensemble averaging from 20 time history analyses.

SANTA CLARA BRIDGE

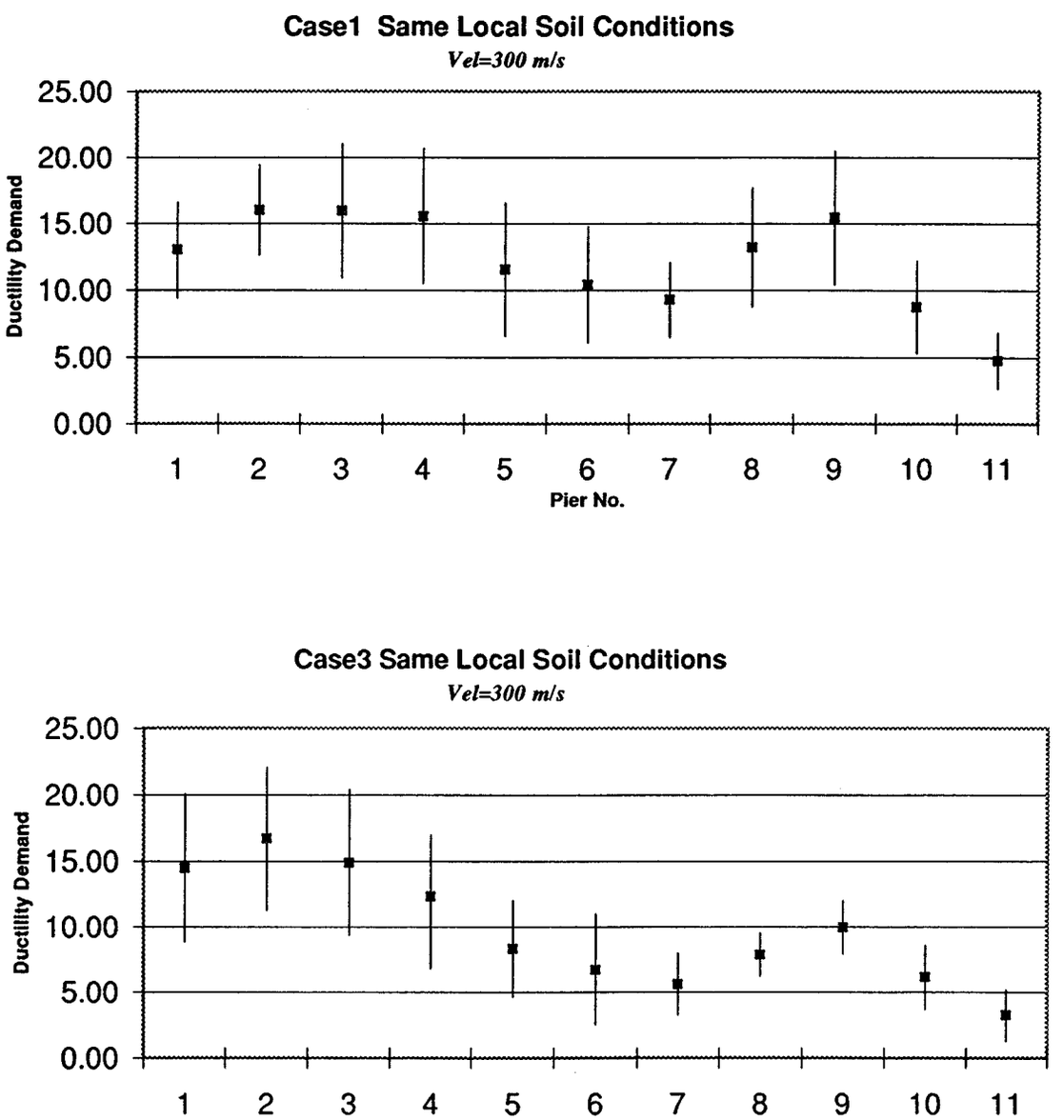

FIGURE 4-57 Mean value (denoted by block square) and mean value plus / minus one standard deviation (denoted by vertical line above and below square) for the peak ductility demand of the various piers of SANTA CLARA bridge, obtained by ensemble averaging from 20 time history analyses.

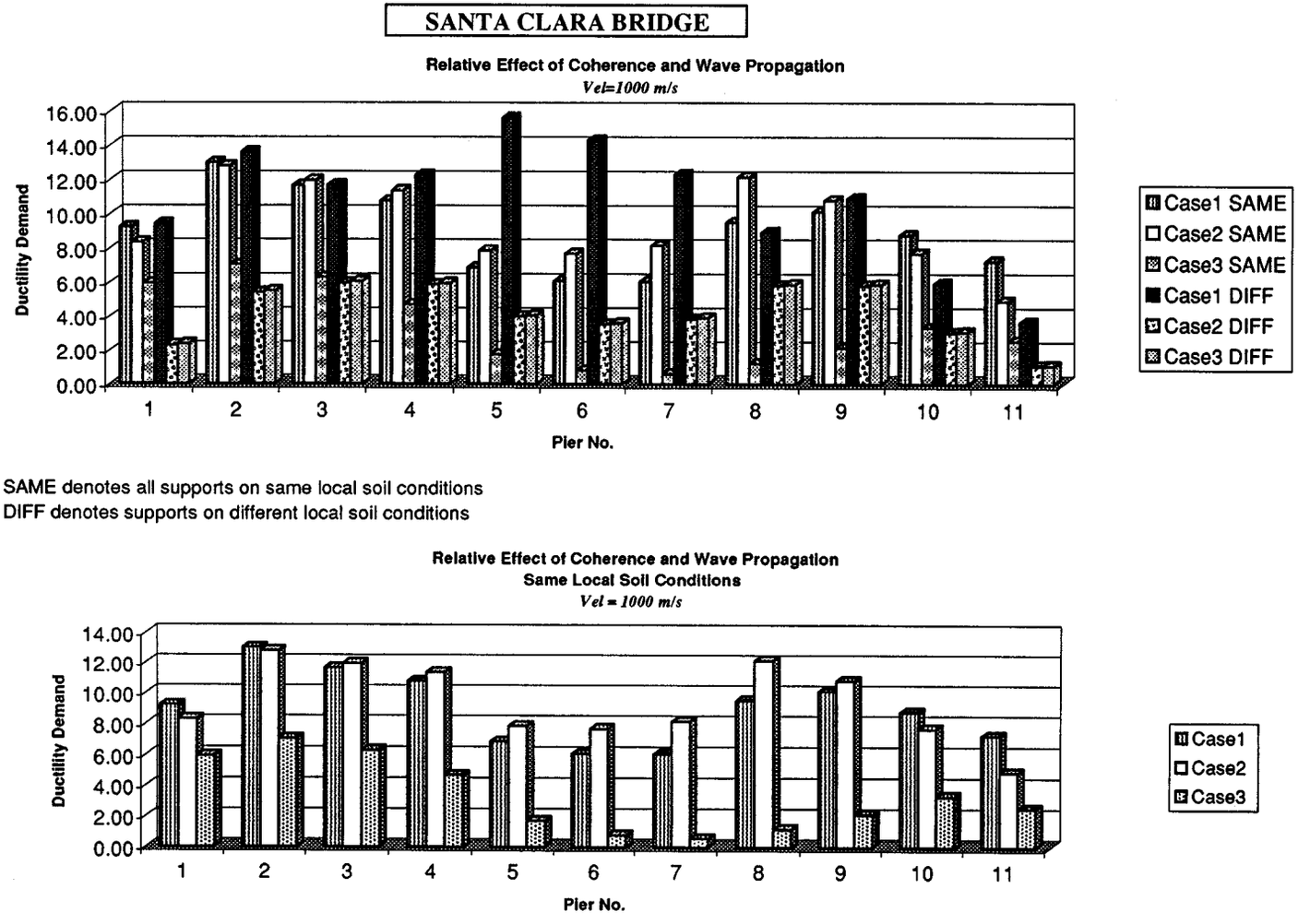

FIGURE 4-58a Bar chart depicting mean values for the peak ductility demand of the various piers of SANTA CLARA bridge, obtained from ensemble averaging from 20 time history analyses. Case 1, 2 and 3 are compared to estimate the relative effect of coherence and wave propagation. The effect of different local soil conditions and the effect of different velocities of wave propagation can also be assessed.

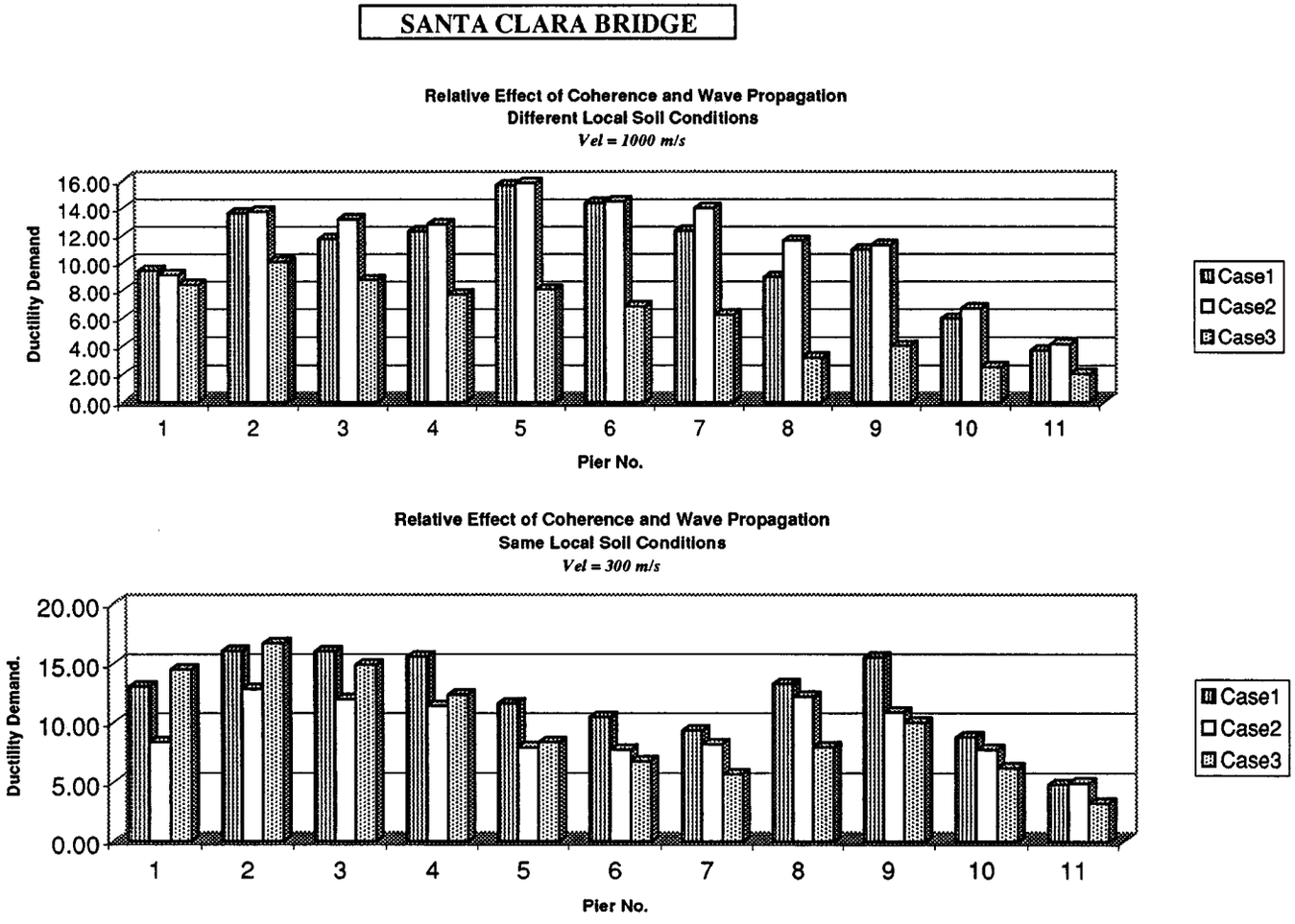

FIGURE 4-58b Bar chart depicting mean values for the peak ductility demand of the various piers of SANTA CLARA bridge, obtained from 20 time history analyses. Case 1, 2 and 3 are compared to estimate the relative effect of coherence and wave propagation. The effect of different local soil conditions and the effect of different velocities of wave propagation can also be assessed.

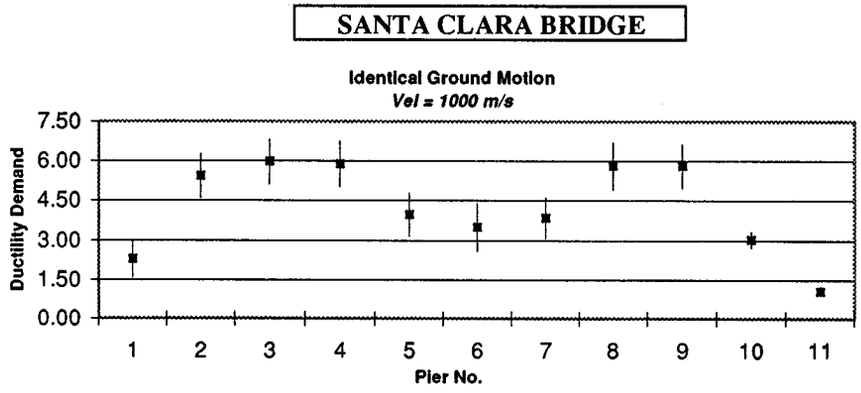

FIGURE 4-59 Mean value (denoted by block square) and mean value plus / minus one standard deviation (denoted by vertical line above and below square) for the peak ductility demand of the various piers of SANTA CLARA bridge, obtained by ensemble averaging from 20 time history analyses, for the case of identical support ground motion.

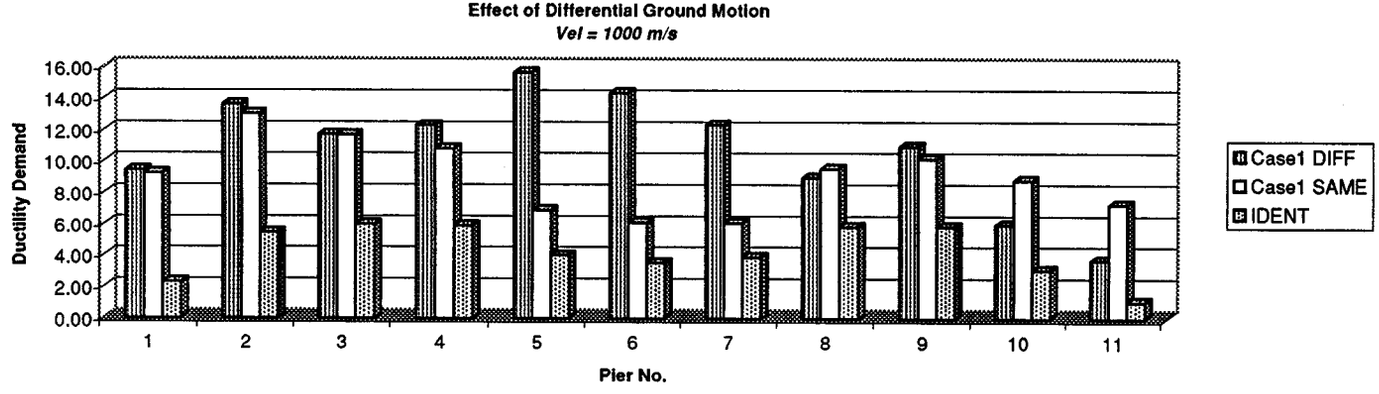

DIFF denotes supports on different local soil conditions
SAME denotes all supports on same local soil conditions
IDENT denotes identical support ground motion

FIGURE 4-60 Bar chart depicting mean values for the peak ductility demand of the various piers of SANTA CLARA bridge, obtained 20 time history analyses. Comparison of cases with differential support ground motion and different local soil conditions, differential support ground motion and same local soil conditions, and identical support ground motion.

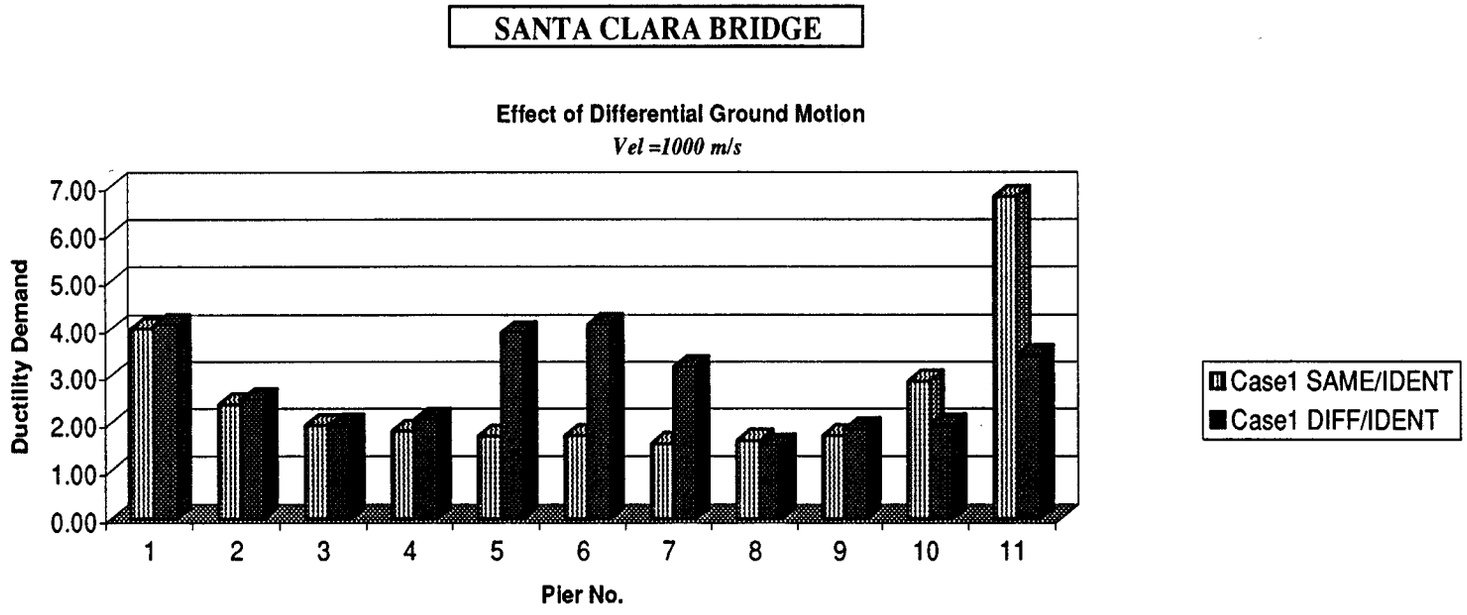

SAME/IDENT denotes the ratio of the peak ductility demand computed using differential support ground motion and same local soil conditions over the peak ductility demand computed using identical support ground motion.

DIFF/IDENT denotes the ratio of the peak ductility demand computed using differential support ground motion and different local soil conditions over the peak ductility demand computed using identical support ground motion.

FIGURE 4-61 Bar chart depicting ratios of mean values for the peak ductility demand of the various piers of SANTA CLARA bridge, obtained by ensemble averaging from 20 time history analyses. The effect of differential support ground motion and different local soil conditions, differential support ground motion and same local soil conditions and identical support gound motion can be assessed.

SECTION 5
GUIDELINES FOR ANALYSIS AND DESIGN OF HIGHWAY BRIDGES

Based mainly on the general observations and conclusions of the analyses performed in Chapter 4 (refer to section 4.4.10), and taking into account the observations and conclusions of other researchers' work (refer to section 4.4.9) and the preliminary analyses carried out in Chapter 3, the following guidelines are proposed for the analysis and design of highway bridges to account for the spatial variation of seismic ground motion:

- *For Bridges That Are Less Than Approximately 1,000 to 1,500 ft in Total Length, And Have All Their Supports on the Same Local Soil Conditions:*

  → *For such bridges, we believe that the relatively small increases in the peak response values due to the spatial variability of seismic ground motion can be taken care of by the various safety margins built in current seismic codes.*

  → *It is therefore recommended that such bridges be analyzed and designed using currently available seismic design practices that do not consider the spatial variability of seismic ground motion.*

- *For Bridges That Are More Than Approximately 1,000 to 1,500 ft in Total Length, Or Bridges of Any Length That Have Supports on Different Local Soil Conditions:*

  → *For such bridges, we believe that the significant increases in the peak response values due to the spatial variability of seismic ground motion can not be taken care of by the various safety margins built in current seismic codes without compromising the overall safety of the structure.*

  → *It is therefore recommended to perform time history dynamic analyses for design purposes, involving response spectrum compatible asynchronous (differential) support ground motion time histories reflecting the (potentially) different local soil conditions, wave propagation and loss of coherence effects.*

  → *The generation of such asynchronous support ground motion time histories can be performed using the methodology presented in this report or analogous methodologies suggested by other researchers.*

  → *It is recommended to consider a minimum of twenty time history analyses of the bridge to get a reliable estimate of the peak response that will be used for design purposes.*

  → *Dynamic analyses of a bridge using asynchronous support ground motion can be done without undue difficulty today using commercially available finite element codes.*

SECTION 6
REFERENCES

1. Abdel-Ghaffar A. M. and Rubin L. I. (1982). "Suspension Bridge Response to Multiple Support Excitations," *Journal of Engineering Mechanics Division,* Vol. 108, pp. 419-435.

2. Abdel-Ghaffar A. M. and Nazmy A.S. (1991). "3D Nonlinear Seismic Behavior of Cable-Stayed Bridges," *Journal of Structural Engineering*, Vol.117, pp. 3456-3476.

3. Abrahamson, N.A. (1985). "Estimation of Seismic Wave Coherency and Rupture Velocity using the SMART 1 Strong Motion Array Recordings," *Report No. UCB/EERC-85/02,* Earthquake Eng. Research Center, Univ. Of California, Berkeley.

4. Abrahamson N. A., Schneider J.F. and Stepp J.C. (1991). "Empirical Spatial Coherency Functions for Application to Soil-Structure Interaction Analyses," *Earthquake Spectra,* Vol. 7, pp. 1-27.

5. Abrahamson, N.A. (1993). "Spatial Variation of Multiple Support Inputs," *Proceedings of 1st U.S. Seminar on Seismic Evaluation and Retrofit of Steel Bridges*, a Caltrans & University of California at Berkeley Seminar, San Francisco, October 18.

6. Arwade, S. (1996). "Analysis of the Effect of Differential Support Motion on a Typical Reinforced Concrete Highway Bridge," *B.S.E. Thesis*, Department of Civil Engineering and Operations Research, Princeton University.

7. Bogdanoff, J.L., Goldberg, J.E. and Bernard, M.C. (1961). "Response of a Simple Structure to a Random Earthquake-Type Disturbance," *Bulletin of the Seismological Society of America*, Vol. 51, No. 2, pp. 293-310.

8. Bolt. B. A., Tsai Y.B., Yeh K. and Hsu M. K. (1982). "Earthquake Strong Motions Recorded by a Large Near-Source Array of Digital Seismographs," *Earthquake Engineering and Structural Dynamics,* Vol. 10, pp. 561-573.

9. Buckle, I.G. (1994). "The Northridge, California Earthquake of January 17, 1994: Performance of Highway Bridges," *Technical Report NCEER-94-0008*, National Center for Earthquake Engineering Research, State University of New York at Buffalo.

10. California Department of Transportation - Division of Structures. (1993). "User's Manual for COLx -- Column Ductility Program."

11. Clough, R.W. and Penzien, J. (1975). Dynamics of Structures, McGraw-Hill.

12. Deodatis, G. (1996a). "Simulation of Stochastic Processes and Fields to Model Loading and Material Uncertainties," Book on "*Probabilistic Methods for Structural Design*" (Editor: Carlos Guedes Soares), Kluwer Academic Publishers.

13. Deodatis, G. (1996b). "Simulation of Ergodic Multi-Variate Stochastic Processes," *Journal of Engineering Mechanics, ASCE*, Vol. 122, No. 8, pp. 778-787.

14. Deodatis, G. (1996c). "Non-Stationary Stochastic Vector Processes: Seismic Ground Motion Applications," *Probabilistic Engineering Mechanics*, Vol. 11, No. 3, pp. 149-167.

15. Deodatis, G. and Shinozuka, M. (1988). "Auto-Regressive Model for Non-Stationary Stochastic Processes," *Journal of Engineering Mechanics*, ASCE, Vol. 114, No. 11, pp. 1995-2012.

16. Deodatis, G. and Shinozuka, M. (1989). "Simulation of Seismic Ground Motion Using Stochastic Waves," *Journal of Engineering Mechanics*, ASCE, Vol. 115, No. 12, pp. 2723-2737.

17. Elishakoff, I. (1983). Probabilistic Methods in the Theory of Structures, John Wiley.

18. Ellingwood, B.R. and Batts, M.E. (1982). "Characterization of Earthquake Forces for Probability-Based Design of Nuclear Structures," *Technical Report BNL-NUREG-51587, NUREG/CR-2945*, Department of Nuclear Energy, Brookhaven National Laboratory, Prepared for Office of Nuclear Regulatory Research, U.S. Nuclear Regulatory Commission.

19. Federal Highway Administration. (1996). "Seismic Design of Bridges," BERGER/ ABAM Engineers, Publication No. FHWA-SA-97-009.

20. Gasparini, D. and Vanmarcke, E.H. (1976). "Simulated Earthquake Motions Compatible With Prescribed Response Spectra," Technical Report, Department of Civil Engineering, Massachusetts Institute of Technology, Publication No. R76-4.

21. Gersch, W. and Yonemoto, J. (1977). "Synthesis of Multi-Variate Random Vibration Systems: A Two-Stage Least Squares ARMA Model Approach," *Journal of Sound and Vibration*, Vol. 52, No. 4, pp. 553-565.

22. Grigoriu, M. (1993). "On the Spectral Representation Method in Simulation," *Journal of Probabilistic Engineering Mechanics*, Vol. 8, No. 2, pp. 75-90.

23. Grigoriu, M. (1995). Applied Non-Gaussian Processes, Prentice-Hall.

24. Gurley, K. and Kareem, A. (1995). "On the Analysis and Simulation of Random Processes Utilizing Higher Order Spectra and Wavelet Transforms," *Proceedings of Second International Conference on Computational Stochastic Mechanics*, Athens, Greece, Balkema, pp. 315-324.

25. Hao, H., Oliveira, C.S. and Penzien, J. (1989). "Multiple-Station Ground Motion Processing and Simulation Based on SMART-1 Array Data," *Nuclear Engineering and Design*, Vol. 111, No. 3, pp. 293-310.

26. Harichandran, R.S. and Vanmarcke, E.H. (1986). "Stochastic Variation of Earthquake Ground Motion in Space and Time," *Journal of Engineering Mechanics*, ASCE, Vol. 112, No. 2, pp.154-174.

27. Harichandran R. S. and Vanmarcke E. H. (1986). "Stochastic Variation of Earthquake Ground Motion in Space and Time," *Earthquake Engineering and Structural Dynamics,* Vol.112, pp. 154-174.

28. Harichandran R. S. (1987). "Correlation Analysis in space-time Modeling of Strong Ground Motion," *Journal of Engineering Mechanics Division*, Vol. 113, pp. 629-634.

29. Harichandran R. S. and Wang Weijun. (1988). "Response of Simple Beam to Spatially Varying Earthquake Excitation," *Journal of Engineering Mechanics Division,* Vol. 114, pp. 1526-1541.

30. Harichandran, R.S. and Wang, W. (1990). "Effect of Spatially Varying Seismic Excitation on Surface Lifelines," *Proceedings of Fourth U.S. National Conference on Earthquake Engineering*, May 20-24, Palm Springs, pp. 885-894 (Vol. 1).

31. Harichandran R. S. and Wang W. (1990). "Effect of Spatially Varying Seismic Excitation on Surface Lines," *Proc. of Fourth U. S. National Conf. On Earthquake Eng.,* Palm Springs, California, Vol. 1, pp. 885-894.

32. Harichandran R. S. and Wang W. (1990). "Response of Indeterminate Two-Span Beam to Spatially Varying Seismic Excitation," *Earthquake Engineering and Structural Dynamics,* Vol. 19, pp. 173-187.

33. Harichandran R. S. (1991). "Estimating the spatial variation of Earthquake Ground Motion from Dense Array Recordings," *Structural Safety,* Vol. 10, pp. 219-233.

34. Harichandran R. S., Hawwari A. and Sweidan B.N. (1996). "Response of Long-span Bridges to Spatially Varying Ground Motion," *Journal of Structural Engineering,* May, Vol. 122, pp. 476-484.

35. Hindy, A. and Novak, M. (1980). "Pipeline Response to Random Ground Motion," *Journal of Engineering Mechanics Division*, ASCE, Vol. 106, No. EM2, pp. 339-360.

36. International Conference of Building Officials. (1994). "Uniform Building Code," Vol. 2.

37. Jennings, P.C., Housner, G.W. and Tsai, N.C. (1968). "Simulated Earthquake Motions," Technical Report, Earthquake Engineering Research Laboratory, California Institute of Technology.

38. Kareem A., Deodatis G. and Shinozuka M. (1997). "Modeling of coherence for stochastic representation of wind, wave and seismic load effects," *Proceedings of ICOSSAR' 97- The 7th international conference on Structural Safety and Reliability,* Kyoto, Japan, 24-28 November, pp. 747-754.

39. Kiureghian A. D. and Neuenhofer A. (1992). "Response Spectrum Method for Multi-support Seismic Excitations," *Earthquake Engineering and Structural Dynamics,* Vol. 21, pp. 713-740.

40. Kiureghian A. D. (1996). "A coherency model for spatially varying ground motions," *Earthquake Engineering and Structural Dynamics,* Vol. 25, pp. 99-111.

41. Kiureghian A. D., Keshishian P. and Hakobian A. "Multiple Support Response Spectrum Analysis of Bridges including Site Response Effect and the MSRS Code," *Report No. UCB/EERC-97/02,* Earthquake Eng. Research Center, Univ. Of California, Berkeley.

42. Kozin, F. (1988). "Auto-Regressive Moving-Average Models of Earthquake Records," Journal *of Probabilistic Engineering Mechanics*, Vol. 3, No. 2, pp. 58-63.

43. Kwan, W-P. (1997). "The Effect of Spatially Differential Seismic Ground Motion on a Typical Three-Span Concrete Bridge," *B.S.E. Thesis*, Department of Civil Engineering and Operations Research, Princeton University.

44. Li, Y. and Kareem, A. (1991). "Simulation of Multi-Variate Non-Stationary Random Processes by FFT," *Journal of Engineering Mechanics*, ASCE, Vol. 117, No. 5, pp. 1037-1058.

45. Li, Y. and Kareem, A. (1993). "Simulation of Multi-Variate Random Processes: Hybrid DFT and Digital Filtering Approach," *Journal of Engineering Mechanics*, ASCE, Vol. 119, No. 5, pp. 1078-1098.

46. Loh C. H., Penzien J., and Tsai Y. B. (1982). "Engineering Analysis of Smart 1 Array Accelerograms," *Earthquake Engineering and Structural Dynamics*, Vol. 10, pp. 575-591.

47. Loh C. H. (1985). "Analysis of Spatial Variation of Seismic Waves and Ground Movements from Smart-1 Array Data," *Earthquake Engineering and Structural Dynamics*, Vol. 13, pp. 561-581.

48. Loh C. H. and Yeh Y. T. (1988). "Spatial Variation and Stochastic Modeling of Seismic Differential Ground Movement," *Earthquake Engineering and Structural Dynamics,* Vol. 16, pp. 583-596.

49. Luco J. E., and Wong H.L. (1986). " Response of a rigid foundation to a spatially varying random ground motion," *Earthquake Engineering and Structural Dynamics,* Vol. 14, pp. 891-908.

50. Masri S. F. (1976). "Response of beams to propagating boundary excitation," *Earthquake Engineering and Structural Dynamics,* Vol. 4, pp. 497-507.

51. Mignolet, M.P. and Spanos, P-T.D. (1987a). "Recursive Simulation of Stationary Multi-Variate Random Processes. Part I," Journal *of Applied Mechanics*, Vol. 54, No. 3, pp. 674-680.

52. Mignolet, M.P. and Spanos, P-T.D. (1987b). "Recursive Simulation of Stationary Multi-Variate Random Processes. Part II," Journal *of Applied Mechanics*, Vol. 54, No. 3, pp. 681-687.

53. Monti Giorgio, Nuti C. and Pinto P.E. (1996). "Nonlinear Response of Bridges under Multi-support excitation," *Journal of Structural Engineering,* Vol. 122, pp. 1147-1159.

54. Nazmy A. S. and Abdel-Ghaffar A. M. (1992). "Effects of Ground Motion Spatial Variability on the response of Cable-Stayed Bridges," *Earthquake Engineering and Structural Dynamics,* Vol. 21, pp. 1-20.

55. Priestley, M.B. (1965). "Evolutionary Spectra and Non-Stationary Processes," *Journal of the Royal Statistical Society*, Series B, Vol. 27, pp. 204-237.

56. Priestley, M.B. (1988). Non-Linear and Non-Stationary Time Series Analysis, Academic Press.

57. Ramadan, O. and Novak, M. (1993). "Simulation of Spatially Incoherent Random Ground Motions," *Journal of Engineering Mechanics*, ASCE, Vol. 119, No. 5, pp. 997-1016.

58. Ramadan O. and Novak M. (1991). "Simulation of Spatially Incoherent Random Ground Motions," *Journal of Engineering Mechanics,* Vol. 119, pp. 997-1016.

59. Rice, S.O. (1954). "Mathematical Analysis of Random Noise," *Selected Papers on Noise and Stochastic Processes*, (Edited by Nelson Wax), Dover, pp. 133-294. (paper originally appeared in two parts in the Bell System Technical Journal in Vol. 23, July 1944 and in Vol. 24, January 1945)

60. Scanlan, R.H.(1976). "Seismic Wave Effects in Soil Structure Interaction," *Earthquake Engineering and Structural Dynamics,* Vol. 4, pp. 379-388.

61. Schneider J.F., Stepp J.C. and Abrahamson N. A. (1992). "Spatial Variation of Earthquake Ground Motion and Effect of Local Soil Conditions," *Proceedings 10 Th. World Conf. in Earthquake Eng.*, Madrid, Spain, Vol. 2, pp. 967-972.

62. Shinozuka, M. and Jan, C-M. (1972). "Digital Simulation of Random Processes and its Applications," Journal *of Sound and Vibration*, Vol. 25, No. 1, pp. 111-128.

63. Shinozuka, M. (1972). "Monte Carlo Solution of Structural Dynamics," Computers *and Structures*, Vol. 2, Nos. 5+6, pp. 855-874.

64. Shinozuka, M. (1974). "Digital Simulation of Random Processes in Engineering Mechanics with the Aid of FFT Technique," Stochastic *Problems in Mechanics*, (Eds. S. T. Ariaratnam and H. H. E. Leipholz), University of Waterloo Press, Waterloo, pp. 277-286.

65. Shinozuka, M. (1987). "Stochastic Fields and Their Digital Simulation," Stochastic *Methods in Structural Dynamics*, (Eds. G. I. Schuëller and M. Shinozuka), Martinus Nijhoff Publishers, Dordrecht, pp. 93-133.

66. Shinozuka, M. and Deodatis, G. (1988). "Stochastic Process Models for Earthquake Ground Motion," Journal *of Probabilistic Engineering Mechanics*, Vol. 3, No. 3, pp. 114-123.

67. Shinozuka, M. and Deodatis, G. (1991). "Simulation of Stochastic Processes by Spectral Representation," Applied *Mechanics Reviews*, ASME, Vol. 44, No. 4, pp. 191-204.

68. Shinozuka, M. and Deodatis, G. (1996). "Simulation of Multi-Dimensional Gaussian Stochastic Fields by Spectral Representation," Applied *Mechanics Reviews*, ASME, Vol. 49, No. 1, pp. 29-53.

69. Shinozuka, M., Kim, J-M. and Purasinghe, R. (1997). "Use of Visco-Elastic Dampers at Expansion Joints to Suppress Seismic Vibration of Bridges," *Second National Seismic Conference on Bridges and Highways,* Sacramento, California, July 8-11.

70. Soong, T.T. and Grigoriu, M. (1993). Random Vibration of Mechanical and Structural Systems, Prentice-Hall.

71. Spanos, P-T.D. and Zeldin, B. (1995). "Random Field Simulation Using Wavelet Bases," *Proceedings of the ICASP-7 Conference*, Paris, France, July 10-13, pp. 1275-1283.

72. Werner, S.D. and L.C. Lee. (1979). "The Three-Dimensional Response of Structures Subjected to Traveling Wave Excitation," *Proceedings of the Second U.S. National Conference on Earthquake Engineering,* 22-24 Aug., Stanford, CA, 1979.

73. Werner, S.D., L.C. Lee, H.L. Wong and M.D. Trifunac. (1979). "Effects of Travelling Seismic Waves on the Response of Bridges," *Proceedings of a Workshop*

on Earthquake Resistance of Highway Bridges, 29-31 Jan., Aug., Palo Alto, CA, 1979.

74. Yamazaki, F. and Shinozuka, M. (1988). "Digital Generation of Non-Gaussian Stochastic Fields," *Journal of Engineering Mechanics*, ASCE, Vol. 114, No. 7, pp. 1183-1197.

75. Yang, J.-N. (1972). "Simulation of Random Envelope Processes,'' Journal *of Sound and Vibration*, Vol. 25, No. 1, pp. 73-85.

76. Yang, J.-N. (1973). "On the Normality and Accuracy of Simulated Random Processes," Journal *of Sound and Vibration*, Vol. 26, No. 3, pp. 417-428.

77. Zerva A., Ang A. H-S. and Wen Y.K. (1988). "Development of differential response spectra for lifeline seismic analysis," *Probabilistic Engineering Mechanics,* Vol. 1, pp. 208-218.

78. Zerva A., Ang A. H-S. and Wen Y.K. (1988), "Lifeline Response to Spatially Variable Ground Motions," *Earthquake Engineering and Structural Dynamics,* Vol. 16, pp. 361-379.

79. Zerva A. (1991). "Effect of Spatial Variability and propagation of seismic ground motions on the response of multiply supported structures," *Probabilistic Engineering Mechanics*, Vol. 6, pp. 212-221.

80. Zerva A. (1992). "Spatial incoherence effects on seismic ground strains," *Probabilistic Engineering Mechanics,* Vol. 7, pp. 217-226.

81. Zerva, A. (1992). "Seismic loads predicted by spatial variability models," *Structural Safety,* Vol. 11, pp. 227-243.

82. Zerva A. (1992). "Seismic Ground Motion Simulation from a Class of Spatial Variability Models," *Earthquake Engineering and Structural Dynamics*, Vol. 21, pp. 351-361.

83. Zerva A. (1994). "On the spatial variation of seismic ground motions and its effects on lifelines," *Engineering Structures*, Vol. 16, pp. 534-546.

84. Zerva A. and Zhang O. (1997). "Correlation Patterns in Characteristics of Spatially Variable Seismic Ground Motions," *Earthquake Engineering and Structural Dynamics*, Vol. 26, pp. 19-39.

Multidisciplinary Center for Earthquake Engineering Research
List of Technical Reports

The Multidisciplinary Center for Earthquake Engineering Research (MCEER) publishes technical reports on a variety of subjects related to earthquake engineering written by authors funded through MCEER. These reports are available from both MCEER Publications and the National Technical Information Service (NTIS). Requests for reports should be directed to MCEER Publications, Multidisciplinary Center for Earthquake Engineering Research, State University of New York at Buffalo, Red Jacket Quadrangle, Buffalo, New York 14261. Reports can also be requested through NTIS, 5285 Port Royal Road, Springfield, Virginia 22161. NTIS accession numbers are shown in parenthesis, if available.

NCEER-87-0001 "First-Year Program in Research, Education and Technology Transfer," 3/5/87, (PB88-134275, A04, MF-A01).

NCEER-87-0002 "Experimental Evaluation of Instantaneous Optimal Algorithms for Structural Control," by R.C. Lin, T.T. Soong and A.M. Reinhorn, 4/20/87, (PB88-134341, A04, MF-A01).

NCEER-87-0003 "Experimentation Using the Earthquake Simulation Facilities at University at Buffalo," by A.M. Reinhorn and R.L. Ketter, to be published.

NCEER-87-0004 "The System Characteristics and Performance of a Shaking Table," by J.S. Hwang, K.C. Chang and G.C. Lee, 6/1/87, (PB88-134259, A03, MF-A01). This report is available only through NTIS (see address given above).

NCEER-87-0005 "A Finite Element Formulation for Nonlinear Viscoplastic Material Using a Q Model," by O. Gyebi and G. Dasgupta, 11/2/87, (PB88-213764, A08, MF-A01).

NCEER-87-0006 "Symbolic Manipulation Program (SMP) - Algebraic Codes for Two and Three Dimensional Finite Element Formulations," by X. Lee and G. Dasgupta, 11/9/87, (PB88-218522, A05, MF-A01).

NCEER-87-0007 "Instantaneous Optimal Control Laws for Tall Buildings Under Seismic Excitations," by J.N. Yang, A. Akbarpour and P. Ghaemmaghami, 6/10/87, (PB88-134333, A06, MF-A01). This report is only available through NTIS (see address given above).

NCEER-87-0008 "IDARC: Inelastic Damage Analysis of Reinforced Concrete Frame - Shear-Wall Structures," by Y.J. Park, A.M. Reinhorn and S.K. Kunnath, 7/20/87, (PB88-134325, A09, MF-A01). This report is only available through NTIS (see address given above).

NCEER-87-0009 "Liquefaction Potential for New York State: A Preliminary Report on Sites in Manhattan and Buffalo," by M. Budhu, V. Vijayakumar, R.F. Giese and L. Baumgras, 8/31/87, (PB88-163704, A03, MF-A01). This report is available only through NTIS (see address given above).

NCEER-87-0010 "Vertical and Torsional Vibration of Foundations in Inhomogeneous Media," by A.S. Veletsos and K.W. Dotson, 6/1/87, (PB88-134291, A03, MF-A01). This report is only available through NTIS (see address given above).

NCEER-87-0011 "Seismic Probabilistic Risk Assessment and Seismic Margins Studies for Nuclear Power Plants," by Howard H.M. Hwang, 6/15/87, (PB88-134267, A03, MF-A01). This report is only available through NTIS (see address given above).

NCEER-87-0012 "Parametric Studies of Frequency Response of Secondary Systems Under Ground-Acceleration Excitations," by Y. Yong and Y.K. Lin, 6/10/87, (PB88-134309, A03, MF-A01). This report is only available through NTIS (see address given above).

NCEER-87-0013 "Frequency Response of Secondary Systems Under Seismic Excitation," by J.A. HoLung, J. Cai and Y.K. Lin, 7/31/87, (PB88-134317, A05, MF-A01). This report is only available through NTIS (see address given above).

NCEER-87-0014 "Modelling Earthquake Ground Motions in Seismically Active Regions Using Parametric Time Series Methods," by G.W. Ellis and A.S. Cakmak, 8/25/87, (PB88-134283, A08, MF-A01). This report is only available through NTIS (see address given above).

NCEER-87-0015 "Detection and Assessment of Seismic Structural Damage," by E. DiPasquale and A.S. Cakmak, 8/25/87, (PB88-163712, A05, MF-A01). This report is only available through NTIS (see address given above).

NCEER-87-0016 "Pipeline Experiment at Parkfield, California," by J. Isenberg and E. Richardson, 9/15/87, (PB88-163720, A03, MF-A01). This report is available only through NTIS (see address given above).

NCEER-87-0017 "Digital Simulation of Seismic Ground Motion," by M. Shinozuka, G. Deodatis and T. Harada, 8/31/87, (PB88-155197, A04, MF-A01). This report is available only through NTIS (see address given above).

NCEER-87-0018 "Practical Considerations for Structural Control: System Uncertainty, System Time Delay and Truncation of Small Control Forces," J.N. Yang and A. Akbarpour, 8/10/87, (PB88-163738, A08, MF-A01). This report is only available through NTIS (see address given above).

NCEER-87-0019 "Modal Analysis of Nonclassically Damped Structural Systems Using Canonical Transformation," by J.N. Yang, S. Sarkani and F.X. Long, 9/27/87, (PB88-187851, A04, MF-A01).

NCEER-87-0020 "A Nonstationary Solution in Random Vibration Theory," by J.R. Red-Horse and P.D. Spanos, 11/3/87, (PB88-163746, A03, MF-A01).

NCEER-87-0021 "Horizontal Impedances for Radially Inhomogeneous Viscoelastic Soil Layers," by A.S. Veletsos and K.W. Dotson, 10/15/87, (PB88-150859, A04, MF-A01).

NCEER-87-0022 "Seismic Damage Assessment of Reinforced Concrete Members," by Y.S. Chung, C. Meyer and M. Shinozuka, 10/9/87, (PB88-150867, A05, MF-A01). This report is available only through NTIS (see address given above).

NCEER-87-0023 "Active Structural Control in Civil Engineering," by T.T. Soong, 11/11/87, (PB88-187778, A03, MF-A01).

NCEER-87-0024 "Vertical and Torsional Impedances for Radially Inhomogeneous Viscoelastic Soil Layers," by K.W. Dotson and A.S. Veletsos, 12/87, (PB88-187786, A03, MF-A01).

NCEER-87-0025 "Proceedings from the Symposium on Seismic Hazards, Ground Motions, Soil-Liquefaction and Engineering Practice in Eastern North America," October 20-22, 1987, edited by K.H. Jacob, 12/87, (PB88-188115, A23, MF-A01). This report is available only through NTIS (see address given above).

NCEER-87-0026 "Report on the Whittier-Narrows, California, Earthquake of October 1, 1987," by J. Pantelic and A. Reinhorn, 11/87, (PB88-187752, A03, MF-A01). This report is available only through NTIS (see address given above).

NCEER-87-0027 "Design of a Modular Program for Transient Nonlinear Analysis of Large 3-D Building Structures," by S. Srivastav and J.F. Abel, 12/30/87, (PB88-187950, A05, MF-A01). This report is only available through NTIS (see address given above).

NCEER-87-0028 "Second-Year Program in Research, Education and Technology Transfer," 3/8/88, (PB88-219480, A04, MF-A01).

NCEER-88-0001 "Workshop on Seismic Computer Analysis and Design of Buildings With Interactive Graphics," by W. McGuire, J.F. Abel and C.H. Conley, 1/18/88, (PB88-187760, A03, MF-A01). This report is only available through NTIS (see address given above).

NCEER-88-0002 "Optimal Control of Nonlinear Flexible Structures," by J.N. Yang, F.X. Long and D. Wong, 1/22/88, (PB88-213772, A06, MF-A01).

NCEER-88-0003 "Substructuring Techniques in the Time Domain for Primary-Secondary Structural Systems," by G.D. Manolis and G. Juhn, 2/10/88, (PB88-213780, A04, MF-A01).

NCEER-88-0004 "Iterative Seismic Analysis of Primary-Secondary Systems," by A. Singhal, L.D. Lutes and P.D. Spanos, 2/23/88, (PB88-213798, A04, MF-A01).

NCEER-88-0005 "Stochastic Finite Element Expansion for Random Media," by P.D. Spanos and R. Ghanem, 3/14/88, (PB88-213806, A03, MF-A01).

NCEER-88-0006 "Combining Structural Optimization and Structural Control," by F.Y. Cheng and C.P. Pantelides, 1/10/88, (PB88-213814, A05, MF-A01).

NCEER-88-0007 "Seismic Performance Assessment of Code-Designed Structures," by H.H-M. Hwang, J-W. Jaw and H-J. Shau, 3/20/88, (PB88-219423, A04, MF-A01). This report is only available through NTIS (see address given above).

NCEER-88-0008 "Reliability Analysis of Code-Designed Structures Under Natural Hazards," by H.H-M. Hwang, H. Ushiba and M. Shinozuka, 2/29/88, (PB88-229471, A07, MF-A01). This report is only available through NTIS (see address given above).

NCEER-88-0009 "Seismic Fragility Analysis of Shear Wall Structures," by J-W Jaw and H.H-M. Hwang, 4/30/88, (PB89-102867, A04, MF-A01).

NCEER-88-0010 "Base Isolation of a Multi-Story Building Under a Harmonic Ground Motion - A Comparison of Performances of Various Systems," by F-G Fan, G. Ahmadi and I.G. Tadjbakhsh, 5/18/88, (PB89-122238, A06, MF-A01). This report is only available through NTIS (see address given above).

NCEER-88-0011 "Seismic Floor Response Spectra for a Combined System by Green's Functions," by F.M. Lavelle, L.A. Bergman and P.D. Spanos, 5/1/88, (PB89-102875, A03, MF-A01).

NCEER-88-0012 "A New Solution Technique for Randomly Excited Hysteretic Structures," by G.Q. Cai and Y.K. Lin, 5/16/88, (PB89-102883, A03, MF-A01).

NCEER-88-0013 "A Study of Radiation Damping and Soil-Structure Interaction Effects in the Centrifuge," by K. Weissman, supervised by J.H. Prevost, 5/24/88, (PB89-144703, A06, MF-A01).

NCEER-88-0014 "Parameter Identification and Implementation of a Kinematic Plasticity Model for Frictional Soils," by J.H. Prevost and D.V. Griffiths, to be published.

NCEER-88-0015 "Two- and Three- Dimensional Dynamic Finite Element Analyses of the Long Valley Dam," by D.V. Griffiths and J.H. Prevost, 6/17/88, (PB89-144711, A04, MF-A01).

NCEER-88-0016 "Damage Assessment of Reinforced Concrete Structures in Eastern United States," by A.M. Reinhorn, M.J. Seidel, S.K. Kunnath and Y.J. Park, 6/15/88, (PB89-122220, A04, MF-A01). This report is only available through NTIS (see address given above).

NCEER-88-0017 "Dynamic Compliance of Vertically Loaded Strip Foundations in Multilayered Viscoelastic Soils," by S. Ahmad and A.S.M. Israil, 6/17/88, (PB89-102891, A04, MF-A01).

NCEER-88-0018 "An Experimental Study of Seismic Structural Response With Added Viscoelastic Dampers," by R.C. Lin, Z. Liang, T.T. Soong and R.H. Zhang, 6/30/88, (PB89-122212, A05, MF-A01). This report is available only through NTIS (see address given above).

NCEER-88-0019 "Experimental Investigation of Primary - Secondary System Interaction," by G.D. Manolis, G. Juhn and A.M. Reinhorn, 5/27/88, (PB89-122204, A04, MF-A01).

NCEER-88-0020 "A Response Spectrum Approach For Analysis of Nonclassically Damped Structures," by J.N. Yang, S. Sarkani and F.X. Long, 4/22/88, (PB89-102909, A04, MF-A01).

NCEER-88-0021 "Seismic Interaction of Structures and Soils: Stochastic Approach," by A.S. Veletsos and A.M. Prasad, 7/21/88, (PB89-122196, A04, MF-A01). This report is only available through NTIS (see address given above).

NCEER-88-0022 "Identification of the Serviceability Limit State and Detection of Seismic Structural Damage," by E. DiPasquale and A.S. Cakmak, 6/15/88, (PB89-122188, A05, MF-A01). This report is available only through NTIS (see address given above).

NCEER-88-0023 "Multi-Hazard Risk Analysis: Case of a Simple Offshore Structure," by B.K. Bhartia and E.H. Vanmarcke, 7/21/88, (PB89-145213, A05, MF-A01).

NCEER-88-0024 "Automated Seismic Design of Reinforced Concrete Buildings," by Y.S. Chung, C. Meyer and M. Shinozuka, 7/5/88, (PB89-122170, A06, MF-A01). This report is available only through NTIS (see address given above).

NCEER-88-0025 "Experimental Study of Active Control of MDOF Structures Under Seismic Excitations," by L.L. Chung, R.C. Lin, T.T. Soong and A.M. Reinhorn, 7/10/88, (PB89-122600, A04, MF-A01).

NCEER-88-0026 "Earthquake Simulation Tests of a Low-Rise Metal Structure," by J.S. Hwang, K.C. Chang, G.C. Lee and R.L. Ketter, 8/1/88, (PB89-102917, A04, MF-A01).

NCEER-88-0027 "Systems Study of Urban Response and Reconstruction Due to Catastrophic Earthquakes," by F. Kozin and H.K. Zhou, 9/22/88, (PB90-162348, A04, MF-A01).

NCEER-88-0028 "Seismic Fragility Analysis of Plane Frame Structures," by H.H-M. Hwang and Y.K. Low, 7/31/88, (PB89-131445, A06, MF-A01).

NCEER-88-0029 "Response Analysis of Stochastic Structures," by A. Kardara, C. Bucher and M. Shinozuka, 9/22/88, (PB89-174429, A04, MF-A01).

NCEER-88-0030 "Nonnormal Accelerations Due to Yielding in a Primary Structure," by D.C.K. Chen and L.D. Lutes, 9/19/88, (PB89-131437, A04, MF-A01).

NCEER-88-0031 "Design Approaches for Soil-Structure Interaction," by A.S. Veletsos, A.M. Prasad and Y. Tang, 12/30/88, (PB89-174437, A03, MF-A01). This report is available only through NTIS (see address given above).

NCEER-88-0032 "A Re-evaluation of Design Spectra for Seismic Damage Control," by C.J. Turkstra and A.G. Tallin, 11/7/88, (PB89-145221, A05, MF-A01).

NCEER-88-0033 "The Behavior and Design of Noncontact Lap Splices Subjected to Repeated Inelastic Tensile Loading," by V.E. Sagan, P. Gergely and R.N. White, 12/8/88, (PB89-163737, A08, MF-A01).

NCEER-88-0034 "Seismic Response of Pile Foundations," by S.M. Mamoon, P.K. Banerjee and S. Ahmad, 11/1/88, (PB89-145239, A04, MF-A01).

NCEER-88-0035 "Modeling of R/C Building Structures With Flexible Floor Diaphragms (IDARC2)," by A.M. Reinhorn, S.K. Kunnath and N. Panahshahi, 9/7/88, (PB89-207153, A07, MF-A01).

NCEER-88-0036 "Solution of the Dam-Reservoir Interaction Problem Using a Combination of FEM, BEM with Particular Integrals, Modal Analysis, and Substructuring," by C-S. Tsai, G.C. Lee and R.L. Ketter, 12/31/88, (PB89-207146, A04, MF-A01).

NCEER-88-0037 "Optimal Placement of Actuators for Structural Control," by F.Y. Cheng and C.P. Pantelides, 8/15/88, (PB89-162846, A05, MF-A01).

NCEER-88-0038 "Teflon Bearings in Aseismic Base Isolation: Experimental Studies and Mathematical Modeling," by A. Mokha, M.C. Constantinou and A.M. Reinhorn, 12/5/88, (PB89-218457, A10, MF-A01). This report is available only through NTIS (see address given above).

NCEER-88-0039 "Seismic Behavior of Flat Slab High-Rise Buildings in the New York City Area," by P. Weidlinger and M. Ettouney, 10/15/88, (PB90-145681, A04, MF-A01).

NCEER-88-0040 "Evaluation of the Earthquake Resistance of Existing Buildings in New York City," by P. Weidlinger and M. Ettouney, 10/15/88, to be published.

NCEER-88-0041 "Small-Scale Modeling Techniques for Reinforced Concrete Structures Subjected to Seismic Loads," by W. Kim, A. El-Attar and R.N. White, 11/22/88, (PB89-189625, A05, MF-A01).

NCEER-88-0042 "Modeling Strong Ground Motion from Multiple Event Earthquakes," by G.W. Ellis and A.S. Cakmak, 10/15/88, (PB89-174445, A03, MF-A01).

NCEER-88-0043 "Nonstationary Models of Seismic Ground Acceleration," by M. Grigoriu, S.E. Ruiz and E. Rosenblueth, 7/15/88, (PB89-189617, A04, MF-A01).

NCEER-88-0044 "SARCF User's Guide: Seismic Analysis of Reinforced Concrete Frames," by Y.S. Chung, C. Meyer and M. Shinozuka, 11/9/88, (PB89-174452, A08, MF-A01).

NCEER-88-0045 "First Expert Panel Meeting on Disaster Research and Planning," edited by J. Pantelic and J. Stoyle, 9/15/88, (PB89-174460, A05, MF-A01).

NCEER-88-0046 "Preliminary Studies of the Effect of Degrading Infill Walls on the Nonlinear Seismic Response of Steel Frames," by C.Z. Chrysostomou, P. Gergely and J.F. Abel, 12/19/88, (PB89-208383, A05, MF-A01).

NCEER-88-0047 "Reinforced Concrete Frame Component Testing Facility - Design, Construction, Instrumentation and Operation," by S.P. Pessiki, C. Conley, T. Bond, P. Gergely and R.N. White, 12/16/88, (PB89-174478, A04, MF-A01).

NCEER-89-0001 "Effects of Protective Cushion and Soil Compliancy on the Response of Equipment Within a Seismically Excited Building," by J.A. HoLung, 2/16/89, (PB89-207179, A04, MF-A01).

NCEER-89-0002 "Statistical Evaluation of Response Modification Factors for Reinforced Concrete Structures," by H.H-M. Hwang and J-W. Jaw, 2/17/89, (PB89-207187, A05, MF-A01).

NCEER-89-0003 "Hysteretic Columns Under Random Excitation," by G-Q. Cai and Y.K. Lin, 1/9/89, (PB89-196513, A03, MF-A01).

NCEER-89-0004 "Experimental Study of `Elephant Foot Bulge' Instability of Thin-Walled Metal Tanks," by Z-H. Jia and R.L. Ketter, 2/22/89, (PB89-207195, A03, MF-A01).

NCEER-89-0005 "Experiment on Performance of Buried Pipelines Across San Andreas Fault," by J. Isenberg, E. Richardson and T.D. O'Rourke, 3/10/89, (PB89-218440, A04, MF-A01). This report is available only through NTIS (see address given above).

NCEER-89-0006 "A Knowledge-Based Approach to Structural Design of Earthquake-Resistant Buildings," by M. Subramani, P. Gergely, C.H. Conley, J.F. Abel and A.H. Zaghw, 1/15/89, (PB89-218465, A06, MF-A01).

NCEER-89-0007 "Liquefaction Hazards and Their Effects on Buried Pipelines," by T.D. O'Rourke and P.A. Lane, 2/1/89, (PB89-218481, A09, MF-A01).

NCEER-89-0008 "Fundamentals of System Identification in Structural Dynamics," by H. Imai, C-B. Yun, O. Maruyama and M. Shinozuka, 1/26/89, (PB89-207211, A04, MF-A01).

NCEER-89-0009 "Effects of the 1985 Michoacan Earthquake on Water Systems and Other Buried Lifelines in Mexico," by A.G. Ayala and M.J. O'Rourke, 3/8/89, (PB89-207229, A06, MF-A01).

NCEER-89-R010 "NCEER Bibliography of Earthquake Education Materials," by K.E.K. Ross, Second Revision, 9/1/89, (PB90-125352, A05, MF-A01). This report is replaced by NCEER-92-0018.

NCEER-89-0011 "Inelastic Three-Dimensional Response Analysis of Reinforced Concrete Building Structures (IDARC-3D), Part I - Modeling," by S.K. Kunnath and A.M. Reinhorn, 4/17/89, (PB90-114612, A07, MF-A01). This report is available only through NTIS (see address given above).

NCEER-89-0012 "Recommended Modifications to ATC-14," by C.D. Poland and J.O. Malley, 4/12/89, (PB90-108648, A15, MF-A01).

NCEER-89-0013 "Repair and Strengthening of Beam-to-Column Connections Subjected to Earthquake Loading," by M. Corazao and A.J. Durrani, 2/28/89, (PB90-109885, A06, MF-A01).

NCEER-89-0014 "Program EXKAL2 for Identification of Structural Dynamic Systems," by O. Maruyama, C-B. Yun, M. Hoshiya and M. Shinozuka, 5/19/89, (PB90-109877, A09, MF-A01).

NCEER-89-0015 "Response of Frames With Bolted Semi-Rigid Connections, Part I - Experimental Study and Analytical Predictions," by P.J. DiCorso, A.M. Reinhorn, J.R. Dickerson, J.B. Radziminski and W.L. Harper, 6/1/89, to be published.

NCEER-89-0016 "ARMA Monte Carlo Simulation in Probabilistic Structural Analysis," by P.D. Spanos and M.P. Mignolet, 7/10/89, (PB90-109893, A03, MF-A01).

NCEER-89-P017 "Preliminary Proceedings from the Conference on Disaster Preparedness - The Place of Earthquake Education in Our Schools," Edited by K.E.K. Ross, 6/23/89, (PB90-108606, A03, MF-A01).

NCEER-89-0017 "Proceedings from the Conference on Disaster Preparedness - The Place of Earthquake Education in Our Schools," Edited by K.E.K. Ross, 12/31/89, (PB90-207895, A012, MF-A02). This report is available only through NTIS (see address given above).

NCEER-89-0018 "Multidimensional Models of Hysteretic Material Behavior for Vibration Analysis of Shape Memory Energy Absorbing Devices, by E.J. Graesser and F.A. Cozzarelli, 6/7/89, (PB90-164146, A04, MF-A01).

NCEER-89-0019 "Nonlinear Dynamic Analysis of Three-Dimensional Base Isolated Structures (3D-BASIS)," by S. Nagarajaiah, A.M. Reinhorn and M.C. Constantinou, 8/3/89, (PB90-161936, A06, MF-A01). This report has been replaced by NCEER-93-0011.

NCEER-89-0020 "Structural Control Considering Time-Rate of Control Forces and Control Rate Constraints," by F.Y. Cheng and C.P. Pantelides, 8/3/89, (PB90-120445, A04, MF-A01).

NCEER-89-0021 "Subsurface Conditions of Memphis and Shelby County," by K.W. Ng, T-S. Chang and H-H.M. Hwang, 7/26/89, (PB90-120437, A03, MF-A01).

NCEER-89-0022 "Seismic Wave Propagation Effects on Straight Jointed Buried Pipelines," by K. Elhmadi and M.J. O'Rourke, 8/24/89, (PB90-162322, A10, MF-A02).

NCEER-89-0023 "Workshop on Serviceability Analysis of Water Delivery Systems," edited by M. Grigoriu, 3/6/89, (PB90-127424, A03, MF-A01).

NCEER-89-0024 "Shaking Table Study of a 1/5 Scale Steel Frame Composed of Tapered Members," by K.C. Chang, J.S. Hwang and G.C. Lee, 9/18/89, (PB90-160169, A04, MF-A01).

NCEER-89-0025 "DYNA1D: A Computer Program for Nonlinear Seismic Site Response Analysis - Technical Documentation," by Jean H. Prevost, 9/14/89, (PB90-161944, A07, MF-A01). This report is available only through NTIS (see address given above).

NCEER-89-0026 "1:4 Scale Model Studies of Active Tendon Systems and Active Mass Dampers for Aseismic Protection," by A.M. Reinhorn, T.T. Soong, R.C. Lin, Y.P. Yang, Y. Fukao, H. Abe and M. Nakai, 9/15/89, (PB90-173246, A10, MF-A02). This report is available only through NTIS (see address given above).

NCEER-89-0027 "Scattering of Waves by Inclusions in a Nonhomogeneous Elastic Half Space Solved by Boundary Element Methods," by P.K. Hadley, A. Askar and A.S. Cakmak, 6/15/89, (PB90-145699, A07, MF-A01).

NCEER-89-0028 "Statistical Evaluation of Deflection Amplification Factors for Reinforced Concrete Structures," by H.H.M. Hwang, J-W. Jaw and A.L. Ch'ng, 8/31/89, (PB90-164633, A05, MF-A01).

NCEER-89-0029 "Bedrock Accelerations in Memphis Area Due to Large New Madrid Earthquakes," by H.H.M. Hwang, C.H.S. Chen and G. Yu, 11/7/89, (PB90-162330, A04, MF-A01).

NCEER-89-0030 "Seismic Behavior and Response Sensitivity of Secondary Structural Systems," by Y.Q. Chen and T.T. Soong, 10/23/89, (PB90-164658, A08, MF-A01).

NCEER-89-0031 "Random Vibration and Reliability Analysis of Primary-Secondary Structural Systems," by Y. Ibrahim, M. Grigoriu and T.T. Soong, 11/10/89, (PB90-161951, A04, MF-A01).

NCEER-89-0032 "Proceedings from the Second U.S. - Japan Workshop on Liquefaction, Large Ground Deformation and Their Effects on Lifelines, September 26-29, 1989," Edited by T.D. O'Rourke and M. Hamada, 12/1/89, (PB90-209388, A22, MF-A03).

NCEER-89-0033 "Deterministic Model for Seismic Damage Evaluation of Reinforced Concrete Structures," by J.M. Bracci, A.M. Reinhorn, J.B. Mander and S.K. Kunnath, 9/27/89, (PB91-108803, A06, MF-A01).

NCEER-89-0034 "On the Relation Between Local and Global Damage Indices," by E. DiPasquale and A.S. Cakmak, 8/15/89, (PB90-173865, A05, MF-A01).

NCEER-89-0035 "Cyclic Undrained Behavior of Nonplastic and Low Plasticity Silts," by A.J. Walker and H.E. Stewart, 7/26/89, (PB90-183518, A10, MF-A01).

NCEER-89-0036 "Liquefaction Potential of Surficial Deposits in the City of Buffalo, New York," by M. Budhu, R. Giese and L. Baumgrass, 1/17/89, (PB90-208455, A04, MF-A01).

NCEER-89-0037 "A Deterministic Assessment of Effects of Ground Motion Incoherence," by A.S. Veletsos and Y. Tang, 7/15/89, (PB90-164294, A03, MF-A01).

NCEER-89-0038 "Workshop on Ground Motion Parameters for Seismic Hazard Mapping," July 17-18, 1989, edited by R.V. Whitman, 12/1/89, (PB90-173923, A04, MF-A01).

NCEER-89-0039 "Seismic Effects on Elevated Transit Lines of the New York City Transit Authority," by C.J. Costantino, C.A. Miller and E. Heymsfield, 12/26/89, (PB90-207887, A06, MF-A01).

NCEER-89-0040 "Centrifugal Modeling of Dynamic Soil-Structure Interaction," by K. Weissman, Supervised by J.H. Prevost, 5/10/89, (PB90-207879, A07, MF-A01).

NCEER-89-0041 "Linearized Identification of Buildings With Cores for Seismic Vulnerability Assessment," by I-K. Ho and A.E. Aktan, 11/1/89, (PB90-251943, A07, MF-A01).

NCEER-90-0001 "Geotechnical and Lifeline Aspects of the October 17, 1989 Loma Prieta Earthquake in San Francisco," by T.D. O'Rourke, H.E. Stewart, F.T. Blackburn and T.S. Dickerman, 1/90, (PB90-208596, A05, MF-A01).

NCEER-90-0002 "Nonnormal Secondary Response Due to Yielding in a Primary Structure," by D.C.K. Chen and L.D. Lutes, 2/28/90, (PB90-251976, A07, MF-A01).

NCEER-90-0003 "Earthquake Education Materials for Grades K-12," by K.E.K. Ross, 4/16/90, (PB91-251984, A05, MF-A05). This report has been replaced by NCEER-92-0018.

NCEER-90-0004 "Catalog of Strong Motion Stations in Eastern North America," by R.W. Busby, 4/3/90, (PB90-251984, A05, MF-A01).

NCEER-90-0005 "NCEER Strong-Motion Data Base: A User Manual for the GeoBase Release (Version 1.0 for the Sun3)," by P. Friberg and K. Jacob, 3/31/90 (PB90-258062, A04, MF-A01).

NCEER-90-0006 "Seismic Hazard Along a Crude Oil Pipeline in the Event of an 1811-1812 Type New Madrid Earthquake," by H.H.M. Hwang and C-H.S. Chen, 4/16/90, (PB90-258054, A04, MF-A01).

NCEER-90-0007 "Site-Specific Response Spectra for Memphis Sheahan Pumping Station," by H.H.M. Hwang and C.S. Lee, 5/15/90, (PB91-108811, A05, MF-A01).

NCEER-90-0008 "Pilot Study on Seismic Vulnerability of Crude Oil Transmission Systems," by T. Ariman, R. Dobry, M. Grigoriu, F. Kozin, M. O'Rourke, T. O'Rourke and M. Shinozuka, 5/25/90, (PB91-108837, A06, MF-A01).

NCEER-90-0009 "A Program to Generate Site Dependent Time Histories: EQGEN," by G.W. Ellis, M. Srinivasan and A.S. Cakmak, 1/30/90, (PB91-108829, A04, MF-A01).

NCEER-90-0010 "Active Isolation for Seismic Protection of Operating Rooms," by M.E. Talbott, Supervised by M. Shinozuka, 6/8/9, (PB91-110205, A05, MF-A01).

NCEER-90-0011 "Program LINEARID for Identification of Linear Structural Dynamic Systems," by C-B. Yun and M. Shinozuka, 6/25/90, (PB91-110312, A08, MF-A01).

NCEER-90-0012 "Two-Dimensional Two-Phase Elasto-Plastic Seismic Response of Earth Dams," by A.N. Yiagos, Supervised by J.H. Prevost, 6/20/90, (PB91-110197, A13, MF-A02).

NCEER-90-0013 "Secondary Systems in Base-Isolated Structures: Experimental Investigation, Stochastic Response and Stochastic Sensitivity," by G.D. Manolis, G. Juhn, M.C. Constantinou and A.M. Reinhorn, 7/1/90, (PB91-110320, A08, MF-A01).

NCEER-90-0014 "Seismic Behavior of Lightly-Reinforced Concrete Column and Beam-Column Joint Details," by S.P. Pessiki, C.H. Conley, P. Gergely and R.N. White, 8/22/90, (PB91-108795, A11, MF-A02).

NCEER-90-0015 "Two Hybrid Control Systems for Building Structures Under Strong Earthquakes," by J.N. Yang and A. Danielians, 6/29/90, (PB91-125393, A04, MF-A01).

NCEER-90-0016 "Instantaneous Optimal Control with Acceleration and Velocity Feedback," by J.N. Yang and Z. Li, 6/29/90, (PB91-125401, A03, MF-A01).

NCEER-90-0017 "Reconnaissance Report on the Northern Iran Earthquake of June 21, 1990," by M. Mehrain, 10/4/90, (PB91-125377, A03, MF-A01).

NCEER-90-0018 "Evaluation of Liquefaction Potential in Memphis and Shelby County," by T.S. Chang, P.S. Tang, C.S. Lee and H. Hwang, 8/10/90, (PB91-125427, A09, MF-A01).

NCEER-90-0019 "Experimental and Analytical Study of a Combined Sliding Disc Bearing and Helical Steel Spring Isolation System," by M.C. Constantinou, A.S. Mokha and A.M. Reinhorn, 10/4/90, (PB91-125385, A06, MF-A01). This report is available only through NTIS (see address given above).

NCEER-90-0020 "Experimental Study and Analytical Prediction of Earthquake Response of a Sliding Isolation System with a Spherical Surface," by A.S. Mokha, M.C. Constantinou and A.M. Reinhorn, 10/11/90, (PB91-125419, A05, MF-A01).

NCEER-90-0021 "Dynamic Interaction Factors for Floating Pile Groups," by G. Gazetas, K. Fan, A. Kaynia and E. Kausel, 9/10/90, (PB91-170381, A05, MF-A01).

NCEER-90-0022 "Evaluation of Seismic Damage Indices for Reinforced Concrete Structures," by S. Rodriguez-Gomez and A.S. Cakmak, 9/30/90, PB91-171322, A06, MF-A01).

NCEER-90-0023 "Study of Site Response at a Selected Memphis Site," by H. Desai, S. Ahmad, E.S. Gazetas and M.R. Oh, 10/11/90, (PB91-196857, A03, MF-A01).

NCEER-90-0024 "A User's Guide to Strongmo: Version 1.0 of NCEER's Strong-Motion Data Access Tool for PCs and Terminals," by P.A. Friberg and C.A.T. Susch, 11/15/90, (PB91-171272, A03, MF-A01).

NCEER-90-0025 "A Three-Dimensional Analytical Study of Spatial Variability of Seismic Ground Motions," by L-L. Hong and A.H.-S. Ang, 10/30/90, (PB91-170399, A09, MF-A01).

NCEER-90-0026 "MUMOID User's Guide - A Program for the Identification of Modal Parameters," by S. Rodriguez-Gomez and E. DiPasquale, 9/30/90, (PB91-171298, A04, MF-A01).

NCEER-90-0027 "SARCF-II User's Guide - Seismic Analysis of Reinforced Concrete Frames," by S. Rodriguez-Gomez, Y.S. Chung and C. Meyer, 9/30/90, (PB91-171280, A05, MF-A01).

NCEER-90-0028 "Viscous Dampers: Testing, Modeling and Application in Vibration and Seismic Isolation," by N. Makris and M.C. Constantinou, 12/20/90 (PB91-190561, A06, MF-A01).

NCEER-90-0029 "Soil Effects on Earthquake Ground Motions in the Memphis Area," by H. Hwang, C.S. Lee, K.W. Ng and T.S. Chang, 8/2/90, (PB91-190751, A05, MF-A01).

NCEER-91-0001 "Proceedings from the Third Japan-U.S. Workshop on Earthquake Resistant Design of Lifeline Facilities and Countermeasures for Soil Liquefaction, December 17-19, 1990," edited by T.D. O'Rourke and M. Hamada, 2/1/91, (PB91-179259, A99, MF-A04).

NCEER-91-0002 "Physical Space Solutions of Non-Proportionally Damped Systems," by M. Tong, Z. Liang and G.C. Lee, 1/15/91, (PB91-179242, A04, MF-A01).

NCEER-91-0003 "Seismic Response of Single Piles and Pile Groups," by K. Fan and G. Gazetas, 1/10/91, (PB92-174994, A04, MF-A01).

NCEER-91-0004 "Damping of Structures: Part 1 - Theory of Complex Damping," by Z. Liang and G. Lee, 10/10/91, (PB92-197235, A12, MF-A03).

NCEER-91-0005 "3D-BASIS - Nonlinear Dynamic Analysis of Three Dimensional Base Isolated Structures: Part II," by S. Nagarajaiah, A.M. Reinhorn and M.C. Constantinou, 2/28/91, (PB91-190553, A07, MF-A01). This report has been replaced by NCEER-93-0011.

NCEER-91-0006 "A Multidimensional Hysteretic Model for Plasticity Deforming Metals in Energy Absorbing Devices," by E.J. Graesser and F.A. Cozzarelli, 4/9/91, (PB92-108364, A04, MF-A01).

NCEER-91-0007 "A Framework for Customizable Knowledge-Based Expert Systems with an Application to a KBES for Evaluating the Seismic Resistance of Existing Buildings," by E.G. Ibarra-Anaya and S.J. Fenves, 4/9/91, (PB91-210930, A08, MF-A01).

NCEER-91-0008 "Nonlinear Analysis of Steel Frames with Semi-Rigid Connections Using the Capacity Spectrum Method," by G.G. Deierlein, S-H. Hsieh, Y-J. Shen and J.F. Abel, 7/2/91, (PB92-113828, A05, MF-A01).

NCEER-91-0009 "Earthquake Education Materials for Grades K-12," by K.E.K. Ross, 4/30/91, (PB91-212142, A06, MF-A01). This report has been replaced by NCEER-92-0018.

NCEER-91-0010 "Phase Wave Velocities and Displacement Phase Differences in a Harmonically Oscillating Pile," by N. Makris and G. Gazetas, 7/8/91, (PB92-108356, A04, MF-A01).

NCEER-91-0011 "Dynamic Characteristics of a Full-Size Five-Story Steel Structure and a 2/5 Scale Model," by K.C. Chang, G.C. Yao, G.C. Lee, D.S. Hao and Y.C. Yeh," 7/2/91, (PB93-116648, A06, MF-A02).

NCEER-91-0012 "Seismic Response of a 2/5 Scale Steel Structure with Added Viscoelastic Dampers," by K.C. Chang, T.T. Soong, S-T. Oh and M.L. Lai, 5/17/91, (PB92-110816, A05, MF-A01).

NCEER-91-0013 "Earthquake Response of Retaining Walls; Full-Scale Testing and Computational Modeling," by S. Alampalli and A-W.M. Elgamal, 6/20/91, to be published.

NCEER-91-0014 "3D-BASIS-M: Nonlinear Dynamic Analysis of Multiple Building Base Isolated Structures," by P.C. Tsopelas, S. Nagarajaiah, M.C. Constantinou and A.M. Reinhorn, 5/28/91, (PB92-113885, A09, MF-A02).

NCEER-91-0015 "Evaluation of SEAOC Design Requirements for Sliding Isolated Structures," by D. Theodossiou and M.C. Constantinou, 6/10/91, (PB92-114602, A11, MF-A03).

NCEER-91-0016 "Closed-Loop Modal Testing of a 27-Story Reinforced Concrete Flat Plate-Core Building," by H.R. Somaprasad, T. Toksoy, H. Yoshiyuki and A.E. Aktan, 7/15/91, (PB92-129980, A07, MF-A02).

NCEER-91-0017 "Shake Table Test of a 1/6 Scale Two-Story Lightly Reinforced Concrete Building," by A.G. El-Attar, R.N. White and P. Gergely, 2/28/91, (PB92-222447, A06, MF-A02).

NCEER-91-0018 "Shake Table Test of a 1/8 Scale Three-Story Lightly Reinforced Concrete Building," by A.G. El-Attar, R.N. White and P. Gergely, 2/28/91, (PB93-116630, A08, MF-A02).

NCEER-91-0019 "Transfer Functions for Rigid Rectangular Foundations," by A.S. Veletsos, A.M. Prasad and W.H. Wu, 7/31/91, to be published.

NCEER-91-0020 "Hybrid Control of Seismic-Excited Nonlinear and Inelastic Structural Systems," by J.N. Yang, Z. Li and A. Danielians, 8/1/91, (PB92-143171, A06, MF-A02).

NCEER-91-0021 "The NCEER-91 Earthquake Catalog: Improved Intensity-Based Magnitudes and Recurrence Relations for U.S. Earthquakes East of New Madrid," by L. Seeber and J.G. Armbruster, 8/28/91, (PB92-176742, A06, MF-A02).

NCEER-91-0022 "Proceedings from the Implementation of Earthquake Planning and Education in Schools: The Need for Change - The Roles of the Changemakers," by K.E.K. Ross and F. Winslow, 7/23/91, (PB92-129998, A12, MF-A03).

NCEER-91-0023 "A Study of Reliability-Based Criteria for Seismic Design of Reinforced Concrete Frame Buildings," by H.H.M. Hwang and H-M. Hsu, 8/10/91, (PB92-140235, A09, MF-A02).

NCEER-91-0024 "Experimental Verification of a Number of Structural System Identification Algorithms," by R.G. Ghanem, H. Gavin and M. Shinozuka, 9/18/91, (PB92-176577, A18, MF-A04).

NCEER-91-0025 "Probabilistic Evaluation of Liquefaction Potential," by H.H.M. Hwang and C.S. Lee," 11/25/91, (PB92-143429, A05, MF-A01).

NCEER-91-0026 "Instantaneous Optimal Control for Linear, Nonlinear and Hysteretic Structures - Stable Controllers," by J.N. Yang and Z. Li, 11/15/91, (PB92-163807, A04, MF-A01).

NCEER-91-0027 "Experimental and Theoretical Study of a Sliding Isolation System for Bridges," by M.C. Constantinou, A. Kartoum, A.M. Reinhorn and P. Bradford, 11/15/91, (PB92-176973, A10, MF-A03).

NCEER-92-0001 "Case Studies of Liquefaction and Lifeline Performance During Past Earthquakes, Volume 1: Japanese Case Studies," Edited by M. Hamada and T. O'Rourke, 2/17/92, (PB92-197243, A18, MF-A04).

NCEER-92-0002 "Case Studies of Liquefaction and Lifeline Performance During Past Earthquakes, Volume 2: United States Case Studies," Edited by T. O'Rourke and M. Hamada, 2/17/92, (PB92-197250, A20, MF-A04).

NCEER-92-0003 "Issues in Earthquake Education," Edited by K. Ross, 2/3/92, (PB92-222389, A07, MF-A02).

NCEER-92-0004 "Proceedings from the First U.S. - Japan Workshop on Earthquake Protective Systems for Bridges," Edited by I.G. Buckle, 2/4/92, (PB94-142239, A99, MF-A06).

NCEER-92-0005 "Seismic Ground Motion from a Haskell-Type Source in a Multiple-Layered Half-Space," A.P. Theoharis, G. Deodatis and M. Shinozuka, 1/2/92, to be published.

NCEER-92-0006 "Proceedings from the Site Effects Workshop," Edited by R. Whitman, 2/29/92, (PB92-197201, A04, MF-A01).

NCEER-92-0007 "Engineering Evaluation of Permanent Ground Deformations Due to Seismically-Induced Liquefaction," by M.H. Baziar, R. Dobry and A-W.M. Elgamal, 3/24/92, (PB92-222421, A13, MF-A03).

NCEER-92-0008 "A Procedure for the Seismic Evaluation of Buildings in the Central and Eastern United States," by C.D. Poland and J.O. Malley, 4/2/92, (PB92-222439, A20, MF-A04).

NCEER-92-0009 "Experimental and Analytical Study of a Hybrid Isolation System Using Friction Controllable Sliding Bearings," by M.Q. Feng, S. Fujii and M. Shinozuka, 5/15/92, (PB93-150282, A06, MF-A02).

NCEER-92-0010 "Seismic Resistance of Slab-Column Connections in Existing Non-Ductile Flat-Plate Buildings," by A.J. Durrani and Y. Du, 5/18/92, (PB93-116812, A06, MF-A02).

NCEER-92-0011 "The Hysteretic and Dynamic Behavior of Brick Masonry Walls Upgraded by Ferrocement Coatings Under Cyclic Loading and Strong Simulated Ground Motion," by H. Lee and S.P. Prawel, 5/11/92, to be published.

NCEER-92-0012 "Study of Wire Rope Systems for Seismic Protection of Equipment in Buildings," by G.F. Demetriades, M.C. Constantinou and A.M. Reinhorn, 5/20/92, (PB93-116655, A08, MF-A02).

NCEER-92-0013 "Shape Memory Structural Dampers: Material Properties, Design and Seismic Testing," by P.R. Witting and F.A. Cozzarelli, 5/26/92, (PB93-116663, A05, MF-A01).

NCEER-92-0014 "Longitudinal Permanent Ground Deformation Effects on Buried Continuous Pipelines," by M.J. O'Rourke, and C. Nordberg, 6/15/92, (PB93-116671, A08, MF-A02).

NCEER-92-0015 "A Simulation Method for Stationary Gaussian Random Functions Based on the Sampling Theorem," by M. Grigoriu and S. Balopoulou, 6/11/92, (PB93-127496, A05, MF-A01).

NCEER-92-0016 "Gravity-Load-Designed Reinforced Concrete Buildings: Seismic Evaluation of Existing Construction and Detailing Strategies for Improved Seismic Resistance," by G.W. Hoffmann, S.K. Kunnath, A.M. Reinhorn and J.B. Mander, 7/15/92, (PB94-142007, A08, MF-A02).

NCEER-92-0017 "Observations on Water System and Pipeline Performance in the Limón Area of Costa Rica Due to the April 22, 1991 Earthquake," by M. O'Rourke and D. Ballantyne, 6/30/92, (PB93-126811, A06, MF-A02).

NCEER-92-0018 "Fourth Edition of Earthquake Education Materials for Grades K-12," Edited by K.E.K. Ross, 8/10/92, (PB93-114023, A07, MF-A02).

NCEER-92-0019 "Proceedings from the Fourth Japan-U.S. Workshop on Earthquake Resistant Design of Lifeline Facilities and Countermeasures for Soil Liquefaction," Edited by M. Hamada and T.D. O'Rourke, 8/12/92, (PB93-163939, A99, MF-E11).

NCEER-92-0020 "Active Bracing System: A Full Scale Implementation of Active Control," by A.M. Reinhorn, T.T. Soong, R.C. Lin, M.A. Riley, Y.P. Wang, S. Aizawa and M. Higashino, 8/14/92, (PB93-127512, A06, MF-A02).

NCEER-92-0021 "Empirical Analysis of Horizontal Ground Displacement Generated by Liquefaction-Induced Lateral Spreads," by S.F. Bartlett and T.L. Youd, 8/17/92, (PB93-188241, A06, MF-A02).

NCEER-92-0022 "IDARC Version 3.0: Inelastic Damage Analysis of Reinforced Concrete Structures," by S.K. Kunnath, A.M. Reinhorn and R.F. Lobo, 8/31/92, (PB93-227502, A07, MF-A02).

NCEER-92-0023 "A Semi-Empirical Analysis of Strong-Motion Peaks in Terms of Seismic Source, Propagation Path and Local Site Conditions, by M. Kamiyama, M.J. O'Rourke and R. Flores-Berrones, 9/9/92, (PB93-150266, A08, MF-A02).

NCEER-92-0024 "Seismic Behavior of Reinforced Concrete Frame Structures with Nonductile Details, Part I: Summary of Experimental Findings of Full Scale Beam-Column Joint Tests," by A. Beres, R.N. White and P. Gergely, 9/30/92, (PB93-227783, A05, MF-A01).

NCEER-92-0025 "Experimental Results of Repaired and Retrofitted Beam-Column Joint Tests in Lightly Reinforced Concrete Frame Buildings," by A. Beres, S. El-Borgi, R.N. White and P. Gergely, 10/29/92, (PB93-227791, A05, MF-A01).

NCEER-92-0026 "A Generalization of Optimal Control Theory: Linear and Nonlinear Structures," by J.N. Yang, Z. Li and S. Vongchavalitkul, 11/2/92, (PB93-188621, A05, MF-A01).

NCEER-92-0027 "Seismic Resistance of Reinforced Concrete Frame Structures Designed Only for Gravity Loads: Part I - Design and Properties of a One-Third Scale Model Structure," by J.M. Bracci, A.M. Reinhorn and J.B. Mander, 12/1/92, (PB94-104502, A08, MF-A02).

NCEER-92-0028 "Seismic Resistance of Reinforced Concrete Frame Structures Designed Only for Gravity Loads: Part II - Experimental Performance of Subassemblages," by L.E. Aycardi, J.B. Mander and A.M. Reinhorn, 12/1/92, (PB94-104510, A08, MF-A02).

NCEER-92-0029 "Seismic Resistance of Reinforced Concrete Frame Structures Designed Only for Gravity Loads: Part III - Experimental Performance and Analytical Study of a Structural Model," by J.M. Bracci, A.M. Reinhorn and J.B. Mander, 12/1/92, (PB93-227528, A09, MF-A01).

NCEER-92-0030 "Evaluation of Seismic Retrofit of Reinforced Concrete Frame Structures: Part I - Experimental Performance of Retrofitted Subassemblages," by D. Choudhuri, J.B. Mander and A.M. Reinhorn, 12/8/92, (PB93-198307, A07, MF-A02).

NCEER-92-0031 "Evaluation of Seismic Retrofit of Reinforced Concrete Frame Structures: Part II - Experimental Performance and Analytical Study of a Retrofitted Structural Model," by J.M. Bracci, A.M. Reinhorn and J.B. Mander, 12/8/92, (PB93-198315, A09, MF-A03).

NCEER-92-0032 "Experimental and Analytical Investigation of Seismic Response of Structures with Supplemental Fluid Viscous Dampers," by M.C. Constantinou and M.D. Symans, 12/21/92, (PB93-191435, A10, MF-A03). This report is available only through NTIS (see address given above).

NCEER-92-0033 "Reconnaissance Report on the Cairo, Egypt Earthquake of October 12, 1992," by M. Khater, 12/23/92, (PB93-188621, A03, MF-A01).

NCEER-92-0034 "Low-Level Dynamic Characteristics of Four Tall Flat-Plate Buildings in New York City," by H. Gavin, S. Yuan, J. Grossman, E. Pekelis and K. Jacob, 12/28/92, (PB93-188217, A07, MF-A02).

NCEER-93-0001 "An Experimental Study on the Seismic Performance of Brick-Infilled Steel Frames With and Without Retrofit," by J.B. Mander, B. Nair, K. Wojtkowski and J. Ma, 1/29/93, (PB93-227510, A07, MF-A02).

NCEER-93-0002 "Social Accounting for Disaster Preparedness and Recovery Planning," by S. Cole, E. Pantoja and V. Razak, 2/22/93, (PB94-142114, A12, MF-A03).

NCEER-93-0003 "Assessment of 1991 NEHRP Provisions for Nonstructural Components and Recommended Revisions," by T.T. Soong, G. Chen, Z. Wu, R-H. Zhang and M. Grigoriu, 3/1/93, (PB93-188639, A06, MF-A02).

NCEER-93-0004 "Evaluation of Static and Response Spectrum Analysis Procedures of SEAOC/UBC for Seismic Isolated Structures," by C.W. Winters and M.C. Constantinou, 3/23/93, (PB93-198299, A10, MF-A03).

NCEER-93-0005 "Earthquakes in the Northeast - Are We Ignoring the Hazard? A Workshop on Earthquake Science and Safety for Educators," edited by K.E.K. Ross, 4/2/93, (PB94-103066, A09, MF-A02).

NCEER-93-0006 "Inelastic Response of Reinforced Concrete Structures with Viscoelastic Braces," by R.F. Lobo, J.M. Bracci, K.L. Shen, A.M. Reinhorn and T.T. Soong, 4/5/93, (PB93-227486, A05, MF-A02).

NCEER-93-0007 "Seismic Testing of Installation Methods for Computers and Data Processing Equipment," by K. Kosar, T.T. Soong, K.L. Shen, J.A. HoLung and Y.K. Lin, 4/12/93, (PB93-198299, A07, MF-A02).

NCEER-93-0008 "Retrofit of Reinforced Concrete Frames Using Added Dampers," by A. Reinhorn, M. Constantinou and C. Li, to be published.

NCEER-93-0009 "Seismic Behavior and Design Guidelines for Steel Frame Structures with Added Viscoelastic Dampers," by K.C. Chang, M.L. Lai, T.T. Soong, D.S. Hao and Y.C. Yeh, 5/1/93, (PB94-141959, A07, MF-A02).

NCEER-93-0010 "Seismic Performance of Shear-Critical Reinforced Concrete Bridge Piers," by J.B. Mander, S.M. Waheed, M.T.A. Chaudhary and S.S. Chen, 5/12/93, (PB93-227494, A08, MF-A02).

NCEER-93-0011 "3D-BASIS-TABS: Computer Program for Nonlinear Dynamic Analysis of Three Dimensional Base Isolated Structures," by S. Nagarajaiah, C. Li, A.M. Reinhorn and M.C. Constantinou, 8/2/93, (PB94-141819, A09, MF-A02).

NCEER-93-0012 "Effects of Hydrocarbon Spills from an Oil Pipeline Break on Ground Water," by O.J. Helweg and H.H.M. Hwang, 8/3/93, (PB94-141942, A06, MF-A02).

NCEER-93-0013 "Simplified Procedures for Seismic Design of Nonstructural Components and Assessment of Current Code Provisions," by M.P. Singh, L.E. Suarez, E.E. Matheu and G.O. Maldonado, 8/4/93, (PB94-141827, A09, MF-A02).

NCEER-93-0014 "An Energy Approach to Seismic Analysis and Design of Secondary Systems," by G. Chen and T.T. Soong, 8/6/93, (PB94-142767, A11, MF-A03).

NCEER-93-0015 "Proceedings from School Sites: Becoming Prepared for Earthquakes - Commemorating the Third Anniversary of the Loma Prieta Earthquake," Edited by F.E. Winslow and K.E.K. Ross, 8/16/93, (PB94-154275, A16, MF-A02).

NCEER-93-0016 "Reconnaissance Report of Damage to Historic Monuments in Cairo, Egypt Following the October 12, 1992 Dahshur Earthquake," by D. Sykora, D. Look, G. Croci, E. Karaesmen and E. Karaesmen, 8/19/93, (PB94-142221, A08, MF-A02).

NCEER-93-0017 "The Island of Guam Earthquake of August 8, 1993," by S.W. Swan and S.K. Harris, 9/30/93, (PB94-141843, A04, MF-A01).

NCEER-93-0018 "Engineering Aspects of the October 12, 1992 Egyptian Earthquake," by A.W. Elgamal, M. Amer, K. Adalier and A. Abul-Fadl, 10/7/93, (PB94-141983, A05, MF-A01).

NCEER-93-0019 "Development of an Earthquake Motion Simulator and its Application in Dynamic Centrifuge Testing," by I. Krstelj, Supervised by J.H. Prevost, 10/23/93, (PB94-181773, A-10, MF-A03).

NCEER-93-0020 "NCEER-Taisei Corporation Research Program on Sliding Seismic Isolation Systems for Bridges: Experimental and Analytical Study of a Friction Pendulum System (FPS)," by M.C. Constantinou, P. Tsopelas, Y-S. Kim and S. Okamoto, 11/1/93, (PB94-142775, A08, MF-A02).

NCEER-93-0021 "Finite Element Modeling of Elastomeric Seismic Isolation Bearings," by L.J. Billings, Supervised by R. Shepherd, 11/8/93, to be published.

NCEER-93-0022 "Seismic Vulnerability of Equipment in Critical Facilities: Life-Safety and Operational Consequences," by K. Porter, G.S. Johnson, M.M. Zadeh, C. Scawthorn and S. Eder, 11/24/93, (PB94-181765, A16, MF-A03).

NCEER-93-0023 "Hokkaido Nansei-oki, Japan Earthquake of July 12, 1993, by P.I. Yanev and C.R. Scawthorn, 12/23/93, (PB94-181500, A07, MF-A01).

NCEER-94-0001 "An Evaluation of Seismic Serviceability of Water Supply Networks with Application to the San Francisco Auxiliary Water Supply System," by I. Markov, Supervised by M. Grigoriu and T. O'Rourke, 1/21/94, (PB94-204013, A07, MF-A02).

NCEER-94-0002 "NCEER-Taisei Corporation Research Program on Sliding Seismic Isolation Systems for Bridges: Experimental and Analytical Study of Systems Consisting of Sliding Bearings, Rubber Restoring Force Devices and Fluid Dampers," Volumes I and II, by P. Tsopelas, S. Okamoto, M.C. Constantinou, D. Ozaki and S. Fujii, 2/4/94, (PB94-181740, A09, MF-A02 and PB94-181757, A12, MF-A03).

NCEER-94-0003 "A Markov Model for Local and Global Damage Indices in Seismic Analysis," by S. Rahman and M. Grigoriu, 2/18/94, (PB94-206000, A12, MF-A03).

NCEER-94-0004 "Proceedings from the NCEER Workshop on Seismic Response of Masonry Infills," edited by D.P. Abrams, 3/1/94, (PB94-180783, A07, MF-A02).

NCEER-94-0005 "The Northridge, California Earthquake of January 17, 1994: General Reconnaissance Report," edited by J.D. Goltz, 3/11/94, (PB193943, A10, MF-A03).

NCEER-94-0006 "Seismic Energy Based Fatigue Damage Analysis of Bridge Columns: Part I - Evaluation of Seismic Capacity," by G.A. Chang and J.B. Mander, 3/14/94, (PB94-219185, A11, MF-A03).

NCEER-94-0007 "Seismic Isolation of Multi-Story Frame Structures Using Spherical Sliding Isolation Systems," by T.M. Al-Hussaini, V.A. Zayas and M.C. Constantinou, 3/17/94, (PB193745, A09, MF-A02).

NCEER-94-0008 "The Northridge, California Earthquake of January 17, 1994: Performance of Highway Bridges," edited by I.G. Buckle, 3/24/94, (PB94-193851, A06, MF-A02).

NCEER-94-0009 "Proceedings of the Third U.S.-Japan Workshop on Earthquake Protective Systems for Bridges," edited by I.G. Buckle and I. Friedland, 3/31/94, (PB94-195815, A99, MF-A06).

NCEER-94-0010 "3D-BASIS-ME: Computer Program for Nonlinear Dynamic Analysis of Seismically Isolated Single and Multiple Structures and Liquid Storage Tanks," by P.C. Tsopelas, M.C. Constantinou and A.M. Reinhorn, 4/12/94, (PB94-204922, A09, MF-A02).

NCEER-94-0011 "The Northridge, California Earthquake of January 17, 1994: Performance of Gas Transmission Pipelines," by T.D. O'Rourke and M.C. Palmer, 5/16/94, (PB94-204989, A05, MF-A01).

NCEER-94-0012 "Feasibility Study of Replacement Procedures and Earthquake Performance Related to Gas Transmission Pipelines," by T.D. O'Rourke and M.C. Palmer, 5/25/94, (PB94-206638, A09, MF-A02).

NCEER-94-0013 "Seismic Energy Based Fatigue Damage Analysis of Bridge Columns: Part II - Evaluation of Seismic Demand," by G.A. Chang and J.B. Mander, 6/1/94, (PB95-18106, A08, MF-A02).

NCEER-94-0014 "NCEER-Taisei Corporation Research Program on Sliding Seismic Isolation Systems for Bridges: Experimental and Analytical Study of a System Consisting of Sliding Bearings and Fluid Restoring Force/Damping Devices," by P. Tsopelas and M.C. Constantinou, 6/13/94, (PB94-219144, A10, MF-A03).

NCEER-94-0015 "Generation of Hazard-Consistent Fragility Curves for Seismic Loss Estimation Studies," by H. Hwang and J-R. Huo, 6/14/94, (PB95-181996, A09, MF-A02).

NCEER-94-0016 "Seismic Study of Building Frames with Added Energy-Absorbing Devices," by W.S. Pong, C.S. Tsai and G.C. Lee, 6/20/94, (PB94-219136, A10, A03).

NCEER-94-0017 "Sliding Mode Control for Seismic-Excited Linear and Nonlinear Civil Engineering Structures," by J. Yang, J. Wu, A. Agrawal and Z. Li, 6/21/94, (PB95-138483, A06, MF-A02).

NCEER-94-0018 "3D-BASIS-TABS Version 2.0: Computer Program for Nonlinear Dynamic Analysis of Three Dimensional Base Isolated Structures," by A.M. Reinhorn, S. Nagarajaiah, M.C. Constantinou, P. Tsopelas and R. Li, 6/22/94, (PB95-182176, A08, MF-A02).

NCEER-94-0019 "Proceedings of the International Workshop on Civil Infrastructure Systems: Application of Intelligent Systems and Advanced Materials on Bridge Systems," Edited by G.C. Lee and K.C. Chang, 7/18/94, (PB95-252474, A20, MF-A04).

NCEER-94-0020 "Study of Seismic Isolation Systems for Computer Floors," by V. Lambrou and M.C. Constantinou, 7/19/94, (PB95-138533, A10, MF-A03).

NCEER-94-0021 "Proceedings of the U.S.-Italian Workshop on Guidelines for Seismic Evaluation and Rehabilitation of Unreinforced Masonry Buildings," Edited by D.P. Abrams and G.M. Calvi, 7/20/94, (PB95-138749, A13, MF-A03).

NCEER-94-0022 "NCEER-Taisei Corporation Research Program on Sliding Seismic Isolation Systems for Bridges: Experimental and Analytical Study of a System Consisting of Lubricated PTFE Sliding Bearings and Mild Steel Dampers," by P. Tsopelas and M.C. Constantinou, 7/22/94, (PB95-182184, A08, MF-A02).

NCEER-94-0023 "Development of Reliability-Based Design Criteria for Buildings Under Seismic Load," by Y.K. Wen, H. Hwang and M. Shinozuka, 8/1/94, (PB95-211934, A08, MF-A02).

NCEER-94-0024 "Experimental Verification of Acceleration Feedback Control Strategies for an Active Tendon System," by S.J. Dyke, B.F. Spencer, Jr., P. Quast, M.K. Sain, D.C. Kaspari, Jr. and T.T. Soong, 8/29/94, (PB95-212320, A05, MF-A01).

NCEER-94-0025 "Seismic Retrofitting Manual for Highway Bridges," Edited by I.G. Buckle and I.F. Friedland, published by the Federal Highway Administration (PB95-212676, A15, MF-A03).

NCEER-94-0026 "Proceedings from the Fifth U.S.-Japan Workshop on Earthquake Resistant Design of Lifeline Facilities and Countermeasures Against Soil Liquefaction," Edited by T.D. O'Rourke and M. Hamada, 11/7/94, (PB95-220802, A99, MF-E08).

NCEER-95-0001 "Experimental and Analytical Investigation of Seismic Retrofit of Structures with Supplemental Damping: Part 1 - Fluid Viscous Damping Devices," by A.M. Reinhorn, C. Li and M.C. Constantinou, 1/3/95, (PB95-266599, A09, MF-A02).

NCEER-95-0002 "Experimental and Analytical Study of Low-Cycle Fatigue Behavior of Semi-Rigid Top-And-Seat Angle Connections," by G. Pekcan, J.B. Mander and S.S. Chen, 1/5/95, (PB95-220042, A07, MF-A02).

NCEER-95-0003 "NCEER-ATC Joint Study on Fragility of Buildings," by T. Anagnos, C. Rojahn and A.S. Kiremidjian, 1/20/95, (PB95-220026, A06, MF-A02).

NCEER-95-0004 "Nonlinear Control Algorithms for Peak Response Reduction," by Z. Wu, T.T. Soong, V. Gattulli and R.C. Lin, 2/16/95, (PB95-220349, A05, MF-A01).

NCEER-95-0005 "Pipeline Replacement Feasibility Study: A Methodology for Minimizing Seismic and Corrosion Risks to Underground Natural Gas Pipelines," by R.T. Eguchi, H.A. Seligson and D.G. Honegger, 3/2/95, (PB95-252326, A06, MF-A02).

NCEER-95-0006 "Evaluation of Seismic Performance of an 11-Story Frame Building During the 1994 Northridge Earthquake," by F. Naeim, R. DiSulio, K. Benuska, A. Reinhorn and C. Li, to be published.

NCEER-95-0007 "Prioritization of Bridges for Seismic Retrofitting," by N. Basöz and A.S. Kiremidjian, 4/24/95, (PB95-252300, A08, MF-A02).

NCEER-95-0008 "Method for Developing Motion Damage Relationships for Reinforced Concrete Frames," by A. Singhal and A.S. Kiremidjian, 5/11/95, (PB95-266607, A06, MF-A02).

NCEER-95-0009 "Experimental and Analytical Investigation of Seismic Retrofit of Structures with Supplemental Damping: Part II - Friction Devices," by C. Li and A.M. Reinhorn, 7/6/95, (PB96-128087, A11, MF-A03).

NCEER-95-0010 "Experimental Performance and Analytical Study of a Non-Ductile Reinforced Concrete Frame Structure Retrofitted with Elastomeric Spring Dampers," by G. Pekcan, J.B. Mander and S.S. Chen, 7/14/95, (PB96-137161, A08, MF-A02).

NCEER-95-0011 "Development and Experimental Study of Semi-Active Fluid Damping Devices for Seismic Protection of Structures," by M.D. Symans and M.C. Constantinou, 8/3/95, (PB96-136940, A23, MF-A04).

NCEER-95-0012 "Real-Time Structural Parameter Modification (RSPM): Development of Innervated Structures," by Z. Liang, M. Tong and G.C. Lee, 4/11/95, (PB96-137153, A06, MF-A01).

NCEER-95-0013 "Experimental and Analytical Investigation of Seismic Retrofit of Structures with Supplemental Damping: Part III - Viscous Damping Walls," by A.M. Reinhorn and C. Li, 10/1/95, (PB96-176409, A11, MF-A03).

NCEER-95-0014 "Seismic Fragility Analysis of Equipment and Structures in a Memphis Electric Substation," by J-R. Huo and H.H.M. Hwang, (PB96-128087, A09, MF-A02), 8/10/95.

NCEER-95-0015 "The Hanshin-Awaji Earthquake of January 17, 1995: Performance of Lifelines," Edited by M. Shinozuka, 11/3/95, (PB96-176383, A15, MF-A03).

NCEER-95-0016 "Highway Culvert Performance During Earthquakes," by T.L. Youd and C.J. Beckman, available as NCEER-96-0015.

NCEER-95-0017 "The Hanshin-Awaji Earthquake of January 17, 1995: Performance of Highway Bridges," Edited by I.G. Buckle, 12/1/95, to be published.

NCEER-95-0018 "Modeling of Masonry Infill Panels for Structural Analysis," by A.M. Reinhorn, A. Madan, R.E. Valles, Y. Reichmann and J.B. Mander, 12/8/95, (PB97-110886, MF-A01, A06).

NCEER-95-0019 "Optimal Polynomial Control for Linear and Nonlinear Structures," by A.K. Agrawal and J.N. Yang, 12/11/95, (PB96-168737, A07, MF-A02).

NCEER-95-0020 "Retrofit of Non-Ductile Reinforced Concrete Frames Using Friction Dampers," by R.S. Rao, P. Gergely and R.N. White, 12/22/95, (PB97-133508, A10, MF-A02).

NCEER-95-0021 "Parametric Results for Seismic Response of Pile-Supported Bridge Bents," by G. Mylonakis, A. Nikolaou and G. Gazetas, 12/22/95, (PB97-100242, A12, MF-A03).

NCEER-95-0022 "Kinematic Bending Moments in Seismically Stressed Piles," by A. Nikolaou, G. Mylonakis and G. Gazetas, 12/23/95, (PB97-113914, MF-A03, A13).

NCEER-96-0001 "Dynamic Response of Unreinforced Masonry Buildings with Flexible Diaphragms," by A.C. Costley and D.P. Abrams," 10/10/96, (PB97-133573, MF-A03, A15).

NCEER-96-0002 "State of the Art Review: Foundations and Retaining Structures," by I. Po Lam, to be published.

NCEER-96-0003 "Ductility of Rectangular Reinforced Concrete Bridge Columns with Moderate Confinement," by N. Wehbe, M. Saiidi, D. Sanders and B. Douglas, 11/7/96, (PB97-133557, A06, MF-A02).

NCEER-96-0004 "Proceedings of the Long-Span Bridge Seismic Research Workshop," edited by I.G. Buckle and I.M. Friedland, to be published.

NCEER-96-0005 "Establish Representative Pier Types for Comprehensive Study: Eastern United States," by J. Kulicki and Z. Prucz, 5/28/96, (PB98-119217, A07, MF-A02).

NCEER-96-0006 "Establish Representative Pier Types for Comprehensive Study: Western United States," by R. Imbsen, R.A. Schamber and T.A. Osterkamp, 5/28/96, (PB98-118607, A07, MF-A02).

NCEER-96-0007 "Nonlinear Control Techniques for Dynamical Systems with Uncertain Parameters," by R.G. Ghanem and M.I. Bujakov, 5/27/96, (PB97-100259, A17, MF-A03).

NCEER-96-0008 "Seismic Evaluation of a 30-Year Old Non-Ductile Highway Bridge Pier and Its Retrofit," by J.B. Mander, B. Mahmoodzadegan, S. Bhadra and S.S. Chen, 5/31/96, (PB97-110902, MF-A03, A10).

NCEER-96-0009 "Seismic Performance of a Model Reinforced Concrete Bridge Pier Before and After Retrofit," by J.B. Mander, J.H. Kim and C.A. Ligozio, 5/31/96, (PB97-110910, MF-A02, A10).

NCEER-96-0010 "IDARC2D Version 4.0: A Computer Program for the Inelastic Damage Analysis of Buildings," by R.E. Valles, A.M. Reinhorn, S.K. Kunnath, C. Li and A. Madan, 6/3/96, (PB97-100234, A17, MF-A03).

NCEER-96-0011 "Estimation of the Economic Impact of Multiple Lifeline Disruption: Memphis Light, Gas and Water Division Case Study," by S.E. Chang, H.A. Seligson and R.T. Eguchi, 8/16/96, (PB97-133490, A11, MF-A03).

NCEER-96-0012 "Proceedings from the Sixth Japan-U.S. Workshop on Earthquake Resistant Design of Lifeline Facilities and Countermeasures Against Soil Liquefaction, Edited by M. Hamada and T. O'Rourke, 9/11/96, (PB97-133581, A99, MF-A06).

NCEER-96-0013 "Chemical Hazards, Mitigation and Preparedness in Areas of High Seismic Risk: A Methodology for Estimating the Risk of Post-Earthquake Hazardous Materials Release," by H.A. Seligson, R.T. Eguchi, K.J. Tierney and K. Richmond, 11/7/96, (PB97-133565, MF-A02, A08).

NCEER-96-0014 "Response of Steel Bridge Bearings to Reversed Cyclic Loading," by J.B. Mander, D-K. Kim, S.S. Chen and G.J. Premus, 11/13/96, (PB97-140735, A12, MF-A03).

NCEER-96-0015 "Highway Culvert Performance During Past Earthquakes," by T.L. Youd and C.J. Beckman, 11/25/96, (PB97-133532, A06, MF-A01).

NCEER-97-0001 "Evaluation, Prevention and Mitigation of Pounding Effects in Building Structures," by R.E. Valles and A.M. Reinhorn, 2/20/97, (PB97-159552, A14, MF-A03).

NCEER-97-0002 "Seismic Design Criteria for Bridges and Other Highway Structures," by C. Rojahn, R. Mayes, D.G. Anderson, J. Clark, J.H. Hom, R.V. Nutt and M.J. O'Rourke, 4/30/97, (PB97-194658, A06, MF-A03).

NCEER-97-0003 "Proceedings of the U.S.-Italian Workshop on Seismic Evaluation and Retrofit," Edited by D.P. Abrams and G.M. Calvi, 3/19/97, (PB97-194666, A13, MF-A03).

NCEER-97-0004 "Investigation of Seismic Response of Buildings with Linear and Nonlinear Fluid Viscous Dampers," by A.A. Seleemah and M.C. Constantinou, 5/21/97, (PB98-109002, A15, MF-A03).

NCEER-97-0005 "Proceedings of the Workshop on Earthquake Engineering Frontiers in Transportation Facilities," edited by G.C. Lee and I.M. Friedland, 8/29/97, (PB98-128911, A25, MR-A04).

NCEER-97-0006 "Cumulative Seismic Damage of Reinforced Concrete Bridge Piers," by S.K. Kunnath, A. El-Bahy, A. Taylor and W. Stone, 9/2/97, (PB98-108814, A11, MF-A03).

NCEER-97-0007 "Structural Details to Accommodate Seismic Movements of Highway Bridges and Retaining Walls," by R.A. Imbsen, R.A. Schamber, E. Thorkildsen, A. Kartoum, B.T. Martin, T.N. Rosser and J.M. Kulicki, 9/3/97, (PB98-108996, A09, MF-A02).

NCEER-97-0008 "A Method for Earthquake Motion-Damage Relationships with Application to Reinforced Concrete Frames," by A. Singhal and A.S. Kiremidjian, 9/10/97, (PB98-108988, A13, MF-A03).

NCEER-97-0009 "Seismic Analysis and Design of Bridge Abutments Considering Sliding and Rotation," by K. Fishman and R. Richards, Jr., 9/15/97, (PB98-108897, A06, MF-A02).

NCEER-97-0010 "Proceedings of the FHWA/NCEER Workshop on the National Representation of Seismic Ground Motion for New and Existing Highway Facilities," edited by I.M. Friedland, M.S. Power and R.L. Mayes, 9/22/97, (PB98-128903, A21, MF-A04).

NCEER-97-0011 "Seismic Analysis for Design or Retrofit of Gravity Bridge Abutments," by K.L. Fishman, R. Richards, Jr. and R.C. Divito, 10/2/97, (PB98-128937, A08, MF-A02).

NCEER-97-0012 "Evaluation of Simplified Methods of Analysis for Yielding Structures," by P. Tsopelas, M.C. Constantinou, C.A. Kircher and A.S. Whittaker, 10/31/97, (PB98-128929, A10, MF-A03).

NCEER-97-0013 "Seismic Design of Bridge Columns Based on Control and Repairability of Damage," by C-T. Cheng and J.B. Mander, 12/8/97, (PB98-144249, A11, MF-A03).

NCEER-97-0014 "Seismic Resistance of Bridge Piers Based on Damage Avoidance Design," by J.B. Mander and C-T. Cheng, 12/10/97, (PB98-144223, A09, MF-A02).

NCEER-97-0015 "Seismic Response of Nominally Symmetric Systems with Strength Uncertainty," by S. Balopoulou and M. Grigoriu, 12/23/97, (PB98-153422, A11, MF-A03).

NCEER-97-0016 "Evaluation of Seismic Retrofit Methods for Reinforced Concrete Bridge Columns," by T.J. Wipf, F.W. Klaiber and F.M. Russo, 12/28/97, (PB98-144215, A12, MF-A03).

NCEER-97-0017 "Seismic Fragility of Existing Conventional Reinforced Concrete Highway Bridges," by C.L. Mullen and A.S. Cakmak, 12/30/97, (PB98-153406, A08, MF-A02).

NCEER-97-0018 "Loss Asssessment of Memphis Buildings," edited by D.P. Abrams and M. Shinozuka, 12/31/97, (PB98-144231, A13, MF-A03).

NCEER-97-0019 "Seismic Evaluation of Frames with Infill Walls Using Quasi-static Experiments," by K.M. Mosalam, R.N. White and P. Gergely, 12/31/97, (PB98-153455, A07, MF-A02).

NCEER-97-0020 "Seismic Evaluation of Frames with Infill Walls Using Pseudo-dynamic Experiments," by K.M. Mosalam, R.N. White and P. Gergely, 12/31/97, (PB98-153430, A07, MF-A02).

NCEER-97-0021 "Computational Strategies for Frames with Infill Walls: Discrete and Smeared Crack Analyses and Seismic Fragility," by K.M. Mosalam, R.N. White and P. Gergely, 12/31/97, (PB98-153414, A10, MF-A02).

NCEER-97-0022 "Proceedings of the NCEER Workshop on Evaluation of Liquefaction Resistance of Soils," edited by T.L. Youd and I.M. Idriss, 12/31/97, (PB98-155617, A15, MF-A03).

MCEER-98-0001 "Extraction of Nonlinear Hysteretic Properties of Seismically Isolated Bridges from Quick-Release Field Tests," by Q. Chen, B.M. Douglas, E.M. Maragakis and I.G. Buckle, 5/26/98, (PB99-118838, A06, MF-A01).

MCEER-98-0002 "Methodologies for Evaluating the Importance of Highway Bridges," by A. Thomas, S. Eshenaur and J. Kulicki, 5/29/98, (PB99-118846, A10, MF-A02).

MCEER-98-0003 "Capacity Design of Bridge Piers and the Analysis of Overstrength," by J.B. Mander, A. Dutta and P. Goel, 6/1/98, (PB99-118853, A09, MF-A02).

MCEER-98-0004 "Evaluation of Bridge Damage Data from the Loma Prieta and Northridge, California Earthquakes," by N. Basoz and A. Kiremidjian, 6/2/98, (PB99-118861, A15, MF-A03).

MCEER-98-0005 "Screening Guide for Rapid Assessment of Liquefaction Hazard at Highway Bridge Sites," by T. L. Youd, 6/16/98, (PB99-118879, A06, not available on microfiche).

MCEER-98-0006 "Structural Steel and Steel/Concrete Interface Details for Bridges," by P. Ritchie, N. Kauhl and J. Kulicki, 7/13/98, (PB99-118945, A06, MF-A01).

MCEER-98-0007 "Capacity Design and Fatigue Analysis of Confined Concrete Columns," by A. Dutta and J.B. Mander, 7/14/98, (PB99-118960, A14, MF-A03).

MCEER-98-0008 "Proceedings of the Workshop on Performance Criteria for Telecommunication Services Under Earthquake Conditions," edited by A.J. Schiff, 7/15/98, (PB99-118952, A08, MF-A02).

MCEER-98-0009 "Fatigue Analysis of Unconfined Concrete Columns," by J.B. Mander, A. Dutta and J.H. Kim, 9/12/98, (PB99-123655, A10, MF-A02).

MCEER-98-0010 "Centrifuge Modeling of Cyclic Lateral Response of Pile-Cap Systems and Seat-Type Abutments in Dry Sands," by A.D. Gadre and R. Dobry, 10/2/98, (PB99-123606, A13, MF-A03).

MCEER-98-0011 "IDARC-BRIDGE: A Computational Platform for Seismic Damage Assessment of Bridge Structures," by A.M. Reinhorn, V. Simeonov, G. Mylonakis and Y. Reichman, 10/2/98, (PB99-162919, A15, MF-A03).

MCEER-98-0012 "Experimental Investigation of the Dynamic Response of Two Bridges Before and After Retrofitting with Elastomeric Bearings," by D.A. Wendichansky, S.S. Chen and J.B. Mander, 10/2/98, (PB99-162927, A15, MF-A03).

MCEER-98-0013 "Design Procedures for Hinge Restrainers and Hinge Sear Width for Multiple-Frame Bridges," by R. Des Roches and G.L. Fenves, 11/3/98, (PB99-140477, A13, MF-A03).

MCEER-98-0014 "Response Modification Factors for Seismically Isolated Bridges," by M.C. Constantinou and J.K. Quarshie, 11/3/98, (PB99-140485, A14, MF-A03).

MCEER-98-0015 "Proceedings of the U.S.-Italy Workshop on Seismic Protective Systems for Bridges," edited by I.M. Friedland and M.C. Constantinou, 11/3/98, (PB2000-101711, A22, MF-A04).

MCEER-98-0016 "Appropriate Seismic Reliability for Critical Equipment Systems: Recommendations Based on Regional Analysis of Financial and Life Loss," by K. Porter, C. Scawthorn, C. Taylor and N. Blais, 11/10/98, (PB99-157265, A08, MF-A02).

MCEER-98-0017 "Proceedings of the U.S. Japan Joint Seminar on Civil Infrastructure Systems Research," edited by M. Shinozuka and A. Rose, 11/12/98, (PB99-156713, A16, MF-A03).

MCEER-98-0018 "Modeling of Pile Footings and Drilled Shafts for Seismic Design," by I. PoLam, M. Kapuskar and D. Chaudhuri, 12/21/98, (PB99-157257, A09, MF-A02).

MCEER-99-0001 "Seismic Evaluation of a Masonry Infilled Reinforced Concrete Frame by Pseudodynamic Testing," by S.G. Buonopane and R.N. White, 2/16/99, (PB99-162851, A09, MF-A02).

MCEER-99-0002 "Response History Analysis of Structures with Seismic Isolation and Energy Dissipation Systems: Verification Examples for Program SAP2000," by J. Scheller and M.C. Constantinou, 2/22/99, (PB99-162869, A08, MF-A02).

MCEER-99-0003 "Experimental Study on the Seismic Design and Retrofit of Bridge Columns Including Axial Load Effects," by A. Dutta, T. Kokorina and J.B. Mander, 2/22/99, (PB99-162877, A09, MF-A02).

MCEER-99-0004 "Experimental Study of Bridge Elastomeric and Other Isolation and Energy Dissipation Systems with Emphasis on Uplift Prevention and High Velocity Near-source Seismic Excitation," by A. Kasalanati and M. C. Constantinou, 2/26/99, (PB99-162885, A12, MF-A03).

MCEER-99-0005 "Truss Modeling of Reinforced Concrete Shear-flexure Behavior," by J.H. Kim and J.B. Mander, 3/8/99, (PB99-163693, A12, MF-A03).

MCEER-99-0006 "Experimental Investigation and Computational Modeling of Seismic Response of a 1:4 Scale Model Steel Structure with a Load Balancing Supplemental Damping System," by G. Pekcan, J.B. Mander and S.S. Chen, 4/2/99, (PB99-162893, A11, MF-A03).

MCEER-99-0007 "Effect of Vertical Ground Motions on the Structural Response of Highway Bridges," by M.R. Button, C.J. Cronin and R.L. Mayes, 4/10/99, (PB2000-101411, A10, MF-A03).

MCEER-99-0008 "Seismic Reliability Assessment of Critical Facilities: A Handbook, Supporting Documentation, and Model Code Provisions," by G.S. Johnson, R.E. Sheppard, M.D. Quilici, S.J. Eder and C.R. Scawthorn, 4/12/9, (PB2000-101701, A18, MF-A04).

MCEER-99-0009 "Impact Assessment of Selected MCEER Highway Project Research on the Seismic Design of Highway Structures," by C. Rojahn, R. Mayes, D.G. Anderson, J.H. Clark, D'Appolonia Engineering, S. Gloyd and R.V. Nutt, 4/14/99, (PB99-162901, A10, MF-A02).

MCEER-99-0010 "Site Factors and Site Categories in Seismic Codes," by R. Dobry, R. Ramos and M.S. Power, 7/19/99, (PB2000-101705, A08, MF-A02).

MCEER-99-0011 "Restrainer Design Procedures for Multi-Span Simply-Supported Bridges," by M.J. Randall, M. Saiidi, E. Maragakis and T. Isakovic, 7/20/99, (PB2000-101702, A10, MF-A02).

MCEER-99-0012 "Property Modification Factors for Seismic Isolation Bearings," by M.C. Constantinou, P. Tsopelas, A. Kasalanati and E. Wolff, 7/20/99, (PB2000-103387, A11, MF-A03).

MCEER-99-0013 "Critical Seismic Issues for Existing Steel Bridges," by P. Ritchie, N. Kauhl and J. Kulicki, 7/20/99, (PB2000-101697, A09, MF-A02).

MCEER-99-0014 "Nonstructural Damage Database," by A. Kao, T.T. Soong and A. Vender, 7/24/99, (PB2000-101407, A06, MF-A01).

MCEER-99-0015 "Guide to Remedial Measures for Liquefaction Mitigation at Existing Highway Bridge Sites," by H.G. Cooke and J. K. Mitchell, 7/26/99, (PB2000-101703, A11, MF-A03).

MCEER-99-0016 "Proceedings of the MCEER Workshop on Ground Motion Methodologies for the Eastern United States," edited by N. Abrahamson and A. Becker, 8/11/99, (PB2000-103385, A07, MF-A02).

MCEER-99-0017 "Quindío, Colombia Earthquake of January 25, 1999: Reconnaissance Report," by A.P. Asfura and P.J. Flores, 10/4/99, (PB2000-106893, A06, MF-A01).

MCEER-99-0018 "Hysteretic Models for Cyclic Behavior of Deteriorating Inelastic Structures," by M.V. Sivaselvan and A.M. Reinhorn, 11/5/99, (PB2000-103386, A08, MF-A02).

MCEER-99-0019 "Proceedings of the 7th U.S.- Japan Workshop on Earthquake Resistant Design of Lifeline Facilities and Countermeasures Against Soil Liquefaction," edited by T.D. O'Rourke, J.P. Bardet and M. Hamada, 11/19/99, (PB2000-103354, A99, MF-A06).

MCEER-99-0020 "Development of Measurement Capability for Micro-Vibration Evaluations with Application to Chip Fabrication Facilities," by G.C. Lee, Z. Liang, J.W. Song, J.D. Shen and W.C. Liu, 12/1/99, (PB2000-105993, A08, MF-A02).

MCEER-99-0021 "Design and Retrofit Methodology for Building Structures with Supplemental Energy Dissipating Systems," by G. Pekcan, J.B. Mander and S.S. Chen, 12/31/99, (PB2000-105994, A11, MF-A03).

MCEER-00-0001 "The Marmara, Turkey Earthquake of August 17, 1999: Reconnaissance Report," edited by C. Scawthorn; with major contributions by M. Bruneau, R. Eguchi, T. Holzer, G. Johnson, J. Mander, J. Mitchell, W. Mitchell, A. Papageorgiou, C. Scaethorn, and G. Webb, 3/23/00, (PB2000-106200, A11, MF-A03).

MCEER-00-0002 "Proceedings of the MCEER Workshop for Seismic Hazard Mitigation of Health Care Facilities," edited by G.C. Lee, M. Ettouney, M. Grigoriu, J. Hauer and J. Nigg, 3/29/00, (PB2000-106892, A08, MF-A02).

MCEER-00-0003 "The Chi-Chi, Taiwan Earthquake of September 21, 1999: Reconnaissance Report," edited by G.C. Lee and C.H. Loh, with major contributions by G.C. Lee, M. Bruneau, I.G. Buckle, S.E. Chang, P.J. Flores, T.D. O'Rourke, M. Shinozuka, T.T. Soong, C-H. Loh, K-C. Chang, Z-J. Chen, J-S. Hwang, M-L. Lin, G-Y. Liu, K-C. Tsai, G.C. Yao and C-L. Yen, 4/30/00.

MCEER-00-0004 "Seismic Retrofit of End-Sway Frames of Steel Deck-Truss Bridges with a Supplemental Tendon System: Experimental and Analytical Investigation," by G. Pekcan, J.B. Mander and S.S. Chen, 7/1/00.

MCEER-00-0005 "Sliding Fragility of Unrestrained Equipment in Critical Facilities," by W.H. Chong and T.T. Soong, 7/5/00.

MCEER-00-0006 "Seismic Response of Reinforced Concrete Bridge Pier Walls in the Weak Direction," by N. Abo-Shadi, M. Saiidi and D. Sanders, 7/17/00.

MCEER-00-0007 "Low-Cycle Fatigue Behavior of Longitudinal Reinforcement in Reinforced Concrete Bridge Columns," by J. Brown and S.K. Kunnath, 7/23/00.

MCEER-00-0008 "Soil Structure Interaction of Bridges for Seismic Analysis," I. PoLam and H. Law, 9/25/00.

MCEER-00-0009 "Proceedings of the First MCEER Workshop on Mitigation of Earthquake Disaster by Advanced Technologies (MEDAT-1), edited by M. Shinozuka, D.J. Inman and T.D. O'Rourke, 11/10/00.

MCEER-00-0010 "Development and Evaluation of Simplified Procedures for Analysis and Design of Buildings with Passive Energy Dissipation Systems," by O.M. Ramirez, M.C. Constantinou, C.A. Kircher, A.S. Whittaker, M.W. Johnson, and J.D. Gomez, 12/8/00.

MCEER-00-0011 "Dynamic Soil-Foundation-Structure Interaction Analyses of Large Caissons," by C-Y. Chang, C-M. Mok, Z-L. Wang, R. Settgast, F. Waggoner, M.A. Ketchum, H.M. Gonnermann and C-C. Chin, 12/30/00.

MCEER-00-0012 "Experimental Evaluation of Seismic Performance of Bridge Restrainers," by A.G. Vlassis, E.M. Maragakis and M. Saiid Saiidi, 12/30/00.

MCEER-00-0013 "Effect of Spatial Variation of Ground Motion on Highway Structures," by M. Shinozuka, V. Saxena and G. Deodatis, 12/31/00.

MULTIDISCIPLINARY CENTER FOR EARTHQUAKE ENGINEERING RESEARCH

A National Center of Excellence in Advanced Technology Applications

University at Buffalo, State University of New York
Red Jacket Quadrangle ▪ Buffalo, New York 14261-0025
Phone: 716/645-3391 ▪ Fax: 716/645-3399
E-mail: mceer@acsu.buffalo.edu ▪ WWW Site: http://mceer.buffalo.edu

University at Buffalo *The State University of New York*

ISSN 1520-295X